Electrotonic Structure and Synaptic Integration in Cortical Neurons

by

Diana Kathryn Smetters

Submitted to the Department of Brain and Cognitive Sciences
in partial fulfillment of the requirements for the degree of

Doctor of Philosophy

at the

MASSACHUSETTS INSTITUTE OF TECHNOLOGY

June 1995

Author .....
Department of Brain and Cognitive Sciences
May 24, 1995

Certified by .....
Mriganka Sur
Professor
Thesis Supervisor

Certified by .....
Tomaso Poggio
Professor
Thesis Supervisor

Accepted by .. ..
Gerald Schneider
Chairman, Departmental Committee on Graduate Students

Electrotonic Structure and Synaptic Integration in Cortical Neurons

by

Diana Kathryn Smetters

Submitted to the Department of Brain and Cognitive Sciences
on May 24, 1995, in partial fulfillment of the
requirements for the degree of
Doctor of Philosophy

Abstract

Cortical neurons receive thousands of synaptic inputs, only a few of which come from any single other cell. The basic nature of cortical computation depends not on this number, but instead on the number of simultaneous inputs necessary to cause the post naptic cell to fire a spike - the degree of functional, as opposed to anatomical, convergence. Using whole-cell patch clamp recording and a combination of techniques allowing the study of both the whole population of inputs to a cell, and its responses to a single input over time, single-fiber inputs to cortical cells are shown to be large, fast, and extremely variable. Assuming linear summation, only 5-50 simultaneous inputs are necessary to generate an action potential. The variability in these inputs - both between the inputs to different cells, across the population of inputs to a single cell, and in a single input over time - is functionally expressed in the variability of output spikes. A number of factors are proposed to account for the variability seen across the population of putatively uniquantal miniature excitatory postsynaptic currents (mEPSCs) seen in a single cell in the presence of tetrodotoxin. Compartmental models of reconstructed neurons are used to show that electrotonic filtering alone is sufficient to generate a large amount of such variability, and is necessary to explain certain features of recorded mEPSCs, including the correlation between event rise time and half width. This analysis is extended to the case of miniature inhibitory postsynaptic currents (mIPSCs) of hippocampal dentate gyrus granule cells. Using computational models designed to match the responses to evoked inputs to known locations, and amputation of the bulk of the dendritic tree, these events are shown to originate almost entirely from proximal sites. Together, these properties allow a single cell to participate in a wide variety of ongoing computations, and providing a rich substrate for both cortical information processing and cortical plasticity.

Thesis Supervisor: Mriganka Sur
Title: Professor

Thesis Supervisor: Tomaso Poggio
Title: Professor

Acknowledgments

> MIT is not a very nice place. But once you've been there, nothing will ever scare you again.
>
> -Steve Kosslyn, Harvard Professor, 1989

Besides those trees that valiantly sacrificed themselves to generate a book that very few people will read, I'd like to thank quite a few people:

My committee: Mriganka Sur, Tomaso Poggio, Christof Koch, and Arthur Lander; for reading this rather long thesis, sometimes on rather short notice; and most importantly, for letting me out. In particular, I'd like to thank Christof for his support, advice, and input over the last few years; and Mriganka, for providing me with the facilities to do the work I wanted to do, even though he wasn't always sure why I wanted to do it. And Jan Ellertsen, for smoothing my passage through MIT, and not killing me at the end for flagrantly disregarding deadlines.

My collaborators, who taught me most of what I know about how to do science, and at the same time were always there for friendship, support, and fun: Sacha Nelson, Ivan Soltesz, the exquisite Manuel Esguerra, Jong-On Hahm, and Istvan Mody.

The current and former members of the Sur lab: Manny, Jong-On, Anna, Young, Louis, Sarah, Ron, Alessandra, Monica, Ary, Paco, Ken, Chris, Carsten, Bhavin, Chenchal, Jittendra, Karina, Sacha, Manuela, Melvin, Darren, and, of course, Preston. You were my teachers, my friends, and always there in a pinch – especially when my thesis was due. And, especially, Martha Meyer, Suzanne Kuffler, Maryann Capehart, and Terry Sullivan, for their attention to detail, ability to make sense out of my sometimes bewildering requests, and tendency to smile in times of crisis.

The people whose fault it was I ended up where I am: Rick Garrison and Jim Garrett, for starting me on this long road; Sylvia Zaremba for making me realize that I didn't want to be a pianist; Wayne Cowart, for showing me that maybe research might be interesting after all; J. P. Bruno for getting me interested in neurons; Peter Pappas from whom I learned that physiology was really cool; and Tom Weiss and Bill Peake, from whom I learned that neurophysiology was the coolest thing of all.

The people without whom I wouldn't have made it through, who provided me advice, support, and encouragement when I needed it most, or who said the right thing at the right time, whether they knew it or not: Christof Koch, Sacha Nelson, Eve Marder, Idan Segev, Larry Abbott, Bill Bialek, Jim Bower, John Rinzel, Bard

Ermentrout, Roger Traub, Brenda Claiborne, Tom Brown, Wayne Cowart, Lyle Borg-Graham, Barry Connors, Irwin Levitan and, certainly, Ivan Soltesz.

My father, for telling me not to panic. My mother, for always being willing to listen. And Anita, for her stability in times of crisis. I'm sure they're all glad this is over at last.

The women of my family, and those I have known, who by doing those things they weren't supposed to, showed me I could be whatever I wanted: Alma, Hilda, Hetty, Harriets one and two, Vera, Punk, and Mary.

My current and former officemates, for putting up with me: Randy, Robert, Louis, Corrie, Bobby, Elliot, and especially Marc and Karl for making it through the last few months.

The moral support contingent: Elizabeth, Rachel, Corrie, Danielle, Barbara, Manny, Sacha, Randy, Robin, Ken, Jim, Diana, Loren, Heather, Jong-On, Gary, Fei, Tony, Todd, Jonathan, Dave, Arun, Jody, Mark, Mark, Libby, Brent, Zhaoping, Eric, Nava, Jan, Yves, Angie, Margaret, Terry and Bill, Debbie, and everybody else I forgot...

And, most importantly, Paul Placeway and Ivan Soltesz – for being there at the beginning and the end, respectively, with love, caring, friendship, and a willingness to listen to me even when I wasn't being altogether rational.

I want to dedicate this to my grandfather, Ralph Hewes, and his sister, Mary Zimmerman, who should have been here to see me finish this thesis; and to Jim Smith, who should have been here to finish his own.

Contents

List of Figures

LIST OF FIGURES

List of Tables

LIST OF TABLES

1

Introduction

The mammalian neocortex is responsible for processing an amazingly diverse body of information – from analyzing early sensory input from all sources and combining those inputs across modalities, to generating plans of action and executing them via an orchestrated motor response. It performs these tasks through a bewildering and ever-increasing number of architectonically and physiologically distinct cortical areas, each specialized in terms of its inputs and outputs [282].

In spite of this specialization of the different cortical areas, their intrinsic cellular makeup and micro-circuitry appears remarkably similar [287, 105]. This suggests that there may be basic computations performed by cortical circuits may be similar in all areas [159, 64]. On this view, specialization to particular tasks would be determined primarily by the input and output connectivity of a particular area, combined with minor differences in its intrinsic circuitry and cellular makeup [216]; examples of the latter being the abundance of small layer 4 cells in primary sensory cortices [192, 287], and the expansion in total cell number in primary visual cortex of all mammals [192, 19, 282].

This implies that an understanding of the computations performed by cortical cells and local cortical circuits will provide a basis for understanding the mechanisms of operation of a wide variety of neural processing across diverse areas of neocortex [181, 63, 64, 259]. While a considerable amount of work over the last 10 years has

demonstrated many of the intrinsic properties of the diverse cortical cell types [49, 166, 111, 113, 136], and the glutamatergic, combined NMDA/non-NMDA makeup of excitatory synaptic connections both intrinsic to the cortex and in the inputs from thalamic afferents [107, 253, 254, 262, 129, 1, 183]; at the same time much less is known about the functional properties of cortical neurons at the level of micro-circuitry – the highly recurrent connectivity between diverse cell types and layers that is the hallmark of the neocortex [64, 287, 258, 262, 261, 264, 60, 108, 162, 182, 181].

A single cortical neuron receives between 5 and 10 thousand excitatory synaptic inputs, from both thalamic afferents and other cortical neurons [62, 287, 192]. As a result of the large divergence of cortical axons [287, 192, 62], it has been estimated that only 1-4 of those synapses come from any single presynaptic cell [287, 62, 74, 116, 255, 256], suggesting a convergence of from 1,000 to 10,000 presynaptic cells onto one postsynaptic cell. How much of an impact does each presynaptic cell have on the output of the postsynaptic cell? Do a thousand presynaptic cells have to be active at once to make the postsynaptic cell fire a spike, or only ten? And does it matter *which* ten – are all inputs to a cortical neuron created the same, or is their function determined by factors such as synapse location or the firing history of the presynaptic cell? Clearly the answers to these questions are basic to our understanding of the operation of neocortical cells.

These are the questions that I will address in this thesis. I have approached these issues using a combination of electrophysiological recording from single neurons in slices of rat and cat visual cortex, anatomical reconstruction of recorded cells, and detailed computational modeling of cellular and synaptic properties. I have chosen to concentrate on visual cortex because of the large body of anatomical and physiological data available. Comparison with this data allows both a greater understanding and analysis of the cellular events studied here, as well as an extrapolation beyond the slice into the impact of cellular and synaptic properties on the response of these cells *in vivo* in response to sensory input.

1.1 Outline of the thesis

The work presented here draws heavily on a previous body of research both on the properties of cortical neurons, and on the nature and properties of synaptic transmission in central neurons. I will therefore begin this thesis with a brief review of the anatomical and cellular properties of cortical neurons, followed by a review and summary of the relevant physiological and theoretical work on synaptic physiology. This review will concentrate on those issues most relevant to the work presented here, for more extensive review the reader is invited to consult the numerous general review works available [192, 287, 165]. More detailed discussion of the literature relevant to particular issues, and review of relevant theoretical and computational work and methods will appear in the appropriate portion of the body of the thesis.

Following the introductory chapter, I will present a summary of electrophysiological and computational methods common to all of the chapters of the thesis. Methods for particular experiments will appear in the introductory section of the relevant chapter.

The body of the thesis is divided into two parts. In the first part, I will address the question of the characteristics of excitatory synaptic inputs to cortical neurons, and how they relate to the output of the cell. This part will attempt to answer the question of how large are the single-fiber inputs to cortical neurons, and how many of them does it take to fire the cell? In other words, what is the *functional*, as opposed to anatomical convergence onto cortical neurons.

In the second part, I will address the question of the factors influencing the response of the postsynaptic cell to these inputs, in particular, how electrotonic filtering and synaptic location influence the effectiveness and properties of a synaptic input. This part can be divided into three subsections. In the first, I will present physiological data on the variability of synaptic inputs, and will use computational modeling to explore how much of this variability could be due to electrotonic filtering, and what influence various cellular and synaptic parameters will have on the synaptic response

at the soma. The simulations in this chapter are supplemented by basic findings presented in the Appendix. In the second section I will present an experimental approach to the question of the role of synaptic location on postsynaptic response, and compare the experimental data with the results of the models in the previous sections. Finally, in the third section, I will address he issue of the generality of the conclusions presented here by applying similar computational techniques to data describing the location of an entirely different class of synapses on an entirely different cell type - GABAergic inputs onto dentate gyrus granule cells of the hippocampus.

1.2 Credits and Publication

While the work presented in this thesis is overwhelmingly my own, various studies were performed in collaboration with other investigators, as summarized below.

The work on cortical synapses presented in chapters 3, 4, 5, and the Appendix was performed in collaboration with Dr. Sacha Nelson, a former postdoctoral fellow and now faculty member at Brandeis university. Besides his contributions to discussions of the work herein, Dr. Nelson and I performed together many of the experiments described in Chapter 3, which also produced a few of the filled cells used in Chapters 4.[1] I performed the other half of the early experiments described in Chapter 3, and all of the cortical physiology used in later chapters, as well as all of the analysis of physiological data presented here, both for chapter 3 and later chapters. I performed all of the histological processing, anatomical analysis, and morphological reconstruction described here, as well as all of the mathematical and theoretical analysis and computational simulations.

As noted in chapter 6, the work on inhibitory synapses onto dentate gyrus granule cells was performed in collaboration with Drs. Ivan Soltesz and Istvan Mody of the University of Texas Southwestern Medical Center at Dallas. All electrophysiology

[1]This series of experiments also included a study on short-term synaptic plasticity of cortical synapses, which is not included here.

for that study was performed by my collaborators. Two granule cells were used for computational modeling, one was filled by Dr. Soltesz, the other, used for preliminary simulations only, was filled by me during the course of other experiments. I reconstructed both of the cells. I performed all of the simulations described here and in the paper, as well as the testing of the event detector using simulated data. In the writing of this chapter I have tried to emphasize the computational analysis of the problem. The work presented in chapter 6 is in press in Neuron [240].

This work was supported by a Howard Hughes Medical Institute predoctoral fellowship, EYO7023 to M. Sur, a NIH eye institute fellowship to S. Nelson, and NS-30549 to I. Mody.

1.3 Literature review

1.3.1 Cortical micro-anatomy and cellular physiology

By the turn of the century, Golgi stains of the neocortex in a variety of species had revealed the bewildering array of cell types making up its cytoarchitectonically defined 6-layered structure [207].[2] This diversity can luckily be described to a first approximation by a small number of morphological classes of cells, which also correspond closely to those divisions based on intrinsic physiological properties and neurotransmitter phenotype.

Cortical neurons can be divided along two different lines, each resulting in two (overlapping) categories of neurons. The first division is between spiny and non-spiny neurons. Spiny neurons, which include the pyramidal cells and the spiny stellate cells of layer IV, are generally considered to be glutamatergic, excitatory neurons [287, 192]. Non-spiny cells (including "sparsely spiny" cell types) are in general GABAergic and hence inhibitory [287, 192]. Along the other axis, there are pyramidal cells, which

[2] In the rat, this 6-layered structure is present, but harder to clearly differentiate. This study will follow the standard practice of lumping together layers II and III, and layers V and VI [287].

make up the largest cell class in the cortex and are its output cells projecting to other cortical areas and subcortical structures [287, 193, 194, 195, 196, 133]; and non-pyramidal cells, a category which includes quite a number of distinguishable cell types (e.g. spiny, sparsely spiny and non-spiny stellates, chandelier cells, basket cells, etc. [197, 106, 241].).

Pyramidal cells (examples of which can be seen in Figures 1-1, 1-2, 4-21, 4-22, 5-44) are distinguished by their pyramidal-shaped soma, and by a long "apical" dendrite extending from the top of the cell body to the pial surface. This dendrite usually gives off a number of side branches close to the soma ("apical obliques"), then extends up to the pial surface where it gives rise to a "tuft" of small branches. There are systematic differences in pyramidal cell morphology both within and between layers. In a large layer V cell (such as that shown in Figure 1-1), the apical obliques and tuft will be separated by up to several hundred microns of isolated apical trunk, while in a smaller layer II/III cell, where the apical dendrite has only a short distance to travel before reaching the pial surface, the boundaries of the obliques and the tuft may overlap and in the smallest cells the distinction may be largely irrelevant. Surrounding the soma will be a cloud of from 3-10 "basal" dendrites, which actually constitute the majority of dendritic membrane in all pyramidal cells [133, 137]. In layer V, pyramids can be divided into "bushy" and "thin" subtypes, the former generating a large apical tuft in layer I, the latter generating many fewer apical branches, and frequently ending in lower layer II/III. Layer IV of the rat contains small spiny stellate neurons, as does layer IV in other species, but in the rat these sometimes maintain a vestigial apical dendrite and are referred to as "star pyramids". Pyramids in Layer VI usually have an apical dendrite which extends only so far as layer IV before ending without branching into an apical tuft [133, 137, 287]. Finally, in the rodent, there are also a reasonable frequency of "inverted pyramids", cells showing normal pyramidal morphology except that for some unknown reason their apical dendrite extends towards the gray matter rather than towards layer I [177]. These subdivisions also correspond to differences in connectivity; for instance "bushy" layer V cells are reported to be the only cell

type projecting to the superior colliculus [108], while "thin" layer V cells project to the contralateral cortex and may project to other cortical areas intrahemispherically.

These differences in morphology and connectivity suggest the likelihood of differences in function between these cell types. Even more suggestive is the finding that these divisions also correspond to differences in intrinsic physiology. Pyramidal cells for the most part fire an adapting train of spikes to an injected current step, have relatively broad spikes, and saturate at maximal firing rates less than around 200 Hz. Two examples of regular-spiking cells, one from cat and one from rat, can be seen in Figure 1-2, together with reconstructions of that rat cell and a different cat pyramidal cell. This broad class of cells has been termed "regular spiking cells", or RS cells, and can be subdivided further on the basis of adaptation characteristics[3] [49, 166, 40, 136]. A subset of pyramidal cells, those large pyramids of layer V and lower layer IV show a different type of intrinsic physiology. These cells respond to injected current with a burst of action potentials, and are known as "intrinsically bursting" (IB) cells [40, 49, 166, 108]. These cells correspond to the "bushy" layer V cells described above [136, 137, 108, 36, 37].

In spite of their high degree of morphological heterogeneity, until recently, only a single physiological class of non-pyramidal cells had been identified. These "fast spiking" (FS) cells make up the majority of smooth non-pyramidal cells in cortex [111, 113]. They respond to an injected current step with a non-adapting train of action potentials, can fire at very high frequency, and have very narrow spikes [49, 166]. Recently they have been identified with the parvalbumin-containing (a Ca^{++}-binding protein) subtype of GABAergic neurons [113, 114], and probably include the basket and chandelier cell types defined morphologically [113, 106]. Three other physiological types of non-pyramidal cells have recently been described in rat frontal cortex. The first of these is the low-threshold spike cell (LT) cell, showing bursts following preceding hyperpolarization, and exhibiting tonic firing to depolarization,

[3]This adaptation, however can vary from a slight frequency reduction towards the end of a train to a total cessation of firing after 4-5 spikes.

similar to thalamic neurons [111, 113, 72]. These are calbindin-positive, and may correspond to "sparsely spiny" cells [113, 112]. Both FS and LT cells are present in all layers. Two other cell types have also been identified in layers II/III. Late-spiking (LS) cells show slowly-developing ramp depolarizations in response to step current injections, which eventually reach firing threshold. Their spike trains are usually of lower frequency than FS cells, and they show slight frequency adaptation [113]. They correspond to neurogliaform cells [113]. Finally, the remaining NP cells have been classed together as regular-spiking non-pyramidal cells (RSNP cells). This class is heterogeneous, including some cells that show a small fast depolarizing notch in response to depolarizing current steps, like a mini-burst; this subgroup includes double bouquet and bipolar cells [113]. Spiny stellates, another non-pyramidal cell class, fire non-adapting trains of spikes, but do not usually fall into the "fast spiking" category, however they have not been analyzed in detail [247, 87].

These differences in intrinsic physiology and cell class have, until recently, not been considered in *in vivo* studies, and hence their relationship to receptive field properties and sensory responses is not yet known. However, cells with different morphologies, or whose somata lie in different layers sample different input populations simply by virtue of the axons their dendrites are able to reach[137, 133, 62, 36]. Additionally, recent evidence both in cortex and on similar cell classes in the hippocampus [82, 83, 261, 264, 164, 163] suggests that these differences in cell class correspond to differences in synaptic response properties (see Table 1.3.3). Combined with the obvious differences in spiking (output) properties of each class, this would provide an opportunity for these cell types to process information in very different ways.

Excitatory synaptic transmission in cortical neurons

Both cortical pyramidal cells and thalamic afferents to cortex are known to use the excitatory amino acid, glutamate, as their major neurotransmitter [62]. Because pyramidal cells receive the bulk of their connections from other pyramidal cells, both

those nearby and those in other cortical areas. excitatory synapses predominate and are estimated to make up 85% of all synapses in cortex [62. 287. 192]. Pyramidal cells receive the vast majority of their excitatory inputs through synapses located on spine heads [192. 287]. while inhibitory inputs are predominantly located on their somata, axon hillocks, and dendritic shafts [192]. For the most part, pyramids have few spines (and hence few excitatory synapses) within 50 μm of their somata [134]. In contrast. spiny stellate cells of layer IV in the cat[4] receive over half of their excitatory inputs onto their dendritic shafts [9, 8].[5] Non-pyramidal, non-spiny neurons receive their excitatory synaptic inputs distributed over their somata and dendrites.

Excitatory synapses onto cortical neurons involve both the N-methyl-d-aspartate (NMDA) and non-NMDA (primarily α-amino-3-hydroxy-5-methyl-4-isoxazolepropionate (AMPA)) subtypes of glutamate receptors[6] [107, 183. 262, 247, 253, 254, 84]. As in many other cell types, the two receptor subtypes seem to be colocalized at single synapses [18, 263, 258, 262]. Presumably because of the high input impedance of spine heads and small distal dendrites, combined with a possibly higher resting potential in the dendrites, significant NMDA contributions can be seen in inputs from single presynaptic axons even when the soma of the postsynaptic cell is as hyperpolarized as -80 mV [264, 262, 183]. This indicates that the site of synaptic input must be significantly depolarized (see chapter 4), as cortical NMDA receptors show a conventional current-voltage relation for that subtype [247], not passing significant current below -50mV in the presence of normal Mg^{++} concentrations.

In addition to the differences in anatomical localization, there appear to be differences in the physiology of synaptic inputs to different cell types and layers. Even

[4]Of which there are few or none in rat [192].

[5]As rats presumably do not have spiny stellate cells, and no recordings in this study were performed in layer IV, this complication will be ignored for the bulk of this study, which is heavily biased towards pyramidal cells.

[6]There is also evidence for the presence of metabotropic glutamate receptors on central neurons [180], but these have been much less extensively studied and will not be considered here. In addition, I will not make a distinction between the other subtypes of non-NMDA receptors, considering primarily the AMPA/CNQX-sensitive class.

the channels underlying the synaptic response may be different in different cell types. For instance, the synaptic responses of pyramids and some interneurons are strikingly different in their kinetics [264, 261]. This may be partially due to the fact that glutamatergic inputs to non-pyramidal cells seem to generate postsynaptic responses with a much more rapid time course than those in pyramidal cells, reflecting differences in the underlying channel kinetics in the two cell classes [83].

Use of whole-cell patch clamp recording and the development of neocortical synaptic physiology

In recent years, the technique of whole-cell patch clamp recording in slices [24, 68] has, through its increased signal-to-noise ratio and its increased pharmacological access to the intracellular milieu, greatly increased our knowledge of synaptic and cellular physiology. However, many of the experiments on synaptic responses in a variety of neuronal subtypes were performed using conventional ("sharp electrode") intracellular recording, and so in comparing data from these studies it is important to consider the differences between these recording methods.[7] There has been some controversy that the significantly higher input resistance and longer time constant seen in whole-cell recordings is due to washout of some normal cellular components contributing additional conductance to the cell [6, 36], but careful studies including use of perforated patch recording techniques support the notion of a somatic shunt underlying a significant fraction of the reduction in R_{in} in sharp electrode recordings [243, 6, 231, 246]. Also, most, if not all, sharp electrode recordings are performed at temperatures above 30°C, while whole-cell recording is frequently performed at room temperature. As a reduction in temperature can increase input resistance and change other cellular properties [257], this may contribute to some of the reported differences

[7] In addition to the increased S/N, the most noted difference between intracellular and whole-cell recording is the likely presence in the former of a somatic shunt, or leakage to ground around the electrode [243, 242, 152]. The importance of this to recordings of synaptic events is discussed in Section A.1.2.

in cellular properties with the two methods. However, some studies have compared whole-cell and sharp electrode recordings under conditions of identical temperature, recording conditions, and animal characteristics [246, 243], indicating that this cannot be whole story. Almost all the recordings here were performed at 34°C, but a small number of cells were recorded between 22 and 34°C for comparative purposes.[8] At reduced temperatures there was a slight increase in R_{in} and decrease in spontaneous mEPSC frequency similar to those reported in from the literature. These changes were small, and would not affect the conclusions presented here.

Additionally, most whole-cell recording (including the data presented here from rat) is performed on tissue from animals significantly younger than those used in intracellular studies (typically postnatal days 9 (P9) to 21)[9] [104, 247, 68, 29]. This becomes an important factor both in comparing data across studies using animals of different ages, and in extrapolating the results of whole-cell studies to the response of these cells in adult animals, as animals may still be undergoing developmental changes in cellular and synaptic properties at these younger ages. It is therefore important to examine both the developmental changes that occur between these younger ages and adulthood, and any changes that may occur in the period from P12 and P28, the ages used for the studies presented here.[10]

A number of studies have examined the morphological and electrophysiological development of rat cortical neurons [174, 175, 177, 176, 109, 110, 29, 30, 147]. In the rat, visual cortical neurons are born between E13 and E22/P0 [16]. They migrate in an inside-out pattern,reaching their final laminar position a few days later [16]. In the visual cortex, their ultimate differentiation may in part be controlled by visual experience, which begins with operation of the photoreceptors after birth [148] and changes dramatically with eye-opening at P13. During this period, from P6-12, retinal axons

[8] As this experiment was somewhat impromptu (the temperature controller broke), no systematic quantitative results will be presented.

[9] This is done because of the increased ease of obtaining whole-cell recordings in the younger animals.

[10] Most of the neurons used here were taken from animals between P14 and P21.

form their contacts with the relay cells of the LGN [16]. In the cortex, differences in cellular morphology corresponding to differences in cell type can be seen as early as P5 [109]. Cells undergo a rapid increase in size, dendritic complexity and number of spines between P3 and P12, which taper off and begin to plateau during the third postnatal week. For the most part, morphological differentiation of pyramidal cells is complete by P21 [174, 109]. After P21, the dendrites continue to increase in length up until P60, but this increase is limited to distal dendritic segments [174]. Between P11 and adult, there is a significant increase in the number of dendritic tips [109], but the basic structure of the cell (as indicated by soma size, number of proximal dendrites, etc) does not change. In all cases, layer V cells develop approximately 3 days in advance of the counterparts in layer II/III [174], possibly due to their earlier arrival in the cortex. Inverted pyramids develop apace with their normally-oriented counterparts [177]. Non-pyramidal cells appear to develop morphologically at the same time as the pyramids of the same layer [175], though it appears that their synaptic development may be somewhat retarded with respect to pyramidal cells, as IPSPs cannot be evoked till several days after it is possible to evoke EPSPs [109, 147]. The major differences between the cells used here and the adult, then, is in the length and number of their distal dendritic segments. This means that the cells used here will be more amenable to space clamp than adult cells, and that it should be considered that discussions of electrotonic filtering in Chapters 4 and 5 may underestimate the impact of electrotonic filtering that will be seen in the adult. Between P14 and P21 (i.e. during the primary period used for study here), cells do continue to increase their dendritic lengths, but their basic structure is largely constant. The major change that cells undergo during this period is in their spine distribution. The density of spines increases by at least two-fold between P9-12 and P21 [174], and the adult pattern of a very low spine density on the most proximal dendritic segments is not established until P21. After P21, spine density first increases and then decreases to approximately the level seen at P21, and there is a continuing loss of proximal spines.

Electrophysiological properties of pyramidal cells appear to develop largely in

concert with their morphological differentiation [167, 109, 110]. Between P3 and P21, there is a gradual decrease in input resistance, time constant, and resting potential [109]. Active properties develop in this period as well, with a gradual decrease in action potential threshold, and an increase in action potential size and speed, amount of persistent Na^+ current, afterhyperpolarization size and complexity, and amount of "sag" current [109, 110, 93, 167, 4]. Bursting cells only appear after P14, in spite of the fact that the morphological distinction between "bushy" and "thin" layer V cells is clearly visible by P5 [110]. In all cases, cells appear electrophysiologically mature by P21, and the changes seen during the age range used here, while significant, are all quantitative changes in cell behavior rather than qualitative ones and should not significantly alter the conclusions below.

Finally, synaptic properties of pyramidal cells appear to develop even before they are morphologically or electrophysiologically mature [29, 30]. Excitatory synaptic inputs [109], showing both NMDA and non-NMDA components [29, 30, 146], can be evoked as early as P3. These do not appear to change in character over the first two postnatal weeks [29, 30], and any changes seen before P21 can be attributed to concomitant changes in membrane time constant [109]. IPSPs in contrast, do not appear until P9, at which point they show a normal reversal potential near the resting potential of the cell [109, 147]. Unfortunately, the development of synaptic properties between P21 and adulthood has not been studied using comparable methods at both ages, so it is difficult to assess whether there is a further period of synaptic development before adulthood.

1.3.2 Synaptic properties of central neurons

Quantal nature of synaptic transmission

Beginning with studies at the neuromuscular junction (NMJ) [55, 56, 280] and gradually expanding, after years of controversy, throughout the central nervous system is a consensus that transmission between neurons is *quantized* [280, 276, 160, 161,

210, 20, 92, 32, 45, 67, 95, 104, 127, 132, 140, 156, 248, 283, 291]. A presynaptic action potential releases not a graded amount of neurotransmitter, but from zero to several hundred vesicles, each containing a "unitary" amount of transmitter. At the NMJ, under normal conditions, the number of quanta released by a single action potential is very large, and the fluctuations in number of quanta released by different action potentials are unseen. In contrast, in the central nervous system, the number of synaptic junctions formed between two neurons can be very small, and the number of quanta released by one action potential is never very large, so in many cases the statistical fluctuations in transmitter release result in significant fluctuations in postsynaptic response between subsequent trials [189, 249, 3, 291]. While quantal synaptic transmission in the central nervous system seems a generally accepted concept at this point, some of its mechanistic details are still under intense debate. It is not known whether a single synaptic connection/release site ever releases more than one vesicle, and hence whether the fluctuations in synaptic amplitude are due to the release of different numbers of vesicles from one site, or from the all-or-none activation of different release sites [191, 126, 95]; a corollary of this fact is that it is still debated whether or not a single vesicle saturates the receptors found locally on the postsynaptic membrane [191, 95, 127, 88], which would imply that release of additional vesicles would have no additional postsynaptic effect. It is not known whether the multiple synaptic connections from one presynaptic cell onto a single postsynaptic partner all produce the same quantal amplitude of response, or have the same probability of release in response to an invading action potential [285, 95, 126]. While it is widely believed that various forms of synaptic plasticity result from modulation of any or all of these parameters of synaptic transmission, other than in a few cases (e.g. paired-pulse facilitation, which is usually due to an increased probability of release to the second of two closely spaced stimuli, due to presynaptic calcium accumulation [161, 92]), it is hotly debated exactly which parameters are subject to change. And finally, it is not known whether different subclasses of synapses differ in some or all of these parameters, and whether membership in a certain subclass can be altered by

the history of synaptic activation [219, 81, 127].

In spite of this uncertainty as to the mechanisms underlying synaptic transmission in the central nervous system, we can still use its well-understood macroscopic features to both examine their functional impact on the behavior of cells, and to explore some of the factors shaping postsynaptic response to a synaptic input.

Functional implications of quantal transmission

At many synaptic connections, at least in the slice preparation, total failures of transmission are frequently seen [189, 249, 3, 291]. While there is a possibility that some of these failures of transmission are due to failures of stimulation of the presynaptic axon, or of branch point failure of action potential propagation [250, 42, 227], there is strong evidence that a significant number of them represent actual failures of transmission [249, 92, 95]. When transmission does occur, the amplitude of the postsynaptic response is characterized by its extreme variability [189, 3, 249, 140, 291], sometimes being seen to fluctuate between discrete, evenly spaced amplitudes, and generating a "peaky" amplitude distribution as a result [140, 247, 67, 104]. This is interpreted as evidence for quantal behavior, with the increments between response amplitude being the amplitude of response to a single "quantum", or vesicle of transmitter.

The fact that in central neurons the probabilistic nature of synaptic transmission is not washed out by the law of large numbers as it is at the NMJ, and shows up in extreme variability of the postsynaptic response, obviously has major impact on the nature of computation performed by neural circuits [34, 189]. It then becomes very important to know what the relationship is between these "noisy" inputs and the output of the postsynaptic cell – is the cell's output affected, or even dominated by synaptic input "noise" [236, 235, 21, 228], or is such "noise" averaged away by requiring hundreds or even thousands of synaptic inputs to be simultaneously active to fire the postsynaptic cell?

This question is particularly important in the neocortex, where single cells (partic-

ularly pyramidal cells) receive between 5,000 and 10,000 excitatory synaptic inputs, while it is suggested that only 1-4 of these inputs come from any single presynaptic cell. Understanding the "unit" by which cortex computes requires knowing what any given synaptic connection might "mean" to the postsynaptic cell – are the local connections between single pre- and postsynaptic cells physiologically strong enough to significantly influence the firing of the postsynaptic cell, or is cortex better seen as a continuum, generating its output only by averaging over large areas of space/large numbers of presynaptic cells.

The answer to this question has far-reaching importance. One of the fundamental questions of neuroscience today is how is information represented by neurons – what is the neural "code" [23]. Classically, neurons were believed to represent information in their average firing rate. If neurons are inherently noisy, incapable of accurately timing or transmitting their outputs [230], this seems to be the inescapable conclusion. On the other hand, a body of recent work has provided evidence that neurons may be capable of representing information in the detailed timing of their spikes [23, 35, 50, 12]. In spite of the seemingly "random" response of a cortical neuron to a visual stimulus, repeated presentation of the same stimulus results in almost exactly the same "random" pattern of spikes in response [12]. Injection of a noisy current waveform designed to mimic the synaptic noise seen *in vivo* results in a train of output spikes which reflect the detailed features of the waveform, not its long-term average. If the "unreliable" single-fiber inputs to a cortical cell are reflected in its (apparently temporally accurate) output, this implies that we must reexamine the notions of neural "noise", and whether these unreliable connections are really in some way functionally effective after all.

To begin to answer these questions, it is first necessary to determine the amplitude of response to single-fiber synaptic inputs to cortical neurons, and its relationship to the threshold level of the postsynaptic cell – how many inputs must be active to make the postsynaptic cell fire a spike. In other words, what is the *functional*, as opposed to anatomical, convergence onto visual cortical neurons?

1.3.3 Functional convergence onto visual cortical neurons

Methods for measuring the properties of synaptic connections

There are a number of established methods for studying the properties of synaptic connections between neurons. A subset of these will be used here, but data from all of them from a large number of cell types and studies is reviewed in Table 1.3.3.

- **Paired recordings:** The most specific method for studying a connection between a synaptically connected pair of cells is to record from both the pre- and postsynaptic neuron. This has the advantage over extracellular electrical stimulation of the presynaptic cell that stimulation failure is not an issue, and connections can be tested in both directions. This has the disadvantage that the number of connections which can be studied is low, due to the difficulty of the technique, and, more importantly, the requirement of repeated penetrations to search for a synaptically connected cell means that it is usually done with sharp electrode recording (the only exception is [156], where the presynaptic cell was recorded intracellularly and the postsynaptic cell using whole-cell techniques). The greatly lowered signal-to-noise ratio of this technique means that connections can only be resolved with averaging, not much information about amplitude fluctuations can be obtained from comparison of single sweeps, and it will be biased towards large-amplitude connections [223, 263, 261, 264, 260]. Additionally, the presence of a somatic shunt induced by the sharp electrode may influence the amplitude and time course of the measured postsynaptic response (see Section A.1.2), and the low frequency response of the high-impedance sharp electrodes make voltage clamp analysis difficult if not impossible. Recent improvements in visualized slice techniques are making this method much more amenable to whole-cell patch recording.

- **Spike-triggered averaging:** A presynaptic neuron is recorded extracellularly (possibly while increasing its firing rate via iontophoresis of glutamate), and

EPSPs are recorded in a postsynaptic neuron by triggering on the time of the extracellularly recorded spikes [262]. This technique has relatively good specificity, though spurious EPSPs might be correlated with the measured spike train. It suffers from the disadvantage that the timing of presynaptic spikes cannot be well-controlled. Additionally, it has in practice been performed with sharp electrode recording from the postsynaptic cell, and hence suffers the disadvantages described above.

- **Minimal stimulation:** Very low-amplitude extracellular stimulation of neighboring cells or fibers is used to find a location where stimulation gives a "threshold" response in the postsynaptic cell – below a certain amplitude of extracellular stimulation, there is no postsynaptic response, and as the stimulus amplitude (or duration) is increased, a postsynaptic response suddenly "appears" which remains relatively constant over a further region of increasing stimulus amplitude. This is interpreted to be a result of stimulation of one, or at most a very small number of presynaptic cells/fibers [249, 168, 3, 209, 291]. In the best uses of this technique, placement of the stimulation pipette next to a candidate presynaptic cell is done under visual control to increase specificity of stimulation [67, 247]. The advantage of this technique is its relative technical simplicity, allowing large numbers of cells and connections to be examined. The disadvantage of this technique is its potential for lack of specificity, as more than one fiber can be stimulated at a time; and the possibility of stimulation failures.[11] It is also impossible, as with spike-triggered averaging, to fill the presynaptic cell and reconstruct the number/location of synapses underlying the recorded connection.

[11] Failures due to transmission failure at axonal branch points are also possible, but they are a hazard of all the techniques mentioned here and may be a feature of normal synaptic transmission [42]. They might be somewhat more common with extracellular stimulation due to the chance of firing only part of an axon, or inducing action potential propagation in an abnormal direction.

- **Spontaneous inputs:** While there is not a lot of spontaneous firing of cells in a brain slice, there is some, and it provides a good metric of the characteristics of the population of inputs to the postsynaptic cell. The advantages of this technique are its extreme simplicity, and the possibility of seeing a large variety of inputs coming in all over the cell and hence getting a measure of the range of possible input characteristics. The disadvantages of this technique are the lack of identifiability of inputs, making it impossible to study the fluctuations of a single input over time or even to know if the same input fires more than once, the fact that only some classes of inputs may be spontaneously active in a slice, leading to a biased sample of a subset of the inputs to the cell; and the fact that spontaneous synaptic inputs are a mix of inputs generated by action potentials in other cells and by the spontaneous, action-potential independent exocytosis of single transmitter quanta, known as "miniature" EPSCs or EPSPs.

- **Miniature EPSCs and EPSPs:** In the presence of TTX, the spontaneous synaptic inputs due to action potentials in other cells disappear, leaving only the "miniature" EPSCs or EPSPs (mEPSCs or mEPSPs, also "minis"). Not only does this give, by subtraction, an estimate of which of the spontaneous events seen without TTX were due to action potentials and how their amplitudes relate to the (putatively uniquantal) minis, but the minis themselves provide a valuable measure of the fundamental "units" of synaptic transmission. Additionally, they have been used to separate pre- and postsynaptic effects of various manipulations (e.g. [157, 155]), as mini frequency is assumed to be determined purely presynaptically, while mini amplitude is assumed to be determined postsynaptically (assuming little change in vesicle filling with most short-term manipulations). This measure does suffer from the same localization issues as does recording spontaneous events, and the potential for bias induced by different frequencies of vesicle release at different classes of synapses [179].

Properties of single-fiber synaptic inputs in a variety of cell types

The properties of single-fiber connections between central neurons have been measured in a variety of cell types over the past 25 years. The results of a large fraction of these studies are summarized in Table 1.3.3. As can be seen, the average amplitude of any given connection is relatively small, on the order of 100-200 μV, as measured with sharp electrodes. This figure is fairly consistent across systems and cell types, a fact which might be considered somewhat unusual given for instance the extreme size difference between a cat spinal motoneuron and a neocortical interneuron. An exception is the more recent work of Thomson *et. al.*[261, 264, 260] in rat sensorimotor cortex, who have observed several extremely strong connections between pyramidal cells, particularly in the deep layers, and from pyramidal cells onto interneurons in the superficial layers. In single sweeps, they have observed EPSP amplitudes as large as 9mV [260].

[12]Recording method used for postsynaptic cell. WC = whole cell patch, SE = sharp electrodes.

Cell Type	Meas[12]	Type[13]	Source	Ref	Amp[14]	Range[15]	Failures	Quantal Amp
Cat Spinal Motoneurons								
Ia	SE	SP	aff	[2]		0.3-1.7 mV[16]		
Ia	SE		aff	[6]	230 μV [17]	85-765 μV[18]		
Ia	SE		aff	[5]		70-700μV[19]		
Ia	SE	MS	aff	[7]				90-100 μV
Rat Cerebellum								
Purkinjie	WC	VMS	GC	[1]	14.4pA[20,19]	2-60pA[16]		$< 40pA$
Rat Hippocampus								
CA1 pyr	WC	P,MS	CA3 pyr	[9]	0.75pA[16]	$< 5pA$[21]	90%[22]	
CA3 int	SE	P	CA3 pyr	[11]		1-4mV[19]	0.53[23]	0.9 mV
CA3 pyr	SE	P	CA3 pyr	[12]	1.4mV	1-2mV[19]	> 0	0.4,0.6 mV
CA3 int	SE	P	CA3 pyr	[4]		0.2-2.5mV	25%	0.79 mV
CA1 pyr	SE	P,MS	CA3 pyr	[15]		85-275μV[24,16,19]	10-44%[25]	85-224 μV
CA3 pyr	WC	VMS	Dentate GC	[8]	1nS	0.24-2.1nS[26]		133pS
CA1 pyr	WC	SP		[14]		3-20pA		
Rat Visual Cortex								
II/III	SE	P	II/III	[10]	0.55mV[16]	0.05-2.08mV[16]		
V	SE	P	V	[13]	0.84mV[16]	0.67-1.18mV[15,16]		
IV non-pyr	WC	VMS	IV non-pyr	[16]		5-90pA		10pA
Rat Sensorimotor Cortex								
II/III pyr	SE	STA	II/III pyr	[19]	0.407mV[16]	0.079-2.3mV[16,27]		
V pyr	SE	P	V pyr	[17]	1.67mV[16]	0.25-5.4mV[16,28]		0.5mV[29]
II/III pyr	SE	P	II/III pyr	[20]	1.003mV[16]	0.22-3.48mV[16,30]		200μV[31]
II/III int	SE	P	II/III pyr	[18]	0.607mV[16]	0-1.1mV[16,32]	73.6%[33]	
V pyr[34]	SE	P	V pyr	[3]	1.33mV	0-3mV	many	
V pyr[35]	SE	P	VI pyr	[3]	1.06mV		few	

Table 1.1: Single-fiber connection strengths measured in a variety of studies.

Relationship of single-fiber inputs to threshold

A number of estimates of the relationship between single-fiber input amplitude and threshold have been made, particularly in hippocampal CA1 pyramidal cells. Using the common value of 150 μV for the average size of a single-fiber input [7, 168], 15-20mV depolarization from rest necessary to fire the postsynaptic cell [7], and assuming linear summation of inputs [130], this has provided an estimate of 100-250 synchronous inputs necessary to cause the postsynaptic cell to spike [7, 168, 259, 181, 223, 6].

More recent estimates using whole-cell recording, however, have provided much

[13]Method used to study connection. P = paired cell recordings, MS = minimal stimulation, VMS = minimal stimulation with visualization of the presynaptic cell, STA = spike-triggered averaging, SP = measurement of spontaneous events, M = measurement of miniature spontaneous events (in the presence of TTX).

[14]Average over all connections tested.

[15]Range of averages seen at single connections.

[16]Average includes failures.

[17]Median amplitude. (Maximum approximately 2mV.)

[18]For putative somatic events, defined by rise times $< 0.5\tau$, half widths $< 0.6\tau$.

[19]Range of event amplitudes seen at single connections.

[23]Estimated probability of release at a single bouton, p.

[21]17.9 pA for pairs where charge transfer was measured. Average charge transfer (corrected for missing pairs) was 170 fC.

[22]Increased to 0-40pA after LTP.

[23]Decreased to 5% after LTP (n=1).

[24]Range of means from minimal stimulation was 95-395μV.

[25]Range from minimal stimulation was 95-395μV.

[26]Range of maximum values across cells was 0.82-5.5nS.

[27]Range of average amplitudes seen in bursting cells: 0.19-0.28mV.

[28]Single sweeps could be as large as 9mV.

[29]As an estimate in some cells.

[30]Selected for strong connections.

[31]Estimated in 4 cells as 179μV, 216μV, 227$\mu V$and 382μV(potentiated).

[32]Maximum average values with repeated activation: 0.24-2.05mV (mean 1.16mV). Single sweeps as large as 5mV.

[33]Failure rate decreased with repeated activation. Failures to first spike: 54-100%, second: 12.2-50%, third: 27-34%.

[34]Single connection, comprised of 2 boutons to separate basal dendrites.

[35]Single connection, comprised of 8 boutons to apical dendrite.

larger estimates for the amplitude of single-fiber inputs (e.g. 1-4mV in CA1 [209]). These studies have come up with much lower numbers of inputs necessary to fire a postsynaptic cell: in cerebellum, 5-50 parallel fiber inputs necessary to bring a Purkinjie cell to threshold [13], and in CA1, 10 inputs [209], or 26 in the presence of inhibition, but only 16 with inhibition blocked [189]. Additionally, several studies provide evidence that the normal fluctuations in synaptic amplitude can have a strong affect on the variability of spike output both *in vitro* (CA1, [189]), and *in vivo* (spinal motoneurons [34]).

As Table 1.3.3 shows, even larger than the amplitude variability at a single connection over time, is the amplitude variability across connections within a single cell class, or even in a single cell. In addition to determining the impact of a particular input on a postsynaptic output, it then becomes equally important to examine the factors that shape postsynaptic response, which determine the variability across the population of inputs to a single cell.

1.3.4 Factors shaping postsynaptic response

There are an extremely large number of mechanisms that can affect the strength of a synaptic connection, for example: number of boutons or release sites making it up, probability of release, number of postsynaptic receptors at each synaptic site and their individual channel conductances, kinetics, and binding properties, number of transmitter molecules released per quantum, the input impedance of the postsynaptic dendrite, its nonlinear properties, and so on. However, if we permit a slight abstraction above the level of mechanism, we can macroscopically lump all of these factors into 4 characteristics of a synaptic connection that control its efficacy. Each of these factors may vary from synapse to synapse, between the boutons making up a single synaptic connection, and even at a single release site over time.

- **Synaptic location:** in a passive cell, electrotonic filtering will affect the amplitude and kinetics of the somatic response to a synaptic input depending on

the location of that input in the dendritic tree [203, 242, 150].

- **Synaptic conductance:** the total conductance opened by any single synaptic input or release of transmitter quantum. If "inputs" are measured as presynaptic action potentials, this may be 0, as there may be a failure of transmission. This parameter subtends any variability in number of boutons, number or characteristics of available postsynaptic channels or number of channels free of desensitization, number of transmitter molecules released (in the absence of synaptic saturation), stochastic fluctuations in the number of channels opened [279], etc.

- **Synaptic kinetics:** differences in the postsynaptic channels (e.g. their subunit composition or state of phosphorylation) or in the distance transmitter must diffuse to reach them may cause differences in their kinetic properties, and hence in the kinetics of the macroscopic currents they generate. While such differences may also cause changes in the synaptic conductance, mathematically we can consider these factors independently.

- **Dendritic nonlinearities:** In addition to the effects of synaptic location mentioned above, variations in the nonlinear properties of the postsynaptic cell dendrites may cause unexpected variations in synaptic response from location to location on the dendritic tree. Until recently, the characteristics of these dendritic nonlinearities were largely unknown, and were a "wild card" in considerations of dendritic computation: they might do anything. In spite of recent increases in our understanding of these properties [252], they are still heavily underdetermined. This thesis endeavors to explore the effects of the first three contributors to synaptic variability alone, and is limited to experimental and computational simulations where that is probably a valid simplification.

Considering synaptic strength in terms of these lumped parameters gives us a great deal of power to draw conclusions about the sources contributing to synaptic

variability in cortical neurons, without getting bogged down in the mechanistic details.

Relationship to quantal variance An important factor in the application of quantal analysis to central synapses is the amplitude variance between quanta at a single synaptic connection [92, 62]. This variance is assumed to be caused by variability in the size of quanta at a single release site either by differences in the number of transmitter molecules in different vesicles, or by stochastic differences in the number of channels opened by different vesicles; or by slight differences in quantal amplitudes at different synapses between the same pre- and postsynaptic cell. Quantal variance causes the width of peaks in the amplitude histogram to increase with peak number [62]. In most applications of quantal analysis, either quantal variance has been assumed to be zero, because the width of the peaks did not increase, or because they were consistently narrower than would be predicted by the baseline noise[36] [95, 45, 285, 223]. This lack of quantal variability was taken to imply that a single quantum saturated the receptors at one postsynaptic site, and that the variance in receptor number between sites at a single connection was minimal or zero (in the case where there were more than one site/connection) [95, 191]. However, it has been estimated that a quantal coefficient of variation of up to 15% might not result in a measurable increase in peak width in typical experimental situations [285]. In cases where quanta were assumed to have some intrinsic variability, this was estimated from the variance of miniature EPSCs occurring in the same cell or cell class. This suffers from the problem that the mEPSCs occur on synapses all over the cell, not just at the connection undergoing quantal analysis. Additionally, if mEPSCs are collected during stimulation (i.e. not in the presence of TTX), they may be contaminated by a certain number of action-potential-dependent EPSCs, which may be multiquantal. Given a population of true mEPSCs, and assuming that the quantal variance (and amplitude) is the same across all synapses onto the cell, then

[36]Indicating that the noise and the peak amplitudes were not independent

one can identify quantal variance with the variance in synaptic conductance described above.[37] However, if any of the other sources of postsynaptic variability mentioned above contribute to the shape of the mEPSC amplitude distribution, then it will not provide a good predictor of quantal variability. A quantitative estimation of the role of the factors above in generating mEPSC variability will therefore have the side benefit of possibly shedding some light on the question of quantal variability and its implications for synaptic saturation.

[37]While the actual mechanism underlying quantal variance may be variance in the size/content of vesicles [17], or in the number of postsynaptic receptors activated at different sites or stochastically at the same site [285], these are all functionally equivalent to a variance of postsynaptic conductance and will be treated as such here.

1.4 Figure Legends

Figure 1-1: Morphology of recorded cell. A layer V cell from a P19 rat, filled with biocytin during the course of recording. On the left is a digitized microscope image taken from the cell at 10x magnification. On the right is a projection of the 3D reconstruction of this cell, scaled to approximately the same size (scale bar is 100 μm). See General Methods for details.

Figure 1-2: Responses of cortical neurons to current injection. A. Responses of a rat layer V pyramidal cell (above) to injected current steps (below). This is a regular-spiking cell, recorded with a K-Gluconate electrode, and shows little adaptation. B. Morphology of cell shown in A. This is a "thin" layer V cell. C. Linear current-voltage relationship for cell shown in A,B. R_{in} is 615.1 $M\Omega$. D. Responses of a cat layer V neuron (above) to injected current steps (below), again in a regular-spiking cell. E. Morphology of *another* cat layer V neuron for comparison to B. F. Current-voltage relationship for the cell shown in D, R_{in} of this cell is 131.6 $M\Omega$.

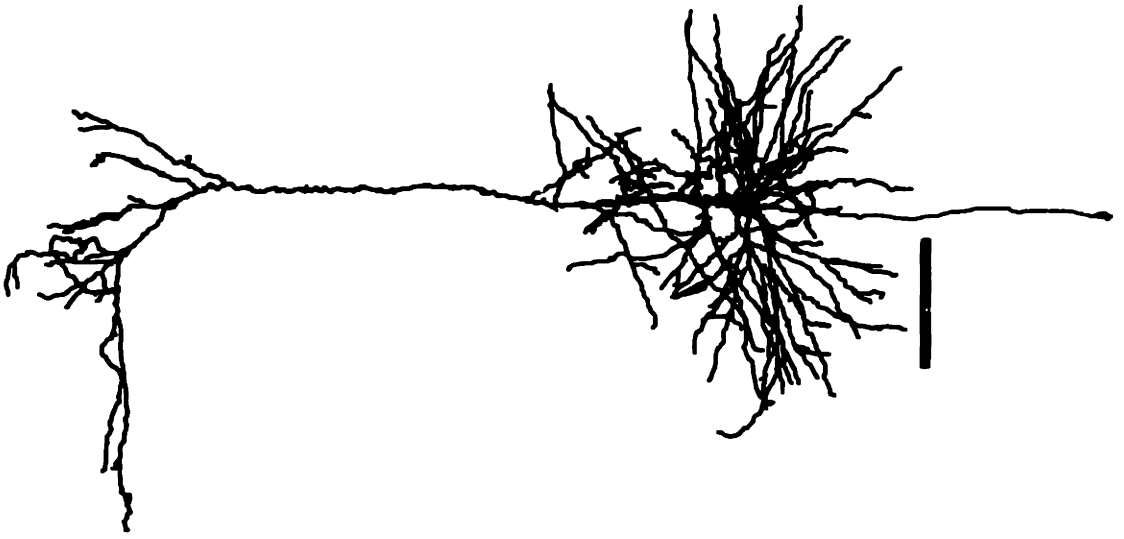

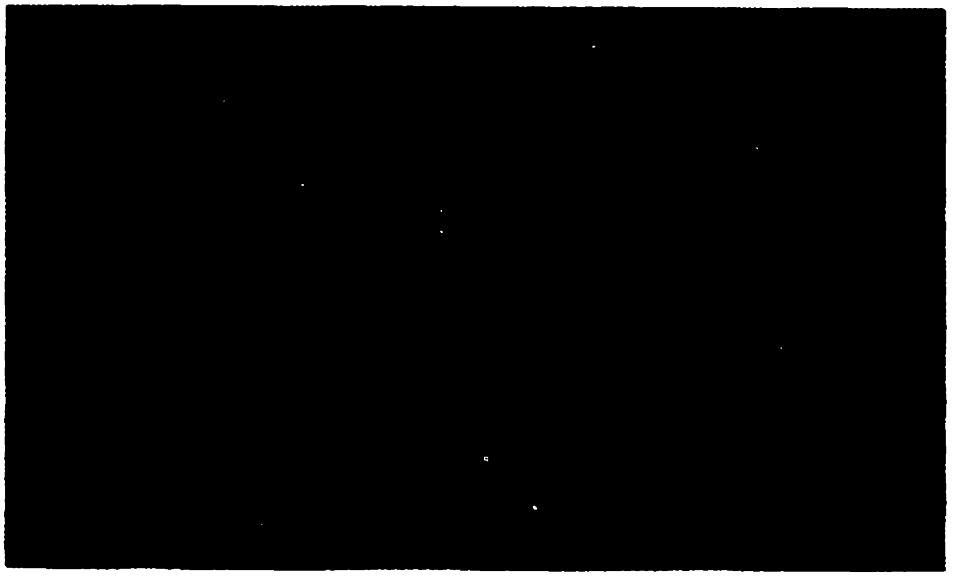

Fig. 1 - 1

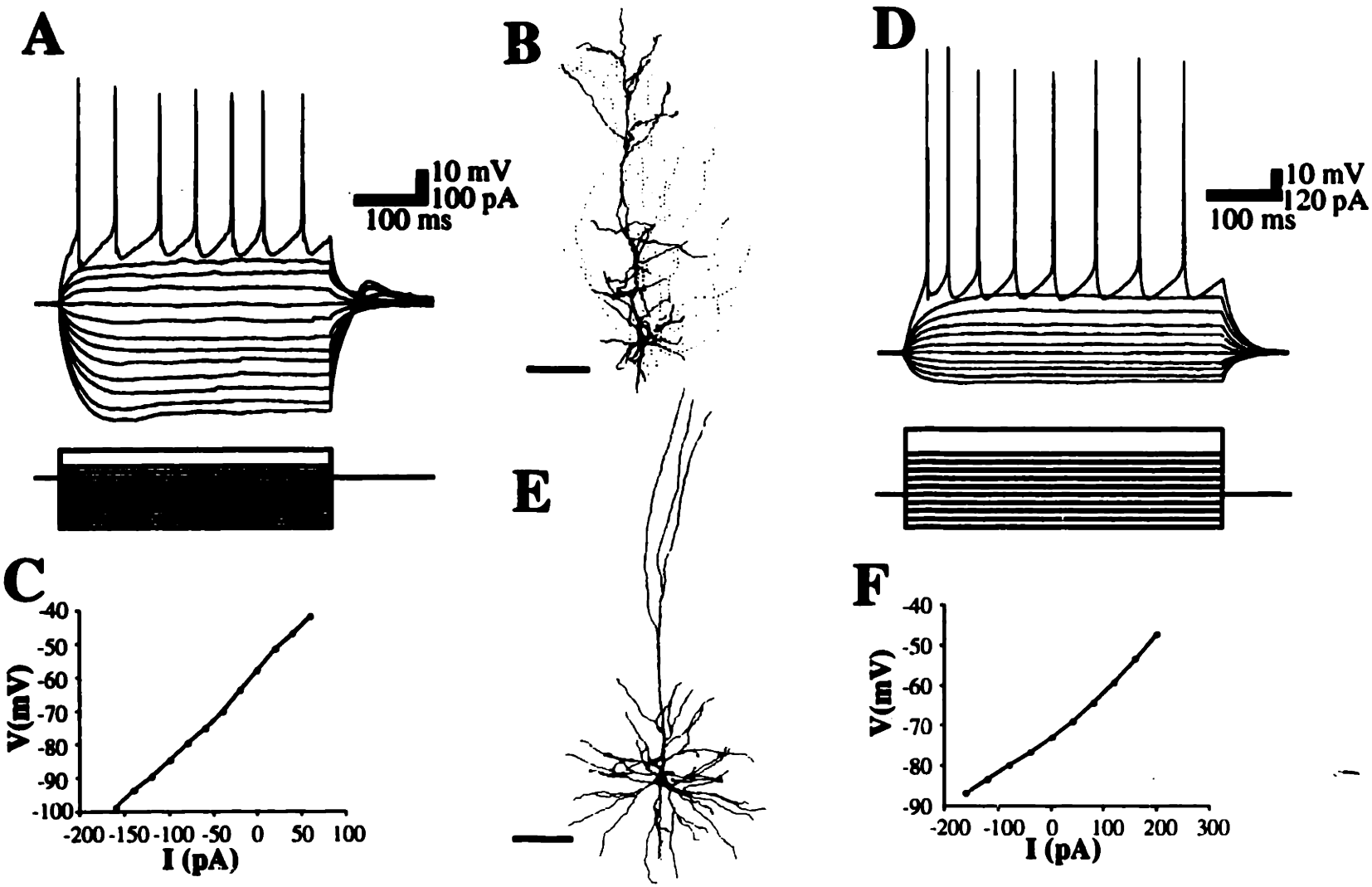
A
10 mV
100 pA
100 ms
B
D
10 mV
120 pA
100 ms
E
C
V(mV)
-40
-50
-60
-70
-80
-90
-100
-200 -150 -100 -50 0 50 100
I (pA)
F
V(mV)
-40
-50
-60
-70
-80
-90
-200 -100 0 100 200 300
I (pA)

Fig. 1 - 2

2

General Methods

This chapter describes those experimental and computational methods which form the basis for all of the work in this thesis. Descriptions of more complex techniques specific to each chapter have been presented in the methods section of the relevant chapter.

2.1 Slice Preparation

Preparation of rat slices Juvenile Sprague-Dawley rats (postnatal day 12-28) were sacrificed by overdose of sodium pentobarbital (120 mg/kg) or ketamine and acepromazine (120/10 mg/kg). The brain was rapidly removed and placed in ice-cold oxygenated artificial cerebrospinal fluid (ACSF), and was then hemisected. The ventral third of each hemisphere was trimmed off, and in some cases the bulk of the diencephalon was removed. The brain was then cut into 400 μm coronal slices with a Vibratome. Slices were used from the most posterior portion of the brain where coronal slices including the full cortical thickness and the white matter could be obtained, anteriorly through the full extent of primary visual cortex to the beginning of the corpus callosum. Recordings were restricted to visual areas. In experiments presented in Chapter 3, only primary visual cortex was used, but in later experiments the more anterior and lateral visual areas were included because they were less significantly curved with respect to the angle used for slicing, and so contained more intact deep-layer pyramidal cells, the apical dendrites of which were frequently sectioned in more posterior slices. Slices were maintained at room temperature submerged in ACSF continuously bubbled with 95% O_2-5%CO_2 (carbogen). Three slices at a time were transfered to the recording chamber, where they were maintained at 34° C at the interface between ACSF and warmed, humidified carbogen. Slices were allowed one hour for temperature equilibration after being transferred to the record-

ing chamber before any penetrations were attempted, and up to an additional hour for recovery after cutting. Except as noted, the ACSF contained (mM): 126 NaCl, 3 KCl, 26 $NaHCO_3$, 1.2-2 $MgSO_4$, 2.5 $CaCl_2$, 10 dextrose in Millipore-filtered water (305 mOsm). In some early recordings, 20mM dextrose was used to increase the rate of spontaneous events. In the experiments described in Chapter 5, 50mM dextrose was used for the same reason.

Preparation of cat slices Cat slices were taken from animals used for *in vivo* whole cell recording after completion of those experiments. Animals (3-4 months old) were induced with Ketamine/Xylazine (30/3 mg/kg), tracheotomized, and then paralyzed with gallamine triethiodide (3.6 mg/hour) and maintained on a respirator anesthetized by isofluorane (1-2%), and O_2/NO_2 (70/30%). Unilateral or bilateral craniotomies were performed over area 17, and the brain was protected by agar and mineral oil for up to 36 hours while whole-cell recording was performed. On completion of those experiments, the craniotomy was enlarged to allow access to additional areas of visual cortex (area 17 was usually too damaged by repeated penetrations to used for slices), the dura was removed, and a 1 cm square chunk of cortex usually from areas 19 or 21 was excised using scalpel cuts. This chunk was immediately placed into iced, oxygenated ACSF. The chunk was then trimmed, and 400 μm slices were cut perpendicular to the pial surface with a Vibratome. Maintenance and recording from slices then proceeded as described above.

2.2 Electrophysiological techniques

2.2.1 Drugs and solutions

Drugs (TTX, CNQX, APV, BMI) were applied by perfusion through the bath solution, except for sucrose and CNQX when used for puffer pipette application (described in the Methods section of Chapter 5). All drugs were dissolved in H_2O except for CNQX, which was either dissolved in H_2O at a concentration of 1 mM, or was dissolved with DMSO at high concentration and then diluted to a concentration of 1 mM with H_2O, to be added to the bath at concentrations of 10 μm or 0.3 μm (final concentration of DMSO < 0.006%). Tetrodotoxin (TTX) and Bicuculline Methiodide (BMI) were obtained from Sigma. CNQX and APV were obtained from Cambridge Biochemicals (Cambridge, UK) or RBI (Worcester, MA).

A number of intracellular solutions were used during the course of these experiments. Those used for the data presented here used Potassium Gluconate (KGlu) or Cesium Fluoride (CsF) as their main salt ($KMeSO_4$ and CsAc were also used in some experiments, but this data is not presented here). These solutions contained

(mM): (KGlu) 120-135 KGlu, 5-10 KCl, 2 $MgCl_2$, 10 N-2- hydroxyethylpiperazine-N-2-ethanesulfonic acid (HEPES), 10 (EGTA), and 1 $CaCl_2$; (CsF) 130-135 CsF, 5-10 CsCl, 2 $MgCl_2$, 10 HEPES, 1 EGTA, 0.1 $CaCl_2$. Solutions were buffered to pH 7.2 and filtered with an 0.2 μm filter (Millipore), and were made in (HPLC grade) Millipore filtered water. In many cases, Lucifer Yellow (0.2%-0.5%, dipotassium salt, Sigma) or biocytin (0.5%-1% Molecular Probes) were added to the recording solution, and the solution was re-filtered. In the case of biocytin, the pH of the solution was also readjusted to 7.2, and the solution was frozen at -20° C in small aliquots until used. The osmolarity of the solution was adjusted to 260-290 mOsm as needed.

2.2.2 Recording and analysis

Whole-cell pipettes were pulled from borosilicate glass (o.d. 1 mm, WPI) using a Brown and Flaming horizontal pipette puller to a final resistance of 1.5-7 $M\Omega$. Recording was performed with an Axopatch-200A (Axon Instruments, Burlingame CA). Series resistance compensation was used whenever possible. Only cells with series resistances under 30 $M\Omega$ were considered acceptable, except where noted for comparative purposes. (Series resistance criteria for use in particular analyses were much stricter than this, this is noted where applicable.) Data were not compared across a change in series resistance of more than 20%. For the experiments reported in Chapter 3, series resistance was checked every few minutes, while for later experiments, series resistance was automatically tested every 5-10 seconds.

KGlu-based recordings were considered acceptable if the cell had a resting potential of greater than -50 mV (relative to potential at withdrawal from the cell), and overshooting action potentials. If either of these factors or the input resistance of the cell changed significantly, recordings were discarded at that point. As recording with Cs-based solutions tended to rapidly depolarize the cell, the main criteria used for accepting such recordings were ability to generate action potentials, initial apparent (and continuing) health (e.g. initial voltage drop on break in), and input resistance. For recordings in the presence of TTX in either case, the remaining parameters besides action potentials were combined with general cellular characteristics (e.g. mEPSC properties) to gauge cell health. A total of 212 neurons (204 rat cells, 8 cat cells) were considered acceptable by these criteria. Membrane potentials in current clamp are corrected for any offset seen on withdrawal from the cell (usually very small), but are not corrected for liquid junction potential. Holding potentials in voltage clamp are not corrected for either of these factors.

Recordings were made in layers II/III or V/VI, as estimated from the relative location of the pipette between white matter and pial surface. If the cell was morphologically recovered, the actual soma location is reported rather than the location of the recording pipette taken from the drawings made during recording. Some of the unre-

covered cells may therefore represent dendritic recordings and therefore their laminar position will be incorrect, however as the number of confirmed dendritic recordings seen in morphologically recovered cells was very low (n=2), thus they should comprise an equally small percentage of the total population. The vast majority of the cells recorded from and recovered are pyramidal cells. It is likely therefore that the majority of those cells whose morphology was not recovered were also pyramidal cells; the large size of most of the recording pipettes used here to obtain low series resistances may have biased us against recording from non-pyramidal cells. When a cell type is reported in the text, it has been confirmed morphologically; cell types postulated purely on physiological grounds are reported as such.

Bipolar stimulating electrodes were constructed from very fine, 0.3 mm, teflon-coated tungsten wire (A&M systems), mounted inside broken glass pipettes with Locktite; some stimulating pipettes were coated with SigmaCote (Sigma) or Sylgard to reduce capacitive artifact. Stimulation was applied through a constant current stimulator (Grass S88) via a stimulus isolation unit (Grass) on current ranges of 10-150 μA (minimal stimulation) and 0.1-1.5 mA (threshold stimulation). Stimulus duration was 50 μsec, and stimulus strength ranged from 1-150 V (1-15 V for minimal stimulation). Stimulating electrodes were usually positioned at either the pial surface or the gray-white border, directly in line with the recording pipette.

Data were filtered at 2-5 kHz and digitized onto videotape at 44 kHz (Neurodata). Off-line, the recordings were sometimes further filtered to 3 kHz before digitization at 5-20 kHz by computer (A/D board in an Intel 486 computer). Digitization was performed using Pclamp software, which was also used for some analysis. Most analysis was performed on Apple Macintosh computers using Axograph (Axon Instruments, Foster City, CA) or software I wrote. The latter included the event detection software, which both detected events and measured their amplitudes, rise times, areas, half widths, and slopes. The event detection used in Chapter 4 and parts of Chapter 3 used a simple combination of an amplitude threshold (usually 1.5-2 times the standard deviation of the noise), minimum time above threshold, and (weak) derivative threshold[1]. Both thresholds could either be set manually or relative to the baseline noise, and were constant for the duration of detection. The same amplitude threshold was used for detecting all events from a single cell. Thresholds were extensively tested to ensure that few if any events were missed, within the limits allowed for by the noise. An additional digital Gaussian filter was included, and sometimes used at 1-2 kHz; it could filter either only the data before an event was detected (and not the buffer used to measure the properties of the detected event), or both the detection and measurement phases. All events detected were screened by eye to remove

[1]The derivative threshold was used sparingly in order to ensure detection of slow, presumably distally generated, events.

as much as possible spurious noise and multiple overlapping events. The latter were not considered in the analysis. A later version of the detector incorporated additional processing to automatically detect overlapping events and inflections on the rising phase of events [10]. The detector used a threshold on a filtered version of the first derivative of the event to look for inflections. The detector incorporated a minimum duration for multiple as well as single events, but sometimes accidentally detected one event as two in rapid succession. It was not considered possible to detect events with an interval between their onsets of less than 1 msec, and "extra" events occuring more frequently than this were removed. These errors did not cause significant changes in the distribution of mEPSC inter-event intervals, however when the reciprocal of the IEIs was taken to obtain instantaneous frequency values, these spurious large frequency values could significantly bias the mean. Therefore, the median instantaneous frequency was usually considered, and then only as an adjunct to the distribution of IEIs. Overlapping events were only used for calculations of event frequency, their shape parameters were not measured unless the overlap could not interfere with them (e.g. the rise time and amplitude of an event with another event late on its falling phase were measured), and they were not included in any averages shown. In this case, events were not extensively screened by hand, removing any chance of experimenter bias in removing particular types of "non-events" from consideration. Events were superficially scanned to remove the pulses used to test access resistance, and to be sure that few, if any, events were missed. Events were scanned with more care in cases where event frequency was very low (e.g. after application of CNQX, see Chapter 5), and a small number of mis-detected noise events would have a noticeable impact on the distribution of mEPSC parameters.

EPSC/EPSP amplitudes were measured as the average of several samples (usually 3) around the peak. 10%-90% rise times were linearly interpolated between successive sample points. In the early portion of the analysis, a design flaw in the routine for measuring rise times caused the rise times for slow events to be overestimated in the presence of large-amplitude noise. Therefore, some of the mean rise times presented here have been biased by these large values. As much as possible, critical data were reanalyzed with the corrected analysis routine, and none of the conclusions (qualitative or quantitative) were significantly altered. Event widths were measured at half-amplitude, and slower half widths tended to be underestimated in the presence of noise (see section 4.3.6). Areas were integrated point-by-point, without additional smoothing. The integration period was determined by the detection software, which attempted to find the point at which the event returned to baseline. It varied for each event. Slopes were estimated using a 5 point centered-difference formula. Inter-event intervals were calculated between the onset of subsequent events. If two events were separated by a noise artifact, or a seal test pulse, their IEI was not calculated as it was not known whether an intervening event might be missed during the seal

test. This put an upper limit on the largest IEI measurable of the interval between seal test pulses (usually 7 seconds, but occasionally 5 or 10). This is more likely to affect the IEI values measured when events are very low frequency and there is a large amount of noise. Absolute frequency values (rather than average instantaneous frequency) are simply the number of detected events divided by the total time period under consideration. This is an optimal estimator of the rate constant of a Poisson process [234], which spontaneous events appear to be.

Differences between parameter distributions were tested using the Komolgorov-Smirnov test [200, 294]. Parameter correlations were tested for significance using Spearman's Rank Test, but R values reported in the text are standard correlation coefficients for ease of interpretability. Due to the very large n's in most samples, even quite small R values are significant. Differences between means were tested using the Mann-Whitney U test [294], as none of the underlying distributions appeared to be normal. Statistical analysis was performed using StatView for the Macintosh, or using macros written for Kaleidagraph [200]. Significance levels are $p<.05$. Values are reported as $Mean \pm Std.Dev.$.

2.3 Histology and reconstruction of cells

In many cases, recording pipettes contained either Lucifer Yellow (0.2%-0.5%, dipotassium salt, Sigma) or biocytin (0.5%-1% Molecular Probes) in order to later visualize the morphology of the recorded neuron. In cases where there was dye in the recording pipette, the locations of all recorded cells and all unsuccessful penetrations were noted on a drawing of the slice[2]. Multiple successful penetrations were sometimes made in the same slice, and these drawings allowed all recorded neurons to be recovered unambiguously. In the cases where there was more than one well-filled neuron in the vicinity of the recording, due to either too close spacing of penetrations, or (more commonly) filling of additional neurons due to extracellular expulsion of dye from the patch pipette, the morphology was not used for subsequent analysis or reconstruction in comparison with the relevant physiology[3] (in cases where all filled neurons were of the same morphological class, tentative class assignment was made to the physiologically-recorded cell).

Slices containing filled neurons were placed in fixative (either 4% paraformalde-

[2]If no dye was included in the pipette, no drawings were made, and in a small number of cases cells were recorded without adequate record of their layer of origin. These are noted as "layer unknown" in the presentation of the data

[3]In several such cases, the cell was reconstructed for simulation, but it was treated as if it was filled without recording from it, and no attempt was made to fit it to physiological data which might have come from another cell.

hyde or 10% neutral buffered formalin) after recording. Some slices were fixed immediately after withdrawal from a recorded cell, others remained in the recording chamber for up to several hours subsequent to any particular recording. Slices remained in fixative for periods from 24 hours to 30 days, with no apparent effect on the ability to recover morphologies. There was a correlation between amount of time before fixation and ability to recover the cell, particularly in the case of biocytin-filled neurons. The somata of some biocytin-filled cells sometimes began to degenerate after conclusion of recording, and at the same time additional transport of biocytin resulted in better filling of the axon with increased time between recording and fixation [27]. Additionally, the soma of recorded cells was sometimes significantly damaged by pulling off the electrode at the conclusion of recording. As all physiological data analyzed was obtained before any significant change in the physiological condition of the cell, I assume that any somatic morphological degeneration occurred after the physiology was obtained [27]. I have therefore used the morphologies of some of these cells in my simulations and analysis, reconstructing the soma morphology as well as possible from the data available.

Fixed slices containing biocytin-filled cells were sunk in 30% sucrose for > 1 hour, and then were sectioned at 60 μm on a freezing microtome into phosphate-buffered saline. After rinsing in PBS, background peroxidase activity was quenched with 1% H_2O_2 and sections were rinsed again. The tissue was then permeated with 0.7% Triton-X100, for 20 minutes, and then incubated for 4 hours to overnight in an avidin-biotin-peroxidase complex (ABC, Vector labs, 1:100 in PBS with 0.7 % Triton-X100). Sections were enhanced in 0.1% $CoCl_2$ in Tris buffer , then reacted with DAB (0.05%) and H_2O_2 (0.01%) in Tris (protocol due to L. Cauller). Sections were mounted from dilute gelatin. They were then cleared in sequential alcohols and coverslipped with DBX. The small size of the sections and the lack of embedding medium made it likely that some sections or fragments would be lost either during sectioning or processing of the tissue. I did not directly measure shrinkage with this technique, but it has previously been estimated to be around 10% [25, 36].

Slices containing Lucifer yellow-filled cells were processed in a number of ways. Some were sunk in sucrose and sectioned as above, then mounted and cleared briefly in alcohols and coverslipped with Krystalon. Some were cleared in methyl salicylate and/or alcohols, and then mounted whole and coverslipped with Krystalon. Some were mounted, cleared and coverslipped in the water-soluble mounting medium Aquamount. By far the most successful protocol, and the one used for most of the slices, was that of B. Claiborne et. al. [43]. Slices were cleared in sequential increasing concentrations of glycerol (20, 40, 50, 70, 90, 95% for 5 minutes each, followed by 3 changes of 100% glycerol for 30 minutes each), then mounted in glycerol (protocol due to B. Claiborne and M. O'Boyle). After examining the slices under fluorescence to determine whether the cells were in the top or bottom half of the slice (in the

z-axis), slices with cells located very deep were flipped over, and then coverslips were sealed with nail polish. This allowed the cells to be as close as possible to the top surface of the slice, which greatly facilitated reconstruction. This latter technique has been estimated to result in a shrinkage of $< 5\%$.

Selected cells were reconstructed using a Eutectics NTS 3D reconstruction system via a Zeiss microscope (all biocytin and some Lucifer Yellow cells), using a 40x water and an 100x oil-immersion objective (1.3 n.a., final magnification 1000x). In some cases, conventional camera lucida drawings were also made at a variety of magnifications (maximum 1250x) to aid in reconstruction. Several Lucifer Yellow-filled cells were scanned in a series of Z sections with a confocal microscope (Biorad, 40x water immersion objective), and the sequential image sections were imported into the NTS system for reconstruction using its video-handling capabilities.

Cells were analyzed quantitatively to varying degrees using the NTS system. Linear shrinkage in the x and y directions was not usually corrected for, however greater apparent shrinkage in the z dimension due to a combination of optical foreshortening and tissue processing was corrected as suggested in the NTS manual.

ASCII text files obtained from the NTS system were converted into input for the simulation program Neuron [85] via a translation program, ntscable, written by John Wathey. The translation was constrained to be accurate between branch points (i.e. segment lengths were constrained to maintain branch point locations) and to generate segments less than $20\mu m$ in length. In all cases, this was significantly less than 0.1λ.

2.4 Compartmental Simulations

Compartmental simulations were performed using standard techniques [90, 124, 205], with the program NEURON (courtesy M. Hines). Reconstructed cells were divided into compartments of less than 20 μm in length between branch points, which always resulted in compartmental lengths less than 0.1 λ. In almost all cells, the initial portion of the axon was retained in the simulations simply for morphological accuracy. It was assumed that the very small diameter of the distal axonal branches would keep them from influencing significantly events seen at the soma, and they were neglected to save computation time. In some cases, simulations were performed of a soma-single cable model. If not otherwise noted, the soma diameter used was $20\mu m$, cable diameter was 1.6 μm, and cable length was 1000 μm. Together with passive properties of: R_m=50,000 Ωcm^2, R_i=200 Ωcm, and C_m=1.0 $\mu F/cm^2$, this gave a cable length of 1.0 λ, which was divided into 20 compartments. In simulations where cable length, diameter, and/or passive properties, were systematically varied, the cable was usually divided into compartments of 0.1 λ (usually less than 20) to save computation time. The time step used was 0.01 msec for voltage clamp simulations and 0.025 msec for

current clamp.

Passive Parameters Except where otherwise noted, all simulations were completely passive - no active conductances were included in the soma, dendrites or axon. "Baseline" passive parameters were: R_m=40,000 Ωcm^2, R_i=100 Ωcm, and C_m=1.0 $\mu F/cm^2$[243]. Variations in all of these parameters were explored, and except as noted all conclusions were robust across a wide range of parameters. Results from simulations using other parameter values, in particular those suggested by Major [150, 154, 104] for cortical pyramidal cells: R_m=50,000 Ωcm^2, R_i=300 Ωcm, and C_m=0.7 $\mu F/cm^2$ ("GM" parameters), will be presented where illustrative for comparison purposes. Somatic voltage clamp was simulated with a simple feedback model. When noted, a resistance in series with the membrane was included to simulate the electrode access resistance normally present in whole-cell voltage clamp recordings (this was neglected in current clamp, see Section A.6 for discussion). Electrode capacitance was not simulated, as the recordings used for comparison were performed in an interface-style chamber, which would minimize excess capacitance due to having the electrode submerged in fluid, and electrode capacitance compensation was always used.

Correction for Spines The presence of spines was corrected for by altering the values of R_m and C_m [89] to compensate for the additional membrane area that spines add to the cell. This is mathematically equivalent to the alternative method of altering dendritic lengths and diameters [251, 102], and it is easier to keep track of particular locations on the cell in the face of changes in passive parameters and spine density assumptions. A number of spine density assumptions were tested. The most simple one was to assume spine density is constant with dendritic length (usual assumed value 1.4 $spines/\mu m$) [22, 33]. It has been noted that spine density can vary as a function of the size of the parent dendrite. Therefore, a more complex spine density function was also used that made density a linear function of parent dendrite diameter. One version of this function was drawn from the average relationship found by Guy Major for a population of layer III cells: $(1.1 + 1.3 \times diameter)$ $spines/\mu m$. The other, used for comparative purposes, was to fit a spine density function for each individual cell by counting the number of spines on a set of dendritic segments of varying diameter, and fitting a linear function to the resulting densities, as per the method of Major [150, 154]. The differences in the outcomes with these varying methods were subtle at best, and so the first two methods were used interchangeably here. Data quantitatively comparing the three methods can be seen in Figure A-61. Average spine areas were taken from the literature [134], as they cannot be accurately measured with the light microscope. In all cases, the assumed spine area depended on parent dendrite diameter as follows: diameter $\leq 1.5\mu m$, area=$1.7\mu m^2$;

$1.5 <$ diameter $< 2\mu m$, area=$1.5\mu m^2$; diameter $\geq 2\mu m$, area=$1.4\mu m^2$[134].

Synaptic Inputs Synapses were simulated as a difference of two exponentials, according to equation 2.1.

$$\begin{aligned} g(t) &= \frac{G_{max}}{Norm}(e^{-t/\tau_D} - e^{-t/\tau_R}) \\ I_{syn}(t) &= g(t)(V_m - E_{rev}) \\ Norm(\tau_R, \tau_D) &= \frac{\tau_R}{\tau_D}^{-\tau_R/(\tau_R-\tau_D)} - \frac{\tau_R}{\tau_D}^{-td/(\tau_R-\tau_D)} \end{aligned} \tag{2.1}$$

The rise and decay time constants were τ_R and τ_D, respectively. G_{max} is the peak synaptic conductance in nS, and $Norm$ is a normalizing constant dependent on τ_R and τ_D, to allow G_{max} to control the synaptic current amplitude independent of kinetics. V_m is the subsynaptic voltage, and E_{rev} is the synaptic reversal potential. "Baseline" values, used unless noted otherwise, are: G_{max}=1nS [17, 104], τ_R=0.1 msec, τ_D=1.0 msec [82], E_{rev}=0mV. Resting membrane potential (and clamp voltage in voltage clamp) was -70 mV. Except where noted, synapses were placed directly onto dendritic shafts, rather than onto explicitly modeled spines, for computational simplicity. The error in neglecting an interposed spine was tested in simulations and found to be negligible for the range of synaptic conductances used here. The effect of including an interposed spine on somatic and subsynaptic response is described in Section A.3.2.

The characteristics of the synaptic response (amplitude, rise time, half width, area, and maximum slope) were measured using the same algorithm used for the experimentally-recorded events, described above. For each synaptic input, these response parameters were measured for both the somatic and the subsynaptic voltage (current clamp); or for the somatic current and the actual synaptic current (voltage clamp). In the latter case, the same parameters were measured for the subsynaptic voltage escape, and the maximum value of the somatic voltage escape[4] was also measured.

[4]With a non-zero series resistance, there will be some somatic voltage escape.

3

Functional Convergence onto Visual Cortical Neurons

Abstract

How many of the thousands of inputs to a cortical neuron need to be active to make it generate an output spike? In this chapter, I have used whole-cell patch clamp recording techniques to study spontaneous synaptic inputs and responses minimal stimulation to characterize the population of single-fiber inputs to individual cortical cells. Individual inputs to cortical neurons are very large (up to several mV), and very rapid in time course. There is enormous variability in the population of inputs to one cell, and between the inputs to different cells. As in many other systems, this variability in amplitude is not just due to differences between synapses, as it is also reflected in the fluctuating response to a single input over time. Given the size of individual inputs, I then estimated the number which must be simultaneously active in order to cause the postsynaptic cell to fire. Spike threshold was measured using synaptic inputs sufficient to generate an action potential on 50% of trials. Single-fiber inputs are large relative to spike threshold, and assuming linear summation, only 5-50 simultaneous inputs would be necessary to generate a spike. This implies that the variability seen at the single input level should be reflected to some degree in the output of the cell. This is indeed the case, as there is considerable variability, both in the probability of the cell spiking with a near threshold input, and in the timing of the resulting spikes.

3.1 Introduction

A single cortical neuron receives 5-10,000 excitatory synaptic inputs [287, 134]. It is estimated that only 1-4 of these contacts come from any single presynaptic cell

[287, 62]. How many of these inputs must be simultaneously active in order to make the postsynaptic cell spike? Must it average over several thousand inputs to generate an output, or are only a few sufficient? In other words, what is the *functional*, as opposed to anatomical, convergence onto the postsynaptic cell?

This question is basic to our understanding of how cortex computes. On the one hand, there is the image of a linear summation unit, or leaky integrator, passively adding up a large number of inputs to generate as noiseless an average as possible before passing judgment. On the other hand, with the recent discovery that single-fiber connections in the CNS are variable and unreliable [189, 140, 3, 249, 291], the possibility that small numbers of inputs are sufficient to generate an output spike raises the specter that this synaptic variability might be passed along to the next cell in the chain, rather than lost in the law of large numbers.

In spite of its seeming simplicity, it is also not a question whose answer is known. Until recently, sharp electrode recordings in hippocampal pyramidal cells had provided an estimate that at least several hundred simultaneous synaptic inputs would be necessary to reach threshold in the postsynaptic cell [7, 6, 223]. With the advent of whole-cell patch clamp techniques, however, the measured input resistances of cells, as well as the amplitudes of their synaptic inputs, have been revised upwards, and hence the estimate of the population size necessary to reach threshold may change as well. This number is also quite likely to vary between brain regions and cell types.

In this chapter, I have used whole-cell patch clamp recording techniques to study the size and characteristics of single-fiber inputs to cortical neurons. I have combined the study of spontaneous synaptic inputs, which allows one to see the range of characteristics of the input population as a whole, with minimal stimulation of one or a small number of fibers to allow the study of single inputs over time. Single fiber inputs to cortical neurons are very large (up to several mV), and very rapid in time course. There is enormous variability in the population of inputs to one cell, and between the inputs to different cells. As in many other systems, this variability in amplitude is not just due to variation between synapses, as it is also reflected in

the fluctuating response to a single input over time [249, 3, 291, 140]. Single-fiber inputs are large relative to spike threshold, and assuming linear summation, only 5-50 simultaneous inputs would be necessary to generate a spike. These findings here are consistent with very recent studies in cerebellum and hippocampus [189, 13].[1] This implies that the variability seen at the level of single inputs should be reflected to some degree in the output of the cell. This is indeed the case, as there is considerable variability both in the probability of the cell spiking with a near threshold input, and in the timing of the resulting spikes.

3.2 Methods

Electrophysiology and stimulation. Preparation of rat and cat slices and recording were performed as in General Methods. The vast majority of cells were recorded using KGlu-based solutions, however a small number were recorded using CsF solutions in order to improve voltage control and decrease intrinsic noise at holding potentials above -30mV. Where data from these cells are presented, the solution is noted; however, there were no differences between the two groups of cells with regards to the conclusions of this study. Spontaneous events and evoked responses were collected off-line for analysis. Evoked responses were sampled at 5-10kHz. For the vast majority of cells presented in this chapter, series resistance and recording criteria were as described in Chapter 1. However, for the small sample of cat cells, and for cells recorded in current clamp, the series resistance criteria were relaxed somewhat to include a few cells with R_s >30$M\Omega$. As these cells were used for current clamp analysis, or for comparison of spontaneous inputs to evoked responses within the same cell (and thus subject to the same series resistance), this should not bias the results. Data from such cells are not included in the amplitude summary plots in Figures 3-7 and 3-8, except in the case of one cat cell with a very high R_s, and 3 cat cells with R_s values in the range of 30-40$M\Omega$. Data from some cells with high R_s values are included in the plots in Figures 3-9B and C, on the effect of R_s on EPSC amplitude. They are not used for further analysis elsewhere in the chapter.

Stimulating electrodes were made as in General Methods. Small, bipolar electrodes were placed at the gray-white matter border, or in layer 1, directly in line with the recording electrode. 1-2 stimuli of 0.05 ms duration were given at 0.33-1 Hz (usu-

[1] These studies were published while this work was in progress.

ally 0.5 Hz, ISI for paired stimuli 20-200 ms, usually 50 ms). For minimal stimulation, stimulus strength was gradually increased till a response began to appear. Such responses failed on a percentage of trials, were uniform in waveform and latency, and appeared to be the result of a single input fiber [168, 209, 156, 140, 249, 3, 291]. As stimulus intensity was increased further, there was a plateau region where the amplitude of the response did not change, though the failure rate sometimes decreased (see Fig. 3-11). Eventually, as the stimulus was increased yet further, response amplitude began to increase, and inhibitory components to the response usually appeared. In some cases, it appeared that 2 fibers, with different latencies and waveforms, were being stimulated; though it is impossible to distinguish this from the case of two synapses from the same axon which generate very different postsynaptic responses. Whenever possible, analysis was restricted to those cases which seemed to be the same single input. In measurements of peak amplitude, kinetics, or failure rates, attention was restricted to an input that occurred at a particular, fixed latency. This seemed to be the best method for avoiding contamination by spontaneous synaptic inputs. Peak amplitudes were measured as the average of three samples in a fixed window following each stimulus. For measurements of evoked event kinetics, individual evoked responses were detected using Axograph and a simple amplitude threshold algorithm. Kinetic parameters were then measured using Axograph. Failure rates were counted by eye, restricting attention to an identified input coming in at a particular latency post stimulus. Failures were counted for both the first and second peak of paired-pulse stimuli, but unless noted, these numbers were not combined. Responses to the first of a pair of stimuli were considered equivalent to responses to a single stimulus alone, and data from these two groups were pooled.

For threshold stimulation, stimulus intensity was increased to the point where the cell generated a spike on 50% of trials. For both large-amplitude (threshold) stimuli and minimal stimulation, stimulus pulses were frequently given in pairs 50 ms apart. Paired-pulse facilitation and depression were both seen, and are discussed in detail in separate publications (Nelson and Smetters, in preparation). In many cases, it was impossible to bring a cell to threshold with white matter stimulation due to powerful feedforward inhibition. Sometimes, however, due to depression of the IPSP combined with facilitation of the EPSP, the cell would spike to the second of a pair of pulses. For each cell presented here undergoing paired stimulation, it is noted whether the responses shown are to the first pulse, the second, or both.

3.3 Results

How can one estimate the importance of individual inputs to the output of a cortical cell? The first step is, of course, to figure out how large are the individual inputs, and what are their properties. The second is to determine what "large" means - large relative to what? In other words, what is the threshold for the cell to generate an output, and how does it sum those inputs to get there? Finally, one can combine these two pieces of information to estimate how many simultaneously active inputs are necessary to generate an output from a cortical cell, and how much the properties of these individual inputs will influence the output of the postsynaptic cell, and hence the information seen by the next cell down the line.

3.3.1 Properties of single-fiber inputs to cortical cells.

How large is a single-fiber input to a cortical neuron? Recording from pairs of synaptically connected neurons, the most accurate technique to determine this number (see Chapter 1), suffers from the problem that at the very most only 2-3 of the inputs to any one cell can practically be studied, and the overall yield of connected pairs is very low. Additionally, the vast majority of these studies have been performed using sharp electrode recording techniques, whose low signal-to-noise ratio makes it difficult to identify very small inputs, or reliably distinguish failures of transmission from non-failures.

What we would like to do is assess the properties of the whole population of inputs to a single cortical cell, and compare them to the properties of an identified input, which can be studied repeatedly over time. To do this practically, I have combined study of spontaneous excitatory inputs to cortical cells, with minimal stimulation designed to evoke responses in one, or at most a small number of fibers at a time.

3.3.2 Properties of spontaneous synaptic events.

Cortical cells in a slice receive a barrage of spontaneous synaptic inputs. Figure 3-3 shows several such events occurring in a cat layer III cell. Such events occur apparently at random, in most if not all cases, with exponentially distributed inter-event intervals suggestive of a Poisson process. Unlike evoked inputs, which occur at known times and can be averaged to increase their signal-to-noise ratio (SNR), spontaneous events must be detected in order to be analyzed. These events presumably arise from synapses located all over the dendrites of the postsynaptic cell, and it is impossible to know which presynaptic cell generated a particular response, or where on the postsynaptic cell it arose. This, however, is also true of all techniques for studying synaptic inputs to cortical cells, with the sole exception of paired recordings combined with successful filling of both cells, and, ideally, electron microscopic analysis of synapse location. Unfortunately, neocortex has none of the supposed simple, laminar organization of input fibers characteristic of the hippocampus – the relative location of two cell bodies is not at all predictive of where on the somadendritic axis they may synaptically connect.

The frequency of spontaneous EPSCs[2] is much lower in slice than it is *in vivo*, and it is sensitive to drugs, the composition of the bath solution, and electrical stimulation; so they do not provide a good method to study the effects of spontaneous activity on the properties of cells *in vivo* [22, 208]. However, in spite of these drawbacks, they give a simple method to rapidly asses the properties of a large number of single-fiber inputs to a single cortical cell, and to compare the distributions so gathered from a large number of cells.

[2]Spontaneous excitatory postsynaptic currents. Miniature excitatory postsynaptic currents, recorded in the presence of tetrodotoxin (TTX, see below), will be referred to as mEPSCs. "Spontaneous events" always refers to sEPSCs.

Single-fiber inputs are large relative to threshold.

Figure 3-4A shows the properties of spontaneous EPSCs (sEPSCs) and EPSPs (sEPSPs) in a rat layer V cell recorded in the presence of bicuculline to block $GABA_A$-mediated spontaneous IPSCs (sIPSCs). These events are large, with a modal amplitude in current clamp frequently $\geq$ 0.5mV; and very rapid in time course. Amplitude distributions in both current and voltage clamp show a characteristic shape, skewed towards larger values. This distribution shape is common to a variety of synaptic input types in a large number of cells [247, 144. 274, 104, 164, 163, 244, 232, 41, 290, 143, 82, 70, 146. 29, 155, 157, 17. 128, 188, 187, 190, 217, 231, 238, 240, 266, 280].

Most spontaneous events are excitatory.

In cortical cells recorded at 34°C at the ages studied here, the vast majority of spontaneous synaptic inputs were excitatory and glutamatergic. Bath application of CNQX ($10\mu M$) blocked almost all events (n=4), and all events recorded in the presence of TTX, APV, and bicuculline (n=4). Figure 3-4B shows traces before (above, V_{hold}=-70mV) and after (below, V_{hold}=-60mV) bath application of CNQX ($10\mu M$) in the absence of bicuculline; in spite of the very high initial frequency of spontaneous PSCs, all events seen here are blocked by CNQX.

There are spontaneous IPSCs in these cells as well, occuring at a lower frequency than sEPSCs. Holding the cell at -40mV, above the reversal potential for $GABA_A$-mediated IPSCs (around -55 with KGlu-based solutions), makes a small population of outward events clearly visible (Fig. 3-4C). Over several seconds (upper trace) outward (upward) IPSCs can be seen to occur at a slower frequency than inward EPSCs (downwards). In this cell, IPSC frequency is 0.307 Hz, while EPSC frequency is 7.36 Hz. The different kinetics of sEPSCs and sIPSCs can be seen in the lower, expanded trace. In cells recorded in the presence of bicuculline, no reversed IPSCs appeared at -40 mV (n=6). Washing in bicuculline methiodide (BMI, $50\mu M$) did not change the frequency of spontaneous PSCs (Fig. 3-4D, same cell as in C), however it did

shift them slightly towards larger amplitudes, presumably due to the usual increase in spontaneous action potential activity seen with BMI in the absence of TTX (see below).

The frequency of sEPSCs and sIPSCs varied from cell to cell. The contribution of each was assessed by counting the number of inward and outward events during time periods of 25-250 seconds, at holding potentials where sIPSCs were clearly visible as outwards events (-50 – -30mV, usually -40mV), in 33 cells. sEPSC frequency was usually 3-4 Hz, but was considerably higher in a few cells. Figure 3-4E shows the percentage of all events which were IPSCs for each cell, broken down by layer and species. The average percentage of IPSCs was 11.9±2.79%, including 2 cat cells with relatively high or very high IPSC frequencies and EPSC frequencies of 2Hz; the median value was only 6.62%. For the vast majority of cells, sIPSC frequency fell into a narrow range (Fig. 3-4F), with a few outliers. Mean sIPSC frequency in these cells was 0.8623±0.372 Hz (median: 0.276Hz). Mean sEPSC frequency counted at -40 mV in these cells was 5.8±1.11 Hz (median: 3.45 Hz), and in the whole population of cells studied was usually 3-4 Hz, unless increased by manipulation of bath osmolarity.[3]

As sIPSCs do not usually form a large fraction of the spontaneous events, this allows excitatory inputs to be studied in the absence of bicuculline with only minor contamination by sIPSCs. Bicuculline, even at low concentrations, increases spontaneous action potential-driven activity and frequently causes seizures, particularly if electrical stimulation is applied. Therefore, this study combines analysis of a small number of cells recorded in bicuculline with a larger number recorded in its absence, to assess the properties of sEPSCs. It must be kept in mind that in these cases up to 15% of the events detected at -70 may be reversed IPSCs, so large numbers of events should be considered to allow robust conclusions in spite of this contamination. However, emphasis was placed on cells which showed very low frequencies or no sIPSCs when held at -40 mV, and all of the conclusions here were robust in the presence

[3]Some of the cells in this sample of 33 were recorded with a bath dextrose concentration of 20 mM, which will mildly increase synaptic event frequency.

of bicuculline. In fact, as event amplitudes shifted slightly towards larger values in the presence of bicuculline,[4] recording in the absence of bicuculline will if anything lead us to underestimate the size of single-fiber inputs to cortical cells. In spite of the relatively small contribution of sIPSCs to the population of synaptic events at these ages, evoked inhibition to large stimuli was quite robust, and frequently able to prevent cell firing.

Voltage dependence of sEPSCs

Figure 3-5A shows average sEPSCs as a function of holding potential for a cell recorded with CsF-based solution. sEPSCs reverse at 0mV, consistent with their being glutamatergic. There is a slight trend towards broadening of the average sEPSC at depolarized potentials, possibly reflecting a contribution of NMDA receptors [29, 146]. Cumulative amplitude distributions for a cell recorded in TTX, APV, and bicuculline (Fig. 3-5B) also show that events reverse at 0mV, and there is a standard increase in distribution slope with increased polarization.

The nature of spontaneous events, however, complicates any more detailed analysis of their voltage dependence. One might be tempted to measure the average slope conductance of sEPSCs by plotting the peak amplitude of the average event[5] vs voltage; or to estimate the range of electrotonic distances events were coming from, or individual event locations, by isolating a uniform population of events (e.g. in APV and bicuculline), and seeing at what point they reversed as a function of their amplitude and kinetics. In the noise-free case, more proximal events would reverse at a lower apparent potential (the true reversal potential) than more distal events, who are not under quite as good voltage control.

The detection threshold for spontaneous events, however, makes such analyses

[4]Due to both increased action potential-driven activity and the fact that any sIPSCs blocked are close to their reversal potential and therefore small in amplitude due to lack of driving force.

[5]Or the average peak amplitude, which is not the same thing due to differences in time course between events.

difficult. As sEPSCs must be detected, rather than occurring at known times, there is always a chance that some small events may escape detection, depending on event size and noise level (see Section 5.3.7). As the cell is depolarized, events decrease in amplitude due to the reduction in driving force, and an increasing proportion of the smallest events are lost below the threshold. This can be seen in Figure 3-5C and D, where the complete amplitude distributions for each holding potential are summarized for the cells in A and B (see legend for explanation of plot). This induces a bias in the measurement of mEPSC parameters and voltage dependence. For instance, the sEPSCs of the cell shown in Fig. 3-5A probably reverse slightly above 0mV. This cell had a small number of sIPSCs (4% of all events at -40mV). At voltages from -40 to 0 mV, only inward events (purely sEPSCs) were detected. At 0 mV, however, a very small number of events (12 inward, 13 outward) were still seen. These presumably comprised the very largest inward sEPSCs, who had not quite reversed but were still visible even with very little driving force, and the low-frequency sIPSCs (the outward events). Averaged together, these events came to an amplitude of 0 pA. Unfortunately, the noise level and detection threshold impose a band around 0mV where no events can be seen.

This effect of losing an increasingly large number of small amplitude events below the detection threshold (which is constant across all events detected in a single cell), means that the slope conductance of sEPSCs would be overestimated if measured from average events at depolarized voltages, as at these voltages only the largest-amplitude events are detectable. It is much better to estimate slope conductance from the event amplitudes measured at very negative potentials, where all or almost all events are detectable (see Section 5.3.7), and use the reversal potential measured from a voltage series such as this one (which will be relatively accurate as DC space clamp errors are usually small [242, 150, 293]) to estimate sEPSC conductance. Similarly, the band around the synaptic reversal potential where no events are visible above the detection threshold makes it difficult or impossible to accurately measure any differences in reversal potential due to location across an otherwise uniform population of synaptic

inputs. The difference in reversal potential between proximal and distal events is subtle, usually less than 20 mV (see Figure 4-35), which is too small to be reliably detected above the noise as events disappear behind the detection barrier surrounding 0 mV.

3.3.3 sEPSC variability within and between cells.

Kinetics of sEPSCs vary both within and between cells.

The individual sEPSCs shown in the lower part of Fig. 3-4A show that, besides the wide variation in sEPSC amplitudes within a single cell, events also vary in kinetics. Distributions of sEPSC kinetic parameters show characteristic skewed shapes similar to that seen for amplitudes (Fig. 3-6A, from the cell shown in Figure 3-4A, recorded in the presence of $50\mu M$ BMI). Even recording events in the presence of TTX, APV, and BMI, to isolate as much as possible a uniform set of purely AMPAergic, uniquantal events, kinetic parameters still show such skewed distributions (Fig. 4-17B).

Kinetic variations between cells. sEPSCs also vary in kinetics between cells. The average of 490 sEPSCs from two layer III cells recorded in the presence of TTX, APV, and BMI are compared in Figure 3-6B and C (also compare traces in Figures 3-4A, 3-12A,B,C lower). These cells show dramatically different sEPSC kinetics (time and amplitude scales are the same for the two averages), in spite of their only slight differences in amplitude, and their presumed uniquantal, purely AMPAergic nature. This difference is not a function of a difference in series resistance, in fact, the cell in C with relatively slow sEPSC kinetics had the lowest R_s of any cell recorded in this study (2 $M\Omega$), and lower that that in B (8 $M\Omega$).

In some cases such extreme kinetic differences in EPSCs have been shown to correspond to differences in cell class (e.g. interneuron vs. regular-spiking cell) [82, 143]; and to be due to differences in underlying AMPA receptor kinetics [83, 142]. Based on the data in [82, 83], it is possible that the cell in Figure 3-6B is an interneuron;

this is, however, not consistent with its low input resistance of 87 $M\Omega$. It was not recovered anatomically, and was recorded entirely in the presence of TTX, so this is the best indication available of its class.

Kinetic variation within a single cell. It is not known whether such heterogeneity in AMPA receptors is present within the population of receptors on one cell, though there have been suggestions of kinetically distinct, bimodally distributed populations of mEPSCs in some cell types [70].

Another potential source of variation in sEPSC kinetics is electrotonic filtering, as these events differ in input location.[6]

sEPSCs are made up of action potential-dependent and independent events.

One source of the large amplitude variability seen among the inputs to on cell is the fact that these events are a mix of responses to action potentials in other cells, and to the spontaneous, quantal exocytosis of transmitter as miniature EPSCs (mEPSCs, or minis). Miniature EPSCs can be studied in isolation by recording in the presence of TTX to block action potentials.[7] Cells vary in the contribution of action potential-dependent events to their sEPSC population, and in the degree of overlap between the amplitudes of these events and the minis. Figure 3-7A and B compares two cells with very different responses to TTX ($1\mu M$). The layer V cell in A loses most of its spontaneous events, and all large-amplitude events, in the presence of TTX. The layer III cell in B, in contrast, shows no such change, and in fact a slight increase in event frequency after washing in TTX. These two cells had sEPSCs of comparable amplitudes before TTX application, but the cell in A showed a very unusual, broad,

[6]The relative contributions of these factors to generating kinetic variability in EPSCs is discussed in detail in Chapter 4.

[7]Unfortunately, there is no corresponding method to study action potential-dependent events alone.

almost peaky amplitude distribution. While on the whole, cells recorded in TTX tended to have fewer very large sEPSCs than did cells recorded without TTX, it is not true that all large-amplitude events are action potential-driven. Figure 3-7C and D show cumulative amplitude distributions for 29 layer II/III cells (C), 27 layer V/VI cells (D), and two cells of unknown layer (C, circles) recorded in the presence of TTX. There is still considerable intra- and inter-cell amplitude variability even among pure uniquantal mEPSCs. There is a tendency for event amplitudes to be slightly smaller than those recorded in the absence of TTX (see Figure 3-8E), particularly in the presence of bicuculline, which promotes the firing of spontaneous action potentials in the slice. There is also a slight, non-significant, trend towards larger amplitude mEPSCs in layer V/VI cells.

3.3.4 Sources of sEPSC variability between cells.

Comparing sEPSC amplitude distributions from different cells reveals an inter-cell variability as large as that within a single cell. While almost all cells show the stereotypical skewed distribution of sEPSC amplitudes (see Figure 3-7A for one of the few exceptions), the range of absolute event amplitudes varies tremendously between cells. Figure 3-8A-C shows cumulative amplitude histograms for 12 rat layer II/III cells, 13 rat layer V/VI cells, and 5 cat cells (4 layer II/III, 1 layer V/VI). The distribution of mean amplitudes for each group is shown in Fig. 3-8D. In spite of the large amount of variation between cells, the variation in the variation is rather small – the coefficient of variation (CV) of sEPSC amplitudes is very close to 0.4 in most cells. The distribution of amplitude CV's for the data in A-C, plus the data for the cells in Fig. 3-7C,D is shown in Fig. 3-8E. A similar degree of inter-cell variability is shown for sEPSPs in current clamp (Fig. 3-8F).

There are a number of likely sources of inter-cell variability in sEPSC amplitudes. One, noted before, is the presence of both spontaneous and miniature synaptic inputs within the population of sEPSCs. However, the large inter-cell variability seen in the

presence of TTX (Fig. 3-7C,D) indicates that this cannot be the only factor involved.

Animal Age The age of the animal might affect sEPSC characteristics in two ways. First, the properties of sEPSCs, in terms of their size, frequency, or underlying receptor makeup, might change during development over the ages studied here. Second, the increase in dendritic length over this period, and hence the degradation of space clamp, may also contribute to changes in recorded sEPSC amplitudes. Figure 3-9A shows the relationship between mean sEPSC amplitude and animal age, for the groups of cells shown above. Cells on this plot can be subdivided into two loose groupings. There is one group, consisting of the vast majority of cells, whose mean sEPSC amplitude changes vary little, if at all, with age, remaining at around 15 pA. There is a second, smaller, group of animals with very large sEPSC amplitudes; and the mean amplitudes of this group appear to decrease with age, merging into that of the more general population by P17. This group is made up from cells of all layers, with and without TTX. There may be more subtle changes in sEPSC amplitude with age, however, they are not visible relative to the large variability in sEPSC properties between cells.[8]

Pharmacological Manipulations Just as TTX will affect the distribution of event amplitudes by restricting attention to mEPSCs, other drugs which affect synaptic responses, such as BMI; or compounds which affect postsynaptic cell properties, such as TTX itself or Cs^+-based recording solutions, may affect sEPSC amplitudes. It is clear from the data in Figures 3-7 and 3-8 that sEPSC amplitude increases significantly in the presence of bicuculline and the absence of TTX, presumably due to the concomitant increase in spontaneous activity in the slice. The change in cellular passive properties after perfusion with Cs^+ might be expected to have some effect on

[8]Or even, occasionally, between sequentially recorded cells in the same slice.

sEPSC amplitudes.[9] Unfortunately, due to the problems of spontaneous bursting and bistable plateau potentials encountered when recording with Cs^+-based solutions in the absence of TTX, too few cells were recorded with such solutions without TTX (similarly, very few cells were recorded using K^+ -based solutions in the presence of TTX).

Series Resistance An unfortunate complication in continuous voltage clamp recording, access resistance (R_s) acts as a low-pass filter to selectively attenuate the amplitudes of the very fastest (usually largest) sEPSCs. This effect, obviously, increases with increasing values of R_s; but less intuitively it also increases with increasing cell size (to do an increase in total capacitance [229] (see Section A.6). Therefore, recordings with the same absolute value of R_s may have in fact undergone different amounts of filtering, depending on the size of the cell involved. Figure 3-9 plots mean (B) and maximum (C) sEPSC amplitude against effective R_s(after the application of series resistance compensation, if any).[10] Both mean and maximum amplitude decrease exponentially with increasing amplitude, as would be expected for the effect of a low-pass filter (see Chapter 4). Both appear to decrease at the same rate with increasing R_s, which is somewhat surprising. Mean amplitude, being heavily determined by the bulk of small events, which are frequently slow and less affected by low-pass filtering (see Chapter 4) would be expected to be less sensitive to R_s. However, mean amplitude does show a slightly smaller proportional reduction in value than does maximum amplitude (80% as opposed to 90%). The effect of R_s on maximum amplitude can only be estimated in this fashion; because we are limited to examining the largest event we happen to see during our period of observation, it

[9]However, this effect may be small. Though Cs^+ increases membrane resistivity by blocking K^+ channels, attenuation of synaptic events is much more dependent on R_i and C_m then R_m (see [242], Chapter 4).

[10]Note that a few cells used here with very high values of $R_s$are only included for comparison, and were not used elsewhere in this study. One cell included in this graph was actually recorded at three different values of R_s , and all three are included for comparison.

is possible that just by sampling we will underestimate maximum event amplitude, particularly in cells where the data collection period is short. However, over a large number of cells it should approximate the true maximum value.

Cell Type Another source of sEPSC variability between cells is, of course, differences in the cells themselves. Unlike hippocampus, blind patch recording in the cortex will sample from a variety of cell types. It has been shown that different cell classes in the neocortex can vary dramatically in the properties of their AMPAergic mEPSCs ([82, 83], see above). Even restricting attention to pyramids (only a very small subset of the cells in this study were non-pyramidal), two nearby pyramids in the same layer can have very different morphologies – for instance the "thin" and "thick" pyramidal cells of layer V [137, 136, 108]. The presence of at least two subpopulations of cells with different sEPSC properties is suggested by the cumulative amplitude distributions shown in Figures 3-7 and 3-8. The cumulative amplitude distributions can be divided into two loose groups; a large one of very steep distributions with few large-amplitude events, and a smaller one with a much more gradual slope and many more large-amplitude events – this latter group resembles those cells recorded in the presence of bicuculline. The former, larger group, corresponds to the "standard" picture of sEPSCs/mEPSCs seen in a number of studies – events predominantly distributed below -20 pA in amplitude [247, 274, 104, 164, 163, 244, 232, 41, 290, 143, 82, 70, 146, 29, 155, 157, 17, 190, 217, 231, 266]. This difference in amplitudes also corresponds to a difference in kinetics, with the events of the "large" group appearing somewhat faster (compare the traces shown in Fig. 3-4A, a "large, fast" cell in bicuculline, with the average event in Fig. 3-6C, a "small, slow" cell). This informal classification scheme may not correspond to systematic differences between cell types, however.

Relationship between current and voltage clamp The similarities between the amplitude histograms in current and voltage clamp shown in Figure 3-4A tempt

one to assume there is a very simple mapping between the amplitude of synaptic events in current clamp and their amplitude in voltage clamp. This is, unfortunately, an oversimplification – it's true for the steady-state case, but with transient inputs it no longer holds (see Figure A-60). Determination of the real, empirical, relationship between these two variables is complicated heavily by the difficulty of detecting events in current clamp. As event amplitudes in current clamp are filtered by the cell membrane, but to a large extent recording noise is not, events in current clamp have a lower SNR than they do in voltage clamp, requiring a relatively higher detection threshold. More importantly, the greatly slowed time course of events in current clamp means that, with any frequency of events, they will frequently overlap, which makes them much more difficult to detect (see General Methods). The net result is that, for equal periods of time, one usually detects many fewer spontaneous events in current than in voltage clamp; and they are probably biased towards the larger end of the amplitude distribution. In the ideal case, low event frequency combined with careful detection might allow one to detect a corresponding number of events in both current and voltage clamp. In that case, the relationship between the two would best be revealed by plotting the event amplitudes of particular relative frequencies in one against the same relative frequency in the other (e.g. plot the 25th percentile amplitude in current clamp against that amplitude in voltage clamp).

3.3.5 What generates EPSC variability within a single cell?

As discussed above, there are a large number of factors which might contribute to the variation in sEPSC amplitudes seen between different cells. It is less obvious what might cause such wide variability in event amplitudes within a single cell. Potential contributors can be divided into two classes. *Intrinsic factors* are differences between synapses due to intrinsic properties of the synapses themselves: differences in postsynaptic receptor subunit composition or number, differences between action potential-dependent events and mEPSCs, differences in firing history of the presy-

naptic cell, etc. *Extrinsic factors* are differences due to the relationship of synapses with the postsynaptic cell: for example, synapse location on the dendritic tree, or the presence of voltage-dependent conductances shaping the postsynaptic response to a synaptic input. (See Section 1.3.4.) Is the effectiveness of a synapse controlled only by its own history – intrinsic factors – with each synapse having an equal possibility of contributing to the output of the cell? Or is the effectiveness of a synapse controlled by its location on the postsynaptic cell?

A number of studies have looked for an effect of synapse location on response amplitude of synaptic location, in the form of electrotonic filtering,[11] is to look for a negative correlation between event rise time and amplitude [244, 247, 163, 164, 274, 104, 209]. As a synapse is moved farther out a dendrite, the response at the soma will decrease in amplitude and increase in time [203, 97, 269]. It is therefore logical that these two variables should be negatively related to one another if event amplitudes and kinetics are indeed shaped by electronic filtering. A large number of studies [244, 247, 163, 164, 274, 104, 209] have concluded that since these two parameters are not strongly negatively correlated, there is no contribution of electrotonic filtering to synaptic event amplitude. In fact, in cortical neurons, these two parameters are indeed not negatively correlated (Figure 3-10A,C), and the fastest (presumably most proximal) events are still extremely variable in amplitude, covering the entire range of amplitudes seen. However, as shown in Figure 3-10D, there is a significant correlation between sEPSC rise time and half width. Such a correlation has been identified in the theoretical literature as the best predictor of a role for electrotonic filtering in the generation of synaptic response shape [203, 97]. This suggests that, in fact, sEPSCs may be subject to a considerable degree of electrotonic filtering; and that the lack of correlation between rise time and amplitude may not be a good predictor of a contribution of synaptic input location to synaptic response shape (see Discussion, Chapter 4).

[11] Rather than in the form of a contribution of spatially inhomogeneous voltage-dependent conductances to synaptic response.

3.3.6 Properties of single inputs over time.

The study of spontaneous events tells us about the population of inputs to a cell – what range of amplitudes, etc., we might expect it to see. However, it doesn't give us a lot of detailed information about individual inputs, most notably their behavior over time – a single input might not be active more than once during the period in which sEPSCs are collected, and even if it was, there is no way to know it. Fluctuations in single inputs over time is both an important source of extrinsic variability, and an additional important factor in determining single fiber response amplitudes. I have therefore used the technique of minimal stimulation (see Methods, [168, 209, 249, 3, 291, 140, 156, 6]) to attempt to repeatedly evoke responses from one, or at most a small number, of input fibers.

Putative single-fiber responses fluctuate randomly in amplitude between a clearly identifiable failure level and one or more response amplitudes. This is shown for 3 cells in Figure 3-111,2, and 4. In most cases, failures (open symbols) are clearly distinguishable from responses (1), but if the noise level is high and responses are small, the distance between the two narrows. If there are spontaneous EPSCs either during the baseline or response period, then the failure amplitude will overlap with that of the responses (2). Responses are usually stable over time, showing occasional mild increases (3, end), or decreases (1,end) in failure rate, which usually recover to baseline in a few seconds. The region of putative single-fiber responses can clearly be identified as stimulus amplitude is increased. At low stimulus amplitudes, all inputs fail to generate a response (B1, left). As the stimulus amplitude is increased, suddenly a response begins to appear (B1, 6V, B3, small response, 20V). As the stimulus is increased further, there is a plateau region where the response amplitude does not increase, but the number of failures may go down [249] (or disappear entirely, without the non-failure amplitude increasing much, B1 15-20V). Finally, as stimulus strength is increased still further, the response suddenly begins to increase, failures disappear, and an inhibitory component may appear as well (B1, 30V, B3, 40V). Figure 3-11B2

shows the mean non-failure amplitude and probability of failure for the data in B1.

Probability of failure. To estimate the number of inputs which must be active to make the postsynaptic cell fire, we must not only estimate their size relative to threshold, but given the fact that transmission in the CNS is apparently fallible [189, 92, 17, 3, 249, 291]; we must also estimate the number of inputs which will actually cause a postsynaptic response given that a certain presynaptic population fires a spike. Unfortunately, minimal stimulation is not an accurate technique with which to estimate failure rates. Even if one is extremely careful, it is always possible that one is stimulating 2 fibers instead of one (though this usually results in clear differences of latency and waveform). This will result in an underestimate of failure rate. If responses are small, it may be difficult to distinguish small responses from failures due to recording noise. As these will probably be misclassified as failures, this will cause an overestimate of failure rates. Using the minimal stimulation technique as presented here, one cannot monitor the action potentials of the presynaptic cell being stimulated. This leaves open the possibility of failures of stimulation. Or there could be branch point failure, where a stimulated axon fails to propagate an action potential to all of its terminals; such failures might be increased due to damage during the slicing procedure. Careful studies have suggested that at least a large fraction of the failures of release seen in slice studies are true failures of release, rather than failures of stimulation or propagation [249, 3]. However, other studies support the idea that failures of stimulation do happen at least in some cases [250]; and that the probability of stimulation failure may vary between slices, cells, electrode placements, etc. Given all of this, it is important to take probabilities of failure estimated using minimal stimulation with a very large grain of salt. In spite of this fact, the distribution of failure probabilities seen in the 27 cases (22 rat cells, 5 cat cells, first stimulus only) of minimal stimulation used here is presented in Figure 3-11C. The mean probability of failure was 37.56±4.223% for rat cells, and 26.15±7.79% for cat cells (overall probability = 35.45±3.82, n=27).

Relationship between meEPSCs and spontaneous events.

Single inputs do vary considerably in amplitude over time. Figure 3-12 shows the properties of single fiber inputs evoked with minimal stimulation in rat and cat cortical cells; and compares their properties to spontaneous events within the same cell. Minimal evoked responses (meEPSCs, traces, left) fluctuate in amplitude between clear failures of transmission and variable levels of response. They vary much less in kinetics and latency (see Figure 3-13) than in amplitude. The amplitude distribution of meEPSCs always overlapped heavily with those of sEPSCs in the same cell (see amplitude histograms, right). This was true in all of the cases which met our criteria for minimal stimulation (rat cells, n=23; cat cells, n=5), suggesting that these evoked responses truly represent single-fiber inputs.

Evoked amplitudes do show varying relationships to the distribution of sEPSCs, depending most likely simply on which region of the sEPSC amplitude distribution the fiber under study was drawn. In some cases (Fig. 3-12A), the peak of non-failure meEPSC amplitudes centered around an amplitude which was towards the largest end of the sEPSC amplitudes seen. In other cases, (Fig. 3-12B), the smallest meEPSC amplitudes were close to the failure peak, and appeared to be smaller than the smallest sEPSCs, because they were below the threshold for spontaneous event detection.[12] In the final group (Fig. 3-12C), meEPSC amplitudes showed a broad distribution; with the sEPSC amplitudes primarily corresponding to the smaller peaks. These relationships are consistent with sEPSCs consisting heavily of miniature EPSCs, and with the meEPSCs consisting of one or more distinguishable quantal levels [140, 191].

Minimally-evoked EPSCs show less kinetic variation than sEPSCs.

Careful examination of the amplitude histograms in Figure 3-12 shows that, while spontaneous events show their characteristic skewed amplitude distribution, mini-

[12]Because meEPSCs occur at known times, even very small events are accessible for analysis, though it may be difficult to distinguish them from failures.

mal evoked events from the same cell do not. Besides the peak near 0 pA representing failures of transmission, they consist of either a Gaussian-type second peak (Fig. 3-12A,B), or a constellation of peaks presumably representing multiquantal inputs (Fig. 3-12C). This can be seen more clearly in Figure 3-11B1,3 and 4, which plots meEPSC amplitude histograms without the failures of transmission (parameters of these distributions are summarized in Table 3.3.6). This suggests that at least in some cases, the processes generating skewed amplitude distributions in sEPSCs may not apply to meEPSCs, which presumably come from a single or small number of input sites on the dendritic tree.[13]

Responses to minimal stimulation also show less kinetic variability than do spontaneous events, having, for instance, a rise time distribution with is narrower and less skewed (Fig. 3-13C, Table 3.3.6). This is consistent either with individual inputs being restricted to a particular time course of response (but response kinetics perhaps being allowed to vary between input fibers); or with the stimulated input coming into a single, or a narrow range of, electrotonic locations on the postsynaptic cell's dendritic tree. This latter interpretation is partially supported by plotting rise time vs half width for evoked and spontaneous events. While in both cases, rise time and half width are significantly correlated ($p<.05$, Spearman), the points for the evoked responses form a narrowly-defined, almost isometric cloud in a restricted region of the shape index space (note different axes for evoked and spontaneous responses, to show more detail of evoked response). Interestingly, while spontaneous EPSCs show no correlation between rise time and amplitude, evoked responses in this particular

[13]Even in the case of uniquantal meEPSCs, if the presynaptic fiber made more than one contact with the postsynaptic cell which fired with low enough probability to never simultaneously release two quanta, an apparently uniquantal input could arise from multiple release sites. As individual release sites from the same presynaptic axon are not constrained to make nearby contacts onto the postsynaptic cell's dendritic tree, and a single axon may make multiple synapses at widely disparate points on the same postsynaptic cell [60], any multiquantal input has the possibility of arising from a number of electrotonically distinct input sites. If a single release site is capable of releasing multiple quanta effectively [191], then even an input which consists of large numbers of quanta might all arise from the same point on the dendritic tree. However, using the technique of minimal stimulation, it is impossible to distinguish these possibilities.

	Mean	SD	CV	Skew
Amplitude				
S1	-42.74	8.78	-0.21	0.43
S2	-40.94	11.95	-0.29	-0.31
Both	-41.69	10.73	-0.26	-0.085
Spont	-17.16	7.37	-0.43	-2.30
Rise Time				
S1	0.95	0.17	0.18	0.38
S2	0.98	0.30	0.30	1.04
Both	0.97	0.25	0.26	1.09
Spont	1.09	0.67	0.63	2.68
Half Width				
S1	4.62	0.62	0.13	0.04
S2	4.59	0.73	0.16	0.09
Both	4.61	0.68	0.15	0.06
Spont	2.16	1.18	0.55	5.28

Table 3.1: Comparison of minimally-evoked and spontaneous event kinetics from the same cell.

fiber (as well as at least several others, data not shown) show a small but significant positive correlation between these two variables. This is quite possibly due to the fact that, the largest, apparently multiquantal evoked responses frequently showed a bit of latency jitter in the onset of each quanta, sometimes leaving a rising-phase inflection. Sometimes this inflection is clearly visible; all these events were removed. In other cases, the inflection was subtle, and might serve to increase rise time and half width relative to amplitude.

3.3.7 Only a small number of inputs are necessary to generate a spike.

Now, armed with an estimate of the size of single-fiber inputs to cortical cells, we can proceed to ask how many of these inputs must be simultaneously active to cause the postsynaptic cell to spike. First, however, we must ask how large are these inputs

relative to the spike threshold of the cell, and what it means for a cell to have a threshold.

Spike threshold was measured by using large-amplitude stimuli to generate responses sufficient to cause the cell to spike on 50% of trials [189]. In many cells, it was not possible to stimulate the cell to threshold from the gray-white matter border. When the stimulus intensity was increased beyond a certain point, powerful feedforward inhibition would overcome excitation and cause the response amplitude to actually decrease with increasing stimulus intensity.[14] Giving pairs of stimuli 50 ms apart frequently enabled the cell to reach spike threshold to the second stimulus, due to simultaneous paired-pulse facilitation of the EPSP and paired-pulse depression of the IPSP (Nelson and Smetters, in prep.).

Figure 3-14 compares the response to threshold stimulation to sEPSPs and minimal evoked EPSPs in two cells, an interneuron from upper layer V (A), and a layer II/III regular spiking cell (B). In A, the mean spontaneous event amplitude was 1 mV, while the modal (most common) spontaneous event amplitude was 0.8 mV and the maximum was 3.4 mV. The threshold voltage, measured as the point where the largest subthreshold EPSPs and spiking traces diverged, was 17.68 mV above rest. One can get a crude measure of functional convergence by assuming linear summation, and simply dividing the threshold voltage by the expected input size, to come up with an estimate of how many inputs are necessary to cause the postsynaptic cell to fire. Using the modal, or most common, spontaneous input size, this corresponds to 21 inputs necessary to bring this cell to threshold; if the largest spontaneous event seen in this cell (3.36) mV is considered instead, that number comes down to 6. Similarly, for the cell shown in B, the threshold voltage was measured as 18 mV above rest, while the modal EPSP amplitude was 0.5 mV,[15] while larger events frequently

[14] Large-amplitude stimuli in the presence of bicuculline almost invariably evoked seizure activity. This problem could probably be avoided by stimulating upper-layer cells from layer IV, which avoids much of the feedforward inhibition.

[15] As the modal EPSP amplitude is always smaller than the mean in these cells due to their skewed amplitude distributions, using this measure suggests if anything a larger number of inputs necessary

reached 1mV in amplitude. This would generate an estimate of 18-36 simultaneous inputs necessary to cause this cell to fire an output. Across these measures, and across cells (including cells whose thresholds were measured using current injection), it was estimated that 5-50 inputs would be sufficient to generate an action potential in the postsynaptic cell. Taking into account an approximate mean probability of failure of 40%, 8-83 input cells much reach threshold nearly simultaneously to cause the postsynaptic cell to spike.

Nature of threshold

An important question in estimating the number of inputs needed to bring a cell to threshold, is what exactly do we mean by threshold?[16] Is the above measure, a fixed amplitude relative to rest, a good measure of what it takes to make a cell spike? Or is a better one the old measure of rheobase (threshold) current injection sufficient to generate a spike? Or, perhaps even more simply, the "naive" notion of a simple voltage threshold – if the cell crosses this point, it will fire – used by many simplified neural models. Theoretical work has systematized these naive notions into three possibilities: a voltage threshold, a current threshold, and a charge (integral of current over time) threshold [97]. Old and recent computational work [71, 118, 97] suggests that cells do in fact operate using the simplest approach, a voltage threshold. The data presented here also strongly support the idea that cells fire more or less when they reach a particular voltage.

Figure 3-14C and D plots the absolute peak amplitude reached by the cells in A (C) and B (D) on each trial, whether the cell spiked or not. In each case, the cell was held at two different voltages with DC current; one the resting potential of the cell, and one depolarized closer to spike threshold (in the case of A, -65 mV and -45 mV; -60 mV and -70 mV in the case of B). Amplitudes plotted in C and D are absolute

to activate the cell than the mean would; while also perhaps being a more representative estimate of the most common case in terms of frequency of inputs, if not average input amplitude.

[16] Or, more importantly, what does the cell mean by threshold?

voltages, the relative amplitudes of EPSPs generated from the two holding potentials varied dramatically. It can be seen in C that whenever the cell crossed a certain potential, (-38mV), it fired an action potential, no matter what voltage it came from or how large of an input it took to get it there. This cell fired only to the second of 2 paired stimuli, apparently because the response to the first (open bars) never quite reached threshold. This suggests that these cells operate at least loosely by a voltage threshold [118]. Therefore, the baseline "resting" potential at which the cell is pushed by other inputs will determine how many additional inputs are necessary to cause it to spike.[17]

Applying a similar analysis to spontaneously firing cells also supports the notion of a voltage threshold. Few cells are spontaneously active in the slice, but a small number of cells seem to undergo random baseline fluctuations (either synaptic or simply noise); when these cells are depolarized to near spike threshold, the random fluctuations cause them to generate apparently random spontaneous activity (Fig. 3-15A1). Plotting the local maxima reached by the membrane potential in such a cell, either the peaks of the small subthreshold fluctuations or the peaks of the spikes, shows a sharp bimodal distribution of amplitudes as a function of time (Fig. 3-15A2), suggesting again that this cell simply fired whenever it happened to reach a particular voltage.

Adaptation, and the inactivation of slow currents, can modulate this voltage threshold behavior. Figure 3-15B1 shows a local maxima plot for a cell filled with CsF, undergoing a pattern of voltage plateaus and burst firing typical of such cells [214] (expanded in B2, bursts indicated by gray bars: further expanded to show actual voltage trajectory in B3). If a narrow window of time is examined, such as that shown in B2, the cell apparently exhibits voltage threshold behavior. All amplitudes are either below a threshold near -60 mV, or above it representing the peaks of spikes. The apparent intermediate points near -20mV can be seen on examination of the volt-

[17]Possibly modulo conductance changes due to background activity, see [22, 208].

age trace in B3, to be the lower peak amplitudes of spikes located in the middle of a burst. However, when the long-term behavior of the cell is studied in B1, it can be seen that as it climbs a depolarizing ramp (at 15 sec and 90 sec, description in legend), its threshold climbs with it, and when it is reset to hyperpolarized state where it no longer fires rhythmic bursts (45 sec and 120 sec) the two bursts it does fire (50 sec and 65 sec) appear to arise from a much lower threshold of near -70 mV. This is likely due to the bistability induced by Cs^+ blockade of K^+ currents in cortical cells [214], and indicates that the state of the slowly adapting currents in these cells can control the absolute value of the voltage threshold. However it also shows (B2), that on short time scales, a fixed voltage threshold may be the best and simplest model of action potential generation. As the estimates of functional convergence generated above were based on the distance from the resting potential to spike threshold at a particular resting potential, they are accurate for that potential – if the cell is hyperpolarized, more inputs will be necessary to fire an output.

3.3.8 Reflection of input variability in output variability.

One consequence of the low apparent numbers of inputs necessary to generate an output spike, is that the law of large numbers does not apply. One of the original arguments about why one would want a large number of inputs to converge to make an output is that "noise" in individual inputs would be washed out through averaging. Given that individual inputs are extremely variable in amplitude and sometimes fail to respond at all (Section 3.3.6, [168, 209, 249, 3, 291, 140, 156, 6], this would seem to be a good idea. Therefore it becomes an important question whether this input variability is in fact reflected in variability in the output of the postsynaptic cell. Simply the fact that one can perform threshold stimulation – where repeated, identical electrical stimuli only generate a spike on some subset of trials, suggests that these fluctuations in synaptic inputs do have functional consequences.

Figure 3-16A shows 20 identical stimuli given to the cell shown in Figure 3-14A, 9

of which generate a spike. Mean spike latency is 31.01 ms, with a standard deviation of 7.29 ms; there is an incredible fluctuation in spike timing when a spike occurs at all. Figure 3-16B shows that spike timing in a regular spiking cell is much less variable (6 of 15 traces contain a spike, same cell as in Figure 3-14B), but is still noticeably so. Mean spike latency is 5.7 ms, standard deviation is 0.52 ms. This is not a product of injury due to breaking the cell membrane, or some artifact of washout - Figure 3-16C shows a series of threshold stimuli given to a cell recorded in cell-attached patch mode. Action potentials are clearly visible through the patch on a subset of trials, and occur with variable latency. This variability is likely due to variation in the underlying synaptic inputs, as can be seen in Figure 3-16D, which shows voltage clamp recording of the threshold stimulus to the cell in Figure 3-16B, which varies considerably in amplitude (CV of peak amplitude = 0.085, CV of spike latency = 0.086).

This "jitter" in spike latency varies between cells, as can be seen by comparing A and B, and in Figure 3-16E, which summarizes this variability for 4 representative cells by plotting the time of each spike relative to the mean spike latency for that particular cell. Individual cells ranged dramatically in the variability of their spike timing, from a cell whose spikes almost completely superimposed, to the extreme variability seen in Fig. 3-16A. Plotting mean spike latency vs the standard deviation of spike times for 9 cells, (Fig. 3-16F, which includes separate points for two cells which spiked to each of 2 or 5 stimuli on some trials) shows a significant correlation ($R=0.948$, $p<0.02$, Spearman Rank Test, correlation still significant if only one stimulus considered for each cell) - longer latency spikes show significantly more jitter. This corresponds well to the fact that longer latency inputs, which are typically assumed to be polysynaptic in nature, are more variable in response. In a chicken-and-egg situation, the fact that spikes are variable in their timing, and longer-latency spikes the most variable, may account for why polysynaptic inputs are so variable in latency and occurrence.

3.4 Discussion

In this chapter I have provided estimates of the range of response amplitudes generated by single-fiber inputs in cortical cells, using both the study of spontaneous events to see the range of properties across the population of inputs to a cell, and minimal stimulation to see the variability in a single input over time. Single-fiber inputs to cortical cells are large, fast, and extremely variable; both across the population of inputs to a cell, and over sequential responses to the same input. I then measured the size of input necessary to reach spike threshold, and combined that with estimates of the average single-fiber input size in those cells to estimate, assuming linear summation, that only 5-50 presynaptic inputs would need to be simultaneously active to cause the postsynaptic cell to fire a spike. Because this number is so low, the variability in the individual synaptic inputs to a cortical cell will have functional consequences for the timing and occurrence of its output.

Species differences. Several differences were noted between the spontaneous excitatory inputs to rat and cat cortical cells. Two cat cells showed an extremely high frequency of spontaneous IPSCs, something that was only seen in 1-2 rat cells under conditions were the slices were otherwise undergoing spontaneous epileptiform activity. The amplitudes of sEPSCs in cat cells were also quite small, on the same order as those rat cells showing the smallest sEPSC amplitudes (Fig. 3-8. There were no apparent differences between rat and cat cells in their response to minimal stimulation (threshold stimulation was not performed in cat cells).. There are a number of possible explanations for these differences in sEPSC amplitudes. It may be due simply to differences in cell size (those cat cells recovered morphologically were equivalent in size to the largest of the rat cells in our sample. This would also exacerbate the effects of series resistance (which was high in 4 of these cells), however this difference was maintained in the 3 cells with low series resistances, and the one cell with a moderate series resistance. The difference, particularly that seen in the increased frequency of

sIPSCs, might correspond to the differences in relative ages of the two animal populations used - however, these differences were not uniform across the population of cat cells studied. Most likely, there are also differences in the health of the slices, as the cat tissue was removed by biopsy from animals that had undergone several days of anesthesia. Unfortunately, our sample of cat neurons is much too small to draw any definitive conclusions about the importance of these differences, or their underlying cause. More striking, however, is the fundamental similarity between rat and cat cortical neurons, in the basic properties of their sEPSCs and meEPSCs. This suggests that the fundamental properties of synaptic integration in cortical neurons may be generic across all cortices.

3.4.1 Size of single-fiber inputs to cortical cells

The strength of this study is in its sampling of the populations of single-fiber inputs and mEPSCs from an enormous number of cells (204 rat cells, 8 cat cells; the cells not explicitly shown here were consistent with the rest). A small number of other studies have used paired recordings with sharp electrodes to characterize in detail the properties of a small number of identified connections between cortical cells (see Table 1.3.3 in Chapter 1 for summary), and an even smaller number of studies have looked at the properties of spontaneous, or miniature synaptic events, or minimal stimulation in cortical cells [29, 30, 146]. This study is the only one to have combined the high signal-to-noise ratio of whole cell patch clamp techniques, used by these latter studies, with the attention to the variations between cortical cell types characteristic of the former; in an identified region of cortex and across a number of cells which is simply not possible with paired recordings.

There are several problems endemic to the electrophysiological analysis of single-fiber input strengths. Using spontaneous events as a way to study the entire population of inputs to a cortical cell makes the tacit assumption that all of these inputs are equally likely to generate spontaneous events. This may not be the case. In cultured

cortical cells, the history of stimulation can bias particular synapses to generate the majority of mEPSCs [179]. In dentate gyrus granule cells, miniature IPSCs seem to preferentially be generated by synapses in the region of the soma and proximal dendrites (see Chapter 6, [240]). In the case of spontaneous events measured in the absence of TTX, particular cells may be prone to spontaneous activity in the slice.[18] There is no way to control for this possibility, though comparing sEPSCs with the responses to minimal stimulation, which may hit some of these normally silent inputs, gives some reassurance that there isn't a population of either very large or very small events out there routinely being missed. The hunt-and-peck method of traditional paired recording is also subject to the same problem, and may be especially biased towards the selection of strong connections due to the low signal-to-noise ratio of sharp electrode recordings. Only visualized techniques, with the ability to select connections between particular classes of cells, combined with a great deal of exhaustive work, will get around this problem with time. Finally, spontaneous EPSCs may be heavily biased towards action potential independent events (mEPSCs), which at least in some cases are of smaller size than the average action potential-driven input; this may cause the average size of single-fiber inputs to be underestimated.

Other studies on the size of inputs to cortical cells, and studies on the size of inputs in other brain regions. Single-fiber connections have a public relations problem. When you ask someone to estimate the size of a single synaptic connection, the usual answer is "small". The number which is most commonly cited in review articles and theoretical expositions of cortical function [181] is on the order of 100-200 μV. That is indeed the number obtained in the pioneering studies of synaptic strength in spinal motoneurons, and in several studies of hippocampal and cortical pyramidal cells (see Table 1.3.3 for summary and references). Most attempts

[18]This is suggested by the occasional appearance of repeated, identifiable, sEPSCs in some cells; in the limiting case a single presynaptic cell firing a relatively high-frequency train of action potentials can be identified by its characteristic response waveform.

at quantal analysis using current clamp recording with sharp electrodes, and/or deconvolution approaches [223, 45] also come up with an average quantal amplitude of 100 μV.

On the other hand, there are several recent studies in hippocampus and cerebellum [6, 189, 13] which come to conclusions very similar to those reached here for cortical cells - single-fiber connections are actually strong, a significant fraction of a millivolt in amplitude. Similarly, the sizes of sEPSCs and mEPSCs measured in a large number of voltage clamp studies in hippocampus [164, 163, 155, 70, 157] and cortex [146, 29, 30, 82, 83] as well as other brain structures [143, 142, 290] have described event properties very similar to those seen here for visual cortex. What is the source of this difference?

One major source of this disparity in size estimates is the difference in techniques. Most early studies of single-fiber connections were performed using sharp electrodes, while it is whole-cell patch clamp recording techniques that have generated these recent measurements of strong synaptic connections. Sharp electrode recordings are theorized to generate a somatic shunt conductance, which will decrease the input resistance of the recorded cell. This can decrease the amplitude of synaptic inputs recorded at the soma in current clamp, but is not sufficient to account for the size of the disparity seen here (see Section A.1.2 for examples of sEPSP amplitude distributions recorded with sharp electrodes and discussion of the difference between these techniques). Most importantly, with the poor signal-to-noise ratio of sharp electrode studies, EPSP amplitudes are measured as an average of failure and non-failure trials as the two cannot be reliably distinguished. If a significant fraction of inputs result in failures, this will drastically reduce the estimated EPSP amplitude.

A second source of this disparity is the difference in animal ages typically used; whole cell techniques are typically performed on juvenile animals, while sharp electrode recordings are typically performed in adults, and the spinal motoneuron studies

were performed in adult cats *in vivo*.[19] Cells from younger animals are smaller, have higher input resistances, fewer voltage dependent conductances [109], and might simply have stronger synaptic inputs.

On the other hand, there is a much simpler explanation for the source of this difference: it doesn't actually exist. While the most commonly cited numbers for single-fiber input strengths are the small ones estimated in early studies, Table 1.3.3 clearly shows that recent sharp electrode studies using paired recording of true single-fiber connections in cortex show connection strengths of similar sizes to those seen here. In the limiting case; it has been shown that responses to single-fiber connections between presynaptic pyramids and postsynaptic interneurons can reach 9 mV in amplitude on single sweeps (cortex, [261]); and can be sufficiently strong to excite the postsynaptic cell to fire with a single presynaptic spike, through a single morphologically-identified release site (hippocampus, [77]). It could be argued that these studies selected for particularly strong connections, to best overcome the low SNR of the recording technique. However, taking this data in combination with that of the present study which looked at the whole population of inputs to cortical cells, it is clear that single-fiber inputs are, on the whole, extremely strong.

A secondary, but still interesting question, is why this perception of weak single-fiber inputs persists in the community of physiologists and theoreticians not directly recording them. One reason is that many of these studies, particularly those using whole-cell techniques, are quite recent, and the earlier studies have been around a very long time. Another reason, at least for computational neuroscientists, is simplicity; if you take a realistic neuronal model, using "standard" passive parameters [243], and place onto its soma a "typical" synaptic conductance input, the response you get is about 200 μVin amplitude (e.g. see Fig. 4-21C). In fact, due to heavy filtering by the membrane capacitance, it is extremely difficult to simulate a large response to a rapid synaptic input in current clamp using standard parameters. This is a very

[19] *In vivo* studies have their own contribution to the problem of cell properties and event size, which will not be addressed here [22, 208].

useful fact, as it can place an important constraint on our estimates of cellular and synaptic parameters.

3.4.2 What generates EPSC variability within a single cell?

As discussed above, there are a large number of factors which might contribute to the variation in sEPSC amplitudes seen between different cells. It is less obvious what might cause such wide variability in event amplitudes within a single cell. Above, I identified two broad classes of factors, intrinsic and extrinsic, which might result in such variability.

In the case of sEPSCs, it is very likely that both types of factors play a role. It was shown above, that sEPSCs consist of both mEPSCs and action potential-dependent events, which can have overlapping but not identical amplitude distributions. This division itself will introduce a certain amount of amplitude variability into the population of sEPSCs. Similarly, there is increasing evidence that within the population of action potential-driven events, the response to a single input can vary over time (see below). Even if a given presynaptic cell fires only one action potential during the time period in which sEPSCs are collected, given the fact that a particular fiber will be in different states on subsequent action potentials, and that there is no reason for different fibers to be in the same state at the same time, this intrinsic variability will generate variation in sEPSCs. This is examined in more detail below.

Extrinsic factors are also likely to play a role in the generation of sEPSC amplitude. Considerable sEPSC variability is still seen in recordings using CsF electrodes in the presence of TTX, APV, and BMI (Fig. 3-7B,C), which isolates as much as possible a uniform, AMPAergic population of uniquantal events, and blocks most of the active conductances in the postsynaptic cell. If extrinsic factors do strongly influence synaptic responses, it becomes a developmental problem – if it matters to the synaptic effectiveness of an axon where on the postsynaptic cell it synapses, then the axon guidance problem becomes not only one of finding the right cell, but of finding

the right piece of the right cell. The fact that in many cell types different presynaptic cell classes do target very limited dendritic regions of the postsynaptic cell (see Chapter 6) suggests that there is some important functional difference between inputs to different locations to the postsynaptic cell.

Figure 3-10 shows that there is no strong negative correlation between the rise times and amplitudes of spontaneous inputs to cortical cells. A number of studies have taken such an absence of correlation as proof that synaptic location does not contribute to the generation of response amplitude [244, 247, 163, 164, 274, 104, 209]. However, there is a problem with this analysis. In spite of the fact that these two variables are not negatively *correlated*, they are negatively related - fast events may cover the entire amplitude range, but slow events are restricted to being small. Computational analysis shows that as these two parameters change with distance at different rates, they should not be expected to be negatively correlated, but instead to show a negative relationship such as this one in the presence of electrotonic filtering (see Chapter 4). And in fact, there is a correlation between event rise times and half widths (Fig. 3-10D) in most cells, which is a much better indicator of an effect of electrotonic filtering [203] (Chapter 4). Together, these facts suggest that electrotonic filtering does play a significant role in the generation of sEPSC amplitude variability. However, the fact that the amplitudes of the fastest events do cover such a wide range, while not evidence against an effect of cable filtering, is evidence *for* the presence of an additional source of sEPSC variability (see Chapter 4 for a much more detailed discussion of these issues).

3.4.3 Properties of single inputs over time

Minimal stimulation was used to study the properties of single-fiber inputs over time. The sharp threshold for minimal stimulation response, combined with the high failure probability and the similarity between meEPSCs and sEPSCs in the same cell all strongly suggest that this increasingly commonly used technique [168, 249, 3, 291,

283, 140, 156] is successful at stimulating one, or at most a small number, of fibers. However, there are problems with this technique, most of which were discussed above. The possibility that one is stimulating 2 or 3 fibers, instead of just one, or that in some cases stimulation or conduction, rather than transmission, may fail, means that results obtained with this technique must be interpreted with caution. The qualitative results of minimal stimulation experiments presented here, that single fiber inputs are variable and quite fallible over time, and that they are consistent in size with being made up of one or a small number of quanta; are all consistent with the results of paired recordings in cortical cells [261, 264, 260, 60].

The most interesting result obtained using minimal stimulation in this study was that the kinetics of meEPSCs are much less variable than those of sEPSCs in the same cell (Fig. 3-13). This conclusion is robust, at least in the subset of tested connections where one fixed-latency input could clearly be identified. If two or more fibers were actually being stimulated, this would, if anything, artificially increase the apparent amount of kinetic variability; failures of stimulation would have no effect on the response kinetics for the successful trials. The example inputs used were unfortunately not uniquantal, and showed mildly peaky, though generally Gaussian amplitude distributions. Therefore any temporal dispersion between release of quanta, or spatial dispersion in the possible multiple release sites involved in this connection will also cause an overestimate of kinetic variability. Therefore, the data presented here provides an upper bound on the amount of kinetic variability in a single fiber inputs. Similarly, because the events subjected to detailed analysis were not uniquantal, they cannot easily be used to estimate the amount of quantal variability at a single release site (rather than between release sites). However, it is clear that, at least in the absence of TTX, single inputs are variable in amplitude, and more notably, for the most part these amplitude distributions are not particularly skewed.[20] These two

[20]The response to the second of two pulses occasionally showed a mildly skewed amplitude distribution, presumably because of a slight bias towards larger-amplitude events induced by paired-pulse facilitation. However, these distributions were always much less skewed than those seen for sEPSCs.

facts will become important in Chapter 4, when they will be used to estimate the relative contributions of various sources of synaptic variability to the generation of skewed sEPSC amplitude distributions.

3.4.4 Estimates of spike threshold

A number of methods have been used to estimate spike threshold in pyramidal cell types throughout the brain [7]. The current or charge injection necessary to produce a spike, the amplitude of a just subthreshold EPSP, the point at which the spike takes off from the surrounding EPSP (measured as divergence from failure trials or by a slope threshold for spike onset), the voltage response to just non-spiking current injections, etc. All of these methods come up with similar answer: spike threshold is approximately 12-20 mV above resting potential in the slice [7, 189, 13, 6], and behaves as an absolute voltage threshold, rather than an amplitude threshold relative to the "resting" membrane potential – if the cell is hyperpolarized, a larger input is necessary to make it spike. The important fact about these facts is that a) these estimates are very consistent, yielding reliable predictions applicable across a variety of cell types; and b) if the cell is depolarized, e.g. by spontaneous background activity *in vivo*, to near firing threshold, only a slight perturbation may be sufficient to make it spike [149]. Influences on the cell, such as neuromodulators, which can alter its resting potential, can dynamically alter the size of an input necessary to reach threshold, as well as simultaneously affecting synaptic integration by changing the input resistance of parts of the cell. Similarly, differences between the intrinsic nonlinear properties of cells, e.g. whether they are bursting or regular-spiking cells, will affect their spike threshold, and hence their degree of functional convergence.

3.4.5 Estimates of functional convergence

Most older estimates of functional convergence have relied on the small estimates of single-fiber input size discussed above; these have resulted in estimates that at

least 100-400 inputs will need to be simultaneously active to make a (in this case, hippocampal) pyramidal cell fire an action potential [7, 6, 259, 181]. While still much smaller than the total number of inputs to the average cell, this estimate is large in the important sense that the properties of the individual inputs making up this threshold cohort will be averaged away.

The estimate of functional convergence obtained here, in contrast, is much smaller - only 5-50 inputs must be synchronously active in order to generate a spike. These numbers are remarkably consistent with those obtained in recent studies in hippocampus [189] and cerebellum [13]. Of course, these estimates must be taken with the usual caveats. If inputs are desynchronized, more of them will be necessary. If they sum nonlinearly, again, more will be necessary. If there is strong inhibition [189], or a lot of background activity increasing the cell's resting conductance [22, 208], more will be necessary. It is a lower bound. In the limiting case of a very small, high input resistance cell such as a hippocampal interneuron, the lowest bound has been reached - a single presynaptic spike, mediated via a single bouton, is sufficient to make the postsynaptic cell fire [77].

Do inputs sum linearly?

It can be easily noted that the threshold synaptic current shown in Figure 3-16 is very large, on the order of 1 nA. While this is on the large end of that seen in our sample, and is much larger than the amplitude of the steady-state current injection necessary to cause spiking, it is not that much larger than that seen in other cells. And yet our apparent voltage threshold of 20mV above rest would suggest that much less current would be required. There are two possible explanations for this fact. The first is that linear summation is not a good model for synaptic integration, that nonlinear interactions between synapses combined with interference by voltage-dependent currents cause combined inputs to be "worth" much less than those single inputs alone. The second is a profound effect of silent, or "shunting" inhibition.

Experimental studies have shown that, in the absence of the nonlinear effects of shunting inhibition, linear summation is indeed a good model for the interaction between EPSPs; even when those EPSPs are generated at sites presumed to be near to one another on the postsynaptic cell [7, 206, 31].

The second explanation for the apparently large size of threshold synaptic currents is that a large component of that synaptic current is in fact inhibitory, acting as a shunt to ground [120, 122, 33]. In fact, when cells undergoing large-amplitude stimuli were depolarized, it was found that they were receiving massive inhibitory input. In many cells, feedforward inhibition was so strong that they could not be brought to spike threshold via large-amplitude stimulation of the white matter – as stimulus intensity was increased, response amplitude first increased, and then decreased as excitation was overwhelmed by inhibition. In the presence of bicuculline, not only were small-amplitude stimuli capable of evoking action potentials from a similar location, such action potentials usually cascaded into full-blown seizure-like activity. Such inhibition has been shown to increase the number of combined synaptic inputs necessary to generate an output [189]. Though it was not tested systematically, a few observations suggested that those cells with the least spike latency jitter tended to be subject to strong inhibition. It is an interesting question of whether shunting inhibition, in addition to preventing spike firing through the powerful influence of basket and chandelier cells on the soma and axon hillock of pyramidal cells [106], also acts to shape the *timing* of an output spike; only allowing the cell to fire in a narrow window of time depending on the time course of the IPSP [117].

3.4.6 Implications for cortical information processing

If you do need only a small number of inputs to generate an output, at least under some circumstances, it has strong implications for the nature of cortical information processing. A recent study has shown that the spike-encoding (threshold) mechanism in cortical cells is very reliable [149] – it will accurately represent the details of the

timing of an input current waveform in the pattern of output spikes, up to some limit. If large, single-fiber inputs are riding on a pattern of background depolarization, they will have a large impact on the detailed timing of the cell's output spikes. This is a far cry from a simple integrate-and-fire model [228, 12].

The data presented above, and similar results obtained in hippocampal pyramids [189] show that indeed, the variability shown to be characteristic of single-fiber inputs appears in the output spike timing of the postsynaptic cell. This is perhaps an ugly side effect of this sensitivity to single inputs – if you average many inputs to make an output, it doesn't much matter if your inputs are noisy. Given the fact that this synaptic "noise" has consequences for the next cell down the line, we are therefore forced to ask whether it actually plays some functional role [86, 28, 5], particularly in the light of the fact that regular spiking cells seem to work very hard to accurately encode the details of their subthreshold inputs [149]. And it is extremely interesting in light of the recent studies suggesting that the timing of spikes in cortex in response to sensory stimuli can be very repeatable [12]. These cells certainly seem to function well in spite of this "noise" – perhaps they are actually doing so because of it (see Chapter 7).

Another interesting question is suggested by the idea that only 1% of the inputs to a cell are required to make it generate an output. Namely, what do you do with the rest? Neural network studies suggest that such wide fan-in could be used to allow the cell to participate in multiple representations; if this is combined with an output encoding mechanism using spike timing rather than just a binary spike-or-don't signal, a given cell could store many input-output transformations. Simple simulations of a realistic pyramidal cell model have in fact used it to store on the order of 100 images [169, 170].

Modulation of dynamic range. Finally, the powerful effect of inhibition on spike failure and spike timing seen in Figure 3-16 suggests an important processing role for all of our above caveats on why this estimate of functional convergence is in fact

a lower bound. As the cell receives more or less background input, or more or less inhibition, or changes the state of its active conductances through short- or long-term modulation [138, 273], it will dynamically change its functional convergence. Even more interestingly, the temporal sculpting effect of shunting inhibition [117], and the dynamics of its active conductances will allow it to change this convergence in time as well as in space; this will allow it to make the timing of its output spikes more or less accurate, and make the window for temporal convergence of its inputs narrower or wider. Given enough inhibition and background activity, the cell would indeed revert to a leaky integrator, when such behavior was suggested by the amount of background activity. This ability to dynamically alter its functional convergence would allow the cell transparently to encode information in different ways depending on the current sensory and motivational context; and would provide a rich substrate for cellular and sensory plasticity.

3.5 Figure Legends

Figure 3-3: Cortical cells receive spontaneous synaptic inputs. Spontaneous synaptic events in a cat layer III cell. The bottom trace shows a stretch of current recorded from a cell voltage-clamped at -70mV. Spontaneous inward synaptic currents can be seen as downwards deflections; there are probably 5 of them in this trace. One event (shown by box) is expanded in the upper trace.

Figure 3-4: Properties of spontaneous synaptic events. A. Amplitude histograms (above) and traces (below) of spontaneous excitatory synaptic inputs to a layer V cell. Events are large, fast, and amplitude distributions show a characteristic skewed shape. Bath solution contains $50\mu M$ bicuculline methiodide (BMI). B. Traces before (above, V_{hold}=-70mV) and after (below, V_{hold}=-60mV) bath application of CNQX ($10\mu M$) in a different cell in the absence of bicuculline. C. Holding a cell at -40mV, above the reversal potential for $GABA_A$-mediated IPSCs, makes a small population of outward events clearly visible. Upper trace: outward (upward) IPSCs can be seen to occur at a slower frequency than EPSCs (downwards). The different kinetics of sEPSCs and sIPSCs can be seen in the lower, expanded trace. D. Amplitude distributions from a layer III cell before and after bath application of BMI ($50\mu M$). E. Relative frequency of sEPSCs and sIPSCs. 33 cells were held at potentials where sIPSCs were clearly visible as outwards events (-50 - -30mV, usually -40mV), and the number of inward and outward events were counted in time periods of 25-250 seconds. No automatic detection was used. Percentage of all events which were IPSCs is plotted for each cell, broken down by layer and species. "Other" cells were ones whose layer was unknown. F. Absolute frequency of sIPSCs in the same population of cells.

Figure 3-5: Voltage dependence of sEPSCs. A. Average sEPSCs from one cell at a number of different holding potentials. sEPSCs reverse at 0mV. B. Cumulative amplitude histograms for events at a variety of holding potentials for a cell recorded in TTX ($1\mu M$), APV ($30\mu M$), and BMI ($50\mu M$). C,D. The detection threshold for spontaneous events complicates interpretations of voltage dependence. These plots summarize the amplitude distributions as a function of voltage for the cells shown in A(C) and B (D). The total length of the bar represents the range of event amplitudes seen. The ends of the box represent the 25th and 75th percentiles, and the bar inside the box is the median amplitude. These cells were recorded using CsF-based solutions.

Figure 3-6: sEPSCs show intra- and inter-cellular variations in kinetics. A. Distributions of sEPSC kinetic parameters show characteristic skewed shapes sim-

ilar to that seen for amplitudes. These parameter distributions are for the cell shown in Figure 3-4A. B,C. Event kinetics vary widely between cells. Averages of 490 sEPSCs from two example cells showing widely different kinetics. Both are rat layer III cells recorded in the presence of TTX (1 μM), APV (30 μM), and BMI (50 μM). B. A cell from a P12 rat. R_{in}= 107.5 $M\Omega$. R_s= 2 $M\Omega$. C. A cell from a P19 rat. R_{in}= 87 $M\Omega$. R_s= 8 $M\Omega$.

Figure 3-7: sEPSCs are made up of action potential-dependent and independent events. A. Amplitude distribution of sEPSCs from a layer V cell showing a large reduction in event frequency and amplitude with bath application of TTX (1μM) to block action potential-dependent events. B. A layer III cell showing no loss of events on washing in TTX, and, if anything, a small increase in the frequency of medium amplitude events. C,D. Cumulative amplitude histograms for mEPSCs recorded in the presence of TTX in 29 layer II/III cells (C) and 27 layer V/VI cells (D). The majority of these cells (solid lines) were recorded in TTX (1μM), APV (30μM) and BMI (50μM), with CsF electrodes and (except in one case) 50 mM bath dextrose, which may increase mEPSC amplitude (see Chapter 5, [278, 281, 275]). Two cells were recorded under the same conditions except with KGlu-filled electrodes (empty squares), and 3 cells were recorded with KGlu electrodes either in TTX alone (circles) or TTX + BMI (lines).

Figure 3-8: Distribution of sEPSC amplitudes across the population of cells. A. Cumulative amplitude distributions for sEPSCs in 10 rat layer II/III cells, and 2 cells of unknown layer (dashed lines with circles). Thick line is for a cell recorded in 50 μM bicuculline. B. Cumulative amplitude distributions for sEPSCs in 12 rat layer V/VI cells. Thick line is for a cell recorded in 50 μM bicuculline (also shown in Figure 3-4A). C. Cumulative amplitude distributions for sEPSCs in 5 cat cells. The only layer V/VI cell, is shown by a thick, dashed line, the rest of the cells were in layer III. D. Cumulative amplitude distributions for 8 rat cells and 1 cat cell (filled circles) in current clamp. Dashed line with squares shows events for an interneuron from upper layer V (also shown in Figures 3-14A and 3-16A). Thick line is for a cell recorded in 50 μM bicuculline (also shown in Figure 3-4A). E. Distribution of mean sEPSC amplitudes for the cells shown in A-C, and the cells shown in Figure 3-7B and C recorded in the presence of 1 μM TTX. "Other" refers to cells whose layer was not recorded. F. Distribution of coefficients of variation of sEPSC amplitude for the cells shown in E.

Figure 3-9: Sources of sEPSC variation between cells. A. Mean sEPSC or mEPSC amplitude vs animal age, for rat cells whose cumulative amplitude distri-

butions were shown in Figure 3-8. B. Mean and C. maximum sEPSC or mEPSC amplitude plotted against effective R_s. Cell layer, species, and whether events were sEPSCs (no TTX) or mEPSCs (with TTX) shown in legend.

Figure 3-10: What generates EPSC variability? A. Rise time and amplitude are not negatively correlated in a large population of sEPSCs from one cell. B. Amplitude and rise time distributions for the cell in A. C. A similar lack of relationship between rise time and amplitude is seen in current clamp (left) and in the presence of bicuculline (right), indicating that it is intrinsic to the cell and not due to other sources of variability, such as heterogeneity of input types.D. Rise times and half widths of sEPSCs are significantly correlated (p¡0.05), suggesting a role for synaptic location in controlling synaptic event amplitude.

Figure 3-11: Variability in a single input over time. A. Variation in a single input over time. Responses to minimal stimulation in 3 cells are plotted as a function of successive stimulus trials. Amplitudes were measured as the average of a fixed 1-ms window located at the peak of the average response. Responses are plotted for both the first (circles) and second (squares) of two paired stimuli (ISI 50 ms). Open symbols were identified as failures. B. Effect of increasing stimulus amplitude. 1. Response amplitude vs stimulus strength, for a single stimulus (the first of a pair). Failures are identified as open symbols. 2. Mean amplitude (error bars are std. error) and % failures as a function of stimulus intensity for the data shown in 1. 3. Response amplitude vs. stimulus strength for another cell. Failures are not identified. C. Histogram of % failures for 27 cells, including 5 cat cells. Single (or first) stimuli only.l

Figure 3-12: Minimal evoked EPSCs are very similar to sEPSCs. Responses to minimal (putatively single-fiber) stimulation are compared to spontaneous events in the same cell for 3 cells. A. Rat layer II/III cell. B. Cat layer III cell. C. Cat layer V/VI cell. Minimal evoked EPSCs (meEPSCs) are shown to the left, including clear failures of transmission. Below each set of traces are shown examples of consecutive sEPSCs from the same cell. To the right are amplitude histograms for larger populations of meEPSCs (upper) and sEPSCs (lower) from each cell. The meEPSC amplitude histograms include a peak near 0 representing failures.[21] Amplitude histograms in B and C were taken from cells undergoing paired pulse stimulation (2 pulses 50 ms apart), and contain responses to both pulses (the traces at left are

[21] Due to the stimulus artifact, the failure peak may not be exactly 0 pA in amplitude. However, its shape is invariant and clearly does not contain a synaptic inflection.

responses to the first pulse only). In B, responses were indistinguishable between the two pulses. In C, responses to the second pulse failed less frequently an tended towards larger amplitudes; they are shown as white bars.

Figure 3-13: meEPSCs show less kinetic variability than spontaneous events. A. Single-fiber responses show a narrow distribution of latencies. Latency of onset (black bars) measured as 5% of peak amplitude[22], and of meEPSC peak (hatched bars) relative to stimulus onset.[23] B. 1,3,4. meEPSC amplitude distributions with failures removed. Distributions are peaky, and Gaussian, rather than skewed, in shape. Responses to both of paired stimuli shown, distributions to first stimulus alone were also unskewed. 2. Skewed distribution of spontaneous EPSC amplitudes for the cell shown in 1. C. Rise time distribution for minimally evoked inputs (left) is narrower and less skewed than that for spontaneous events in the same cell (right). D. Rise time vs half width plot for evoked responses (both stimuli, left) and spontaneous events (right). E. Rise time vs amplitude plot for evoked responses (both stimuli, left) and spontaneous events (right). A, B1,2, C-E all show data from the same cell.

Figure 3-14: Only a small number of inputs are necessary to bring the postsynaptic cell to threshold. A. Spontaneous inputs and minimal evoked responses in a layer V non-pyramidal cell (left). Increasing the amplitude of the stimulus was sufficient to bring the cell to threshold on 50% of trials (right). Inset shows responses to intermediate levels of stimulation, where distinguishable inputs appeared to be added sequentially as the stimulus intensity was increased. B. Threshold stimulation in a regular-spiking neuron. Spontaneous EPSPs are shown in inset. This cell only spiked to the second of two paired pulses at an interval of 50ms. C,D. Histograms of peak amplitude of either the EPSP or the spike, depending on whether the cell spiked or not. Each cell was held at 2 potentials, and the absolute voltage, rather than the voltage relative to the holding potential, is shown. C. Data for the cell shown in A. Responses to the first of the two paired pulses are shown as white bars, the second as black. D. Data for the cell shown in B, black and white bars show the two different holding potentials.

Figure 3-15: Cells utilize a voltage threshold for firing. A1. Layer V cell firing spontaneously in a slice when depolarized to near threshold with DC current.

[22] As response amplitude varies between trials, this onset measure will introduce a certain amount of variability in and of itself.

[23] As peak latency is measured relative to the stimulus, not to onset, onset variability will be convolved with intrinsic and noise-induced variability in peak latency.

Cell fires randomly due to baseline fluctuations and sEPSPs. 2. Local maxima of data for cell in 1. A longer stretch of data from the cell in 1 (data shown in 1 has time axis values appropriate for its location in 2) was low-pass filtered, and its local maxima were detected using a simple derivative sign algorithm. This finds the peaks of both the spikes and the subthreshold baseline fluctuations, similar to the analysis for evoked inputs shown in Figure 3-14C,D. Local maxima are plotted against time, and suggesting that every time the cell goes above a critical voltage, it fires. B1. Local maxima plot for cell filled with CsF and exhibiting bursting and plateau behavior. This cell went through periods of 0.5Hz bursts on an increasingly depolarized plateau. When hyperpolarized by injected current (at 40 and 115 seconds in B1), it remained at a lower stable point with only occasional bursting, and then began to climb to the same plateau. 2. Expansion of one of these bursting periods shows the same voltage threshold behavior as in the cell in A. Periods during individual bursts are indicated by gray bars. 3. Expansion of the data shown in 2, to show the structure of individual bursts. Each burst consisted of 4-7 spikes, with the middle spikes much shorter than the first or last. These middle spikes produce the intermediate-amplitude maxima in 2. Times in 2, 3 correspond to the appropriate section of 1.

Figure 3-16: Variability in inputs is reflected in output variability. A. 20 identical stimuli to the cell shown in Figure 3-14A, 9 of which generate a spike. B. Spike timing in a regular spiking cell is much less variable. Note different time base than in A. C. Variability in output spike timing is not a result of injury to the cell. Threshold stimuli were applied to a cell recorded in cell-attached patch mode, and show a similar pattern of failures and variability. D. Voltage clamp of the threshold synaptic EPSP in B. E. Variation in spike times around the mean latency for the cells in A and B, and 2 other regular-spiking cells. F. Significant correlation between spike latency and standard deviation of spike time, for 7 cells. One cell measured from spikes to threshold stimuli in voltage clamp ($p<0.02$). Two cells fired to multiple sequential stimuli - one (shown in C) to both of two paired stimuli, and the other to all 5 of a 5-stimulus train (ISI 50 ms in both cases), the responses to each stimulus is shown as a separate point.

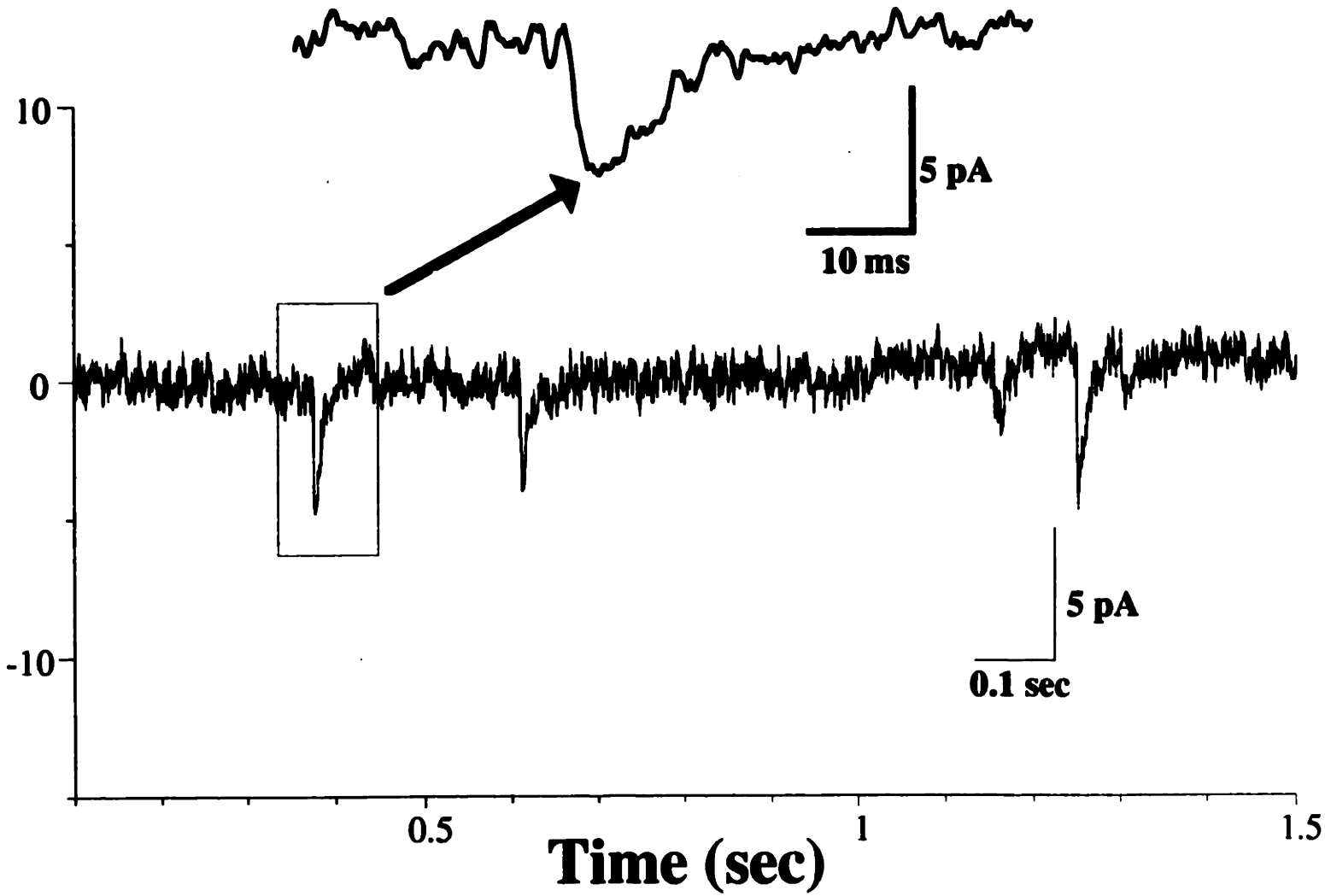

Fig. 3 - 3

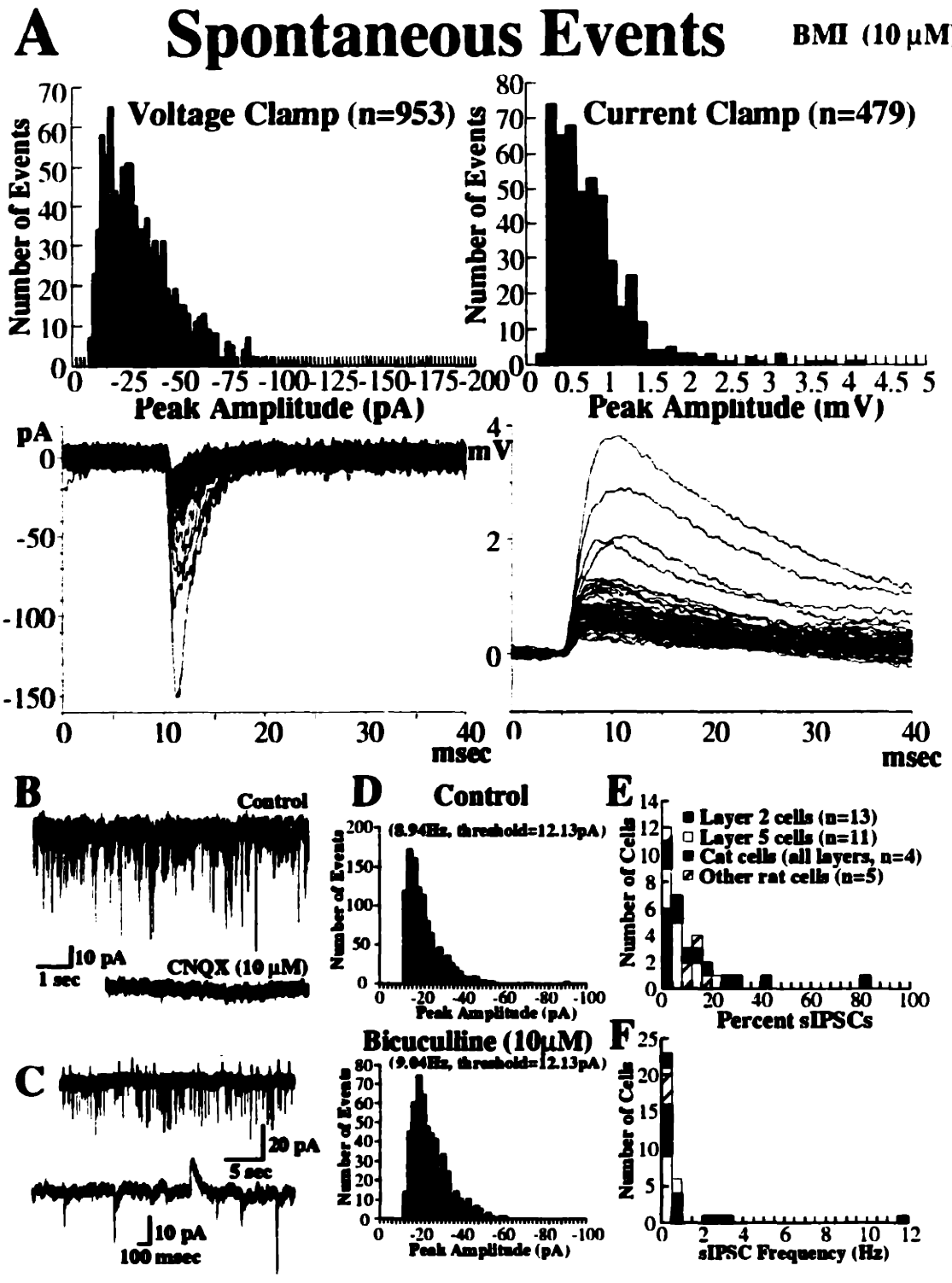
A
Spontaneous Events
BMI (10 μM)
Voltage Clamp (n=953)
Current Clamp (n=479)
Number of Events
Peak Amplitude (pA)
Peak Amplitude (mV)
pA
mV
msec
B
Control
10 pA
1 sec
CNQX (10 μM)
C
20 pA
5 sec
10 pA
100 msec
D
Control
(8.94Hz, threshold=12.13pA)
Bicuculline (10μM)
(9.04Hz, threshold=12.13pA)
E
Layer 2 cells (n=13)
Layer 5 cells (n=11)
Cat cells (all layers, n=4)
Other rat cells (n=5)
Number of Cells
Percent sIPSCs
F
sIPSC Frequency (Hz)

Fig. 3 - 4

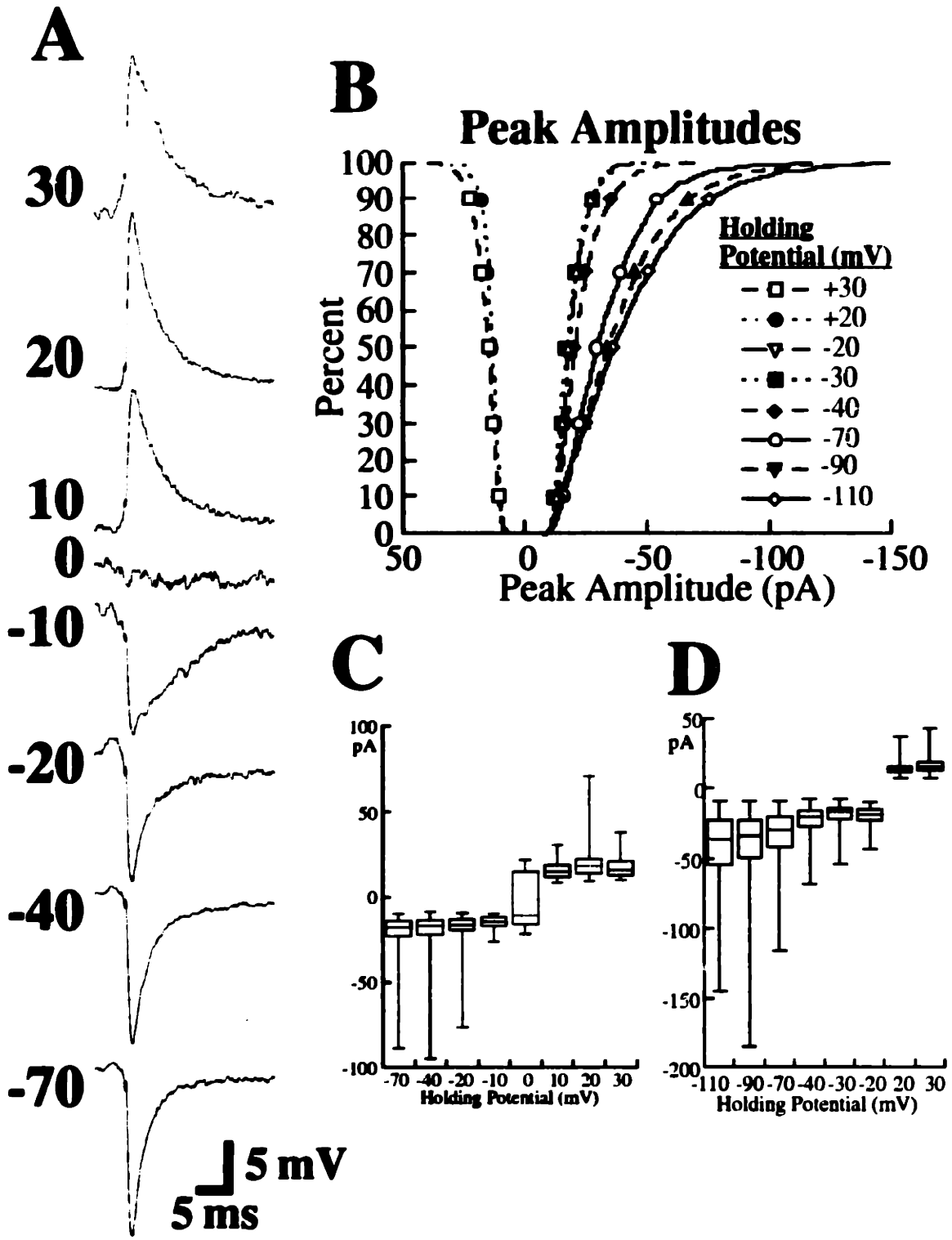
A
30
20
10
0
-10
-20
-40
-70
5 mV
5 ms
B
Peak Amplitudes
Percent
Peak Amplitude (pA)
Holding Potential (mV)
+30
+20
-20
-30
-40
-70
-90
-110
C
pA
Holding Potential (mV)
D
pA
Holding Potential (mV)

Fig. 3 - 5

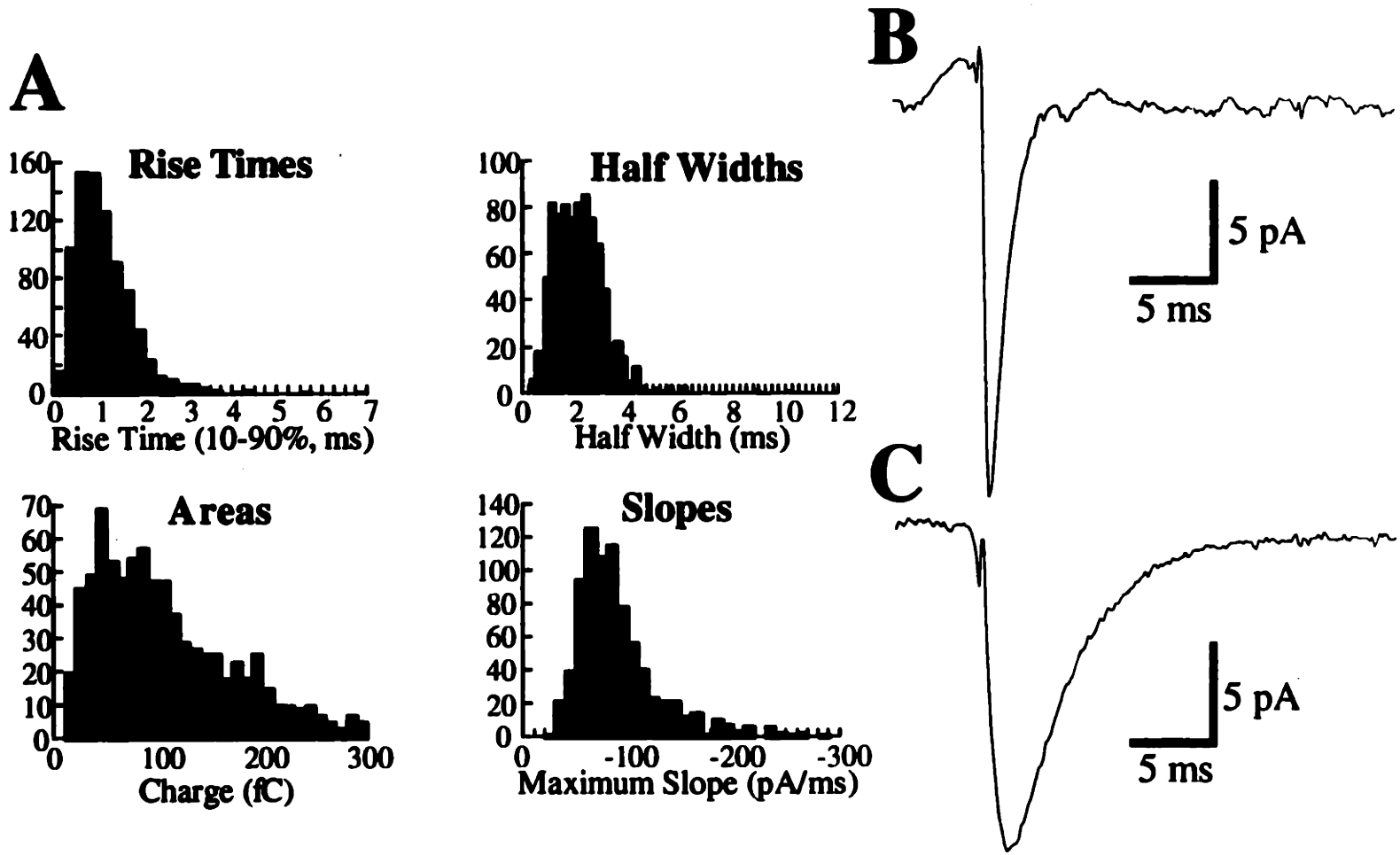
A
Rise Times
160
120
80
40
0
0 1 2 3 4 5 6 7
Rise Time (10-90%, ms)
Half Widths
100
80
60
40
20
0
0 2 4 6 8 10 12
Half Width (ms)
Areas
70
60
50
40
30
20
10
0
0 100 200 300
Charge (fC)
Slopes
140
120
100
80
60
40
20
0
0 -100 -200 -300
Maximum Slope (pA/ms)
B
5 pA
5 ms
C
5 pA
5 ms

Fig. 3 - 6

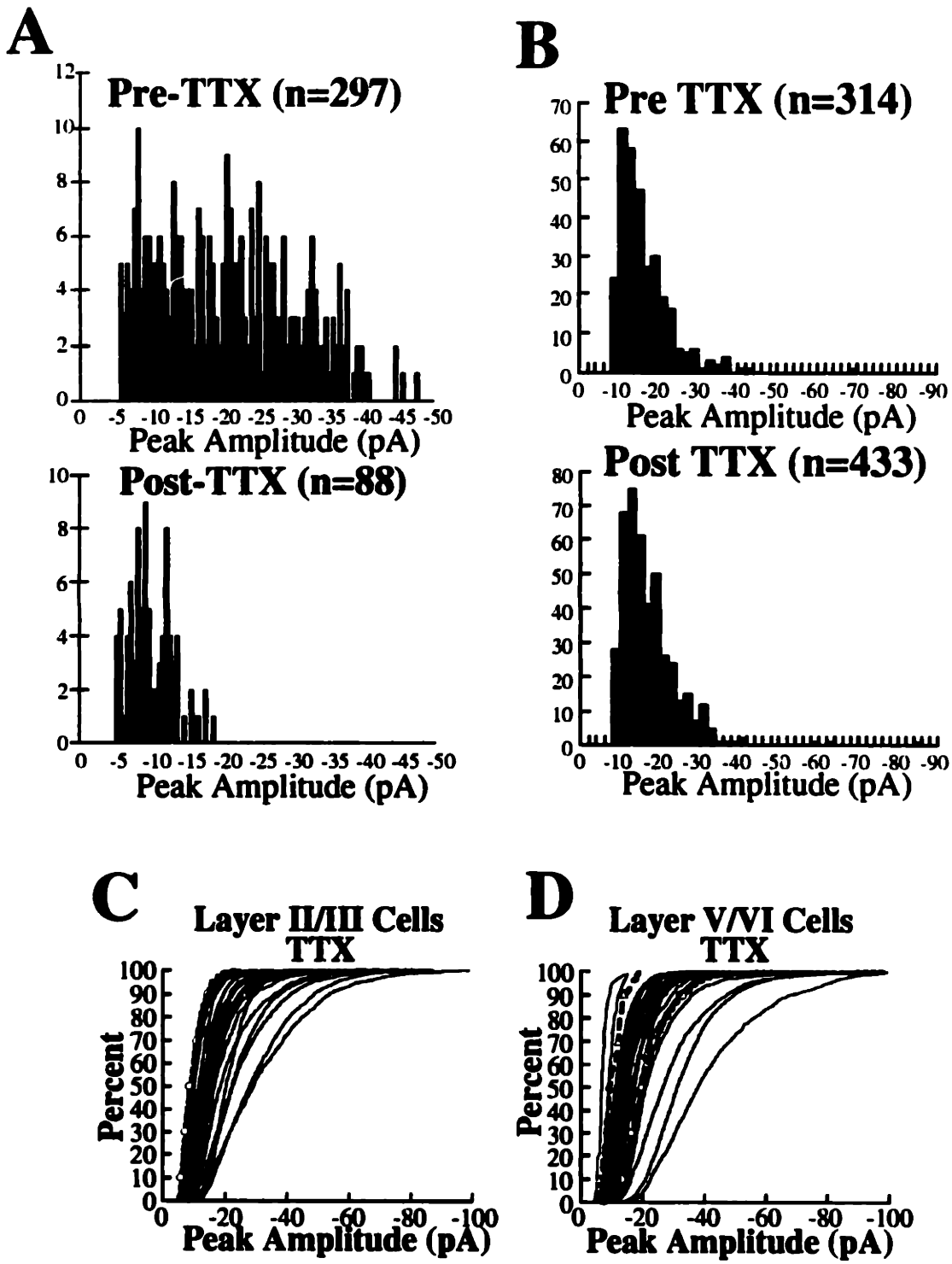
A
Pre-TTX (n=297)
Peak Amplitude (pA)
Post-TTX (n=88)
Peak Amplitude (pA)
B
Pre TTX (n=314)
Peak Amplitude (pA)
Post TTX (n=433)
Peak Amplitude (pA)
C
Layer II/III Cells
TTX
Percent
Peak Amplitude (pA)
D
Layer V/VI Cells
TTX
Percent
Peak Amplitude (pA)

Fig. 3 - 7

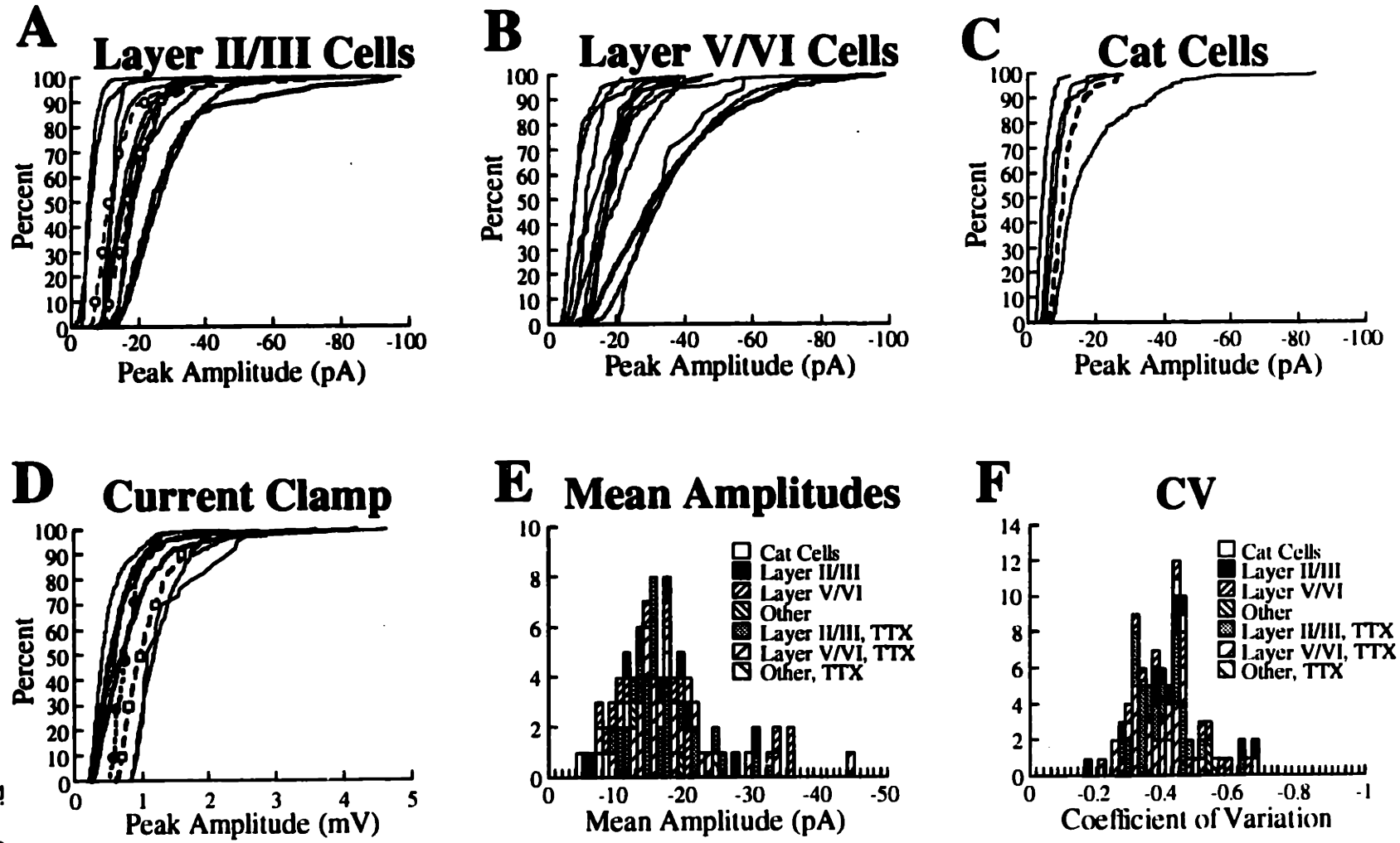
A
Layer II/III Cells
Percent
Peak Amplitude (pA)
B
Layer V/VI Cells
Percent
Peak Amplitude (pA)
C
Cat Cells
Percent
Peak Amplitude (pA)
D
Current Clamp
Percent
Peak Amplitude (mV)
E
Mean Amplitudes
Cat Cells
Layer II/III
Layer V/VI
Other
Layer II/III, TTX
Layer V/VI, TTX
Other, TTX
Mean Amplitude (pA)
F
CV
Cat Cells
Layer II/III
Layer V/VI
Other
Layer II/III, TTX
Layer V/VI, TTX
Other, TTX
Coefficient of Variation

Fig. 3 - 8

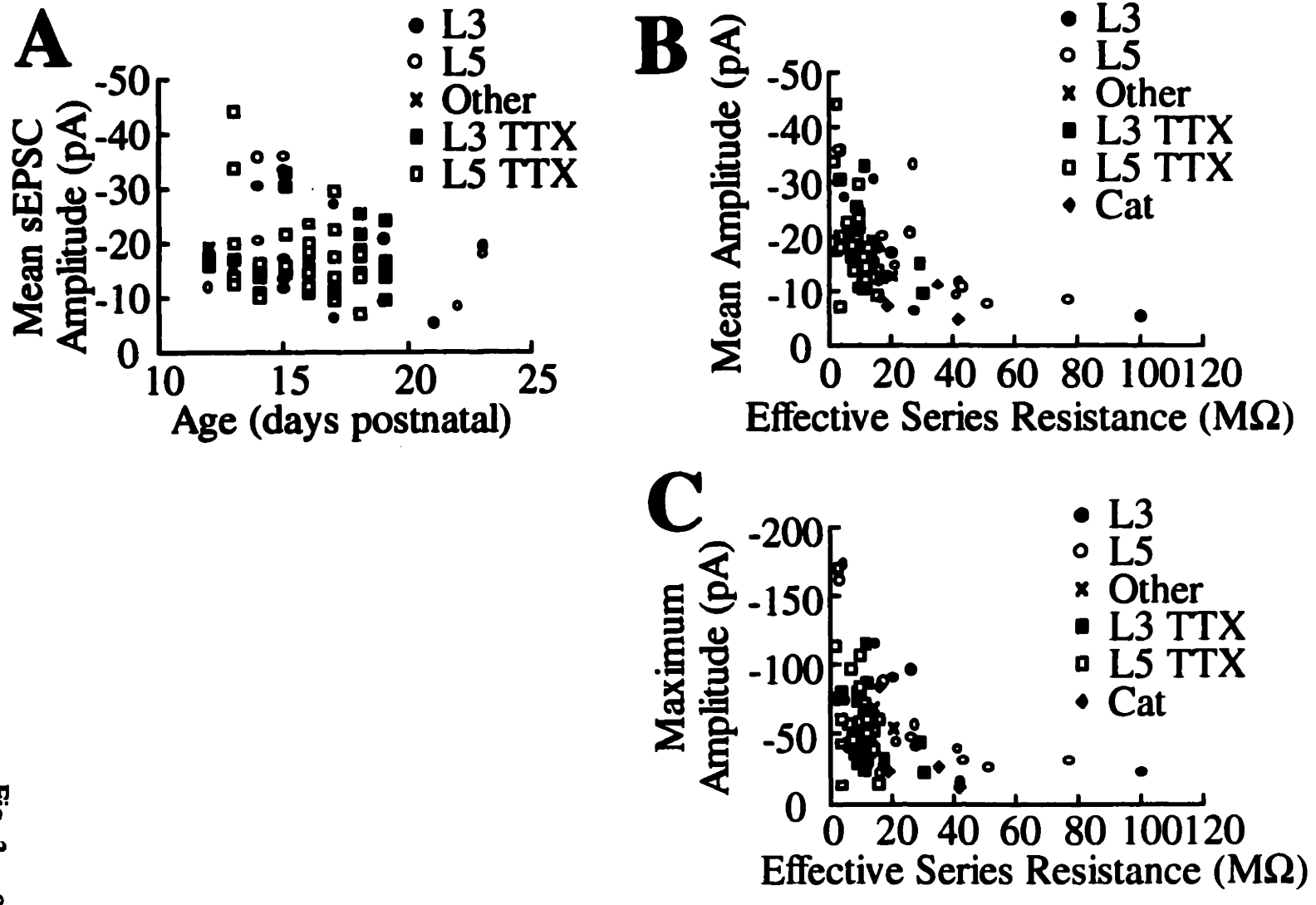
A
Mean sEPSC Amplitude (pA)
-50
-40
-30
-20
-10
0
10
15
20
25
Age (days postnatal)
L3
L5
Other
L3 TTX
L5 TTX
B
Mean Amplitude (pA)
-50
-40
-30
-20
-10
0
0 20 40 60 80 100120
Effective Series Resistance (MΩ)
L3
L5
Other
L3 TTX
L5 TTX
Cat
C
Maximum Amplitude (pA)
-200
-150
-100
-50
0
0 20 40 60 80 100120
Effective Series Resistance (MΩ)
L3
L5
Other
L3 TTX
L5 TTX
Cat

Fig. 3 - 9

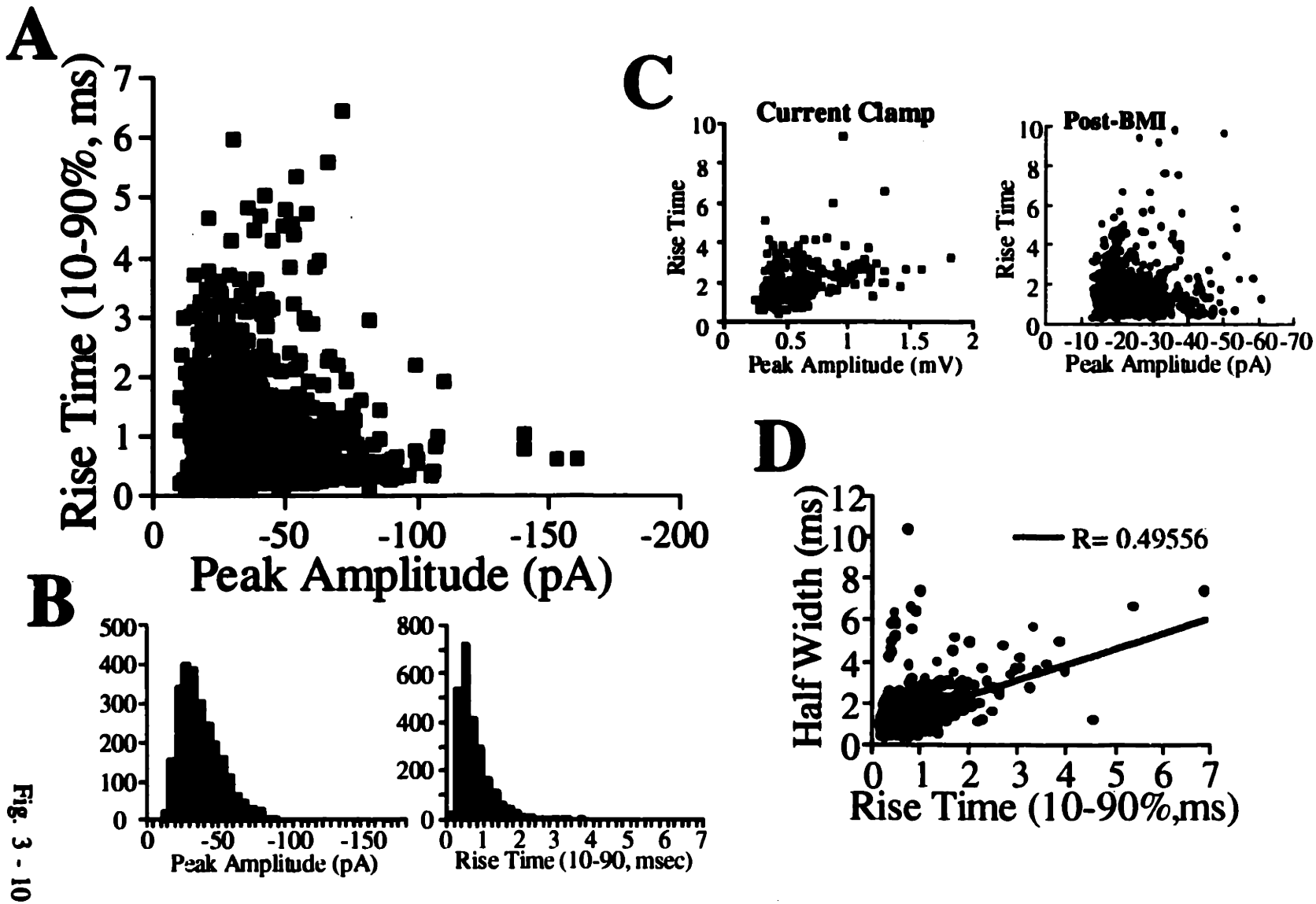
A
Rise Time (10-90%, ms)
Peak Amplitude (pA)
B
Peak Amplitude (pA)
Rise Time (10-90, msec)
C
Current Clamp
Post-BMI
Rise Time
Peak Amplitude (mV)
Peak Amplitude (pA)
D
Half Width (ms)
R= 0.49556
Rise Time (10-90%,ms)

Fig. 3 - 10

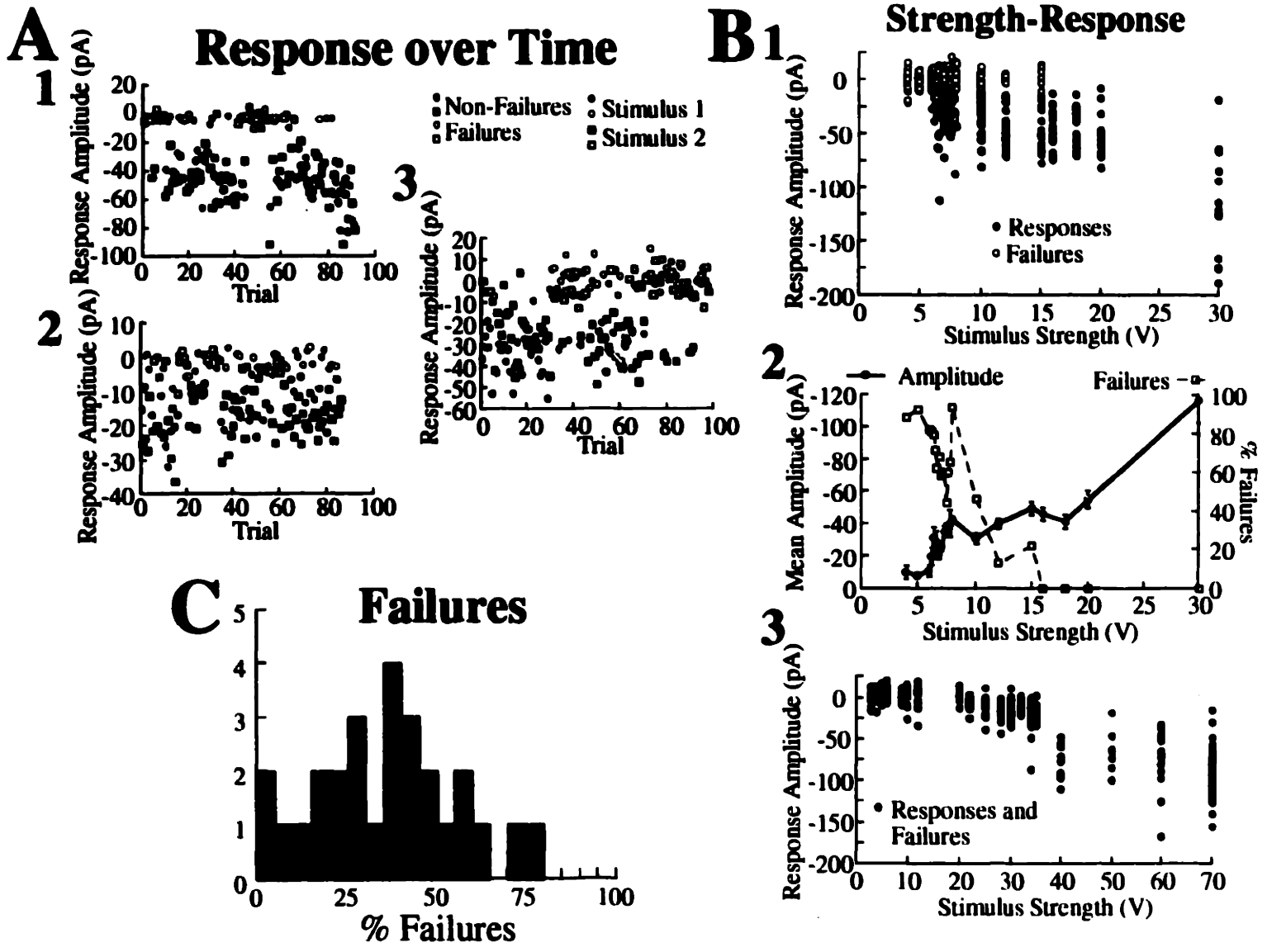
A
Response over Time
1
2
3
Non-Failures
Failures
Stimulus 1
Stimulus 2
Response Amplitude (pA)
Trial
B
1
Strength-Response
Responses
Failures
Stimulus Strength (V)
2
Amplitude
Failures
Mean Amplitude (pA)
% Failures
3
Responses and Failures
C
Failures
% Failures

Fig. 3 - 11

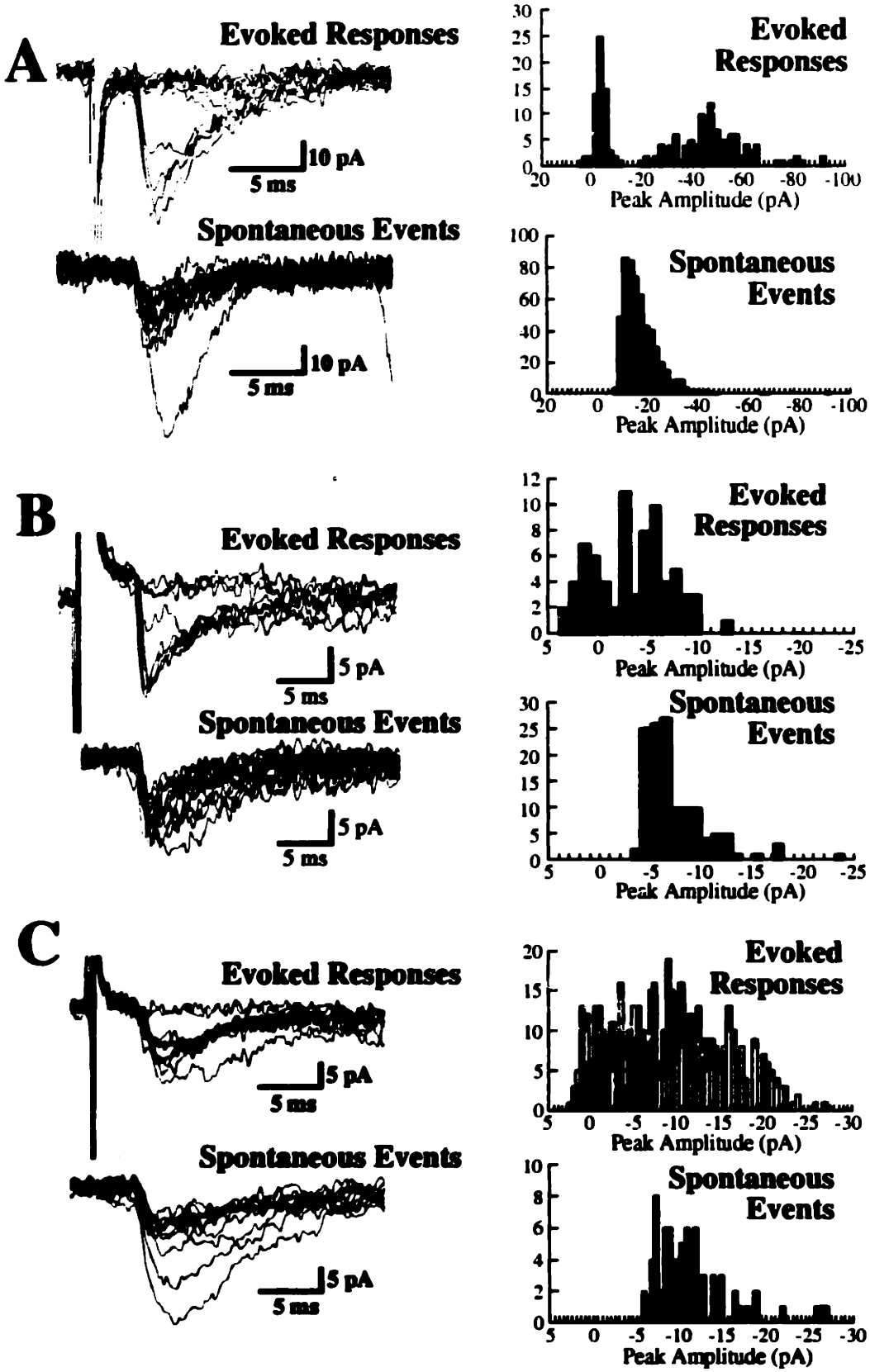
A
Evoked Responses
10 pA
5 ms
Spontaneous Events
10 pA
5 ms
Evoked Responses
Peak Amplitude (pA)
Spontaneous Events
Peak Amplitude (pA)
B
Evoked Responses
5 pA
5 ms
Spontaneous Events
5 pA
5 ms
Evoked Responses
Peak Amplitude (pA)
Spontaneous Events
Peak Amplitude (pA)
C
Evoked Responses
5 pA
5 ms
Spontaneous Events
5 pA
5 ms
Evoked Responses
Peak Amplitude (pA)
Spontaneous Events
Peak Amplitude (pA)

Fig. 3 - 12

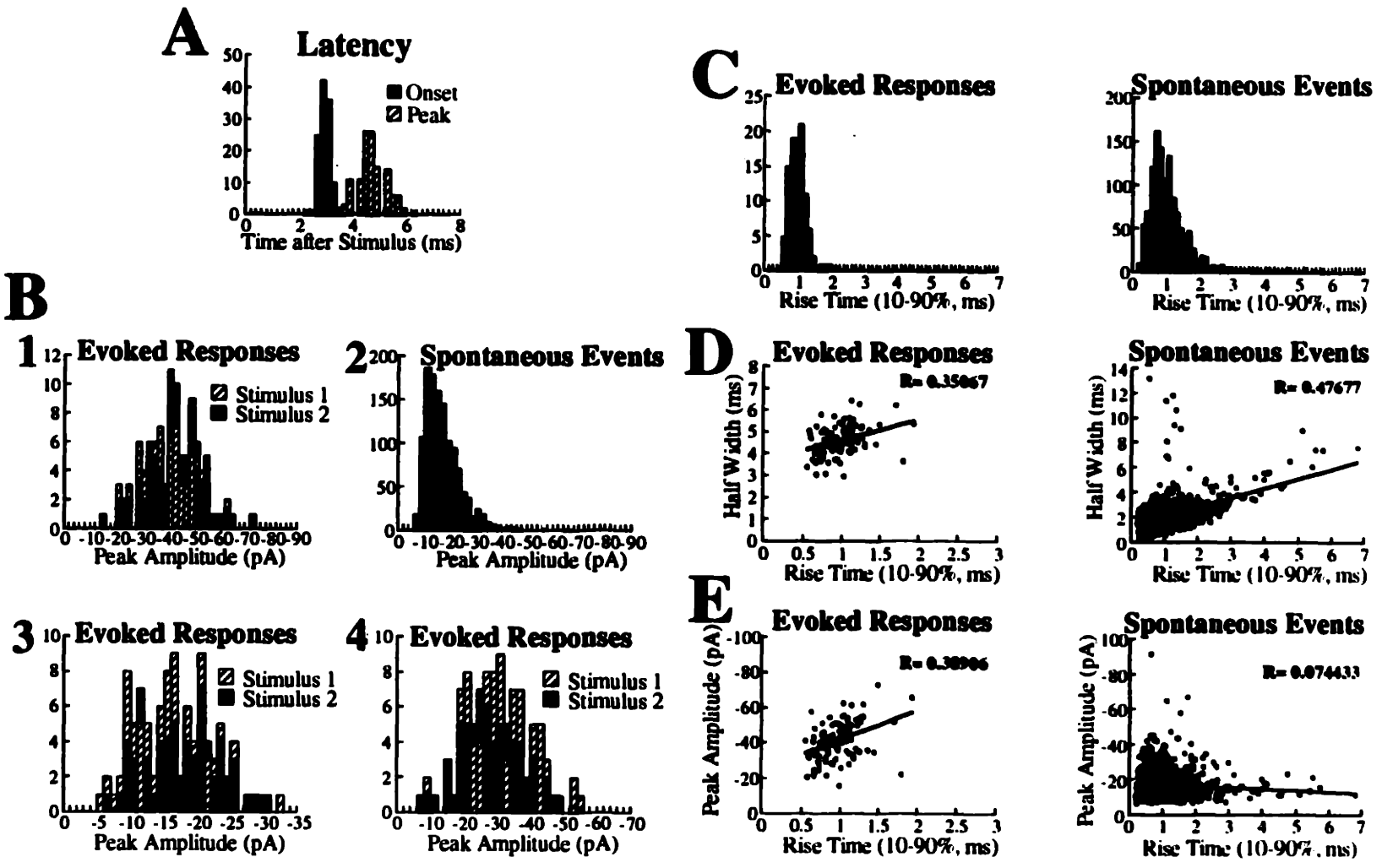
A
Latency
Onset
Peak
Time after Stimulus (ms)
B
1
Evoked Responses
Stimulus 1
Stimulus 2
Peak Amplitude (pA)
2
Spontaneous Events
Peak Amplitude (pA)
3
Evoked Responses
Stimulus 1
Stimulus 2
Peak Amplitude (pA)
4
Evoked Responses
Stimulus 1
Stimulus 2
Peak Amplitude (pA)
C
Evoked Responses
Rise Time (10-90%, ms)
Spontaneous Events
Rise Time (10-90%, ms)
D
Evoked Responses
R= 0.35067
Half Width (ms)
Rise Time (10-90%, ms)
Spontaneous Events
R= 0.47677
Half Width (ms)
Rise Time (10-90%, ms)
E
Evoked Responses
R= 0.38906
Peak Amplitude (pA)
Rise Time (10-90%, ms)
Spontaneous Events
R= 0.074433
Peak Amplitude (pA)
Rise Time (10-90%, ms)

Fig. 3 - 13

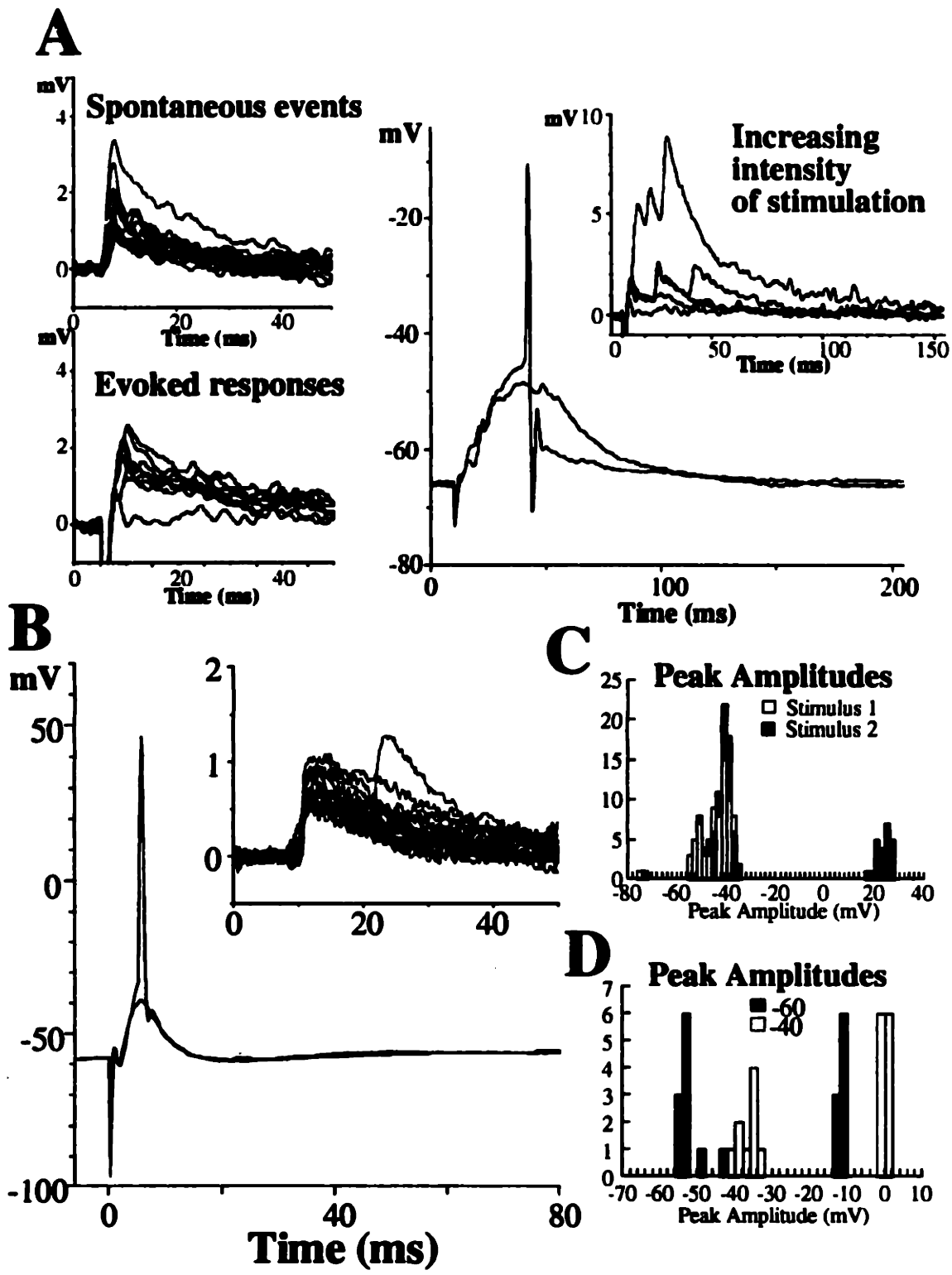
A
Spontaneous events
mV
Time (ms)
Evoked responses
Increasing intensity of stimulation
B
C
Peak Amplitudes
Stimulus 1
Stimulus 2
Peak Amplitude (mV)
D
Peak Amplitudes
-60
-40
Peak Amplitude (mV)
Time (ms)

Fig. 3 - 14

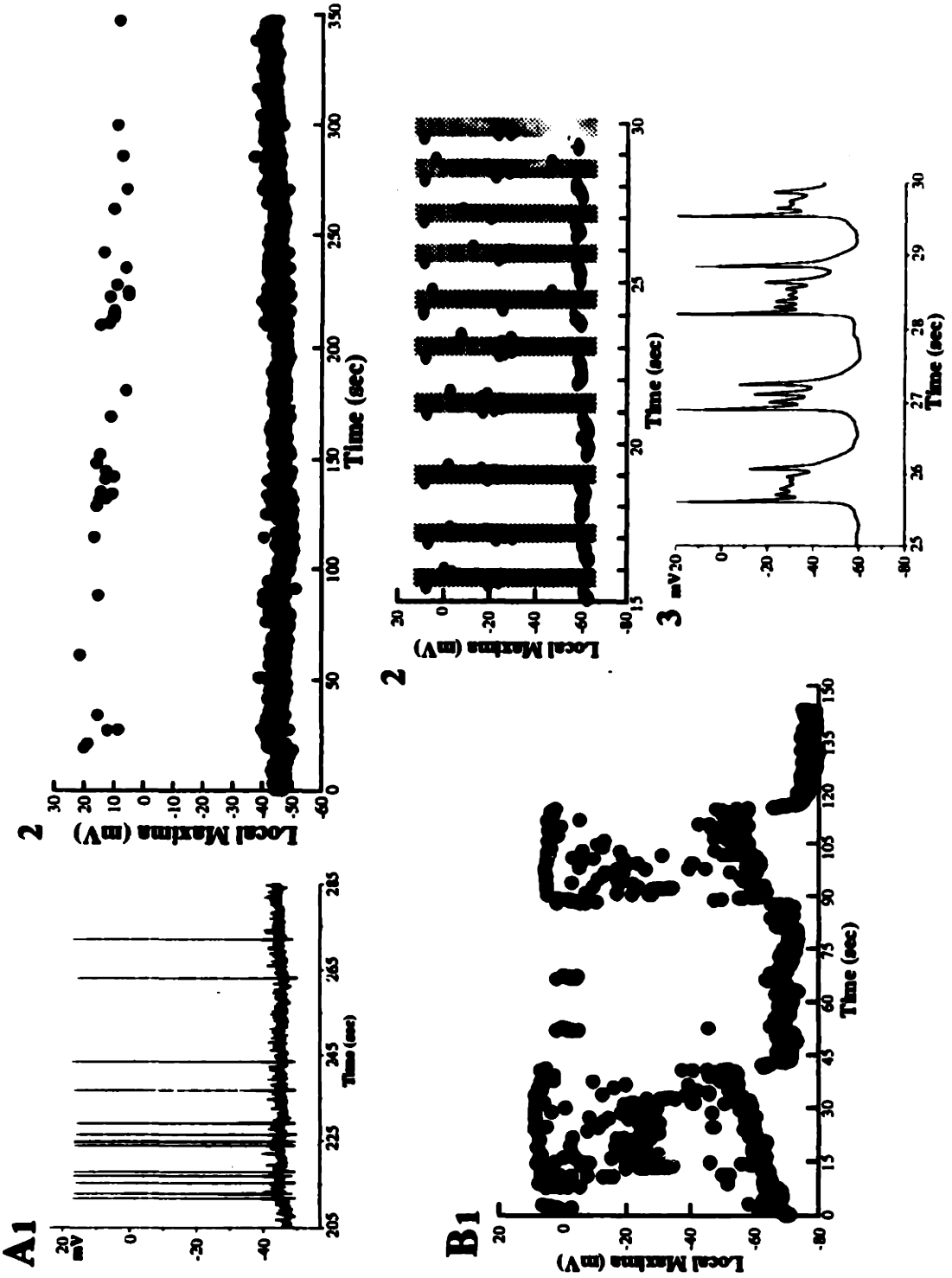

Fig. 3 - 15

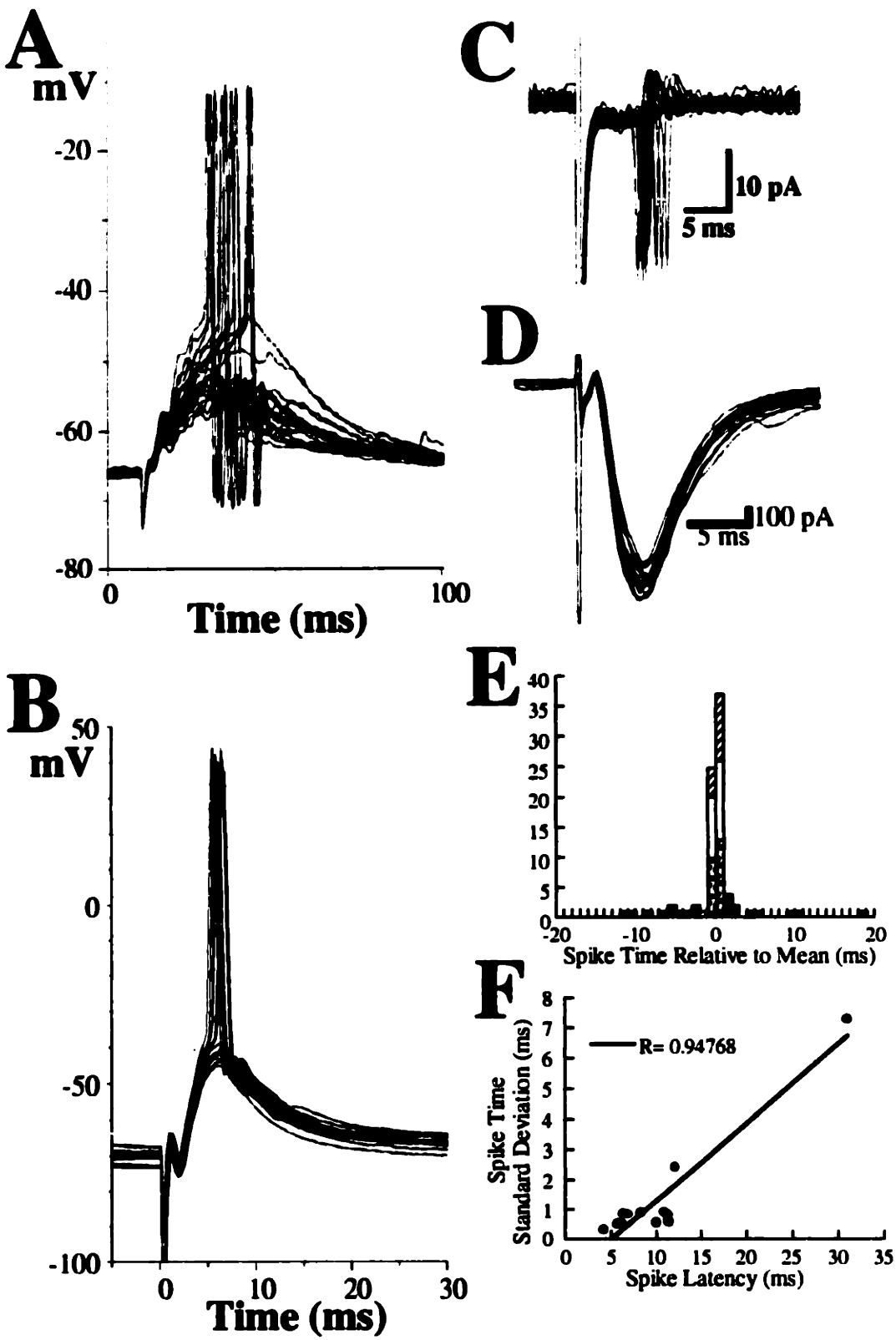
A
mV
-20
-40
-60
-80
0
100
Time (ms)
C
10 pA
5 ms
D
100 pA
5 ms
B
50
mV
0
-50
-100
0
10
20
30
Time (ms)
E
40
35
30
25
20
15
10
5
0
-20
-10
0
10
20
Spike Time Relative to Mean (ms)
F
R= 0.94768
Spike Time
Standard Deviation (ms)
8
7
6
5
4
3
2
1
0
0
5
10
15
20
25
30
35
Spike Latency (ms)

Fig. 3 - 16

4

The Role of Electrotonic Structure in Generating Synaptic Variability in Cortical Neurons

Abstract

Does electrotonic filtering contribute to synaptic variability? Even uniquantal, AMPAergic miniature EPSCs show a remarkable degree of amplitude variability and skewed parameter distributions. In this chapter, compartmental simulations are used to show that electrotonic filtering alone is capable of generating most, but not all of the variability seen in mEPSCs. Methods for detecting the presence of electrotonic filtering and other potential sources of synaptic variability are developed and applied to experimentally-measured mEPSCs. This analysis shows that there is strong evidence for the influence of electrotonic filtering on mEPSC shape and amplitude distributions, but that other sources of variability are likely to be present as well. Electrotonic filtering and one of these additional sources of variability together are shown to be sufficient to qualitatively match all of the properties of mEPSCs measured experimentally.

4.1 Introduction

What controls the effectiveness of a synaptic input? Are all synapses created equal, or are some synapses inherently different from others? In chapter 3, we saw that there was extreme variability in the population of spontaneous inputs to a single cell (see Figure 3-8), between the spontaneous inputs to different cells, and even in the

response to a single input over time (see Figure 3-12). Here we begin to address the question of what factors generate this enormous variability.

One obvious difference between synaptic inputs to a cell is their location on the dendritic tree. In the case of cortical pyramidal cells, more than 80% of their excitatory synaptic inputs come from other cortical pyramidal cells. If we for the moment ignore the sometimes subtle differences in layer and intrinsic physiology (see Section 1.3.1) of these source pyramids, it might be said that this 80% of the excitatory synapses come from a more or less uniform population of input cells, and are distinguished primarily by the location of the synapse on the postsynaptic surface. More accurately, different subpopulations of pyramids (and other inputs) select particular regions of the postsynaptic cell onto which to synapse [62, 287, 36]; this can be most clearly seen in the hippocampus, where the laminated structure makes it clear that a particular region of a cell, not just the cell as a whole, is the desired synaptic target of a presynaptic cell class (see Chapter 6). This suggests that the location of a synapse must have some major impact on its function, to make it worth the developmental cost of this point-to-point wiring.

What effect does synaptic location have on synaptic effectiveness? With the recent demonstration that the dendrites of neocortical pyramidal cells contain a large array of voltage-dependent conductances and can support spiking behavior [115, 39, 252, 158, 184], it may be that different inputs are positioned to activate these dendritic nonlinearities. However, it may be that these conductances are only activated by large numbers of simultaneous inputs to the same dendritic region, or inputs activated at high frequency (as suggested by the limited Ca^{++} response seen in the dendrites with low-frequency stimulation [213]). In this case, this would not explain the high degree of variability seen in small spontaneous synaptic inputs, or in response to minimal stimulation at different sites.

Does synapse location affect the response to small, single synaptic inputs? As early as 1959, it was suggested that the location of a synapse would drastically alter the synaptic response seen at the soma simply due to passive filtering by the

cell membrane [201]. Since that time, the effects of cell morphology and membrane characteristics, or *electrotonic structure* on electrical signals has been analyzed in great detail (for review, see [205, 124, 269, 97, 90]). More recently, several computational studies have strongly supported a role for electrotonic filtering in controlling the shape and amplitude of synaptic inputs as measured at the soma in pyramidal cells[242, 150, 152, 153, 151, 154].

4.1.1 Chapter Summary

What impact does cable filtering have on the population of responses seen at the soma? More importantly, does it play a major role in generating synaptic variability across the *population* of synaptic inputs? This chapter attempts to determine the contribution of cable filtering to the distribution of responses seen at the soma, and to evaluate the impact of synaptic and cellular parameters on these distributions.

To simplify the problem, I have concentrated on as uniform as possible a population of synaptic inputs. Terminals throughout the central and peripheral nervous system spontaneously release neurotransmitter vesicles even in the absence of action potentials, generating so-called "miniature" synaptic inputs, or minis [280, 276]. These events are putatively uniquantal, and can be easily recorded in the presence of tetrodotoxin (TTX), which blocks sodium action potentials. To obtain a uniform population of minis for study, I have recorded excitatory miniature EPSCs (mEPSCs) mediated purely by the AMPA subtype of glutamate receptor, under conditions in which most nonlinearities in the postsynaptic cell's response should be blocked (see methods for details). This population of synaptic inputs should be as intrinsically uniform in kinetics and conductance as possible. In spite of this fact, they still show the extensive amplitude variability described in Chapter 3, and skewed distributions of all parameters (Figure 4-17). To understand how much of this variability could be due to cable filtering, I have used computational simulations of visual cortical neurons. The results suggest that cable filtering does indeed play a major role in

generating synaptic variability under these conditions, but that it is not sufficient to explain all of the data.

4.2 Methods

4.2.1 Electrophysiology

Electrophysiological recording from slices of juvenile rat visual cortex was performed as described in the General Methods (Chapter 2). All data presented here were recorded in the presence of tetrodotoxin (TTX, 1 μM), 2-amino-D-phosphonovaleric acid or 2-amino-D,L-phosphonovaleric acid (APV, 30 μM) and Bicuculline Methiodide (BMI, 50 μM) to isolate putative AMPA-only events. All remaining events under these conditions were blocked by bath application of 10 μM 6-cyano-7-nitroquinoxaline-2,3-dione (CNQX, see data in Figure 3-4C and Figure 5-47), indicating that these remaining events were mediated by AMPA receptors alone.

Pipette solution contained (in mM): 130 CsF, 10 CsCl, 10 HEPES, 1 EGTA, 0.1 Ca^{++}, 2 $MgCl_2$. Intracellular Cs^+ blocks K^+ channels and $GABA_B$ receptors [73]. Additionally, any Cs^+ released extracellularly while forming the seal may act to attenuate anomalous rectifier (H-type) currents [166]. Extracellular TTX blocks somatic and dendritic Na^+ currents, as well as much or all of the persistent Na^+current [93, 4]. Together these effects "passivize" the cell, blocking most of its subthreshold nonlinear response.

4.2.2 Morphological Reconstruction

Cells recorded in rat or cat visual cortical slices were filled with biocytin or Lucifer yellow and reconstructed as described in the General Methods (Section 2.3). Cells were corrected for Z-dimension shrinkage as described. No additional shrinkage correction was applied except where noted, due to the uncertainty in the appropriate correction to use [150, 154].

4.2.3 Simulation of Response Distributions

Simulations of reconstructed neurons were performed as described in the General Methods (Section 2.4). The goal of these simulations was not to model the cell's response to a single synaptic input, but instead to simulate the population of spontaneous mEPSCs recorded in a single cell. Therefore, a method was needed to generate

a simulated *distribution* of responses. The basic paradigm used is shown in Figure 4-20: an identical synaptic input was placed sequentially onto each compartment of the cell, and the properties of the response at the synaptic input site and at the soma were measured. These were then used to estimate the distributions of these various parameters as follows: the number of excitatory synapses onto a compartment was estimated to be the same as the number of spines on that compartment, consistent with results from electron microscopy showing that the vast majority of excitatory synapses on pyramidal cells come onto their spines, and that there is usually 1 synapse/spine [287, 192].[1] The number of spines (and hence synapses) was estimated from the spine density models described above. As noted there, spine density was usually assumed to be constant or to be a simple linear function of dendrite shaft diameter; all conclusions presented here were robust across the various spine density functions described (see Section A.3.1). Each synaptic input was assumed to have an equal probability of generating a mEPSC,[2] and therefore each spine contributed one "measured" set of synaptic response parameters to the simulated "population". This population data was then used to generate histograms and cumulative probability distributions of various parameters. In some cases, the number of spines in each compartment was scaled down to decrease the total number of points to be plotted (usually by a scale factor of 0.3). A fractional number of spines was rounded up to 1. This will not affect the shape of the distribution unless there are a significant number of compartments with a very small number of spines; this was determined not to be the case, and all plots had the same shape in either their reduced or full versions

[1] A recent study has shown that the spiny stellate cells of layer IV in cat in fact get a majority of their excitatory synaptic input onto their shafts [8], however such cells were not considered in this study. I did not record in layer IV (see General Methods), and in addition, rats do not have classical spiny stellate cells, instead having a modified pyramidal type with a very small apical dendrite (the "star pyramid", [62]), therefore the conclusions of that study may not scale easily to this species.

[2] For the conclusions here to be valid it is not necessary that every synapse onto a cell should routinely produce at least one mEPSC in the course of an experiment. It is not even necessary that each synapse on the tree actually has an equal probability of producing an mEPSC – it might be, for instance, that past history of presynaptic release and/or potentiation could affect the probability of any single bouton releasing a vesicle in TTX [179, 155]. All that is required is that the probability of any given synapse generating a mEPSC is independent of that synapse's location on the postsynaptic cell – that, for instance, there isn't some amazing tendency for apical oblique inputs to generate mEPSCs at a much higher rate than other synapses. The conclusions presented here are indepdendent of a certain degree of bias in the locations generating mEPSCs, but extreme bias will alter the conclusions.

4.3 Results

4.3.1 mEPSCs show extensive amplitude variability.

Spontaneous EPSCs recorded in the presence of TTX (mEPSCs) show a remarkable degree of amplitude variability in both current and voltage clamp (Figure 4-17A). Amplitude histograms show the characteristic skewed shape (Fig. 4-17A, top) seen in a wide variety of cell types under very different conditions [247, 144, 274, 104, 164, 163, 244, 232, 41, 290, 143, 82, 70, 146, 29, 155, 157, 17, 128, 188, 187, 190, 217, 231, 238, 240, 266, 280]; such distributions are seen for most of the mEPSC parameters typically measured (Fig. 4-17B). While the shape of the amplitude distribution is common across all cells, the absolute amplitudes vary widely from cell to cell (Fig. 4-17C and Table 4.3.1).

What factors control this synaptic variability? Potential contributors can be divided into two classes. *Intrinsic factors* are differences between synapses due to intrinsic properties of the synapses themselves: differences in postsynaptic receptor subunit composition or number, differences in firing history of the presynaptic cell, etc. *Extrinsic factors* are differences due to the relationship of synapses with the postsynaptic cell: for example, synapse location on the dendritic tree, or the presence of voltage-dependent conductances shaping postsynaptic response to a synaptic input. (See Section 1.3.4.) Is the effectiveness of a synapse controlled only by its own history - intrinsic factors - with each synapse having an equal possibility of contributing to the output of the cell? Or is the effectiveness of a synapse controlled by its location on the postsynaptic cell?

Cell	Layer	N	Amplitudes (pA or mV)				Rise Times (ms)			
			Mean	SD	CV	Skew	Mean	SD	CV	Skew
Voltage Clamp										
1	III	2804	33.83	16.71	0.49	1.81	0.97	0.68	0.71	2.31
2	III	1526	30.68	13.118	0.43	0.96	0.92	0.59	0.65	3.04
3	III	2276	16.69	6.98	0.42	1.62	1.32	0.83	0.62	3.33
All		4500	27.15	14.35	0.53	1.35	1.08	0.74	0.69	2.94
Current Clamp										
1	III	559	0.94	0.60	0.64	2.35	2.57	1.75	0.68	3.12
2	III	569	0.67	0.44	0.66	2.90	3.16	2.52	0.80	2.51
3	III	46	0.61	0.30	0.49	1.27	5.01	2.59	0.52	1.04

		Widths (ms)				Areas (fC)			
Voltage Clamp									
1		2.10	0.88	0.42	1.56	104.88	60.59	0.58	1.31
2		1.72	0.68	0.39	2.09	80.47	48.77	0.61	1.26
3		2.07	1.09	0.53	2.88	59.41	37.97	0.64	1.48
All		2.00	0.95	0.48	2.65	82.73	54.19	0.66	1.45
Current Clamp									
1		11.77	6.89	0.59	2.58	14.70	19.39	1.32	4.59
2		12.20	8.00	0.66	2.23	10.72	13.70	1.278	2.90
3		19.28	11.21	0.58	0.89	12.31	10.34	0.84	0.94

		Slopes (pA/ms)				
Voltage Clamp						
1		95.25	48.03	0.50	2.39	
2		89.67	31.78	0.35	0.87	
3		52.40	16.98	0.32	0.87	
All		78.06	35.63	0.46	1.73	
Current Clamp						
1		0.79	0.38	0.49	2.15	
2		0.67	0.23	0.35	0.85	
3		0.47	0.13	0.26	0.73	

Table 4.1: Measured mEPSC parameter values from 3 layer III cells recorded in the presence of TTX (1 μm), APV (30 μm), and Bicuculine (50 μm). "All" is a pool of 4500 events, made up of 1500 consecutive events selected from each cell.

Recent studies have suggested that synaptic location, through the effects of electrotonic filtering, can have a major impact on the somatic response to a synaptic input [242, 150, 154, 152, 153, 151]. As mEPSCs come from all over the cell, each should be subject to a different degree of electrotonic filtering (Fig. 4-18). Does such filtering contribute to the generation of mEPSC variability?

4.3.2 Does electrotonic filtering contribute to mEPSC variability?

Cable filtering causes distally-generated events to be reduced in amplitude and slowed in time course. Therefore, if cable filtering contributes to mEPSC shape, one might expect these two parameters to be negatively correlated. MEPSCs do not show a strong negative correlation between rise time and amplitude (Fig. 4-19A,C, R=.256 for 3 pooled cells, similar results presented in [247, 163, 164, 104, 244, 144, 274, 41]). In fact the fastest events, presumably from the most proximal synaptic locations, cover the whole range of measured amplitudes. This can be seen more clearly in Figure 4-19D, which shows the amplitude distributions of subpopulations of events with increasingly faster rise times [104, 41] In theory, this should restrict attention to increasingly proximal events; if the shape of the amplitude distribution is determined by synaptic location it might be expected to be uncovered by this technique in the form of shifts to the right (a bias towards larger events) in the amplitude distributions for putatively more proximal events. In reality, all of these distributions overlap very closely. Similar results obtained from recordings of synaptic events in a number of cell types [244, 247, 163, 164, 274, 104, 209] have been taken in other systems to mean that cable filtering does not contribute to the generation of mEPSC amplitude variability [244, 209, 247, 163, 164, 274, 104, 144].

There are, however, features of Figure 4-19A supportive of a role for cable filtering: while the fastest events cover the entire range of amplitude variability, the slowest events do not; as rise times increase, events are restricted to smaller and smaller

amplitudes (see Figure 4-31). Similarly, consideration of the largest events in Figure 4-19 shows that they are uniformly fast.

Several factors complicate interpretation of the results shown in Figure 4-19. While intuitively it seems that a significant role for cable filtering should cause a negative relationship between rise time and amplitude, in the case of a complex cell the relationship between these parameters may not be one of linear correlation. And in using "fast" rise times as a criterion to select for synaptic inputs close to the soma, it is important to know the quantitative change of rise time with distance in these cells – in other words, how fast is fast? These questions are difficult to examine experimentally – it is very hard to unequivocally identify the site of origin of mEPSCs to compare their amplitude and shape with their source location [179, 189].[3] I therefore turned to compartmental simulation to more quantitatively evaluate the potential role cable filtering could play in the generation of mEPSC variability.

4.3.3 How much variability can be produced by cable filtering alone?

I used computational simulations to set up conditions under which electrotonic filtering was the *only* source of synaptic variability, and then asked how much of the experimentally observed mEPSC variability it could account for. Simulated distributions of mEPSC parameters were generated by placing a synaptic input identical in conductance and kinetics sequentially onto each point of a reconstructed cortical cell, measuring the parameters of the resulting response at the soma, and using the known distribution of spines as a metric of synapse location to generate an expected simulated mEPSC distribution of each parameter (see legend to Figure 4-20, Meth-

[3]Using paired recordings or other methods of activating a small population of inputs to a cell with the potential to locate their synaptic contacts both removes the possibility of examining the range of variability that can be produced across the whole cell, and requires recording without TTX, increasing the likelihood of multiquantal release and the involvement of postsynaptic Na^+ currents in the shaping of mEPSCs.

ods for details). In this case, each underlying synaptic input has the same size and shape, and any variation seen at the soma comes only from electrotonic filtering of the response on its way from the synapse.

Amplitudes

Cable filtering is sufficient to generate skewed voltage clamp amplitude distributions very similar to those seen experimentally (Fig. 4-21A, mean = 27.91 pA, CV = 0.573). This histogram was generated from simulation of the cell shown in Figure 4-21B, with inputs to the apical dendrite shown in gray. As would be predicted from the distribution of spines [134] (see Figure A-61A), more than 80% of the simulated mEPSCs are generated in the basal dendrites, less than 250 μm from the soma. In spite of this proximal site of origin, they are still subject to profound attenuation (Fig. 4-21D). Amplitude decreases rapidly, faster than exponentially, with distance, due to the very rapid kinetics of the mEPSCs [82] (see Fig. A-63. Even inputs only 100 μm from the soma lose approximately 50% of their amplitude due to electrotonic filtering. This implies that if one wishes to select "close", mostly unfiltered events, one must use extremely stringent criteria and be satisfied with looking at only a very small subpopulation of events.[4]

Cable filtering has less of an effect in current clamp (Fig. 4-21C, F) - the simulated amplitude distribution is narrower than that seen experimentally and unskewed (CV = 0.248), and the decrement of amplitude with distance plateaus at a relatively high level. In current clamp, all events are filtered by the time constant of the cell membrane, not leaving many high-frequency components to be filtered by synaptic location. Additionally, prominent reflections from dendritic terminations reduce the amount of attenuation (see Figure A-57).

[4]Due to the lower number of spines on the very proximal dendrites [134], it is possible that the number of events coming from <50 μm from the soma, or even closer, will be very small. However, this proximal reduction in spine density does not develop till after the ages of the animals used here (see Section 1.3.1).

The amount of skew seen in the simulated current clamp amplitude distribution depended both on the cell and the parameters used (see Figures 4-38,A-64). The distribution for the cell in Figure 4-21 is one of the less skewed. Absolute amplitudes are also quite small (mean=0.227±0.056mV, experimental pooled mean=0.796mV, 3 cells, see Table 4.3.1), though voltage clamp peak amplitudes are in the experimental range. Modifications of these parameters or the other assumptions of these simulations will be necessary to improve the match between simulation and data (see Section 4.3.8).

These results are general. A number of pyramidal cells were simulated as in Figure 4-21, and in all cases cable filtering alone was sufficient to generate skewed (or in one case, broad, see D) amplitude distributions in voltage clamp (Fig. 4-22). In some cells, cable filtering alone is sufficient to generate a skewed amplitude distribution in current clamp (Fig. 4-22A, CV=0.364).

Rise Times

Cable filtering alone generates skewed rise time distributions in current and voltage clamp similar to those seen experimentally (Fig. 4-23A,B). Rise time increases slowly, almost linearly, with distance across the whole dendritic tree (Fig. 4-23C). Even in simulations, rise time and amplitude do not appear to be negatively correlated (though quantitatively they are, Fig. 4-23D, R=.774). Though rise time increases, and amplitude decreases with distance as predicted, the relationship between these two parameters is not linear. Even in a simple soma and cable model (Fig. 4-23D, inset), a plot of amplitude vs rise time shows a concave V-shape. For the full cell model, this relationship appears as a cloud of points, rather than a simple V, corresponding to the multiple differently-shaped cables making up the cell. The basic concave shape, while less noisy than the experimental relationship, is still in many ways basically similar to it (compare Fig. 4-23D to Fig. 4-19A). As in the experimental case, events with the fastest rise times cover much of the observed amplitude range, and slow

events are restricted to only small amplitudes. There are still disparities between the experimental and simulated distributions, however, which are addressed below.

4.3.4 Sensitivity of response parameters to synaptic location

The reason for this lack of negative correlation between rise time and amplitude can be seen if we examine more closely the relationship between response shape and location on the cell. The parameters of the somatic response: amplitude, rise time, half width, area, and maximum rate of rise, each change in their on characteristic way as the synapse is moved out the dendrite. This is illustrated in Figure 4-24 using a simple soma and cable model. These relationships are, for each parameter, very similar in both voltage (Fig. 4-24A,B) and current clamp (Fig. 4-24C,D).

Three parameters, amplitude, area, and maximum rate of rise, show a quasi-exponential relationship with distance. Each falls off initially very rapidly, and then eventually plateaus. Maximum rate of rise shows the steepest dependence on distance, changing 5-fold within 100 μm of the soma (Fig. 4-24B,C). This extremely rapid falloff is due to the fact that this parameter is the most dependent on high-frequency components in the synaptic current, and therefore the most sensitive to cable filtering. It may therefore serve as the best, almost binary, indicator of "close" synapses. Peak amplitude shows a similar, if less steep, decrement with distance (Fig. 4-24A,B). Again, this parameter is very sensitive to synaptic location over a narrow region close to the soma (i.e. it changes significantly for a small change in synapse location), but it is very insensitive to movement of the synapse in more distal regions. While area (shown only in Figure 4-24D, the pattern in voltage clamp is basically identical) also shows an exponential-type relationship with distance, the rate of decay is very slow, and it may not reach its plateau level within the dendritic extent of the cell. It is therefore sensitive to change in synapse location throughout most or all of the tree. However, the total decrement in area (charge) is approximately the same as the

amount of DC voltage decrement in the cell [201, 205, 97, 269], and hence may not be practically visible in a cell of limited dendritic extent. In an infinite cable, all of these parameters, including area, would eventually continue their exponential decay to zero [97].

Two other parameters, rise time and half width, show a linear dependence on distance from the soma (Fig. 4-24A,B,C,D, also see Figure 4-23C). They can also show pronounced termination effects close to the end of a cable (simulations assume sealed end boundary conditions), but these effects are modest in simulations of real cells (see Fig. 4-23C). The time constants of rise and decay obtained by fitting Equation 2.1 to these simulated EPSCs behave very similarly to rise time and half width, respectively. However, τ_D shows very pronounced termination effects, decreasing sharply near the end of the cable (data not shown).[5] Again, in an infinite cable, these termination effects should not occur, and rise time should continue to increase until decreasing amplitude renders it immeasureable [97].

So in practice, rise time and half width are sensitive to movement of the synapse across all or most of the dendritic tree, and may serve well as index variables of absolute synaptic location.[6] A given change in dendritic distance (e.g. 100 μm) will produce the same absolute change in rise time, for instance, no matter where the original synaptic location was in the tree. On the other hand, the absolute change in rise time or half width may be very small if the movement of the synapse is not a large one. Therefore amplitude or maximum rate, which can show very large relative

[5]Because of the difficulty in accurately fitting exponential functions to even these noise-free traces (extensive hand-tuning of the initial conditions was necessary to find the optimal fits, and even in this purely linear model, some simulated EPSCs had obviously biexponential decays), fits were not attempted to simulated EPSCs from a full cell model. Therefore it is difficult to estimate how severe these termination effects are likely to be in real cells. However, the cylinder used for these simulations was similar to a collapsed equivalent cylinder model – its diameter was quite thick. Termination effects for other parameters, such as half width, increased in cable models whose diameters approached those of real cell dendrites. Therefore I expect that this effect on the fitted τ_D is underestimated here.

[6]The same is true for τ_R and τ_D , however care must be paid to the difficulty of accurate fitting and the possibility of termination effects.

changes in their values for a small movement of the synapse over the proximal region of the dendritic tree, are more sensitive indicators of relative synaptic location in these regions. These parameters are not unique identifiers of synapse location; the fact that the dendritic tree is made up of multiple different cables, rather than the single uniform one used for illustration here, means that the graph for a real cell would be a cloud of points rather than a single curve. However, the different cables generally show reasonably similar relationships (see Figure 4-21D for amplitudes, Figure 4-23C for rise times), and so these relationships can probably be used predictively even in the context of a complicated cell.

Finally, the very different relationships these two classes of parameters show to distance can be used to explain the lack of correlation between rise time and amplitude shown in Figure 4-23D. As amplitude decays exponentially with distance, while rise time increases only linearly, these two parameters should not be neatly negatively correlated with one another. Instead, they should show this concave relationship similar to that seen in the data (compare to Figure 4-19) (See section 4.3.5 for further discussion.)

These different rates of change of the various parameters with distance causes the distributions of these parameters from across the cell to undergo a complex scaling of parameter values (Fig. 4-25). This results in an "axis compression" effect, where one small region of a cell can represent a wide range of parameter values while another, larger region generates only a much narrower range of values. This can be seen most clearly in the case of the amplitude or maximum slope histograms in Figure 4-25, where the region of the cell $< 50\ \mu m$ from the soma (black bars) generates all of the long right-hand tail of the histogram, while values from other parts of the cell are compressed to the left of the histogram. These plots also show clearly that parameters whose distributions are qualitatively very similar in shape, such as amplitude and rise time, actually have totally different underlying relationships to the structure of the cell.

4.3.5 Parameter correlations: How to detect a contribution of electrotonic filtering to mEPSC shape.

Section 4.3.3 and following have shown that cable filtering alone is sufficient to generate a large fraction of the variability seen in spontaneous synaptic inputs to cortical cells. Does it in fact do so? Section 4.3.4 argued that the lack of negative correlation between rise time and amplitude is not good evidence against a role for cable filtering in the generation of mEPSC shape. What *is* a good way to look for evidence of cable filtering shaping experimentally-measured synaptic inputs?

In 1967, Rall made the first theoretical attempt to use the waveform of a synaptic response to determine the location of the underlying synaptic input on the cell surface [203, 206]. He identified a number of measured parameters of the synaptic waveform, or relationships between parameters, that were useful in distinguishing source location; he termed these parameters *shape indices.* The most useful shape index he identified was a linear correlation between rise time and half width (see Figure 3 in [206]); the presence of such a correlation both indicated a strong effect of cable filtering on the underlying synaptic current, and could be used quantitatively to predict the electrotonic distance of the synaptic input from the soma [203, 206, 100, 98, 96, 211]. However, this study normalized all synaptic inputs to have the same peak amplitude at the soma,[7] and concerned itself purely with the generation of synaptic waveform kinetics. The strong dependence of somatic response amplitude on synaptic location may provide an additional source of information about the role of electrotonic filtering in generating synaptic response shape.

Additionally, there are a number of additional potential sources of variability in synaptic responses besides cable filtering alone. It is important to assess what effects, if any, these will have on the shape indices used to assess the effects of filtering.

[7]Though the majority of Rall's earlier work emphasized linear current inputs and analytical solutions, this study and quite a number of the papers that came after it on synaptic transients used conductance inputs and purely computational and graphical approaches [203].

Other sources of synaptic variability.

In the case of real mEPSCs, there are several factors that complicate the picture considerably. These are, most importantly (see section 1.3.4:

- conductance variability between synapses
- kinetic variability between synapses
- noise
- series resistance

In the real world, all synapses are not guaranteed to be identical, and may show subtle or even radical differences in their underlying synaptic conductance or kinetics. In fact, even repeated activation of the same synaptic connection can generate responses with highly variable amplitudes and possibly kinetics (see Figure 3-12, [249, 291, 3, 6, 209, 17]). If the same synapse can generate a variable response over time, then it stands to reason that a population of synapses can easily vary from each other - think of them as single, variable synapses each caught at a particular point in time.

The underlying biophysical basis for these variations are most likely to be a difference in the aggregate of postsynaptic receptor-channels found at a particular synapse. Having different numbers of channels at different synapses will generate variability in peak synaptic conductance, as will releasing varying amount of neurotransmitter in each vesicle (assuming that postsynaptic receptors are not saturated). Having a heterogeneous assortment of channels with different kinetic properties will result in a difference in the macroscopic synaptic kinetics seen from that site; this could be easily due to heterogeneity in the subunits the of AMPA receptor found at different synapses, or to different phosphorylation states of the receptor-channels [268, 267]. These differences between synapses, if large enough, are another potential source of

explanation of the variability seen in spontaneous synaptic events. However, they still leave any variability seen in a single input over time unexplained.

In the case of action-potential driven events, there are several additional mechanisms that can generate variability in the same input over time. Synaptic transmission in the CNS is unreliable [17, 189, 249, 3] (see Figure 3-11). A synaptic bouton can fail to release any neurotransmitter in response to an incoming action potential. When an axon makes more than one synaptic contact onto a postsynaptic cell (which occurs frequently, even between cortical pyramidal cells [60]), this means that any combination of those boutons might release transmitter in response to a spike, resulting in variability at least in the amplitude of the synaptic response. Such amplitude variability will be magnified if the postsynaptic receptors are not saturated by a single vesicle of transmitter [191, 88], and if each bouton is capable of releasing more than one vesicle with some probability. If the kinetics of the channels present at these different synaptic contacts vary, then the response to this single input will have variable kinetics. However, there are two additional important sources of kinetic variability at a multi-bouton synaptic connection. First, those boutons could be located at different places on the postsynaptic cell [60], and hence would be subject to different degrees of cable filtering. Second, those boutons might not always release their vesicles with exact synchrony, which would smear the timing of the somatic response [286]. A primary reason for studying miniature synaptic events in this context is that they are putatively, or at least predominantly, uniquantal (but see [274]), and are therefore not subject to either of these additional sources of variability.

There are two more complications introduced by the experimental situation itself. Noise makes it difficult to record synaptic parameters accurately, and may mask subtle relationships between them, particularly when the changes in parameters with distance are small (see Figure 4-29). Series resistance adds an additional low-pass filter similar to the cable itself, selectively affecting the larger, faster, more proximal inputs (see Figures 4-25, 4-38, A-65, and A-66). In some cases it strengthens or even induces correlations between various parameters. But usually, series resistance acts

to mask the effect of cable filtering, by filtering selectively those events which *aren't* already filtered by the cable.[8] Events that seem relatively impervious to electrotonic location might have actually undergone dramatically different degrees of cable filtering, but their different shapes at the soma will be rendered almost identical by the action of series resistance.

How do these different sources of variability affect the relationship between synaptic shape indices, and are there reliable ways to detect them experimentally? We will attempt to answer these questions by using simulations to explore the effect of these sources of synaptic variability, alone and in combination.

Variability in the absence of cable filtering: Conductance variability

If we assume that synaptic kinetics are uniform, and vary only the conductance of a synapse, what happens to the shape indices? To start, we will remove as many of the other complicating factors described above as possible. Consider a synapse onto a single-compartment, spherical neuron, which will undergo no cable filtering. Let the series resistance be 0 $M\Omega$.

In this case, if you change only the peak conductance of the synapse (G_{max} in equation 2.1), the following happens:

- Rise time and half width remain *constant* (as do τ_R and τ_D).
- Amplitude, maximum slope, and area all increase proportionally to reflect the change in conductance:[9]

[8] This seeming uncanny selectivity can be understood simply by realizing that those events which are strongly filtered by the cable have no high-frequency components left when they reach the soma to be affected by the series resistance, while proximal inputs, less affected by the cable, are much more sensitive to R_s.

[9] If you add conductance variability to a system without perfect space clamp and no access resistance (to prevent subsynaptic voltage change), this proportionality only holds up to a point. When the synaptic conductance becomes large enough, the subsynaptic voltage escape will reduce the synaptic driving force enough to reduce the peak synaptic current. This will mean that the amplitude, maximum slope, and area will all be lower than predicted from the amount of conductance

$$area/amplitude = maxrise/amplitude = CONSTANT \qquad (4.1)$$

Assuming no significant saturation effects, in the case of conductance variation alone, all parameters that are proportional to conductance (amplitude, maximum slope, and area), will obviously be correlated with one another (Fig. 4-26A). The distributions of these parameters will show the same shape as the underlying conductance distribution (data not shown).

Kinetic variability

Now, again in a single compartment, say we assume the synaptic conductance is constant but allow the synaptic kinetics (in the form of τ_R and τ_D) to vary, independently of each other. Then:

- Amplitude is constant.
- Rise time, half width, area, and maximum slope (as well as τ_R and τ_D, the fitted time constants of rise and decay) all vary with the kinetics.
- τ_R and τ_D(the underlying synaptic time constants) are not independently related to any of the measured parameters (e.g. if you change τ_D it can have an effect on rise time). However, the rise is very quick, so area (charge) is mostly (but not completely) determined by τ_D, the time constant of decay. Similarly,

increase, and may not even change in proportion with each other. Eventually, if the conductance becomes large enough, the synaptic kinetics may be affected as well. It is important to realize that this effect occurs long before the synapse "saturates" - i.e. when the subsynaptic potential reaches the reversal potential of the synapse and no current flows at all. A noticeable decrease in response can occur when the subsynaptic voltage increase reduces the driving force by as little as 20% [203]. It is also important to realize that this may happen with different conductance values at different locations on the cell. Fine distal branches will experience saturation effects with much smaller synaptic conductances than those required to cause saturation on large proximal dendrites [120].

maximum rate of rise is primarily determined by τ_R.[10]

The following relationships between parameters are seen in this case (constant conductance, no cable filtering):

- There is a trend towards a loose correlation between rise time and half width (Fig. 4-27B1), simply because things with slow rise times cannot have infinitely short half widths.[11]
- Area and half width are very tightly correlated (Fig. 4-26B2).[12]
- Maximum rate of rise is the maximum value of the limit of *amplitude/risetime* as the measurement period goes to 0. Therefore (Fig. 4-26B3):

$$maximumrate \propto 1/risetime \tag{4.3}$$

The next step: interactions between kinetic and conductance variability.

Now, if we allow in our single compartment model (i.e. no cable filtering effects) both variation in peak synaptic conductance and in synaptic kinetics as described above, we will see the following in recorded responses:

- Rise time, half width, and the decay time constant are determined only by the synaptic kinetics, independent of peak conductance.

[10]Maximum rate of rise and τ_R, the synaptic rising time constant, are related according to:

$$maximumrate \propto 1/\tau_1^{3/4} \tag{4.2}$$

[11]If the distribution of τ_S is narrower than used here, this correlation is much tighter, but the resulting values of rise time and half width cover only a very narrow range.

[12]As maximum conductance is fixed, area cannot be increased by changing peak current amplitude, only by adding to the tail of the synaptic current which will also increase half width.

- Peak amplitude is determined only by conductance, not kinetics. Maximum rate of rise and area are both scaled according to conductance as well, but in addition are also determined by the synaptic kinetics. Therefore, to isolate kinetic effects, normalize both maximum rate and area by peak amplitude.

The following relationships are seen between parameters in this case (no cable filtering, both kinetic and conductance variability):

- Rise time is determined only by the synaptic kinetics, and amplitude only by conductance. Therefore these two variables are independent (Fig. 4-26C1).

- There is a weak relationship between rise time and half width determined by the kinetics (Fig. 4-26C2), this is unaffected by the presence of conductance variability.

- Any relationship between area and width is determined by kinetic variability, as conductance variability does not affect half width. These two parameters will be correlated in the presence of any kinetic variability, but the affect of conductance on area will make the relationship a noisy one (Fig. 4-26C3a). Normalizing area by peak amplitude (see above) should leave a clear correlation between these two parameters in the presence of kinetic variation (Fig. 4-26C3b).

- Similarly, a relationship between maximum rate and $1/risetime$ is determined by kinetic variability, but made noisier by conductance effects on maximum rate (Fig. 4-26C4a). Again, normalizing maximum rate by amplitude will isolate the kinetic effects (Fig. 4-26C4b).

- Any relationship between amplitude and area or maximum rate of rise is determined by conductance variation only. It is, unfortunately, not simple to normalize out the effects of kinetic variation on area or maximum rate to see the effect of conductance change alone.

Effects of Cable filtering alone

In Figure 4-27A, a synapse is moved sequentially out a simple soma-cable model. The underlying synaptic inputs are identical, so the only source of variability in mEPSC parameters is electrotonic filtering. All parameters are altered by cable filtering, but in different ways (see section 4.3.4). We know that rise time and half width both depend linearly on distance, while amplitude, maximum slope, and area all depend quasi-exponentially on distance. In this case, the following relationships between parameters would be expected:

- Amplitude and rise time show the concave V-shaped relationship presented in Figure 4-23D (Fig. 4-27A1).
- Rise time and half width would be correlated linearly with each other (Fig. 4-27A1).
- Cable filtering will induce a (possibly nonlinear) negative relationship between area and half width - area decreases with distance, while half width increases (Fig. 4-27A2). Area and rise time behave similarly (not shown). Normalizing area by peak amplitude does not adequately compensate for the effects of cable filtering (Fig. 4-27A2), leaving a positive correlation with half width.
- Peak amplitude can be correlated to some degree with either maximum slope or area, depending on the relative rate of fall of each (Fig. 4-27A3).
- Maximum slope is the instantaneous limit of $amplitude/risetime$. Therefore it might also be expected to be proportional to $1/rise$, but it isn't as cable filtering has a much more severe effect on maximum slope than rise time (Fig. 4-27A4). Normalizing by peak amplitude to partially compensate for cable filtering restores some correlation (Fig. 4-27A4).
- If Equation 2.1 were fit to the simulated mEPSCs, the resulting time constants τ_R and τ_D should depend linearly on distance and hence ought to be correlated,

similarly to rise time and half width (section 4.3.4). However, τ_D can show strong termination effects which may mask this relationship.

The presence of any of these parameter relationships might be taken as good evidence for the presence of cable filtering in this simple case, but a strong correlation between rise time and half width is probably the best indicator of the presence of cable filtering [203, 206, 100, 98, 96, 211].

Interactions between cable filtering and other sources of variability.

In Figure 4-27B, C and D, the two other potential sources of synaptic variability discussed are added to our simple soma-cable model. As above, amplitude, area, and maximum slope are scaled in proportion to variation in underlying conductance.[13]. Kinetic variability affects everything but peak amplitude[14] Cable filtering, of course, affects all synaptic parameters.

Comparing the corresponding parts of Figure 4-27B, C and D, it can be easily seen that the effects of cable filtering overwhelmingly dominates the relationships between most pairs of synaptic parameters; these relationships resemble a "noisy" version of the ones in A, generated by cable filtering alone. While closer examination shows that in fact some of these relationships are reflective of the nature of inputs underlying them, these other sources of variability only express themselves within the constraints put down by electrotonic filtering (see Section 4.3.5). These relationships are examined in more detail below:

- Cable filtering induces a relatively tight correlation between rise time and half width (Fig. 4-27A1,C1,D1), even in the presence of kinetic variability.[15]

- Peak amplitude and rise time show the concave V-shaped relationship induced

[13]Assuming that we are in the linear synaptic regime and can ignore saturation effects.
[14]Except in the presence of non-zero access resistance, see below.
[15]Conductance variability has no effect on these parameters (Fig. 4-27B1).

by cable filtering,[16] regardless of the presence of other sources of variability (Fig. 4-27A1, B1, C1, D1); these only serve to add additional "noise" to this relationship, filling in some areas of the plot.

- Area/Amplitude shows a very tight correlation with half width (Fig. 4-27B2, C2, D2). While careful examination shows this relationship has the same shape as the corresponding one seen with cable filtering alone (Fig. 4-27A2), its great similarity to the correlation seen in the presence of kinetic variability without cable filtering (Fig. 4-26B2, C3b) prevents it from being experimentally useful.

- Area and half width show a noisy negative correlation in the absence of kinetic variability (Fig. 4-27A2,B2). Kinetic variability alone (without cable filtering) induces a strong positive correlation between these two parameters (Fig. 4-26B2). In the presence of both of these sources of variability (Fig. 4-27C2,D2), these effects cancel each other out, leaving at best a very weak correlation in either direction. The major complication in this case arises from the fact that some combinations of synaptic kinetics will be much more affected by cable filtering than will others. So in some sense, even a single cable will have a multitude of simultaneous "electrotonic lengths" seen by different synaptic inputs depending on their individual kinetics (see section A.4).

- In the generation of the relationships between slope, amplitude and area, the presence of conductance variability dominates over the effects of cable filtering (Fig. 4-27B3), resulting in families of events linearly related in these parameters, rather than showing the somewhat nonlinear relationship seen with cable filtering alone (Fig. 4-27A3). However, both of these effects give rise to approximately equal degrees of correlation. Kinetic variability predominantly acts to add noise to the effects of cable filtering (Fig. 4-27C3). In the case of max-

[16]Surprisingly, this is just the relationship that has been previously used as evidence *against* the presence of cable filtering (see Section 4.3.2).

imum slope, the resulting relationship is very similar to that seen with cable filtering alone. However, the relationship between area and amplitude is filled in, as the variation in kinetics means that proximal events (those with the largest amplitudes) are no longer restricted to having large areas (area being relatively unaffected by cable filtering). Distal events, however, are restricted to having both small amplitudes and small areas by the dominant effects of cable filtering, resulting in compression of the left hand side of the plot. Adding conductance variability (Fig. 4-27D3) does not significantly change these relationships, though it adds a significant degree of noise to that between maximum slope and amplitude.

- Both cable filtering (Fig. 4-27A4) and kinetic variability (Fig. 4-26B3,C3b) induce a correlation between slope (or normalized slope) and $riseime^{-1}$. Such a relationship, particularly in the normalized parameter, is seen in all conditions (Fig. 4-27B4,C4,D4), but it is difficult to uniquely attribute its source.

The examples shown here used a very large degree of kinetic variability, much larger than that likely to appear in in a single cortical neuron.[17] The same effects are seen with much narrower kinetic distributions, but the amount of variability induced by the kinetics is much smaller. This acts to improve correlations between variables, both those induced by other sources of synaptic variability, and those induced by the kinetics themselves. For instance, the correlation between rise time and half width in the presence of kinetic variability alone is much tighter than that shown here when the amount of kinetic variation is smaller. However, in that case, the resulting changes in synaptic parameters (rise time, half width, etc) due to the kinetic variation is so small as to be experimentally irrelevant – the resulting correlations act more by adding correlated noise to the data than by inducing a large-scale structure to it on their own. And as shown here, they are dominated by the effects of cable filtering.

[17] It would have been reflected in a wide variation in the kinetics seen with single-channel recordings within identified cell classes [267, 83, 142].

A correlation between rise time and half width, therefore, still remains the best indicator of the presence of cable filtering in all cases. Additionally, normalizing amplitude and maximum slope by area may provide an indication, albeit a noisy one, of the distribution of these parameters due to cable filtering alone.

Test of the analysis method.

These methods were tested on a population of recorded mEPSCs subject to a simulated increase in conductance variability. The measurements of mEPSCs recorded in one cell at -70mV were compared with those same events combined with the population of events measured in the same cell at a holding potential of -110mV (data not shown). In theory, this change in holding potential should simply increase the driving force by a factor of 1.57, and be approximately equivalent to an shift in the conductance distribution,[18]. The two populations together are approximately equivalent to a stretched version of the original conductance distribution.[19] As predicted for a pure change in the underlying conductance distribution, amplitude, area and maximum slope all show a similar stretch in their distributions, and the normalized parameters (amplitude, area, and maximum slope normalized by either amplitude or area) are unchanged. Again, as predicted,rise time shows no change between the two holding potentials. However, half width shows an apparently linear shift towards larger values at -110mV.[20]

[18]This assumes that no significant portion of the distribution was previously hidden in the noise. As discussed in Section 5.3.7, this does not appear to be the case. Out of approximately 1500 events detected at -110mV, only 15 were of amplitudes that suggested they would have been detected at -110mV and not at -70. The two amplitude distributions do nearly superimpose on scaling one by a constant factor.

[19]They are actually equivalent to the original conductance distribution summed with a shifted version of itself, but in the case of these particular distributions, this can be thought of as a stretch in the distribution shape.

[20]This could be due to the increased availability of anomalous rectifier conductances at this voltage. The addition of larger widths across the amplitude distribution is not what would be expected as a result of events now being larger relative to the noise, that would cause a selective increase in the widths of small-amplitude events. Saturation effects would cause a selective increase in the widths of large-amplitude events.

In spite of this, and as predicted, the relationship between rise time and half width is unaffected by this "conductance variability". The relationship between rise time, area, and amplitude is similarly unaffected, as all three are scaled to the same degree by the "conductance" change. The only affect not in concert with the predictions above is the change in the relationship between half width and area (or amplitude). Conductance increase alone should simply stretch this relationship along the area axis, while leaving the width dimension unchanged. For large amplitude events, this is approximately what happens. However, larger width events are added at all amplitudes, and for smaller amplitude events, there is not the expected increase in amplitude for a given width. The net result is that the change in the area-half width plot mimics kinetic variability almost more than conductance variability. This suggests that either hyperpolarization is not a pure model of conductance change, or that interpretation of the experimental relationship between half width and area must be done with caution.

Attempting to constrain the problem: looking at a selected subclass of events.

One approach to getting around the effects of cable filtering, and to see the other sources of variability contributing to the shape of synaptic events, is to try to restrict attention to proximally-generated, mostly unfiltered events (for instance, see Section 4.3.2, and Chapter 6). There are two major drawbacks to this approach: first, it is difficult to unequivocally select "proximal" events *a posteriori*. Cable filtering places a number of constraints on event shape (see Section 4.3.5), notably that the largest, fastest events are the most likely ones to be generated proximally. [21] However, kinetic and/or conductance variability may shape the size and speed of events independent of their location, so deciding what is "large enough" or "fast enough" to be considered probably proximal is difficult without some *a priori* knowledge of the

[21] Notice that the opposite does not hold.

degree of cable filtering likely to be present in a particular cell. Second, there may only be a few events that are generated proximally enough to be considered unfiltered. In the case of inhibitory inputs [287, 192, 106](see Chapter 6), or excitatory inputs to non-pyramidal cells [26, 27, 77], many of which are somatic, proximal inputs may predominate. On the other hand, in the case of excitatory synaptic inputs to pyramidal cells, the number of proximally-generated events may be very small. None of these inputs occur on the soma, and there are very few spines located on the most proximal 50 μm of the dendrites [134].

To see how this would work in practice, I selected the 25% of events with the fastest rise times in Figure 4-27B,C and D in an attempt to minimize the impact of cable filtering on the resulting parameter relationships. This technique is not completely accurate, particularly in the presence of kinetic variability; while the events thus selected come predominantly from proximal locations, a few events from as far away as the midpoint of the dendritic cable (0.5 λ) are selected as well. And a certain number of proximally-generated events with slow kinetics are missed. The selection is not particularly stringent, as it encompasses most of the events generated in the most proximal 20% of the cable; this region is still subject to a reasonable amount of filtering.

In spite of these facts, the parameter relationships for this "proximal" population resemble more closely those seen in the absence of cable filtering. In particular, rise time and amplitude (Fig. 4-28A1, B1) are predominantly uncorrelated, and rise time and half width show the loose correlation induced by kinetic variability alone (Fig. 4-28A2, B2). The relationship between area and half width is similar to that seen with conductance variability alone (compare Figure 4-28B2 and Figure 4-26C3a,b). When area is normalized by amplitude, it narrows as expected to a very tight correlation as expected (Fig. 4-28B2), however, it shows a very similar pattern in the absence of conductance variability (Fig. 4-28A2), and this behavior is very similar to that seen in the presence of full cable variability; together these facts suggest that it is risky to base any conclusions on this plot. This apparent lack of filtering effects breaks

down when it comes to the relationship between maximum slope or area and peak amplitude (Fig. 4-28A3, B3) which is similar to that seen in the corresponding plot for all events. Both amplitude and maximum slope have still undergone a significant degree of filtering, even in this population. This can be seen in Figure 4-28A3, where only kinetic variability and cable filtering were present in the simulations. The variability in peak amplitude is a result of cable filtering, in spite of the selection of only the most rapid events.

Better methods for selecting proximal events. As amplitude and maximum rate of rise change significantly faster with distance than does rise time, it is hard to unequivocally select the "fastest" events based on rise time and be sure that they really are unaffected by cable filtering of their amplitudes or maximum rates. As noted above, maximum slope is actually the most sensitive marker for proximal synapses. It is non-unique, as it varies with both conductance and kinetics, but if one is willing to end up with that population of closest events with the fastest kinetics and largest amplitudes, which is the only population which can be identified as proximal with any conviction (but see below), it is the best marker. Rall has additionally suggested normalizing slope by peak amplitude (as was done above) [206], as selection based on slope would give a population of proximal synapses, such a normalization would remove most of the effects of conductance variability.[22]

Nonuniqueness and constraints induced by cable filtering.

In the presence of all three of these sources of synaptic variability, a proximally-generated event with slow kinetics and small conductance is indistinguishable from a distal fast event with a large conductance. We cannot uniquely derive the synaptic location from the EPSC shape, even if the electrotonic structure of the cell is

[22]This technique was not used above as a sharp slope criterion really does select the most proximal events, but therefore yields too few events to be used for population analysis, and in addition, it has not been routinely used experimentally.

completely known.

However, we can constrain the answer. We cannot tell how many of the slow events are really intrinsically slow events generated on the soma, rather than fast events generated distally and then filtered without further experimental data (see chapters 5,6). We also cannot tell how many of the small events are actually generated proximally with small conductance (and potentially variable kinetics). But we can put a bound on the problem from the other end. Given the presence of cable filtering, and assuming a passive dendritic tree, very fast events *cannot* come from a significantly distal site. By measuring the fastest event we see at the soma, and simulating the response at the soma to an event with those kinetics placed distally on the cell (assuming knowledge of the cell's morphology and passive properties), we can say what are the fastest events that *could* have come from this site. We can also say how large that fastest event would have to have been for us to detect it at the soma (see Chapter 6 for just such an analysis). Such an analysis requires, as above, identifying a putatively proximal event. However it escapes some of the usual problems with such an analysis; as only a few events are required, selection criteria can be very strict, and should succeed even if the number of true proximal events are small.

Correlated sources of variability.

In the analyses above, we have relied on the very fundamental, and perhaps unwarranted, assumption that these multiple sources of variability are *independent.* In other words, there is no systematic relationship between the kinetics of a synapse and its peak conductance, or between its location and either its conductance or kinetics. It is biologically plausible that there would be some systematic relationship between these variables: for instance, AMPA receptors with slower kinetics might also have lower single-channel conductances, or tend to aggregate less tightly, meaning that slower synapses would generate smaller EPSCs even in the absence of electrotonic filtering.

There are also plausible mechanisms for generating systematic relationships be-

tween synaptic location and EPSC parameters. In many systems, but most notably the hippocampus, inputs from different presynaptic cell types are systematically segregated on the postsynaptic cell. If the presynaptic neuron in some way controls the behavior of the postsynaptic component of the synapse, this would allow different parts of the cell to have synapses made up of different kinetic classes or numbers of receptors. Or more simply, the axons of these different presynaptic cell types could release differently-sized vesicles, generating different peak amplitudes of mEPSCs in the absence of receptor saturation.[23] It has been suggested in alpha-motoneurons that the only way to explain the lack of decrement seen in peak EPSP amplitude resulting from activation of single 1a inputs with increasing distance from the soma (as measured by shape indices from the rise time vs. half width plot), is to postulate a systematic increase in synaptic conductance for more distal synapses [95].

In the worst case, these factors could even conspire to violate the constraints described above, imposed by cable filtering on response shape (Section 4.3.5). All of those constraints were *relative*, based on selecting events that are larger or faster than others in the same cell. If, for some very perverse reason, nature chose to put very slow or small synaptic inputs onto the soma of a cell, and increasingly fast or large inputs farther out,[24], then in fact the largest and/or fastest events seen might not be the most proximal ones. While such collusion is possible, it does not make good biological sense. This would maximize the attenuation of current on its way to the soma, and thus waste a lot of energy in pumping ions back to their starting places without using them to send an effective signal. It would also drastically curtail the

[23]Even more simply in the absence of TTX, these presynaptic cell types could make different numbers of contacts with their postsynaptic partner, thus incurring different failure rates and response amplitudes, without requiring any differences in the release process or postsynaptic receptors between inputs.

[24]This would have the potentially productive effect of reducing the amount of variability between synapses on the same cell as seen at the soma [95, 89, 53]. However this would cost the cell in temporal resolution of its synaptic inputs. A similar effect can be achieved using an arrangement of active dendritic conductances to equalize the somatic impact of synapses across the dendritic tree [51, 52, 53], without loss of temporal resolution. It is more likely that this is the approach actually taken by cells [184, 252, 214, 292].

cell's ability to respond to rapidly changing signals in its inputs - those signals would be lost due to filtering in the distal dendrites, and simply not represented proximally if those inputs were limited to very slow time courses.

Another, perhaps more plausible, scenario is that correlation between these sources of variability would act to mimic the effects of cable filtering when it was not present (e.g. receptor kinetics could be organized so that increasing rise times always were associated with increasing half-widths, etc). However, in this case they would still obey the constraints on synaptic response shape described in the previous paragraph. This suggests that it is a good idea not to rely only on relative measures of synaptic size and speed, but to compare those values both to the results of quantitative simulations and to those obtained in other cell types.[25]

4.3.6 Series resistance and noise.

Series resistance. As described in detail in Section A.6 (also see [242, 150]), series resistance preferentially filters proximally-generated events, which are not already filtered by the cable. As a result, series resistance can drastically reduce the amount of synaptic variability measured at the soma (see Figures 4-38 and A-65). This effect is independent of the presence of conductance variability – the relative change in EPSC parameters is the same regardless of underlying conductance, it only depends on the frequency components of the synaptic current left when it reaches the soma.

In contrast, series resistance interacts with kinetic variability in a complicated manner. Those events with faster kinetics will be much more severely affected by series resistance. Again, only those rapid events which are not already filtered by the cable will be subject to this effect. In the absence of cable filtering (e.g. in the single compartment model discussed above), series resistance can generate amplitude

[25] However, it can be difficult to compare absolute numbers in studies performed in different laboratories. Different standards for access resistance, recording conditions (particularly temperature), and most important, measurement techniques (sampling rate, interpolation techniques, filtering) can affect the synaptic parameter values measured.

variability from a group of events with varying kinetics and uniform conductance (the fastest events have their amplitudes severely reduced by R_s, while the slower events are relatively untouched). Given creative choices of the distributions of τ_R and τ_D, it is possible to generate histograms of all synaptic parameters similar to those seen in cortical neurons in a single compartment model purely from the combination of kinetic variability and series resistance.[26] However, in this case, the parameter correlations are entirely different from that seen in the presence of cable filtering (data not shown). In particular, the relationship between rise time and amplitude is a convex, positive correlation, rather than the concave V-shape seen in both simulations of cable models and the data. Additionally, rise time and area show a strong positive correlation, rather than being uncorrelated or showing the mild negative correlation they do in the presence of cable filtering. These effects may complicate the interpretation of some studies.

Noise. Measurement of mEPSC parameters is complicated by noise; both the usual experimental noise (approximately Gaussian and additive) and several other sources of low-frequency "noise". These include exogenous sources of low-frequency (e.g. 60 Hz) noise, and endogenous sources of low-frequency noise. For accurate measurement of an EPSC, one must also accurately measure the baseline, as well as identify the endpoint of the EPSC. The latter is also obscured both by noise and by baseline drifts and the occurrence of other PSCs. Both of these latter effects increase in probability as the current (EPSC) duration increases (as in slower, more distal events), and increase in impact as the amplitude of the EPSC is reduced. Therefore they will tend to selectively impact the parameters of distally-generated EPSCs, and will also have more impact on those parameters which require measurements to be made over all or a large part of the EPSC: area and half width.

I have used simulations to assess the impact of some of these noise sources on the

[26] Kinetic variability as shown above is already sufficient to generate broad or skewed distributions of all parameters except amplitude without including a nonzero R_s.

measurement of EPSC parameters. In the simplest case, Gaussian noise was added to each simulated mEPSC. Peak amplitude measurements are unaffected (Fig. 4-29A), except for the very smallest (most distal) events. Rise times and half widths of proximal events (smaller values) are similarly unaffected (Fig. 4-29A). However, measured rise times of distally generated events (larger values) are systematically larger in the presence of noise. In contrast, the half widths of distally generated events are systematically smaller with noise. Most strikingly, the addition of noise causes measured half widths to plateau at a value of approximately 5 ms, with no further increases as the synapse is moved more distally. At that point, the synaptic current has decayed to the level that a noise swing will go below the half-amplitude mark, effectively curtailing the mini in the "eyes" of the measurement algorithm. The effect on maximum rate is exactly the opposite: smaller values (more distal synapses) are unaffected by the presence of noise, while larger values (proximal inputs) are systematically reduced by the presence of noise, as the slope of the noise itself begins to be measured rather than the slope of the EPSC. However, in spite of these large effects, Gaussian noise has little effect on the correlations between parameters, other than to increase the amount of scatter (Fig. 4-29C).

As a simple model of these other sources of low-frequency noise, I added noise to the baseline measurement as well as to the mEPSC itself. As all amplitudes, areas, etc, are measured relative to this baseline, this will have far-reaching effects on mEPSC parameters. In this case, the noise in the baseline was the same as that added to the rest of the EPSC; this is an overestimate of this particular source of noise, as the experimentally-measured baseline is averaged, and will be less subject to noise than the points of the EPSC themselves. However, it does not take into account the additional, and possibly even larger, sources of noise mentioned above, so serves as an example of a medium-bad case. Amplitude, rise time, and maximum slope were not significantly more affected by the presence of baseline noise than by noise in the EPSC trace itself (data not shown, see Figure 4-29A). However, half width (Fig. 4-29B, left), and area (Fig. 4-29B, right) were much more significantly affected when the baseline

was noisy than when the traces alone were contaminated by noise. Again, the effect of the additional noise source on half width is much more pronounced on distally-generated events (larger values), though instead of a systematic reduction in measured half widths as is seen with simple Gaussian noise, adding baseline noise adds a large degree of scatter in the measured values of distal half widths. The effect of baseline noise on area is even more pronounced. This somewhat artificial method of inducing noise first of all causes the area measurement to sometimes be negative. Besides that, these values are incredibly scattered, showing essentially no correlation with the true, noise-free values. In contrast to the lack of effect of Gaussian noise alone, adding baseline noise does significantly affect the relationships between parameters. It strongly increases the scatter in the relationship between distally generated rise times and half widths (Fig. 4-29D, left), and practically reverses the direction of the relationship between area and half width (Fig. 4-29D, right).

Testing for the effects of noise in recorded mEPSCs. To test the effect of noise on measured parameter values, a population of 1031 events from one cell were fit according to Equation 2.1, and synaptic shape parameters were measured from the fits, on the theory that the fitted values will be less susceptible to experimental noise. Figure 4-30A shows the relationships between the values of each parameter measured from the fits and those measured from the raw data traces. Tight correlations between directly measured and fitted amplitudes and areas (Fig. 4-30A1,A2) suggest that in fact these parameters may be well-estimated in the experimental data. The latter is a surprising finding in light of the results presented in Figure 4-29. The strong correlation between area and integration period (Fig. 4-30C) suggests a tendency for baseline drift to interfere with area measurements. Estimates of half width are somewhat more susceptible to noise (Fig. 4-29). Half width as measured from the data systematically underestimates the value measured from the fits (Fig. 4-30A3), as expected from simulations. However, the size of the error is independent of the synapse location (actual half width), while the simulations would predict that the error would

have increased with increasing half width (synapse distance from the soma). Most surprisingly, rise time showed the worst correspondence between measured and fitted values. This result suggests that rise times are consistently overestimated and that the amount of error increases as the rise time increases (Fig. 4-30A4).[27] In any case, these results suggest that our models of experimental noise are inadequate, but that parameters measured directly from the data rather than from fits are robust enough for analysis.

Is area a robust parameter? The results presented on page 167 and in section 4.3.5 imply that caution should be used in the interpretation of mEPSC area measurements. Area is frequently used as a robust measure of EPSC characteristics, as it is relatively impervious to electrotonic filtering, and, because it is averaged over a long period is thought to be relatively impervious to noise. In the presence of simple, Gaussian noise, area is indeed a fairly robust measure – as can be seen in Figure 4-29B, noise adds scatter uniformly across all events, and the estimation of area in the presence of noise is unbiased. In theory, if one low-pass filters the data sufficiently, the area estimate should only improve. However, in practice, area estimates are very sensitive to other sources of noise, particularly low-frequency noise, and previous studies have concluded that peak amplitude can be a more robust measure than area, [131], even under relatively optimal conditions. Most importantly, in practice, one can only integrate an EPSC for a limited amount of time before noise or the presence of another mEPSC would bias the area estimate. This means that the integration period must be limited. There are two approaches to doing this: integrate each area for a fixed period, or adaptively choose the integration period based on the duration of the mEPSC. The latter allows use of the minimum integration period possible for any given event, thus minimizing the probability of the occurrence of a second mEPSC

[27]This was discovered to be partially due to a design flaw in the algorithm used to measure rise times, which led to significant overestimates of rise times in slow events, but little error for rapid events. The algorithm was fixed and critical data was reanalyzed with the new algorithm. In any case, no conclusions were altered by the error.

or significant baseline drift during the integration. However, it does require accurate detection of the end of the mEPSC, which is much more difficult for smaller events. This may bias the area measurement, as can be seen in Figure A-60A,B Right. There are two other methods for estimating area which may get around this problem. The first is to integrate for a fixed period, adding the same potential for bias to all events. This approach is frequently taken, however, the integration period is usually chosen to be quite short, to minimize the low frequency noise effects mentioned above. This has some extremely undesirable effects. One is that it is effectively measuring the area under the peak of the event, rather than the event as a whole. Instead of being relatively impervious to electrotonic filtering, this "short-area" measure is in fact somewhere between peak amplitude and area in its attenuation characteristics (data not shown), decreasing exponentially with distance, though somewhat more slowly than amplitude. It also has none of the theoretical advantages of measuring area itself and none of the intuitive advantages of measuring peak amplitude. The prefered approach may be to integrate area for a fixed window long enough to contain the longest mEPSC. However, this requires carefully selecting events and analyzing only those area values for which this entire period is free of contamination.

A third method which may get around some of the problems endemic to the other two is that used on page 169: fitting a function to the mEPSC, and then measure the area under the function rather than the mEPSC itself. While time-consuming, this approach is likely to be the most robust; however the fitting of exponential functions is notoriously ill-conditioned and one must be careful to avoid systematic fitting errors which will bias the area estimate. Surprisingly given the arguments above, application of this technique suggests that area measurements are, as expected *a priori* extremely robust in practice, at least in the data presented here. However, given the considerations mentioned above, it is important to consider the effects of various noise sources in analyzing any or all mEPSC parameters.

4.3.7 Evidence for cable filtering of mEPSCs.

Now, at last, armed with this understanding of how these candidate sources of synaptic variability manifest themselves in EPSC parameters and parameter correlations, we can finally return to our original question: is there experimental evidence that cable filtering does influence mEPSC shape?

Before returning to the parameter correlations introduced above, let us look more closely again at the relationship between mESPC rise time and peak amplitude. The idea that the concave, V-shaped relationship between these parameters might actually be indicative of electrotonic filtering is not an intuitive one. However, it is true that if cable filtering does shape mEPSCs, then slower events should have a tendency to be smaller. This holds true for the mEPSCs recorded in cortical cells. While fast events cover the whole range of amplitudes, slow events are restricted to being very small; similarly the largest events tend to have very rapid rise times (Fig. 4-31D). I have examined this in more detail by dividing the population of mEPSCs into 5 non-overlapping subpopulations with increasingly slower 10-90% rise times, and comparing their averages (Fig. 4-31A) and cumulative amplitude distributions (Fig. 4-31B). Progressively slower subpopulations of events tended to show progressively smaller amplitudes.[28]

The classical measure of electrotonic filtering in a cable model is the degree of correlation between rise time and half width [203, 206]. The simulations performed above showed that this is best predictor of a significant effect of electrotonic filtering in the generation of mEPSC shape (Fig. 4-32A), even in a morphologically complex cell composed of multiple cables, and in the presence of multiple other sources of synaptic variability. In fact, there is a strong correlation between these variables both for the events of a single cortical neuron (an example is shown in Figure 4-32B, R=.6, $p < .0001$) and in the pooled set of 4500 mEPSCs from 3 cells used above (Fig. 4-

[28]This effect is minimized here by restricting most of the divisions of the event pool to contain some of the faster events. See Figure 6-48 for a more striking example of this type of analysis.

32C, expanded in D, R=0.583, $p < .0001$). This indicates that electrotonic filtering does significantly affect the shapes of mEPSCs. Though these correlations are highly significant due to the large number of points involved, the R values themselves are not particularly satisfying. Simulated mEPSCs show a correlation on the order of R=0.95 between rise time and half width. Other sources of effective synaptic variability, such as recording noise and kinetic variability (if present) will act to lower the absolute degree of correlation.

Evidence for other sources of mEPSC variability from parameter correlations.

Electrotonic filtering, though present, is likely not to be the only source of mEPSC variability. The data presented in Figure 4-19D and E, showing that the amplitude distributions of (overlapping) faster and faster subpopulations of events are basically the same, while not evidence for the absence of electrotonic filtering, is evidence that there must be some other factor present in addition to electrotonic filtering to explain all of the variability in the data.

Figures 4-33A and B show that there are strong correlations between both area and maximum slope and amplitude, which from the discussion above, are good evidence for the presence of conductance variability. Additionally, mEPSCs show a reasonable correlation between area and half width (Fig. 4-33C), supporting the presence of kinetic variability in this population of mEPSCs.

As a check on the robustness of these conclusions, equation 2.1 was fit to a population of 1031 events from 1 cell, and the shape parameters were measured from the fits to these events [274], in the hopes of reducing parameter contamination by noise. The parameter correlations obtained between these fitted parameters were unchanged from those measured from the raw traces (Fig. 4-30B), though the strength of correlation between area and half width was somewhat reduced.

Unfortunately, it is difficult to assess directly the amount of kinetic and conduc-

tance variability present in a population of inputs to a cell, because of the confounding effects of cable filtering. Section 4.3.5 presented one approach that has been taken to overcome this problem - using the kinetics of the synaptic events themselves to attempt to select a subpopulation unaffected by electrotonic filtering [41]. Applying this approach to mEPSCs from one cell yielded changes in the correlations between parameters predicted in Section 4.3.5 (data not shown). Limiting attention to the 25% of events with the fastest rise times drastically reduces the correlation between rise time and half width (population: R=.6, n=1492; fastest events: R=.361, n=362), as would be expected if we had removed the effects of electrotonic filtering. The correlation between area and half width was basically unchanged (population: R=.575, fastest events: R=.563). The correlations between area and amplitude and slope and amplitude became even stronger (area: population: R=.782, fastest events: R=.879, slope: population: R=.823, fastest events: R=.905), strongly supporting a contribution of conductance variability to the generation of mEPSCs.

As will be shown below, a simple model incorporating both cable filtering and conductance variability is consistent with almost all of the available data. However, there is one further parameter relationship which suggests that something else may be going on. Figure 4-34A shows that for simulated data, as might be expected from the appearance of Fig. 4-24A, rise time and amplitude actually show a very close inverse relationship to one another purely as a result of electrotonic filtering. However, real mEPSCs show no such relationship (Fig. 4-34B), instead showing a v-shaped relationship similar to that seen for rise time and amplitude directly. This inconsistency may be partially, but not entirely explained by the other sources of variability introduced above. Figures 4-34C-E show this relationship in a simple soma-cable model in the presence of cable filtering and either conductance (C) or kinetic variability (D) alone, or both together (E). While these plots are somewhat more similar to the experimental relationship, they still leave much to be desired. It is not clear whether a combination of the more complex morphology of a real cell, different assumptions about the nature of underlying synaptic parameter distributions, and experimen-

tal noise would together be sufficient to replicate the experimental relationship; or whether an additional factor not discussed here must also be playing a role.

4.3.8 Is cable filtering alone sufficient to explain mEPSC variability?

Evidence has been provided that electrotonic filtering does play a role in generating mEPSC variability. Simulations in Section 4.3.3 showed that such filtering is sufficient to generate most or all of the amplitude variability seen in voltage clamp. However, as described above (and see discussion), there is experimental evidence that other sources of variability play a role in shaping mEPSCs. Additionally, further analysis of the simulations suggest that at least one other such source of variability is *a priori* necessary to explain all of the variety in measured mEPSC parameters – electrotonic filtering alone cannot do so.

What cable filtering can't do.

As shown in Figure 4-21C, simulated amplitude distributions in current clamp do not always show the skewed shape seen in the data. In fact, all parameters which are subject to a considerable degree of intrinsic low-pass filtering: current clamp amplitudes, areas in both current and voltage clamp, and voltage clamp amplitudes under conditions of very high series resistance, in many cases show narrow, sometimes Gaussian-like simulated distributions (Fig. 4-35, left, but see Fig. 4-22A), while the experimental distributions for all of these parameters are skewed (Fig. 4-35, right). Together, these results suggest that cable filtering alone is not always sufficient to generate all of the aspects of mEPSC variability seen experimentally.

Addition of conductance variability.

If one compares responses to mEPSCs originating from different boutons, some or all of differences seen in their conductance or kinetics may arise from their different

locations on the postsynaptic cell.[29] Therefore it is optimal to look for evidence of conductance and or kinetic variability in the response to release from a single, identified bouton, though this may underestimate the total amount of conductance and kinetic variability seen across the population of inputs.

Such independent evidence for the presence of conductance variability in mEPSCs evoked even at a single synapse over time can be seen in the work of Bekkers and Stevens [17], who showed that it was possible to generate skewed amplitude distributions when evoking vesicle release with sucrose from a single bouton in cultured hippocampal neurons.

If electrotonic filtering alone is not sufficient to explain all of the measured mEPSC variability, will the addition of other sources variability allow a complete match to the data? To answer this question, I simulated mEPSC distributions from reconstructed cells, and incorporated conductance variability by generating a distribution of mEPSCs of varying amplitudes from each point on the cell. This is the most restricted way of extending the original model, as addition of kinetic variability adds a large degree of nonuniqueness, and there is no a priori constraint on what distribution of kinetic parameters to use. The evidence for the presence of conductance variability from parameter correlations presented above is quite strong (in contrast to the case for kinetic variability, which is a bit more shaky). Additionally, there is very strong evidence for the presence of conductance variability at central synapses from other studies [17, 274]. Most notably, Bekkers and Stevens have shown that in cultured hippocampal neurons repeated activation of a single bouton with sucrose generates mEPSCs with a skewed amplitude distribution [17]. It is therefore important to see if the addition of conductance variability alone is sufficient to supplement the effects of cable filtering and produce simulated mEPSC parameter distributions that match

[29]This is particularly a problem in the case of minimal stimulation or paired recording, where multiquantal release may also confound interpretation of the data. Even if one considers the kinetic and/or amplitude variability in the subpopulation of presumed uniquantal release events, these events from the same presynaptic axon may in fact arise from boutons widely separated on the postsynaptic cell (e.g. see Thomson and West, 1994 [259]).

those seen experimentally.

Adding conductance variability can indeed generate skewed current clamp amplitude and area (data not shown) distributions (Fig. 4-36, box). Any conductance distribution with a slight amount of skew is sufficient to greatly increase the match between the real and simulated parameter distributions (in fact even a Gaussian distribution may be sufficient). The resulting area distributions in fact more closely reflect the conductance distribution used in the simulations than they do any effect of electrotonic filtering [17]. This suggests that the shape of the experimental area distribution may be a good starting point as an estimate of the true conductance distribution in these cells.

Adding even the large amount of conductance variability shown in the bottom panel does not damage the match between other parameters and the data, in fact it only improves it. This can be seen on the right, where voltage clamp amplitude and rise time distributions are shown for the same 2-Gaussian conductance distribution shown on the left. The skew of these distributions is also somewhat increased, but the predominant effect is simply a smoothing of their previous shape. This suggests that the data is consistent with the presence of a reasonable degree of conductance variability.

In the presence of conductance variability, cable filtering still strongly influences mEPSC shape.

Even in the presence of extensive variability in synaptic conductance (Fig. 4-37), there is still a very strong relationship between amplitude and distance, showing a powerful effect of cable filtering on synaptic shape (also see Sections 4.3.5 and 4.3.5). While proximal events cover a wide range of amplitudes, due to their wide variation in underlying conductances, distal events are limited to being very small events in spite of the fact that they have the same conductance distribution as the proximal events. The tight correlation between rise time and half width (R=.905) in this noise-free case

is a good indicator of the continued presence of cable filtering. There is a reduction in the correlation between rise time and amplitude (R=.540), resulting in a relationship between the two variables very similar to the experimental one (Fig. 4-37), is not indicative of a lack of cable filtering, and is in fact primarily determined by it.

How much conductance variability do we need?

We have seen from the discussion above that there is evidence for the presence of multiple sources of variability in the generation of the distributions of mEPSC parameters. How much do each of these sources contribute to the generation of mEPSC variability?

As noted above, it is difficult to assess directly the total amount of conductance and kinetic variability present in the population of inputs to a cell. One alternate approach is to ask, quantitatively, how much additional variability is needed to explain all of the experimental findings. Addition of conductance variability was shown to be sufficient, in the presence of cable filtering, to replicate the experimental distributions of mEPSC and mEPSP parameters. We can therefore put a bound on the relative contributions of cable filtering and other sources of variability by asking exactly how much conductance variability is necessary to generate the full range of mEPSC/mEPSP variability seen experimentally?

Unfortunately, the answer is "it depends". It does depend, on exactly how much variability can be generated by electrotonic filtering alone. While it is true that with the "standard" parameters used for most of the simulations shown here, the cell shown in Figure 4-21B does indeed have unskewed current clamp amplitude and area distributions, for other cells (Fig. 4-22A), and other sets of parameters (Fig. 4-38, which uses the same cell morphology as in Figure 4-35), it is possible to generate significantly more skewed distributions of these parameters purely by electrotonic filtering. Many of the parameter changes which increase the amount of skew (e.g. increase in synaptic conductance, changes in passive parameters, slowing of synaptic

kinetics) also increase the amplitude of simulated current clamp events into the experimental range, a necessity for any adequate model of mEPSP generation. Therefore, to adequately answer this question, we must much first more tightly experimentally constrain both the passive and synaptic parameters used in simulations.

Even then, the answer we come up with will probably not be unique, as these sources of variability are redundant (as can be seen in Figure 4-36) – addition of extra sources of variability does not always qualitatively change the resulting parameter distributions, it may simply smooth them. However, it should be possible to put an upper bound on the amount of mEPSC variability that could have been generated purely by electrotonic effects. Such simulations are the subject of the next chapter.

4.4 Discussion

Electrotonic filtering is sort of like crime. In this day and age, everybody accepts that it occurs, but everybody assumes it would never happen to *them* – or to the data they record. Its existence is treated with an unusual combination of flagrant disregard and total acceptance. Electrotonic filtering does exist, it is a logical consequence of the basic properties of neurons and their membranes [201, 205, 97, 269]. However, it is one thing to acknowledge its theoretical existence, but quite another to understand its effects in a particular experimental situation. Only recently have we started to understand to what extent electrotonic filtering will impact any particular signal in any particular cell, with its complex morphology and passive properties [242, 150, 152, 153, 151, 154]. The conclusions of a number of recent theoretical studies, however, are simple: electrotonic filtering has a larger impact on more classes of cellular signals than previously considered [242, 150, 154].

In this chapter, I have shown using computational simulations that on its own, electrotonic filtering can generate most of the characteristics of mEPSC parameter distributions.

I have then attempted to answer the question of whether, in fact electrotonic

does contribute to mEPSC variability, and whether any other sources of variability are involved as well. To do this I used simulations to examine the correlations between synaptic parameters generated by cable filtering and other sources of synaptic variability, to see what aspects of these correlations could be used as evidence for the presence of these factors. I also identified which of the synaptic parameters are most useful for identifying location or other characteristics of the source synapse (see Section 4.3.4).

4.4.1 Electrotonic filtering is necessary to explain some characteristics of mEPSCs.

I have examined the parameter correlations present in experimentally-measured mEPSCs, and used these results to conclude that while electrotonic filtering does play a significant role in generating mEPSC variability due to the correlation between mEPSC rise times and half widths, other sources of variability (notably kinetic and conductance variability) also are likely to be present. I have used one such additional source, conductance variability, to show that a small amount of additional variability is sufficient, together with cable filtering, to match the general characteristics of the distributions of all mEPSC parameters. While kinetic variability may also play a role, conductance variability and cable filtering together are sufficient to reproduce the data.

These conclusions are at odds with those of other studies which have strongly downplayed the role of electrotonic filtering in shaping EPSC/IPSCs [209, 41, 244, 163, 164, 144, 145, 217, 94], however, these studies all relied on the lack of relationship between EPSC/IPSC kinetics (usually rise time) and amplitude to draw their conclusion that PSC amplitude was not determined by filtering. As shown above, amplitude and rise time have vastly different relationships to underlying synaptic structure, and hence their relationship to each other is complex to say the least. Rall's original work on identifying the input location of an EPSP from its shape

[203, 206] avoided the question of amplitude entirely, by normalizing all synaptic conductances to generate the same EPSP amplitude at the soma. That work concentrated on using purely kinetic metrics, particularly plots of rise time and amplitude, as a marker of electrotonic filtering and as an indicator of synaptic source location. Notably, a correlation between rise time and half width, indicative of a strong effect of electrotonic filtering, has been found in almost every study that has looked for one – both in the data presented here (Figure 4-32), and in the data from a variety of other systems, both in miniature and action potential-dependent events [206, 96, 100, 162, 262, 289, 163, 164, 274, 184, 259, 182, 150, 104, 128]. Perhaps most tellingly, using sucrose to evoke mEPSCs from increasingly distal regions of the dendrites of cultured hippocampal cells gives rise to events with increasingly smaller amplitudes and slower time courses, matching the predictions of electrotonic filtering [19].

Unfortunately, the presence of noise and the effects of series resistance make it difficult to interpret correlations between mEPSC parameters. For instance, noise can induce a positive correlation between time to peak and amplitude [126], hiding the true relationship between these parameters. It is therefore risky to rely entirely on these correlations to assess what underlies the variability of mEPSCs. Additionally, it could be that a conspiracy of factors make it appear that filtering is truly shaping events (see Section 4.3.5), while all events are really proximal. Or, electrotonic filtering could play an important role in shaping mEPSCs, but in practice we could be unable to detect more than the most proximally-generated events which could be largely free of filtering (but see Figure 4-28, Chapter 6). Can we be sure that electrotonic filtering really plays a major role in generating mEPSC variability? In addition to the evidence from other studies presented above for the presence of electrotonic filtering and other sources of variability in generating mEPSC amplitude distributions, Chapter 5 presents an experimental attempt to directly assess the role of electrotonic filtering in generating mEPSC shape.

If we accept a role for electrotonic filtering in generating mEPSC variability (and

even if we don't), the next important question is: what else contributes? First, can we say *a priori* that there has to be something else? The answer to that appears to be yes. Even if the passive parameters of the cell model used in Figure 4-35 could be tweaked sufficiently (as in Figure 4-38) to account for all of the data, there is additional positive evidence that something else must be playing a role. First, the parameter correlations presented in Figure 4-33 suggest that both kinetic and conductance variability add to the generation of mEPSC variability. Second, the fact that the fastest events seen in Figure 4-19 cover the whole range of amplitude values, and that progressively faster subsets of the data have similar amplitude distributions, suggests strongly that some other source of variability (possibly in addition to cable filtering) is generating very fast events with a wide range of amplitudes. Finally, a number of other studies have presented strong experimental evidence for both conductance [17, 274, 95] and kinetic variability [190] in the generation of minimal events in other systems. The answer, however, may be system- and synapse-dependent – in some cell types [41], the relationship between rise time and amplitude is not of the standard concave form seen in Figure 4-19A, instead being completely scattered. These cells are likely candidates for a large degree of kinetic variability between their synapses, and perhaps a less significant role for cable filtering.

4.4.2 Electrotonic filtering is not sufficient to explain all of mEPSC variability.

As discussed above, and as can be seen from the simple observation that the fastest events in a plot of rise time vs amplitude cover the whole range of observed amplitudes (Fig. 4-19), at least one additional source of variability is necessary to explain the experimentally-measured properties of mEPSCs. I have suggested two additional sources of synaptic variability, namely conductance and kinetic variability, which might account for the rest. These properties were suggested on *a priori* grounds, and an attempt was made to define them abstractly enough that they encompassed

a wide variety of mechanisms. However, do they, together with cable filtering, span the whole space of possible sources of variability? In a very limited set of cases, the answer is yes. If we limit ourselves to a completely passive cell (possibly one whose electrotonic properties are allowed to be nonuniform), with synaptic inputs described by Equation 2.1, then the only parameters subject to change are those that describe the passive properties of the cell or the synapse location (cable filtering), the peak amplitude of the synapse or its reversal potential (conductance variability), and the kinetic parameters τ_R and τ_D (kinetic variability). In this limited, abstract, mathematical universe, we can say that those are the only sources of synaptic variablity.

What happens in a more complicated system? Do all of the biological mechanisms we can think of really reduce to these simple mechanisms? In a lot of cases, they do. Any variance in the release process that affects the postsynaptic cell (i.e. if the receptors aren't saturated) will act as a source of conductance variability or kinetic variability, depending on whether there is a change in the amount of transmitter released (discrete or continuous)/number of channels opened, or in the time course of transmitter release or degradation. Perhaps in the biological case, these two effects (conductance and kinetic changes) cannot happen independently, but we can still treat them mathematically as if they do. If we widen our allowable range of models for the postsynaptic cell, i.e. the factors that contribute to cable filtering, things get more complicated. Nonuniformities in the cable structure of the cell, e.g. those due to localized inhibition, simply add an additional source of variability. If those nonuniformities are allowed to vary over time, at least to a limited degree (e.g. transient large-conductance inhibitory inputs to a portion of the cell), they can probably be encompassed in our extended version of cable filtering by considering them as multiple synchronous spatial differences in cable properties, as we dealt with variability in a single input over time by reducing it to differences between different inputs each of which would be in a unique state, as no single input is likely to be seen twice during the usual periods of observation. With the addition of nonlinear conductances, however, all bets are off.

This study is one showing the plausibility of electrotonic filtering as a source of synaptic variability.

Control of EPSC/EPSP amplitude The data presented on correlations between rise time and half width in this and other studies strongly supports a major role for electrotonic filtering in the generation of mEPSC shape. However, a much more contentious question is how much it contributes to generation of mEPSC *amplitude*. As noted above, every study that has looked for a correlation between synaptic input amplitude and kinetics has failed to find one, and usually such studies have concluded that either electrotonic filtering does not contribute to the generation of EPSC/EPSP properties (those studies looking only at rise time vs amplitude), or that it contributes to EPSC shape, but not to amplitude (those studies looking at rise time vs half width plots). In particular, the pioneering studies which used shape indices such as these to compute probable synaptic location for inputs to alpha motoneurons [206, 100] showed that for those, action potential-dependent inputs, there was no relationship between computed synaptic location and synaptic amplitude; and in one case it was suggested that distal inputs were actually systematically larger in amplitude than proximal ones [100].

There are two major, additional factors which come into play when one moves from mEPSCs to action potential-driven events (or events recorded in the absence of TTX). One is the fact that a given presynaptic cell can make multiple contacts on the postsynaptic cell, sometimes in widely different locations [60], providing a source of conductance variability between single-axon inputs. This is strongly exacerbated in the case of massed, rather than minimal electrical stimulation – there are a number of studies using such population stimulation to show that, in fact, EPSC/EPSP kinetic parameters change as predicted by cable theory as the stimulus is moved farther away from the soma [289, 6], however it is impossible to effectively compare amplitudes resulting from such stimuli as the number of fibers stimulated may vary widely.

The second is dendritic nonlinearities. While such nonlinearities have not been

studied in motoneurons, recent work in cortex has shown that the dendrites of pyramidal cells contain sufficient concentrations of Na^+ channels to support propagation of action potentials [252]. Work using Ca^{++} imaging [213], and the fact that mEPSCs are unaffected by bath application of Cd^{++} or other heavy metals,[30] suggests that mEPSCs themselves to not significantly activate these dendritic nonlinearities, but it is clear multiple inputs arriving under normal conditions will [37]. These nonlinearities may be differentially distributed in the dendrites [214, 292], and it has been suggested in some systems that they are in fact designed primarily to overcome the effects of electrotonic filtering by boosting synaptic signals [36, 37, 214, 292].

The remaining question, therefore, is what are the relative contributions of electrotonic filtering and these other sources of variability in generating the shapes of mEPSC parameter distributions? Unfortunately, that question can not be answered uniquely, as these multiple sources of variability are redundant. If we limit ourselves to the case of cable filtering and conductance variability alone, we can ask the more constrained question: how much conductance variability is necessary, in addition to cable filtering, to match quantitatively the distributions of mEPSC parameters from particular cells? To answer this question, however, we must use experimental data to limit the characteristics of both the cells and the mEPSCs under study – we must use the passive properties of particular cells to attempt to match the mEPSC parameter distributions measured from those same cells.

[30]These compounds block all Ca^{++} channels. They are usually employed to show that mini release itself is independent of Ca^{++}, but at the same time their lack of effect on mEPSC amplitude distributions demonstrates that dendritic Ca^{++} conductances are not significantly involved in the generation of mEPSC amplitude or shape.[172]

4.5 Figure Legends

Figure 4-17: MEPSCs show extensive amplitude variability. A. Traces (below) and amplitude histograms (above) illustrate the variability of the the amplitude and kinetics of miniature excitatory postsynaptic events (mEPSCs) recorded both in voltage clamp (left) and current clamp (right). Amplitude histograms show characteristic skewed shape. All cells showed similar amplitude variability and skewed distributions, though the absolute amplitudes varied between cells. B. Other parameters also show large variability and skewed distributions. Data from the same cell as A. C. Voltage clamp amplitude distributions from 20 cells are shown schematically. Each horizontal bar represents the amplitude distribution measured in one cell. The range of event amplitudes is shown by the bar length. Boxes indicate the portion of each distribution lying within the 25th and 75th percentiles. The center line the median (50th percentile). The mean amplitude is shown as a black diamond. Gray boxes represent events from layer V/VI cells, while white boxes represent events from layer II/III cells. The hatched box is from a cell of unknown layer. The cell marked a was recorded with a potassium gluconate-based solution in the absence of APV. The cell marked b was recorded with a KGlu solution at a temperature of 24.6°C. All other events were recorded in the presence of TTX (1 μM), APV (30 μM), and BMI (50 μM).

Figure 4-18: Could cable filtering contribute to amplitude variability? The effect of synaptic source location on the shape of synaptic current measured at the soma is schematized on the left. Currents coming from more distal synapses are smaller and slower than those originating more proximally.

Figure 4-19: mEPSCs show no correlation between rise time and amplitude. mEPSCs show no strong negative correlation between rise time and amplitude in either voltage clamp (R=.284) (A, amplitude and rise time distributions shown in B) or current clamp (C, R=.096). D. Amplitude distributions are generated for restricted subpopulations of events with increasingly faster rise times: all events, events with 10-90% rise times < 1.5 msec, 1.0 msec, 0.5 msec, and 0.25 msec, identified as 1-5, respectively.

Figure 4-20: Simulation paradigm used. Basic organization of all simulations used in this chapter. Synaptic inputs are placed sequentially onto each point of a reconstructed cell or cable model, and the resulting responses are used together with the distribution of synapses to generate simulated distributions of response parameters (see Methods for details). Synaptic inputs are controlled by four parameters:

location; G_{max}, the peak synaptic conductance; and τ_R and τ_D, the rising and decaying time constants. The effects of cable filtering are measured as the effect of input location on response properties. Changing G_{max} simulates the effects of a change in peak synaptic conductance. Changing τ_R and τ_D simulates the introduction of kinetic variability. (See Section 1.3.4.)

Figure 4-21: Cable filtering alone can generate skewed amplitude distributions similar to those seen experimentally. A. Simulated voltage clamp amplitude distribution shows the same amplitude variability and skewed shape seen experimentally. All underlying synaptic inputs were the same, cable filtering is the only source of variability. Input sites on the apical dendrite (including the proximal apical trunk) are shown as gray bars, basal sites in black. B. Small rat layer V pyramidal cell used for simulations shown here. Scale bar is 100 μm. C. Simulated current clamp amplitude histogram, inputs to the apical dendrite are shown in gray. This histogram is significantly narrower and less skewed than those seen experimentally. D. Relationship between peak response amplitude at the soma (circles) and synaptic input site (squares) and distance of the synaptic input from the soma (measured as dendritic path length). Apical inputs are shown as white symbols. Peak amplitude decreases extremely rapidly with distance, reaching a plateau $< 200\mu m$ from the soma, within the extent of the basal dendrites. There is little decrement in the subsynaptic current amplitude, indicating that loss of input current due to decreased driving force at the input site does not contribute significantly to the decrease in somatic amplitude. The vertical bar at 50 μm indicates that inputs more proximal than that may be overrepresented (see text).[31] Key in F is for D, E and F. E (expanded in F). The relationship between current clamp amplitude (at soma and synapse) and synaptic location. The relative decrement in somatic response amplitudes with distance (seen in F) is not very large in this cell, resulting in the narrow distribution of current clamp peak amplitudes shown in C. The detailed shape of the cell is reflected in the response amplitudes (subsynaptic amplitudes in E, to a lesser extent somatic amplitudes in D). In E, a close correspondence can be seen between the branching structure of the cell and the pattern of increasing subsynaptic amplitude with increasing distance (e.g. compare the three main branches of the apical tuft of the cell in B with the three lines of apical (white) subsynaptic responses (squares) on the right in E).

Figure 4-22: Most cells generate skewed voltage clamp amplitude distributions from cable filtering alone. Simulated voltage clamp amplitude distri-

[31] Removing these extra large-amplitude events in A would actually increase its similarity to experimental distributions by removing the bulge at the right end of the distribution.

butions for 5 additional cells. A. Large rat layer V pyramid. In this cell, the current clamp amplitude distribution is also skewed. B. Rat layer III pyramid. C. Cat layer V pyramid. D. Rat layer III pyramid. E. Thin rat layer V pyramid. All cells but D were filled with biocytin, the cell in D was filled with Lucifer yellow and reconstructed with a confocal microscope (see General Methods). All cells are at the same scale, scale bars are 100 μm. In A and C the pronounced distal tuft of these cells generates a cluster of very small amplitude events when measured at the soma, appearing as a "bump" on the left of the histogram. If such events exist, they would probably be below the threshold for event detection, and so would never be measured experimentally.

Figure 4-23: Cable filtering alone generates skewed rise time distributions in both voltage and current clamp. A. Voltage clamp and B. current clamp rise time distributions corresponding to the amplitude distributions shown in Fig. 4-21 A and C. C. Rise time increases slowly, almost linearly, with distance across the whole dendritic tree. D. Relationship between rise time and amplitude for this cell and a simple soma-cable model (inset).

Figure 4-24: Measured synaptic parameters show different relationships to distance. The relationship between the parameters of the somatic response (amplitude, rise time, half width, area, and maximum rate of rise, and location is illustrated using a simple soma and cable model (parameters: R_m=40,000 Ωcm^2, R_i=100 Ωcm, C_m=1.0 $\mu F/cm^2$, τ_R=0.1 msec,τ_D=1.0 msec, G_{max}=1 nS, R_s=0 $M\Omega$. The curves are, for each parameter, very similar in both voltage (A,B) and current (C,D) clamp. Area is shown only in D, the pattern in voltage clamp is basically identical. See text for discussion (section 4.3.4).

Figure 4-25: Similar parameter distributions have different underlying relationships to cell structure. Histograms of synaptic response parameters are color-coded according to synaptic location on the cell at lower left. The cell is divided up into regions of increasing 50 or 100 μm distance from the soma, as shown by the colored circles, and in the key above the cell. Three effects can be seen: first, an "axis compression" effect, where one small region of a cell can represent a wide range of parameter values while another, larger region generates only a much narrower range of values. Second, parameters whose distributions are qualitatively very similar in shape actually have totally different underlying relationships to the structure of the cell. Third, low-pass filtering of the synaptic signal, in the form of added series resistance in voltage clamp or looking at a parameter that is intrinsically low-pass filtered, such as current clamp amplitudes, or areas, has a much stronger effect on

proximal inputs than on distal ones.

Figure 4-26: Sources of synaptic variability other than cable filtering. A. Effect of conductance variation alone on parameter correlations. 1000 synaptic inputs were simulated in a single compartment model (length = diameter = 80 μm, to give the same total surface area as a full cell model). The kinetics of each input were identical (τ_R=0.1 ms and τ_D=1.0 ms), but the peak conductance, G_{max}, was evenly distributed between 0.0 and 5.0 nS. As EPSC slope, amplitude, and area are all proportional to conductance, they are tightly correlated with one another. B. Kinetic variation alone. In the same single-compartment model, 2000 synaptic inputs were simulated that varied widely in their kinetics: τ_R and τ_D were drawn independently from flat distributions which ranged from 0.05-1.5, and from 1.0-10.0 ms, respectively. G_{max} was fixed at 1 nS. Peak amplitude was therefore constant, but all other synaptic parameters varied with the kinetics. B1. There is a weak correlation between rise time and half width. B2. Area and half width are tightly correlated. B3. Maximum slope is tightly correlated with Rise Time^{-1} (B3). C. Parameter relationships in the presence of both conductance and kinetic variability. 2000 simulated EPSCs were generated in the same single-compartment model, and both G_{max} and τ_R and τ_D were allowed to vary (independently) according to the distributions described above for A and B, respectively. C1. Amplitude and rise time are independent. C2. Rise time and half width show the same mild correlation described for B1. C3a,C4a. Relationships between area and half width and maximum slope and Rise Time^{-1}. C3b,C4b Same relationships with area and slope normalized by peak amplitude. See text. Passive parameters for these simulations: R_m =40,000 Ωcm^2, R_i =100 Ωcm, C_m =1.0 $\mu F/cm^2$, and R_s =0 $M\Omega$.

Figure 4-27: Effects of cable filtering in combination with other sources of synaptic variability. A. Relationships between parameters seen in the case of cable filtering alone. An identical synapse was moved sequentially out a simple 1-λ soma-cable model, and synaptic parameters were measured. B. Relationships between parameters seen in the presence of both cable filtering and conductance variability. A single synaptic input was moved sequentially out a simple soma-cable model as described in A. At each location, 30 points were simulated with varying values of G_{max}. In this case, G_{max} was distributed as the sum of two Gaussians, with means of 0.75 and 1.5 nS (σ = .3 nS). Similar results were seen with the flat distribution of peak conductances used above (Fig. 4-26A,C). C. Relationships between parameters seen in the presence of both cable filtering and kinetic variability. Simulation as described in A, except at each location on the model, 50 EPSCs were simulated with kinetics drawn from the distribution used in Figure 4-26B. D. Relationships between parameters seen in the presence of cable filtering, kinetic variability, and

conductance variability. Simulations as described in A, 50 inputs simulated at each input location. Conductance distribution used taken from B, kinetic distributions same as C. Relationships pictured in D1-4 same as B1-4, described above. See text for discussion.

Figure 4-28: Selection of fastest events allows some examination of underlying kinetic variability. Simulated EPSCs from Figure 4-27 were sorted according to 10-90% rise time, and the 25% of events with the fastest rise times were selected in an attempt to minimize the impact of cable filtering on the resulting parameter relationships. A. Kinetic variability plus cable filtering. 1) Amplitude vs rise time. 2) Half width vs rise time. 3) Maximum slope and area vs amplitude. B. Cable filtering, and both conductance and kinetic variability. Graphs 1-4 as in A. See text for discussion.

Figure 4-29: Effect of noise on the measurement of mEPSC parameters. A. Effects on parameters of adding noise. Simulated parameter distributions were generated as in Figure 4-21 from the cell pictured in 4-21E. Gaussian noise (σ=3pA) was added to the simulated EPSC traces, which were then filtered at 3kHz with a digital Gaussian filter before parameter values were measured. EPSC length was taken as whole simulated time period (50.0 ms), and was the same for each EPSC - no attempt was made to detect the end of the EPSC, as is done with experimental mEPSCs. The value of each parameter in the presence of noise is plotted against the value measured from same location in the noise-free case. Diagonal lines indicate the identity relationship. B. The addition of low-frequency noise was modeled by repeating the simulations in A and adding the same Gaussian noise to the measured baseline value. Amplitude, rise time, and maximum slope were not significantly more affected by the presence of baseline noise than by noise in the EPSC trace itself (data not shown, see A). Half width (B, left), and area (B, right) were much more significantly affected when the baseline was noisy than when the traces alone were contaminated by noise. Both panels show the parameter measured in the presence of Gaussian noise alone (filled triangles), and with both Gaussian trace noise and baseline noise (open circles). C. Parameter correlations in the presence of Gaussian noise alone. Simulations and parameters as shown in A. D. Additional effects of baseline noise on parameter correlations. Parameter correlations for simulations and parameters shown in B.

Figure 4-30: Assessing the robustness of experimental parameter correlations. A population of 1500 events from one cell were fit according to Equation 2.1 using a Chebyshev algorithm (Axograph). 1031 events yielded adequate fits. Synaptic

shape parameters were measured from the fits in order to examine the susceptibility of typical measurement methods and parameter correlations to noise. A. Directly measured values are plotted against those measured from the fits to each event for: 1. Amplitude 2. Area. 3. Half Width. 4. Rise time. The gray line is the line of best fit to the data points. The black line in 3 and 4 is the identity relationship (the slope of the best fit line in 1 and 2 is 1.0). B. Parameter correlations measured from the fits. B1) There is still a strong correlation between rise time and half width (relationship for direct measurement shown in Figure 4-32B). B2) Area and half width are still somewhat correlated. B3) Rise time and amplitude are completely uncorrelated. C. There is a strong correlation between area and integration period, suggesting a tendency for baseline drift to interfere with area measurements.

Figure 4-31: Cable filtering is necessary to explain some features of the data. Three layer III cells were selected on the basis of recording quality, and 1500 events from each were pooled to generate this population distribution (total N = 4500). Rise times range from 0.1-10 msec, and the rise time distribution is skewed. The population of mEPSCs were divided into non-overlapping subpopulations with increasingly slower rise times by arbitrarily binning those events with rise times < 0.5 ms, 0.5-1.0 ms, 1.0-1.5 ms, 1.5-2 ms, and > 2 ms. A. Averages of these subpopulations of cortical mEPSCs. B. Cumulative amplitude distributions for the five subpopulations shown in A. Note that populations of mEPSCs with distinct and progressively slower rise times show progressively smaller amplitudes (see also Figure 6-48). C. Amplitude and rise time distributions for the total population of events shown in A and B. D. There is no strong negative correlation between rise time and amplitude in this population of events (R=.256). Note that while fast events cover the whole range of amplitudes, slow events are restricted to being small.

Figure 4-32: Correlation between rise time and half width suggests the presence of cable filtering. A. Simulations (of the same cell shown in Figure 4-21, see legend to that figure for details) predict that in the presence of cable filtering alone, there should be a strong correlation between rise time and half width [203, 206]. B. Data from one cell recorded in the presence of TTX (1 μM), APV (30 μM), and BMI (50 μM), showing a reasonably strong correlation between rise time and half width (R=0.54, n = 1489 events). Other cells tested showed similar, if not stronger, correlations, with R values of around 0.6. C. 4500 events pooled from three cells also show a strong relationship between rise time and half width (R=0.579). D. Plot in C shown on expanded scale. This strong relationship holds between events with smaller rise times and half widths, and is not simply a feature of slower events.

Figure 4-33: Correlations between parameters provide evidence for additional sources of variability. Other parameter correlations are shown for the population of 4500 events pooled from three cortical cells (see above). A. Strong correlations between maximum slope and amplitude (R=.809), and B. area and amplitude (R=.785) suggest the presence of conductance variability in the generation of these events, although to some degree such a relationship can be generated by electrotonic filtering alone (see Section 4.3.5 and Figure 4-27). C. A positive correlation between area and half width strongly suggests the presence of kinetic variability (R=.535). Without kinetic variability, cable filtering would be expected to generate a negative relationship between these parameters, even in the presence of conductance variability. D. A strong positive correlation between Area/Amplitude and half width supports either the presence of kinetic variability (see Figure 4-26), or cable filtering, or both (see Figure 4-27). These relationships were all seen for each of the three cells pooled here when taken individually, and so are not simply artifacts of combining events from different cells with different properties.

Figure 4-34: Lack of relationship between amplitude and inverse rise time cannot be easily explained. A. Simulated mEPSCs show a very tight inverse relationship between rise time and amplitude (shown as a linear correlation between amplitude and the inverse of rise time). B. Real mEPSCs show no such correlation. Amplitude is plotted against inverse rise time for events in one cell. Kinetic and conductance variability can account for some, but not all, of the experimental relationship. Amplitude is plotted against the inverse of rise time for events in a soma-cable model in the presence of cable filtering and C. conductance variability, D. kinetic variability, and E. both conductance and kinetic variability.

Figure 4-35: Cable filtering alone cannot match all of the characteristics of recorded mEPSC distributions. As shown in Figure 4-21C, simulated amplitude distributions in current clamp do not always show the skewed shape seen in the data. In fact, all parameters which are subject to a considerable degree of intrinsic low-pass filtering: current clamp amplitudes, areas in both current and voltage clamp, and voltage clamp amplitudes under conditions of very high series resistance, all show narrow, sometimes Gaussian-like simulated distributions, while the experimental distributions for all of these parameters are skewed. This is shown here for simulated current clamp amplitude and area distributions, on the left, compared to their skewed counterparts from actual data, on the right. Area, in particular, shows very little decrement over the distance ranges present in this cell. According to cable theory, area should decrease approximately as steady-state voltage [201, 205, 97, 269], this can be seen both in the truly exponential decrease shown in Figure 4-24D, and here in the similarity between the simulated area distribution and the distribution of DC

transfer impedances shown at the bottom of the figure. Together, these results suggest that cable filtering alone is not always sufficient to generate the mEPSC variability seen experimentally.

Figure 4-36: Adding conductance variability generates mEPSC variability consistent with data. Effects of adding conductance variability. Conductance variability is specified in terms of a probability distribution of peak synaptic conductances (G_{max}) occurring at each synaptic connection. In the box, current clamp amplitude distributions are compared for various distributions of underlying synaptic conductances. The conductances used here was in the linear range, so the desired conductance distribution was convolved with the result of standard constant-conductance simulations to arrive at the simulated variable-conductance distributions. The resulting current clamp amplitude distributions are shown for the following conductance distributions: constant (top, parameters as in standard simulations, cable filtering alone generates variability); Gaussian (middle, Gaussian distribution has mean of 1 nS, σ=0.5 nS); and a skewed sum of two Gaussians (bottom, means 0.75 and 1.5 nS, σ=0.3 nS).[32] Absolute amplitudes are still not as large as those seen experimentally (compare to Figure 4-17), however (see section 4.3.8), but the shape of the distribution is much more realistic. Right panel: Adding even the large amount of conductance variability shown in the bottom panel does not damage the match between other parameters and the data, but in fact only improves it. Voltage clamp amplitude and rise time distributions are shown for the same 2-Gaussian conductance distribution shown on the left.

Figure 4-37: Cable filtering still controls mEPSC characteristics in the presence of significant conductance variability. A. Plot of voltage clamp peak amplitude vs distance for simulations with 2-Gaussian underlying conductance distribution shown in Figure 4-36 (compare to Figure 4-21A). B. Amplitude vs distance plot for current clamp for the same underlying conductance distribution, showing that while cable filtering is less dominant under these conditions, it still plays a major role in shaping events. C (expanded in D). Voltage clamp amplitude vs. rise time for the events shown in A still shows the same concave shape as seen in the constant conductance simulations (compare to Figure 4-23D). But the area near the origin has filled in and the whole plot is somewhat more noisy. In fact it now bears a striking similarity to the usual experimental amplitude vs rise time plot (compare to Figure 4-19A).

[32] Any skew to the conductance distribution will increase the skew of the amplitude distribution, this data should not be interpreted to support a model of sums-of-Gaussian conductance distributions [274], an exponential or lognormal distribution would perform just as well.

Figure 4-38: Effects of parameters on degree of amplitude variability in current and voltage clamp. Effects of changing passive and synaptic parameters on simulated voltage and current clamp amplitude histograms (shown at top for comparison). Simulated cumulative amplitude distributions produced in the cell shown in Figure 4-21B. Baseline distributions used the following parameters: R_m=40,000 Ωcm^2, R_i=100 Ωcm, and C_m=1.0 $\mu F/cm^2$; τ_R=0.1 ms, τ_D=1.0 ms. A. Slowing the kinetics of the synaptic current input decreases the amount of attenuation it will undergo on the way to the soma. The standard amplitude histograms (above) are generated with τ_R= 0.1 msec, τ_D= 1.0 msec. An example amplitude histogram generated with τ_R= 0.2 msec, τ_D= 1.5 msec is shown in both current and voltage clamp. To the right of each amplitude histogram is shown a cumulative probability plot comparing the amplitude distributions generated with each of three sets of kinetics. B. Changing passive parameters can increase the skew of the distributions in both current and voltage clamp. The absolute effect of a particular value of R_s depends on parameters of both the cell and the synaptic input (see Figure A-66), as can be seen comparing the curves for R_s=10 with two different sets of passive parameters (the curve for R_s=0 with "GM" parameters is shown in B). D. Increasing the synaptic conductance in current clamp into the saturation range both moves the amplitudes measured at the soma into the experimental range, and increases the skew of the amplitude distribution (histogram at left). Cumulative amplitude distribution at right compares amplitudes normalized to the somatic response amplitude seen with that synaptic conductance (to allow comparison on one graph); as synaptic conductance increases the slope of the cumulative distribution decreases, indicating an increase in variability, and the midpoint of the normalized distribution moves to the left, indicating an increase in skew. Increasing the synaptic conductance beyond 5 n fails to further change the distribution shape, presumably due to increasing saturation. Cumulative amplitude distribution from B, using "GM" parameters, is included for comparison.

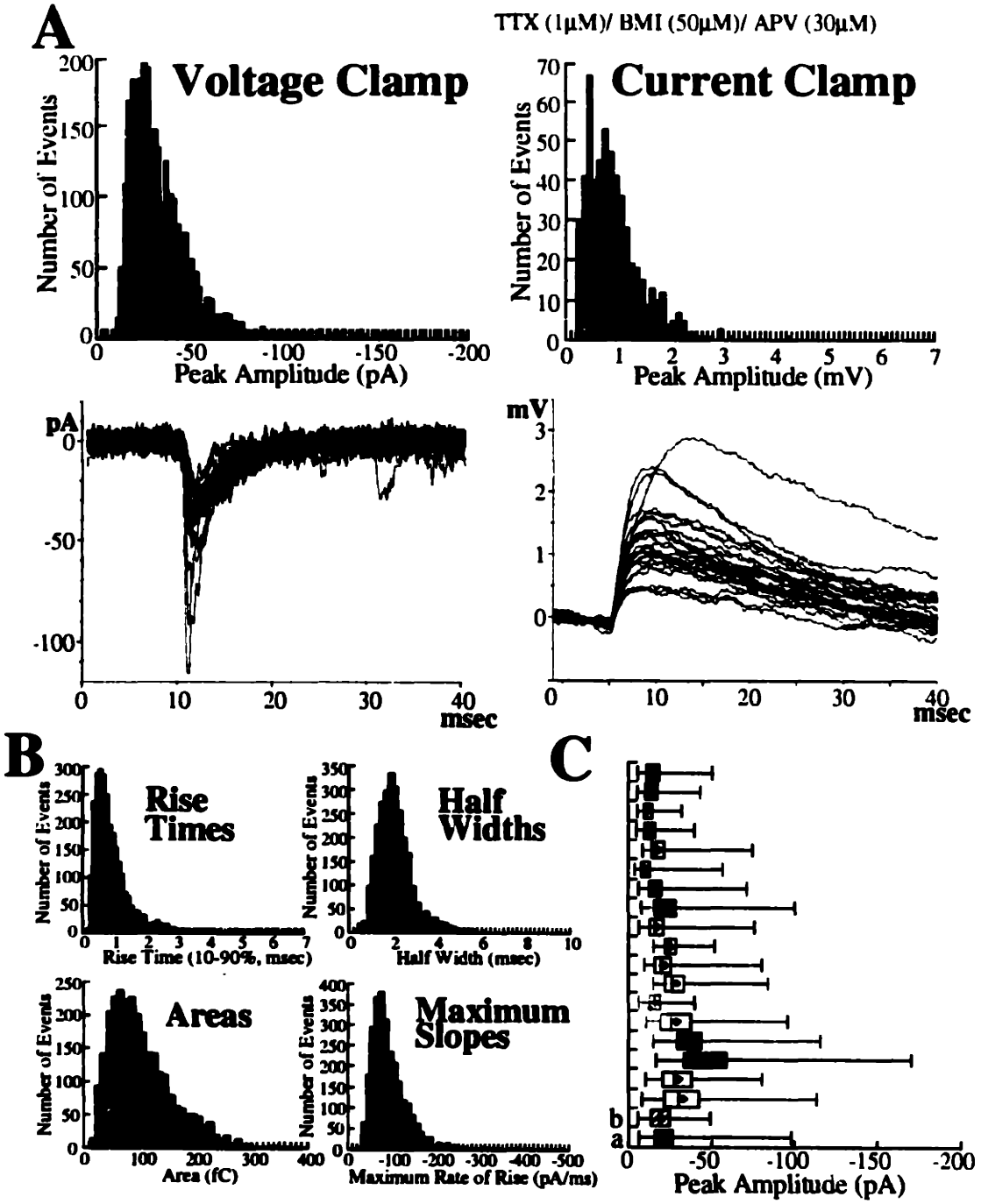
A
TTX (1μM)/ BMI (50μM)/ APV (30μM)
Voltage Clamp
Number of Events
Peak Amplitude (pA)
Current Clamp
Number of Events
Peak Amplitude (mV)
pA
msec
mV
msec
B
Rise Times
Rise Time (10-90%, msec)
Half Widths
Half Width (msec)
Areas
Area (fC)
Maximum Slopes
Maximum Rate of Rise (pA/ms)
C
b
a
Peak Amplitude (pA)

Fig. 4 - 17

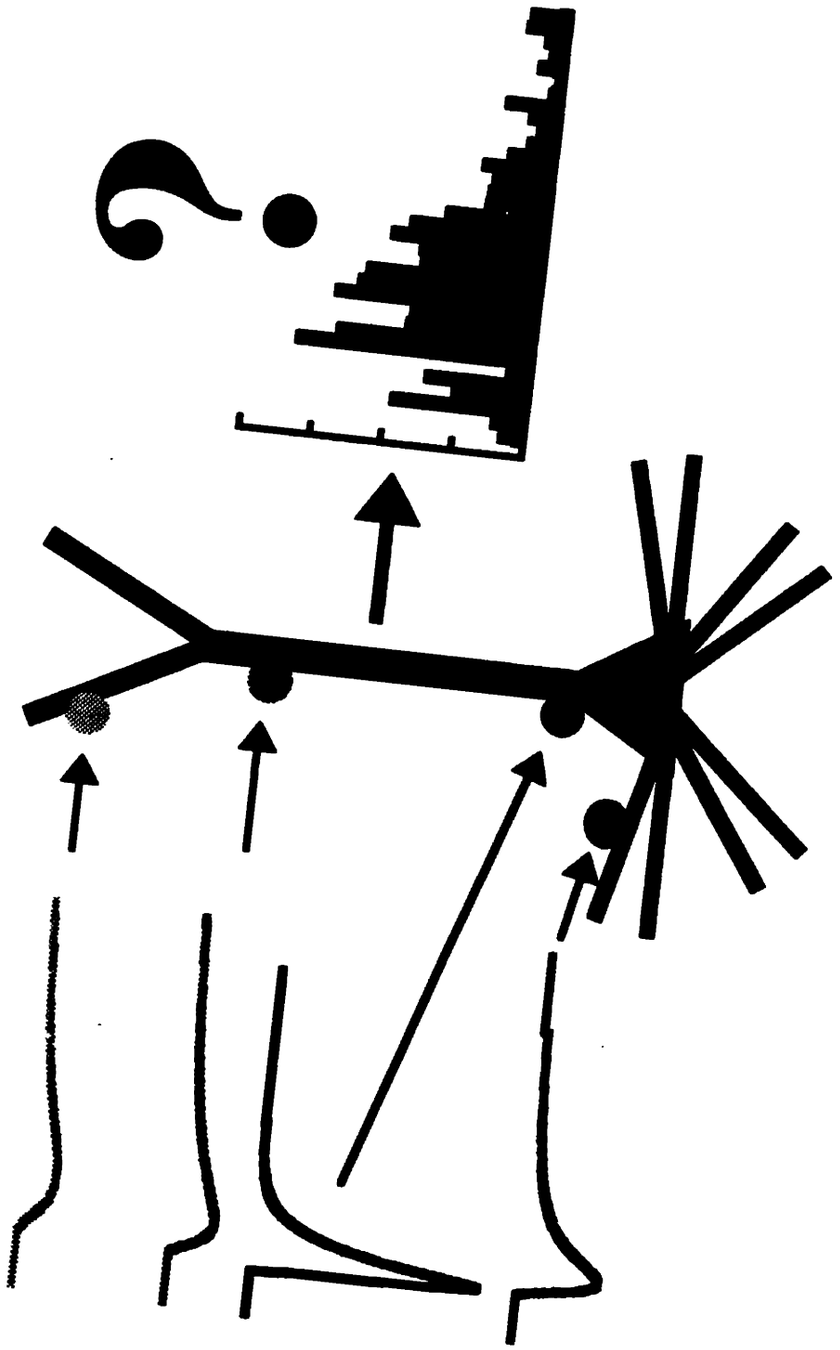

Fig. 4 - 18

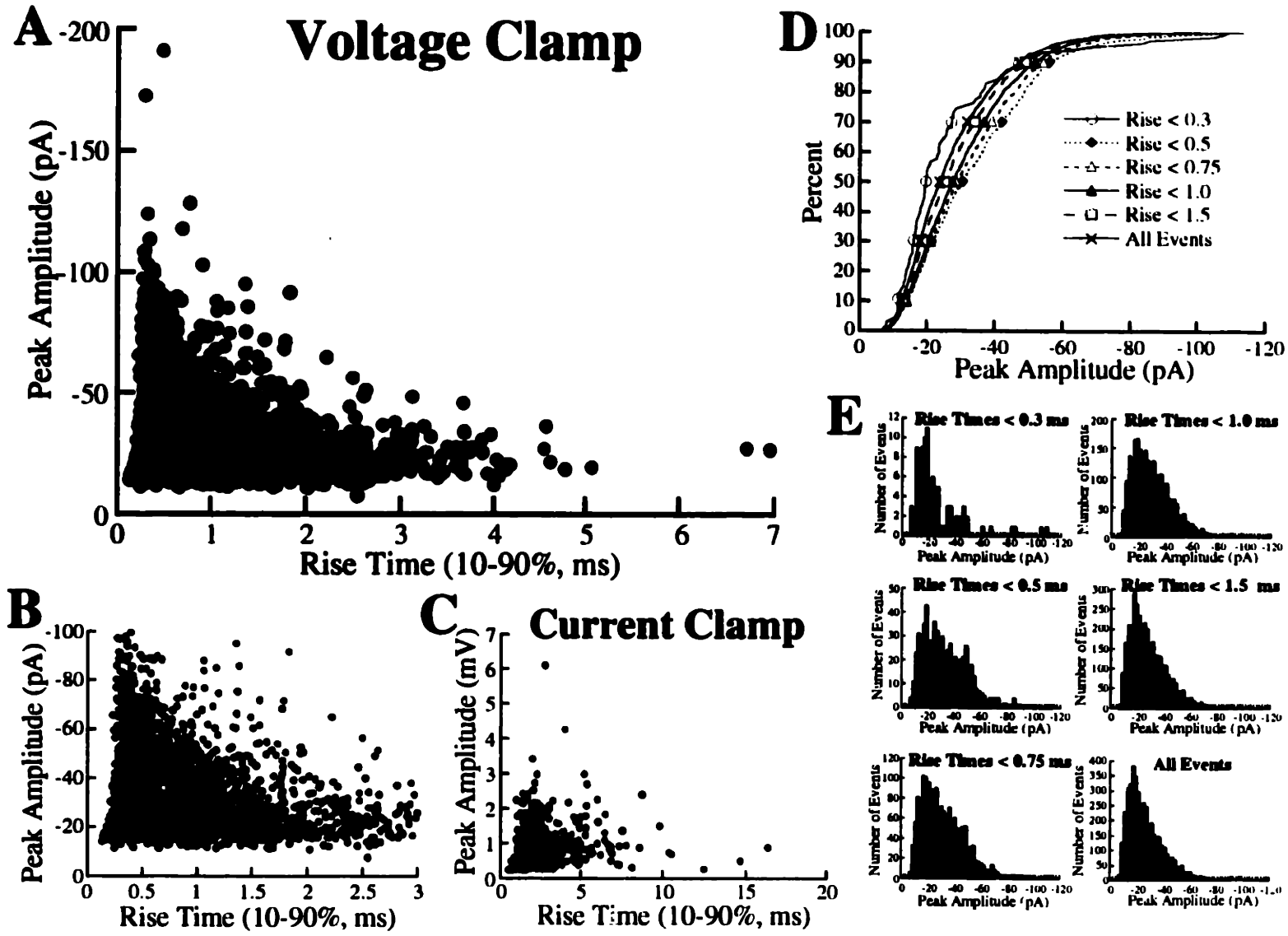
A
Voltage Clamp
Peak Amplitude (pA)
Rise Time (10-90%, ms)
B
Peak Amplitude (pA)
Rise Time (10-90%, ms)
C
Current Clamp
Peak Amplitude (mV)
Rise Time (10-90%, ms)
D
Percent
Peak Amplitude (pA)
Rise < 0.3
Rise < 0.5
Rise < 0.75
Rise < 1.0
Rise < 1.5
All Events
E
Rise Times < 0.3 ms
Rise Times < 1.0 ms
Rise Times < 0.5 ms
Rise Times < 1.5 ms
Rise Times < 0.75 ms
All Events
Number of Events
Peak Amplitude (pA)

Fig. 4 - 19

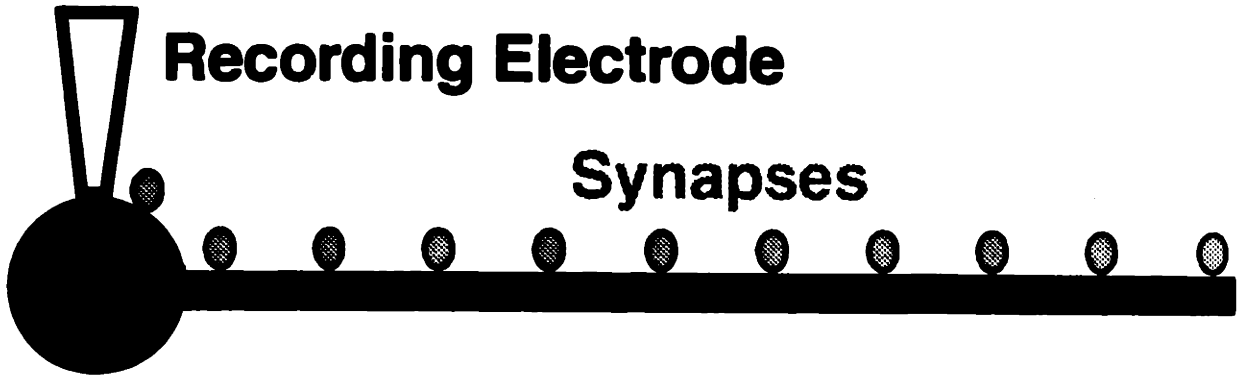

$$I_{syn} = g(t)\,(v - Erev)$$

$$g(t) = Gmax\,(e^{-t/\tau_2} - e^{-t/\tau_1})$$

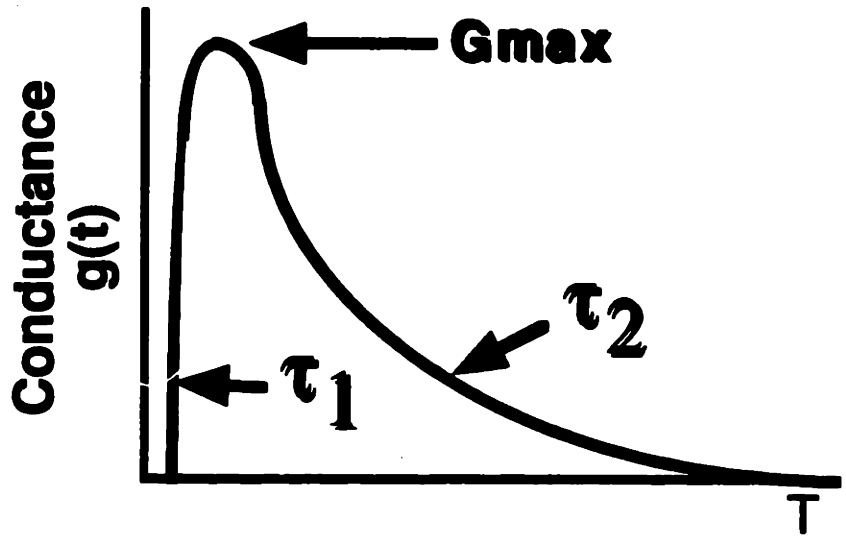

Conductance Variability:
change Gmax

Kinetic Variability:
change τ_1 , τ_2

Fig. 4 - 20

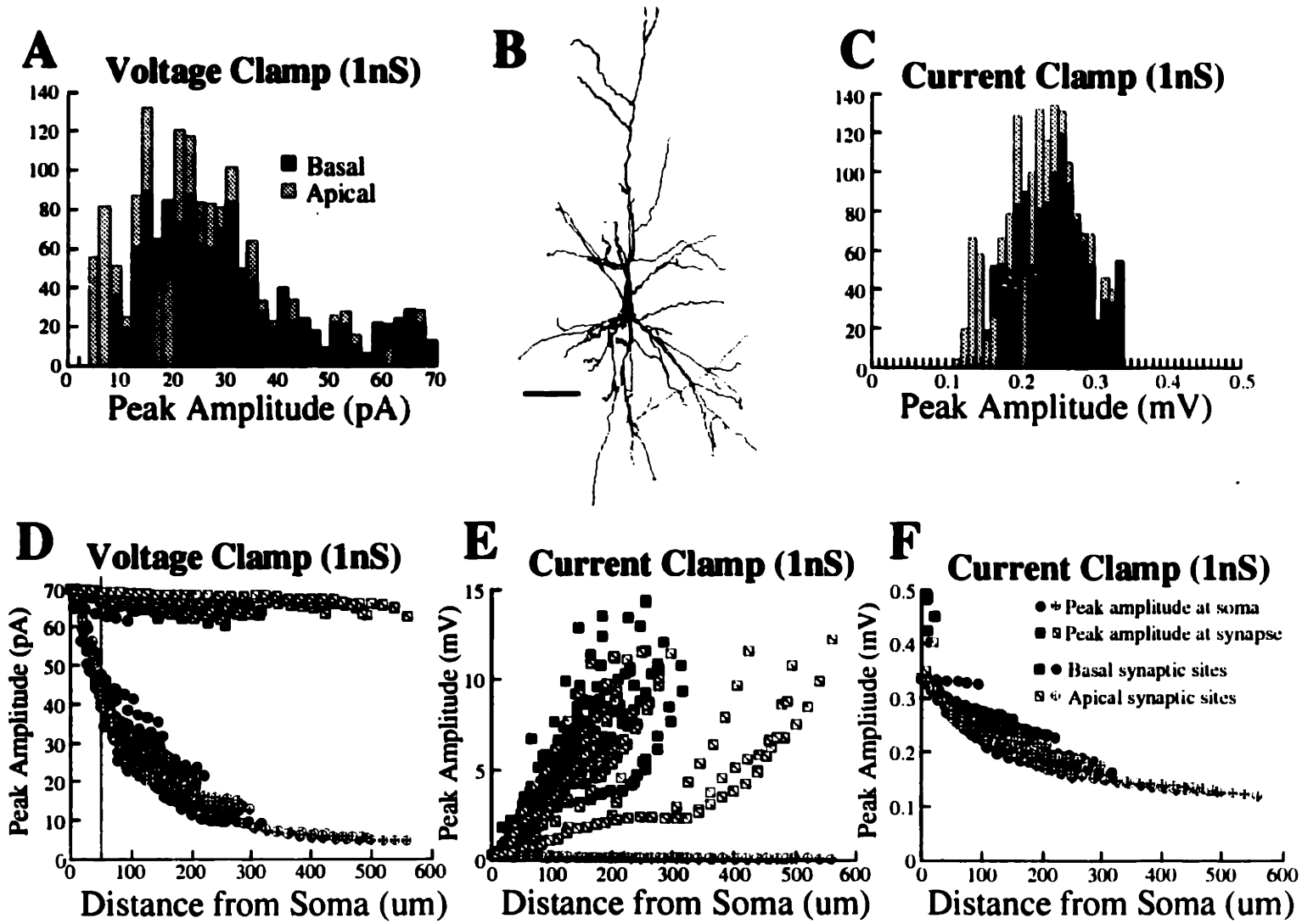
A
Voltage Clamp (1nS)
Basal
Apical
Peak Amplitude (pA)
B
C
Current Clamp (1nS)
Peak Amplitude (mV)
D
Voltage Clamp (1nS)
Peak Amplitude (pA)
Distance from Soma (um)
E
Current Clamp (1nS)
Peak Amplitude (mV)
Distance from Soma (um)
F
Current Clamp (1nS)
Peak amplitude at soma
Peak amplitude at synapse
Basal synaptic sites
Apical synaptic sites
Peak Amplitude (mV)
Distance from Soma (um)

Fig. 4 - 21

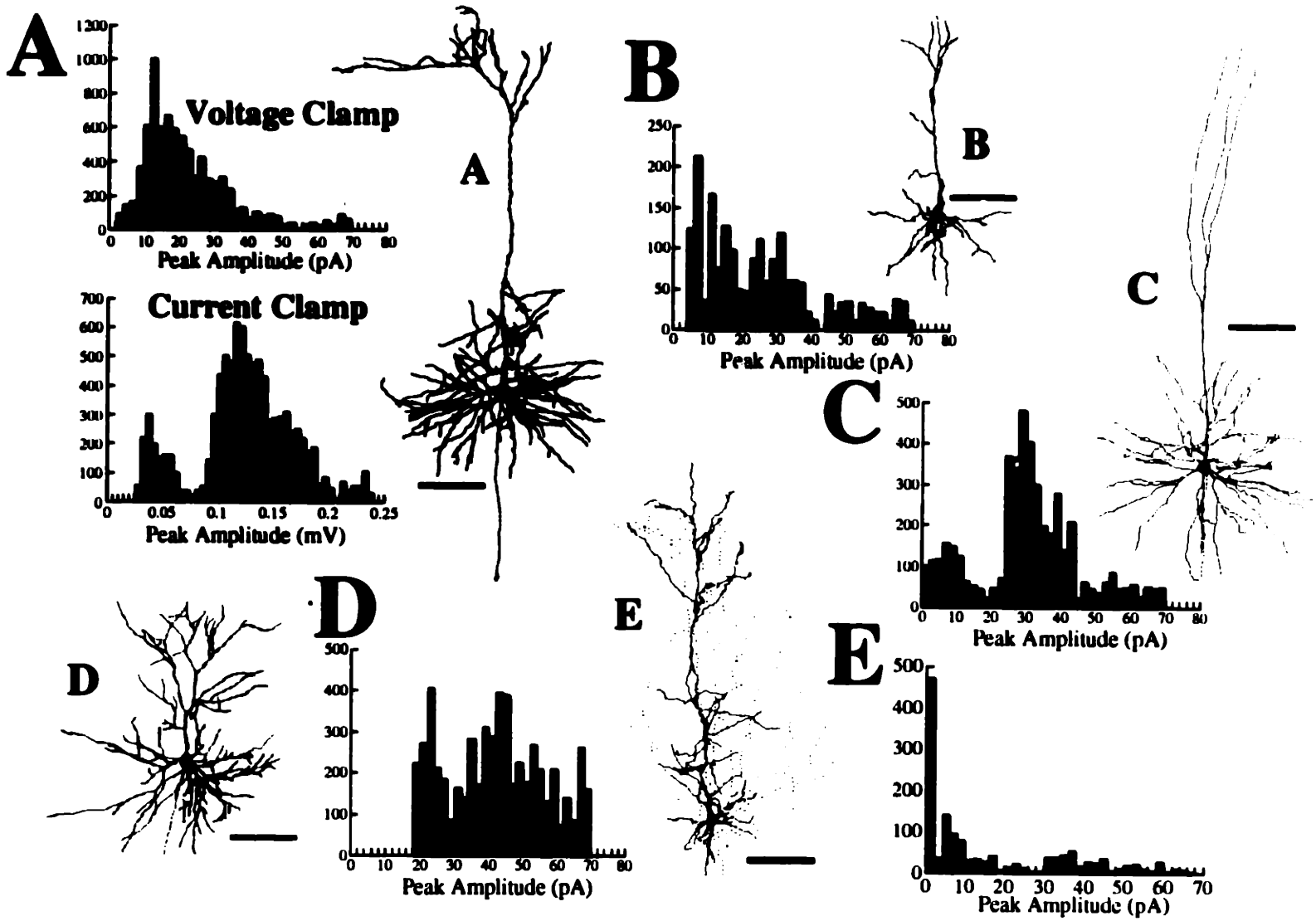
A
Voltage Clamp
Peak Amplitude (pA)
Current Clamp
Peak Amplitude (mV)
A
B
Peak Amplitude (pA)
B
C
Peak Amplitude (pA)
C
D
Peak Amplitude (pA)
D
E
Peak Amplitude (pA)
E

Fig. 4 - 22

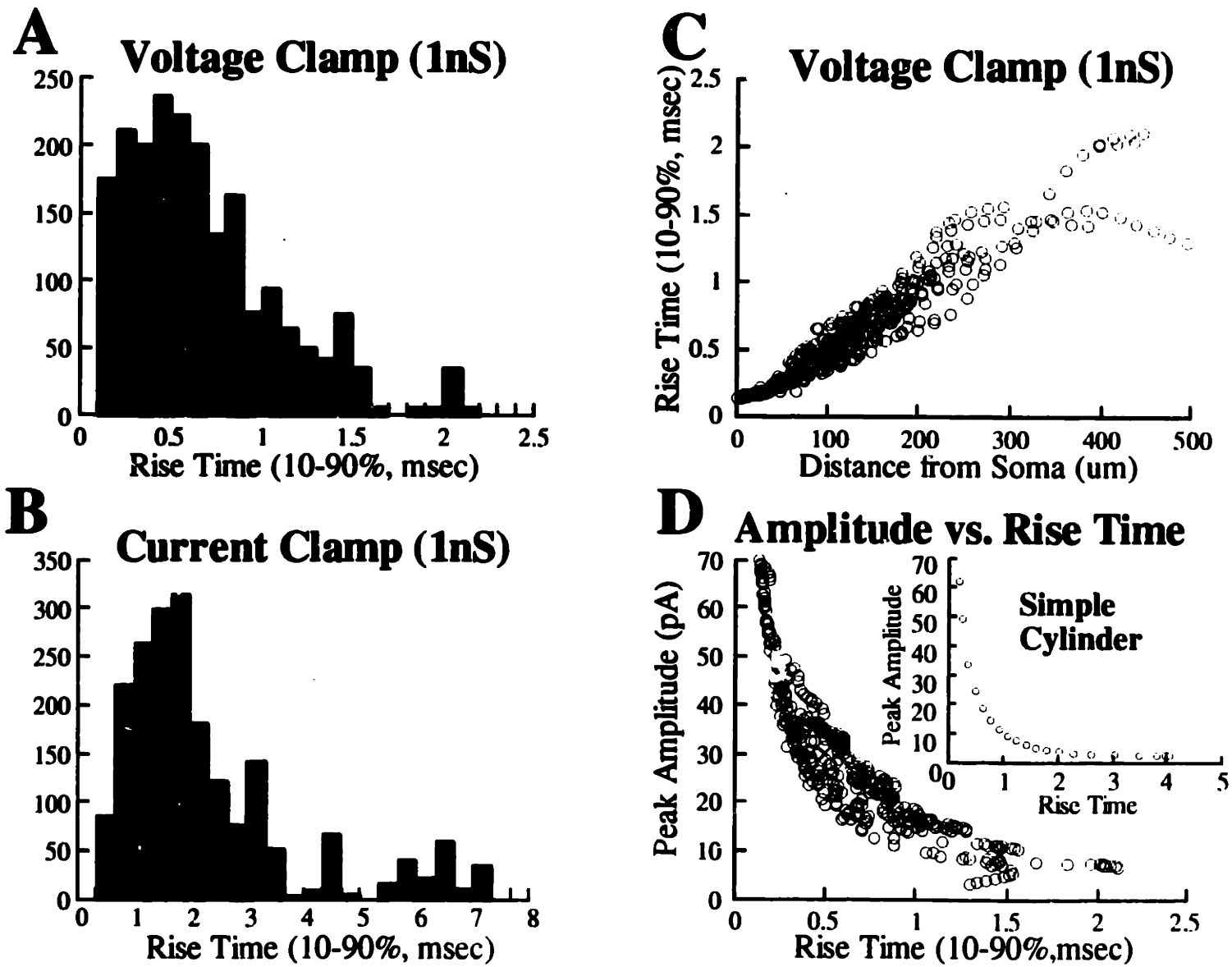
A
Voltage Clamp (1nS)
250
200
150
100
50
0
0
0.5
1
1.5
2
2.5
Rise Time (10-90%, msec)
B
Current Clamp (1nS)
350
300
250
200
150
100
50
0
0
1
2
3
4
5
6
7
8
Rise Time (10-90%, msec)
C
Voltage Clamp (1nS)
Rise Time (10-90%, msec)
2.5
2
1.5
1
0.5
0
0
100
200
300
400
500
Distance from Soma (um)
D
Amplitude vs. Rise Time
Peak Amplitude (pA)
70
60
50
40
30
20
10
0
0
0.5
1
1.5
2
2.5
Rise Time (10-90%,msec)
Simple
Cylinder
Peak Amplitude
70
60
50
40
30
20
10
0
0
1
2
3
4
5
Rise Time

Fig. 4 - 23

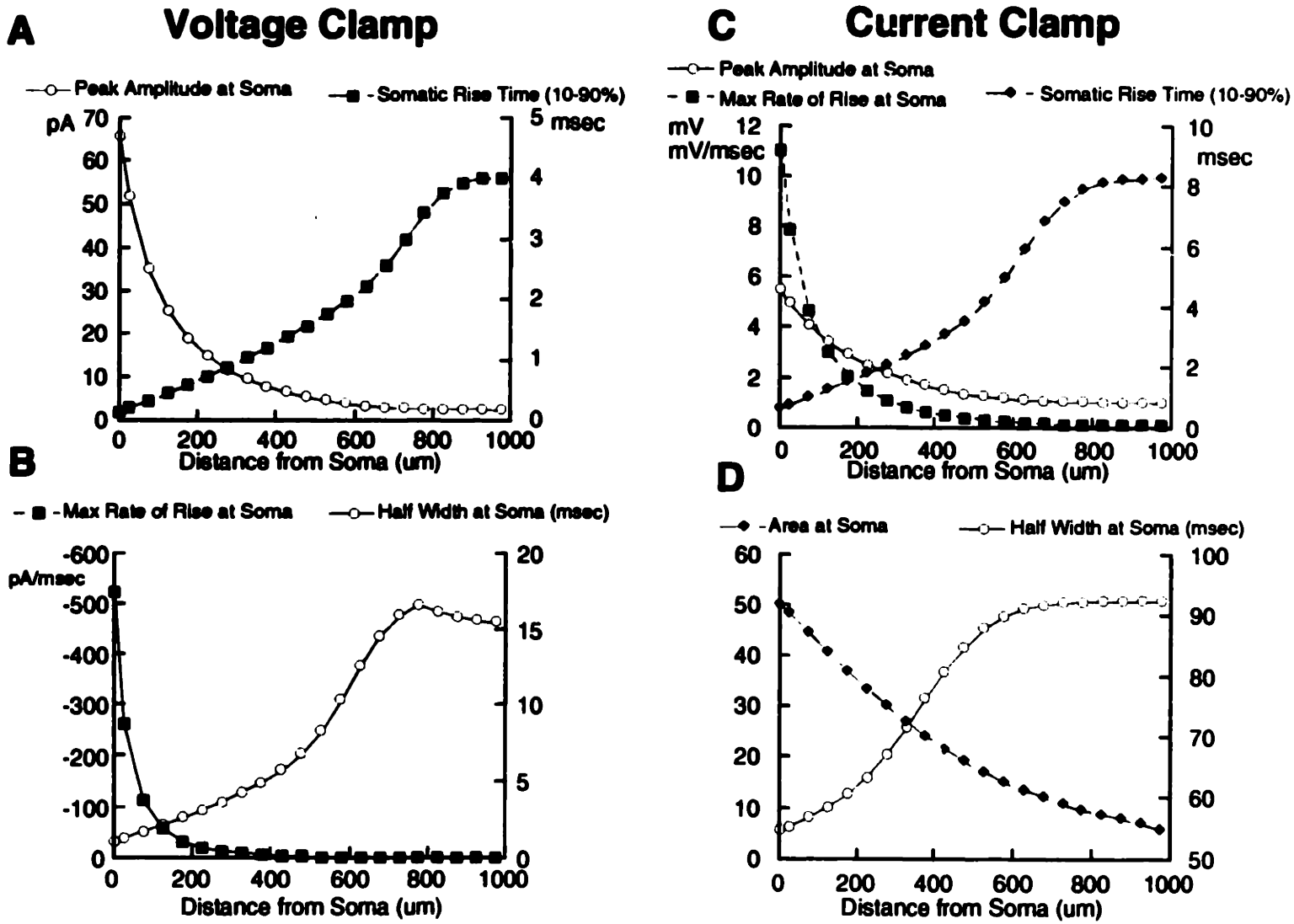
A
Voltage Clamp
Peak Amplitude at Soma
Somatic Rise Time (10-90%)
pA
70
60
50
40
30
20
10
0
5 msec
4
3
2
1
0
0
200
400
600
800
1000
Distance from Soma (um)
B
Max Rate of Rise at Soma
Half Width at Soma (msec)
-600
pA/msec
-500
-400
-300
-200
-100
0
20
15
10
5
0
0
200
400
600
800
1000
Distance from Soma (um)
C
Current Clamp
Peak Amplitude at Soma
Max Rate of Rise at Soma
Somatic Rise Time (10-90%)
mV
12
mV/msec
10
8
6
4
2
0
10
msec
8
6
4
2
0
0
200
400
600
800
1000
Distance from Soma (um)
D
Area at Soma
Half Width at Soma (msec)
60
50
40
30
20
10
0
100
90
80
70
60
50
0
200
400
600
800
1000
Distance from Soma (um)

Fig. 4 - 24

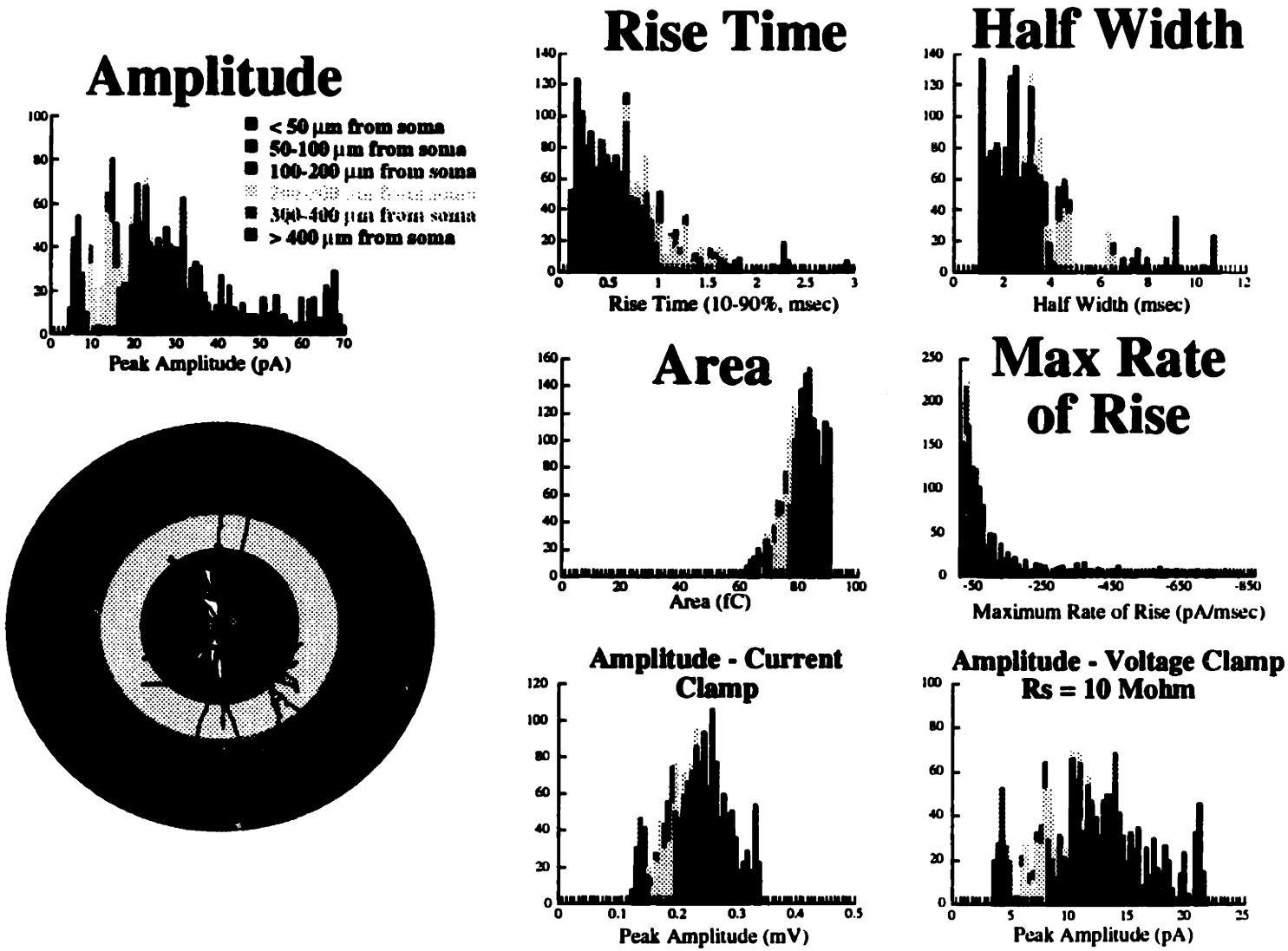
Amplitude
< 50 µm from soma
50-100 µm from soma
100-200 µm from soma
300-400 µm from soma
> 400 µm from soma
Peak Amplitude (pA)
Rise Time
Rise Time (10-90%, msec)
Half Width
Half Width (msec)
Area
Area (fC)
Max Rate of Rise
Maximum Rate of Rise (pA/msec)
Amplitude - Current Clamp
Peak Amplitude (mV)
Amplitude - Voltage Clamp Rs = 10 Mohm
Peak Amplitude (pA)

Fig. 4 - 25

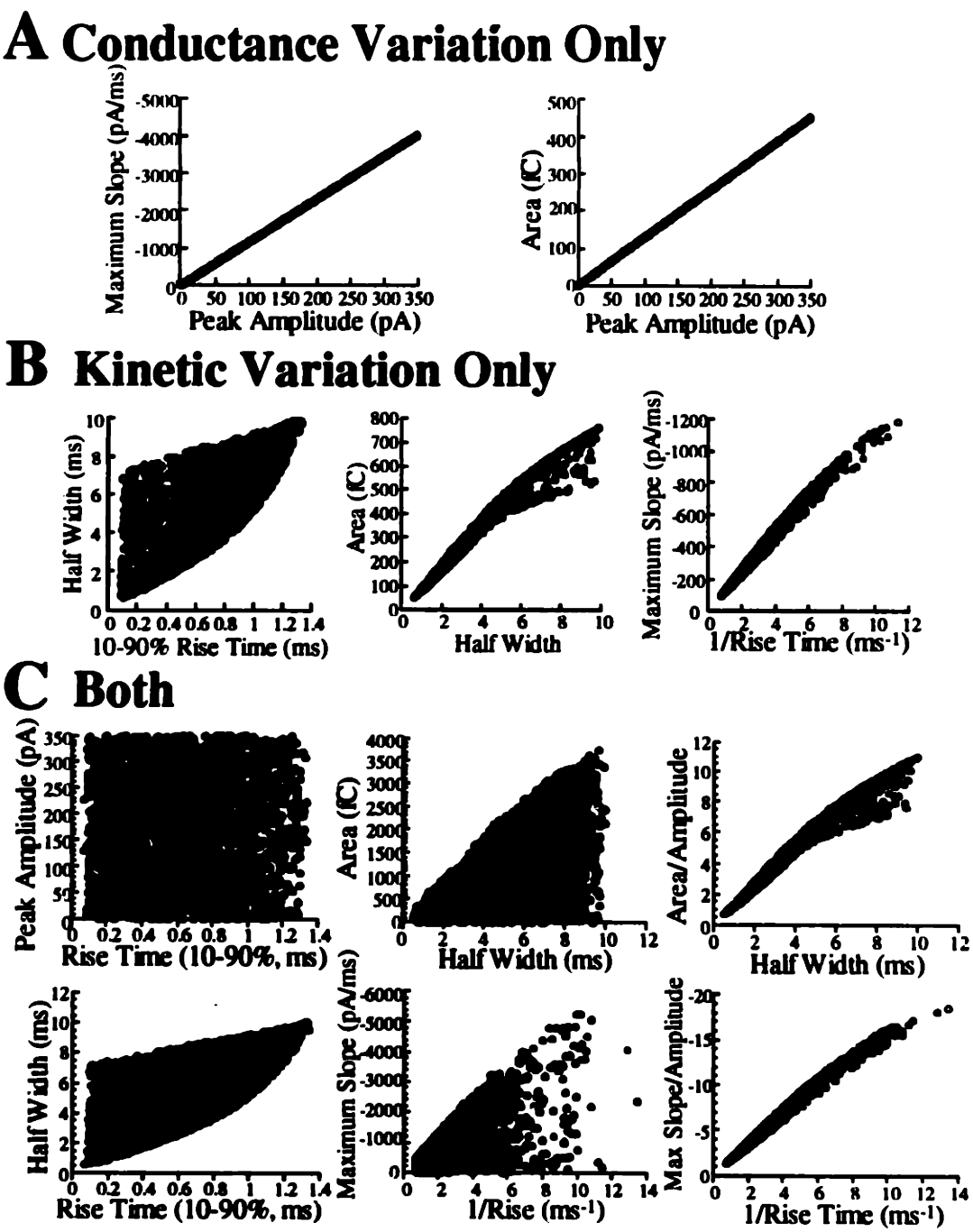
A Conductance Variation Only
Maximum Slope (pA/ms)
Peak Amplitude (pA)
Area (fC)
Peak Amplitude (pA)
B Kinetic Variation Only
Half Width (ms)
10-90% Rise Time (ms)
Area (fC)
Half Width
Maximum Slope (pA/ms)
1/Rise Time (ms-1)
C Both
Peak Amplitude (pA)
Rise Time (10-90%, ms)
Area (fC)
Half Width (ms)
Area/Amplitude
Half Width (ms)
Half Width (ms)
Rise Time (10-90%, ms)
Maximum Slope (pA/ms)
1/Rise (ms-1)
Max Slope/Amplitude
1/Rise Time (ms-1)

Fig. 4 - 26

A Cable

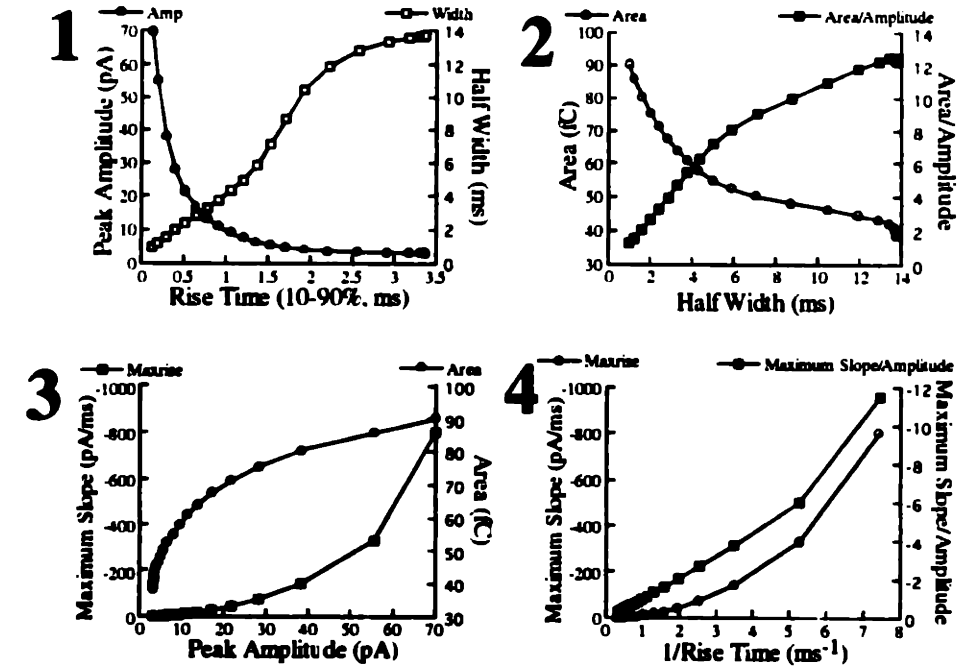

B Cable plus Conductance

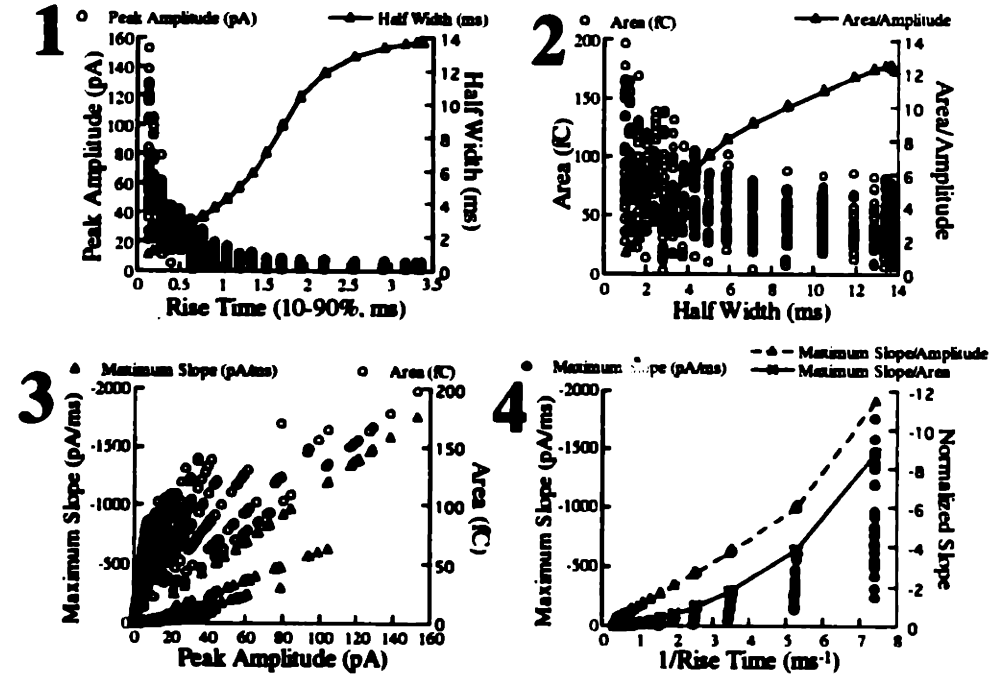

C Cable plus Kinetics

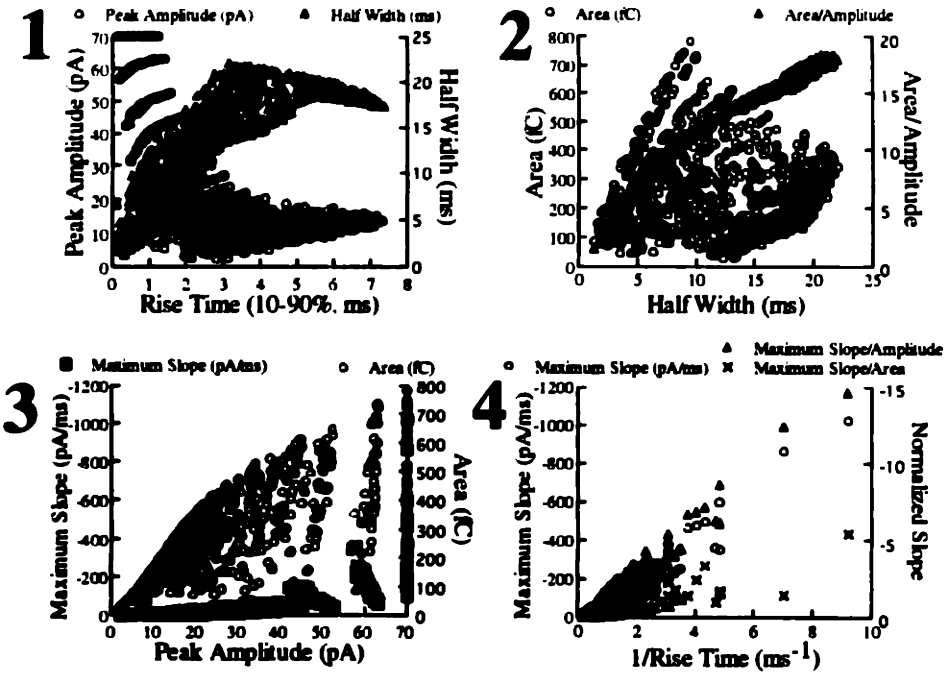

D Cable plus Both Conductance and Kinetics

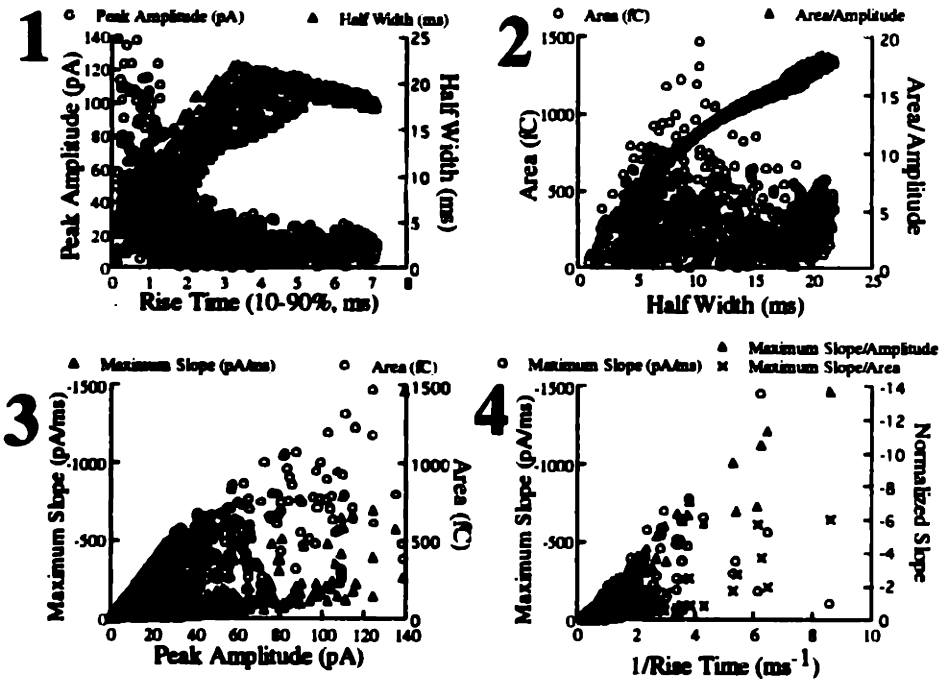

Fig. 4 - 27 p. 2

A Fastest Events, Cable plus Kinetics

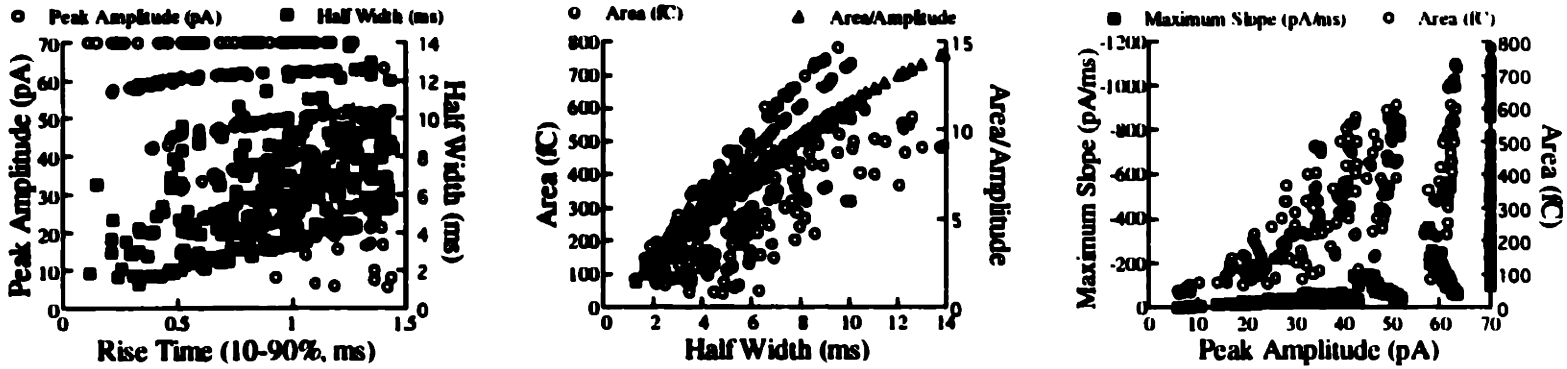

B Fastest Events, Cable plus both Conductance and Kinetics

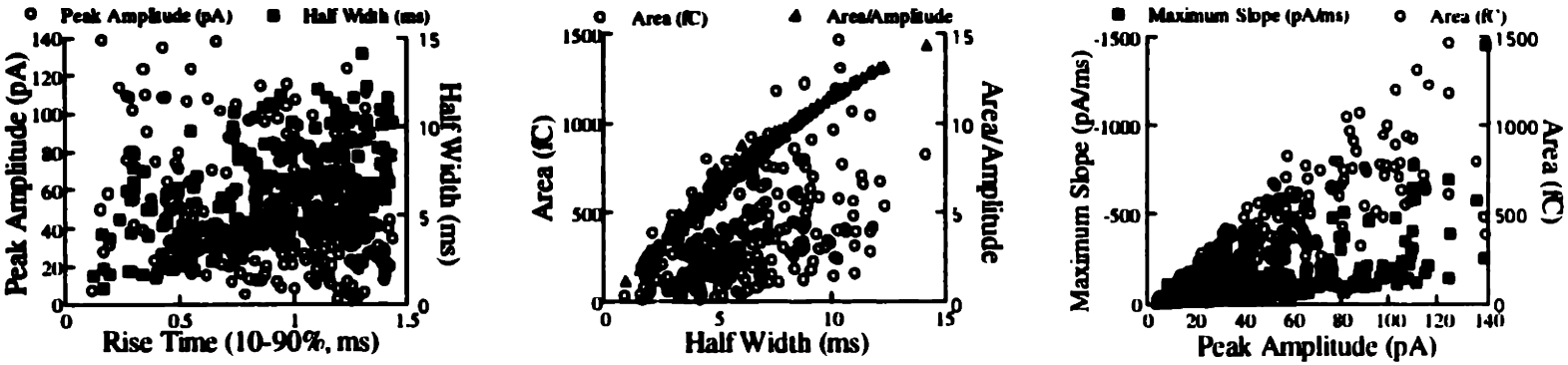

Fig. 4 - 28

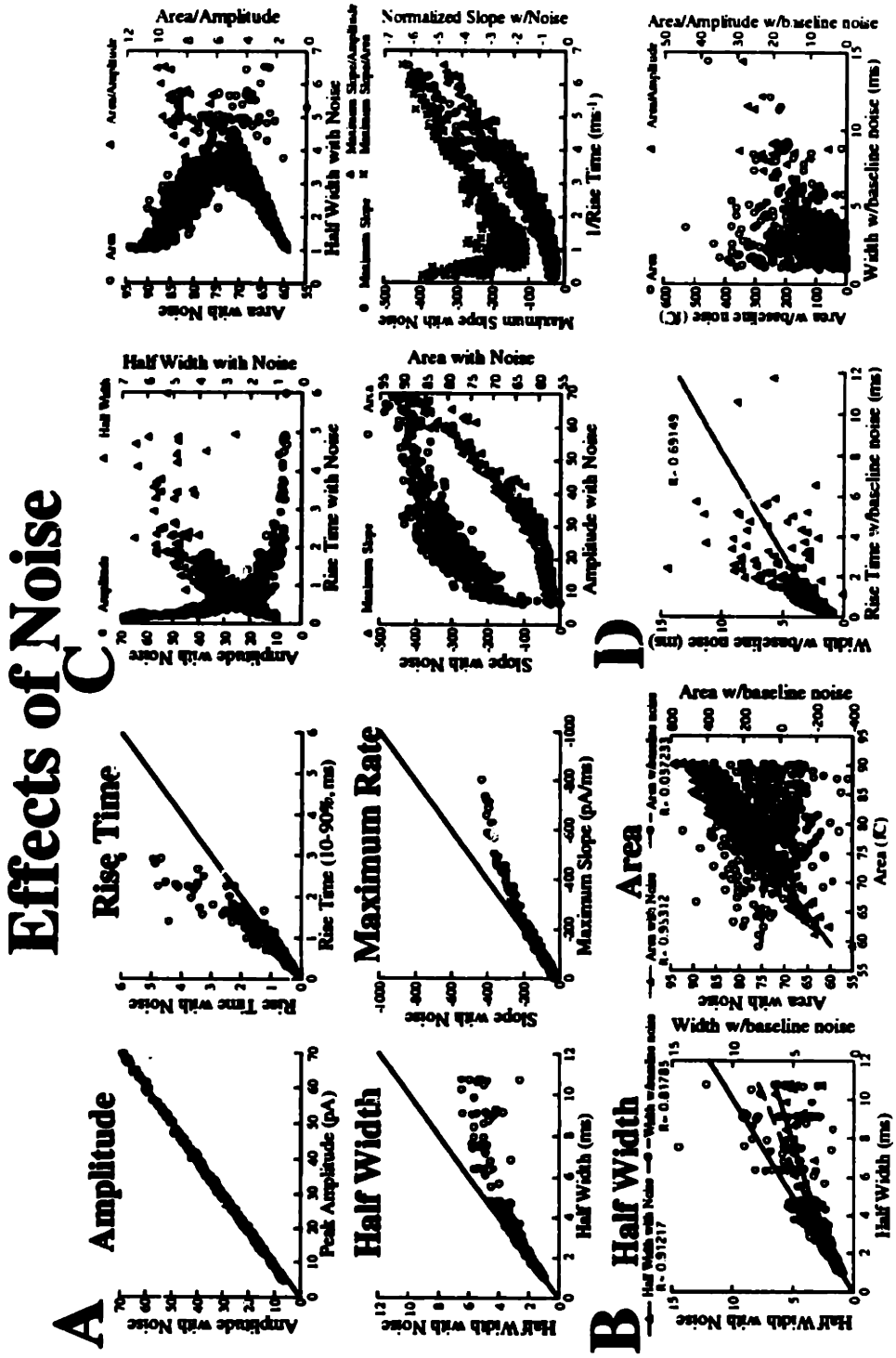
Effects of Noise
A
Amplitude
Peak Amplitude (pA)
Amplitude with Noise
Rise Time
Rise Time (10-90%, ms)
Rise Time with Noise
Maximum Rate
Maximum Slope (pA/ms)
Slope with Noise
Half Width
Half Width (ms)
Half Width with Noise
B
Half Width
Half Width (ms)
Width w/baseline noise
Area
Area (fC)
Area with Noise
Area w/baseline noise
C
Amplitude
Rise Time with Noise
Half Width
Half Width with Noise
Maximum Slope
Amplitude with Noise
Area
Area with Noise
Area/Amplitude
Half Width with Noise
Normalized Slope w/Noise
1/Rise Time (ms-1)
Area/Amplitude w/baseline noise
Width w/baseline noise (ms)
D
Rise Time w/baseline noise (ms)
Area w/baseline noise (fC)

Fig. 4 - 29

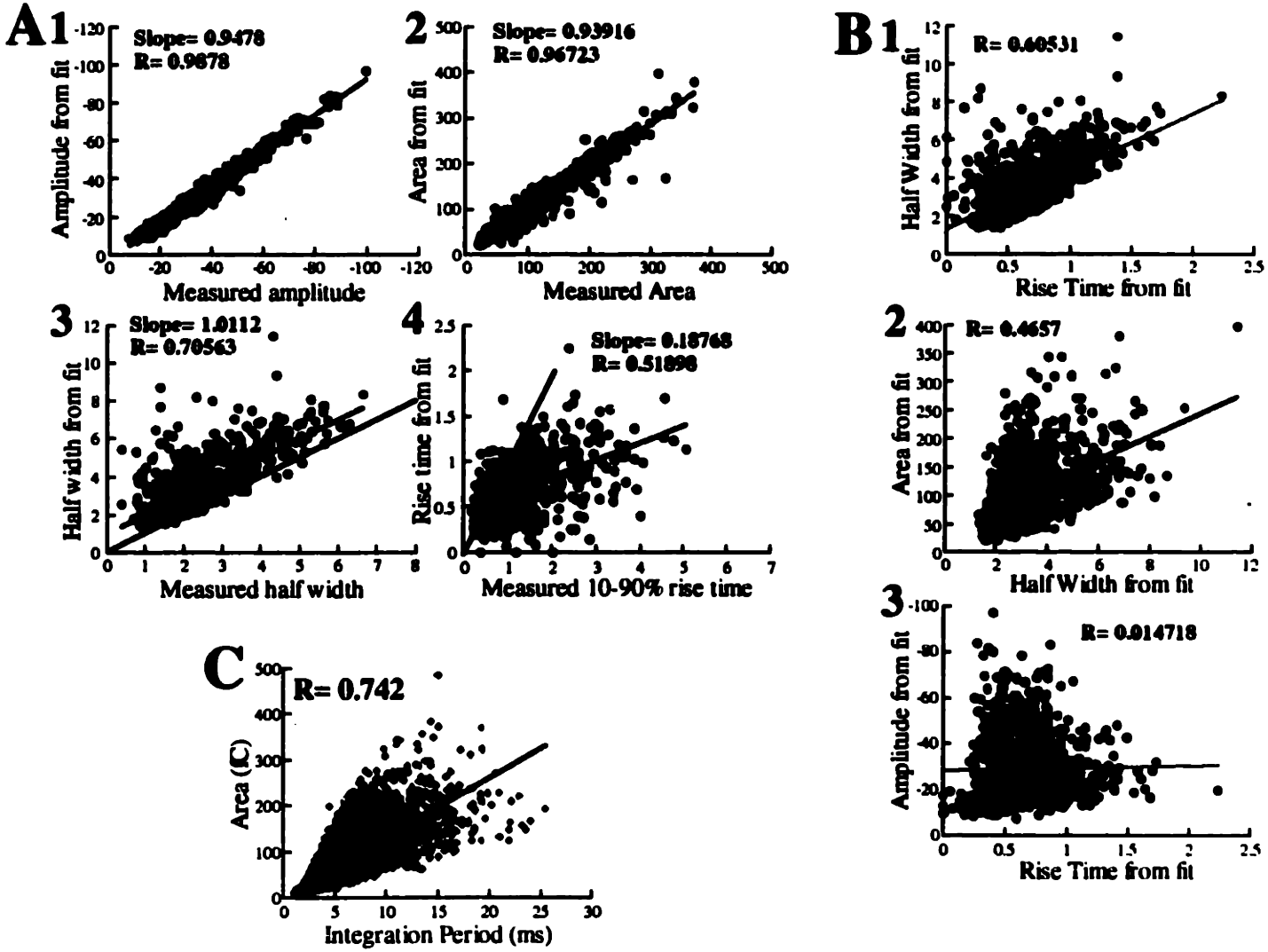
A1
Slope= 0.9478
R= 0.9878
Amplitude from fit
Measured amplitude
2
Slope= 0.93916
R= 0.96723
Area from fit
Measured Area
3
Slope= 1.0112
R= 0.70563
Half width from fit
Measured half width
4
Slope= 0.18768
R= 0.51898
Rise time from fit
Measured 10-90% rise time
B1
R= 0.60531
Half Width from fit
Rise Time from fit
2
R= 0.4657
Area from fit
Half Width from fit
3
R= 0.014718
Amplitude from fit
Rise Time from fit
C
R= 0.742
Area (C)
Integration Period (ms)

Fig. 4 - 30

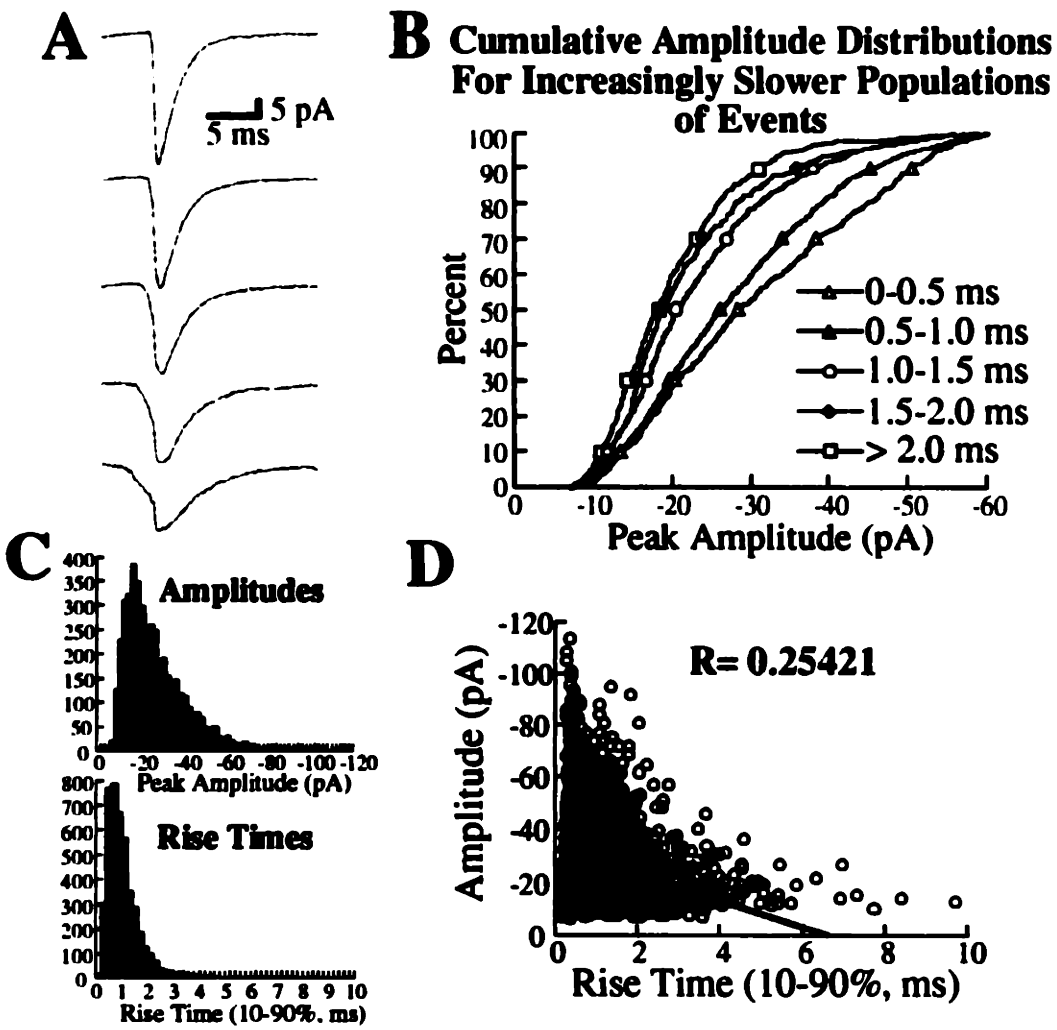
A
5 pA
5 ms
B
Cumulative Amplitude Distributions
For Increasingly Slower Populations
of Events
Percent
0-0.5 ms
0.5-1.0 ms
1.0-1.5 ms
1.5-2.0 ms
> 2.0 ms
Peak Amplitude (pA)
C
Amplitudes
Peak Amplitude (pA)
Rise Times
Rise Time (10-90%, ms)
D
R= 0.25421
Amplitude (pA)
Rise Time (10-90%, ms)

Fig. 4 - 31

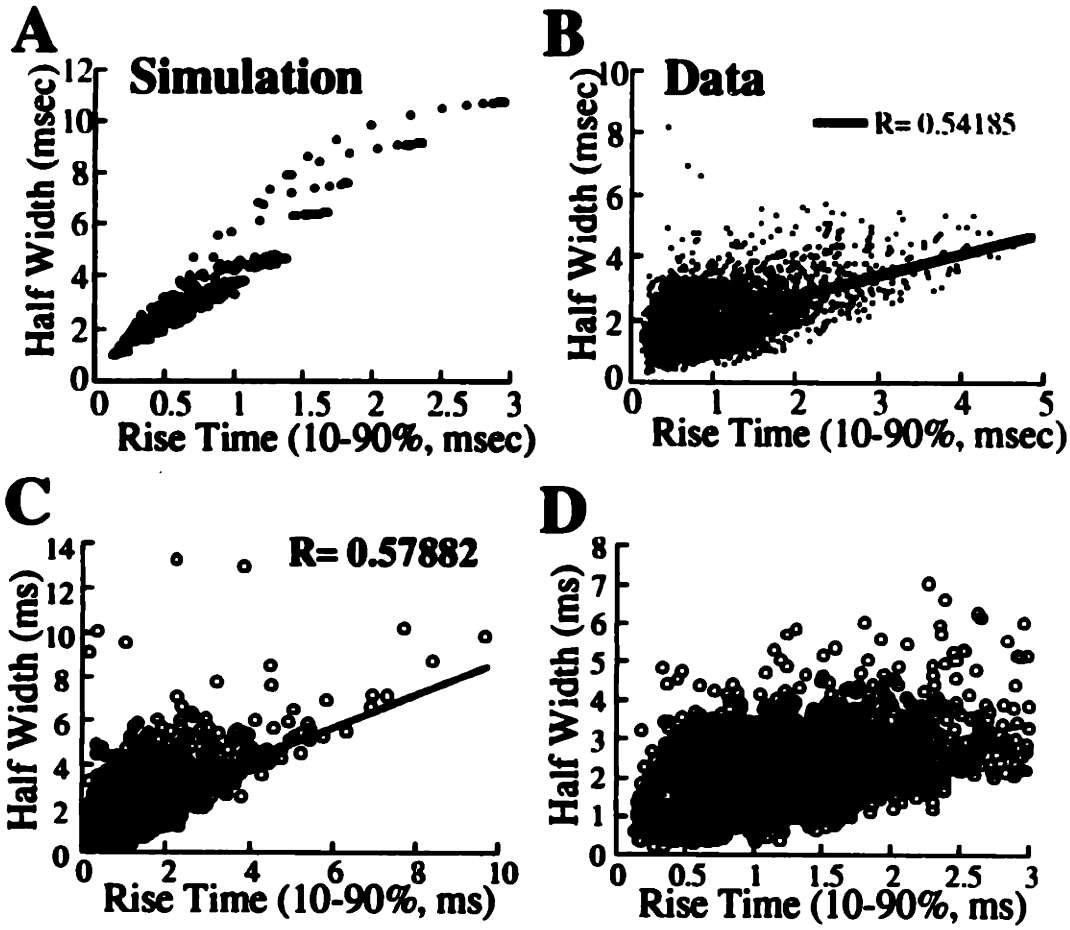
A
Simulation
Half Width (msec)
Rise Time (10-90%, msec)
B
Data
R= 0.54185
Half Width (msec)
Rise Time (10-90%, msec)
C
R= 0.57882
Half Width (ms)
Rise Time (10-90%, ms)
D
Half Width (ms)
Rise Time (10-90%, ms)

Fig. 4 - 32

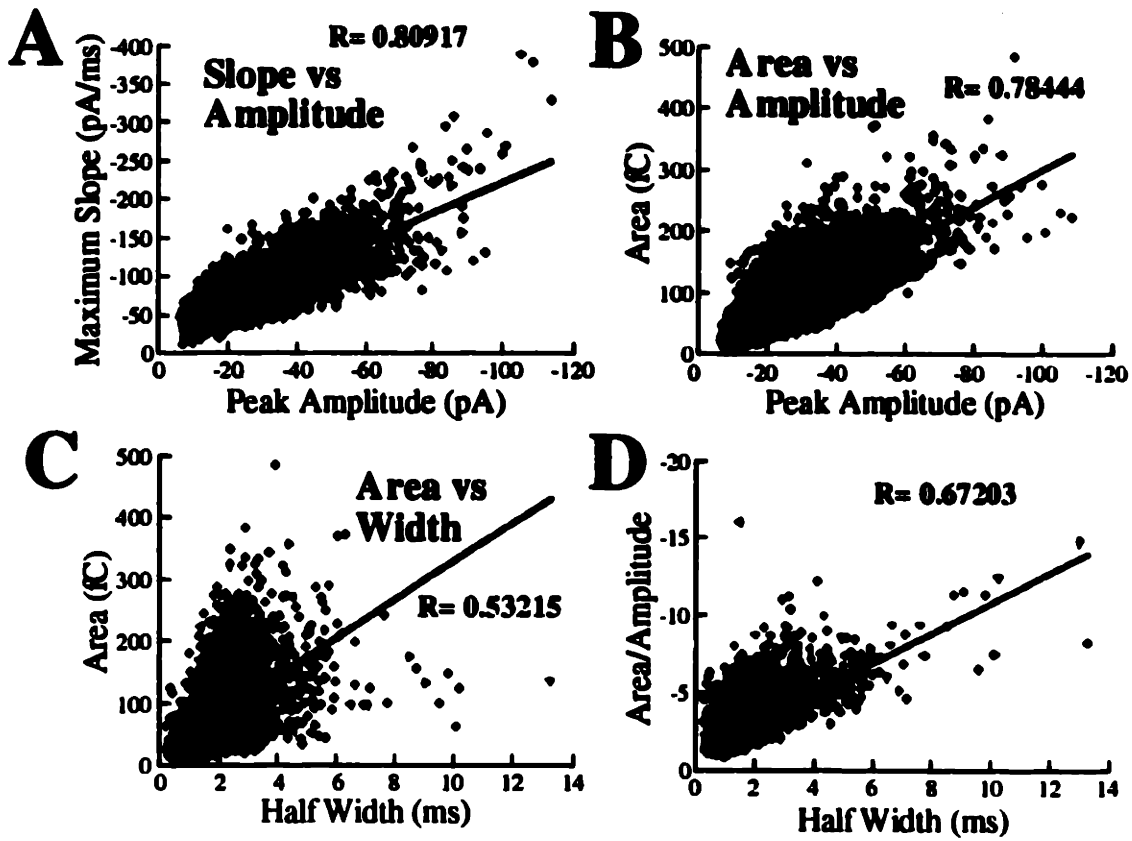
A
R= 0.80917
Slope vs
Amplitude
Maximum Slope (pA/ms)
-400
-350
-300
-250
-200
-150
-100
-50
0
0
-20
-40
-60
-80
-100
-120
Peak Amplitude (pA)
B
Area vs
Amplitude
R= 0.78444
Area (fC)
500
400
300
200
100
0
0
-20
-40
-60
-80
-100
-120
Peak Amplitude (pA)
C
Area vs
Width
R= 0.53215
Area (fC)
500
400
300
200
100
0
0
2
4
6
8
10
12
14
Half Width (ms)
D
R= 0.67203
Area/Amplitude
-20
-15
-10
-5
0
0
2
4
6
8
10
12
14
Half Width (ms)

Fig. 4 - 33

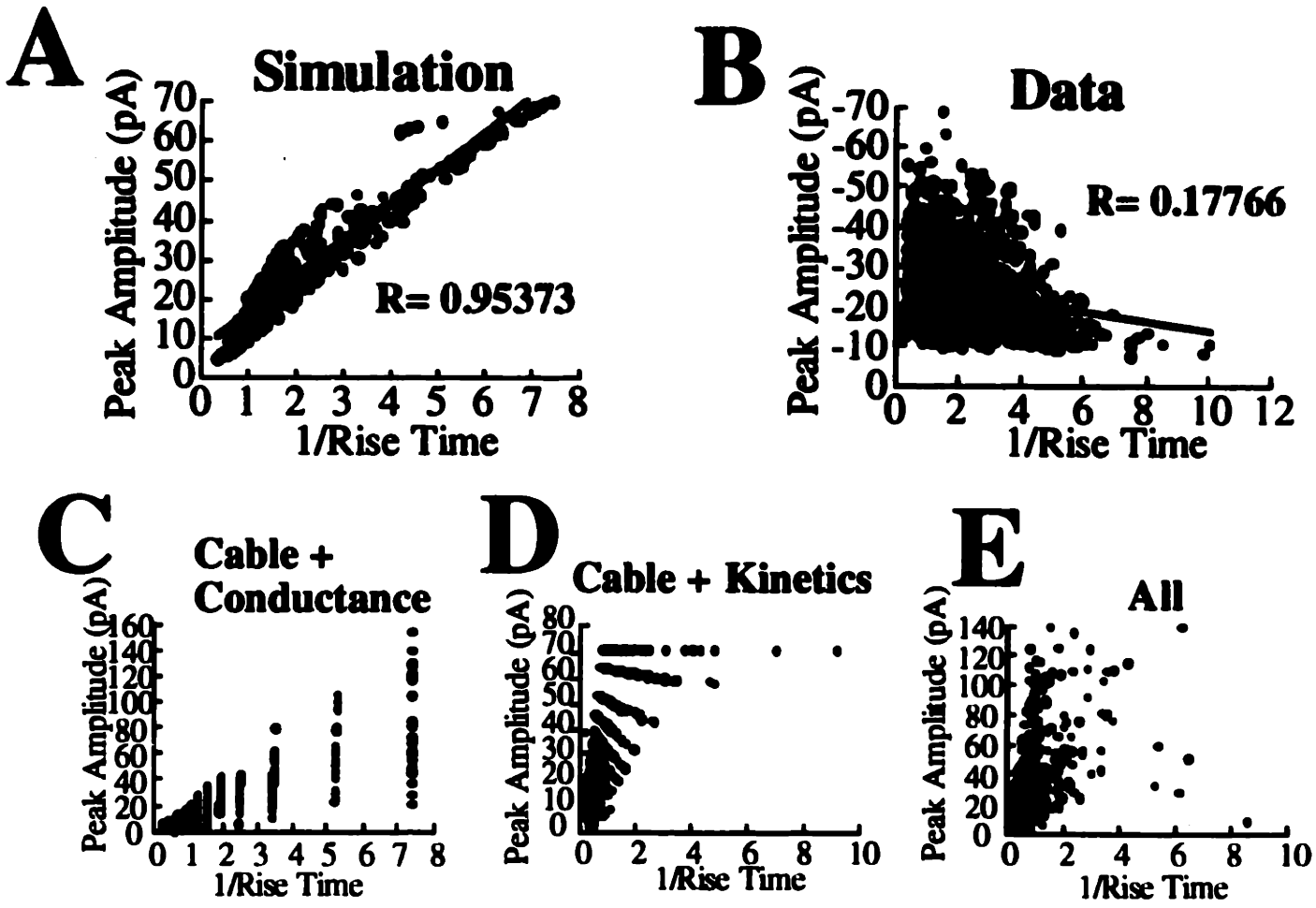
A
Simulation
Peak Amplitude (pA)
1/Rise Time
R= 0.95373
B
Data
Peak Amplitude (pA)
1/Rise Time
R= 0.17766
C
Cable +
Conductance
Peak Amplitude (pA)
1/Rise Time
D
Cable + Kinetics
Peak Amplitude (pA)
1/Rise Time
E
All
Peak Amplitude (pA)
1/Rise Time

Fig. 4 - 34

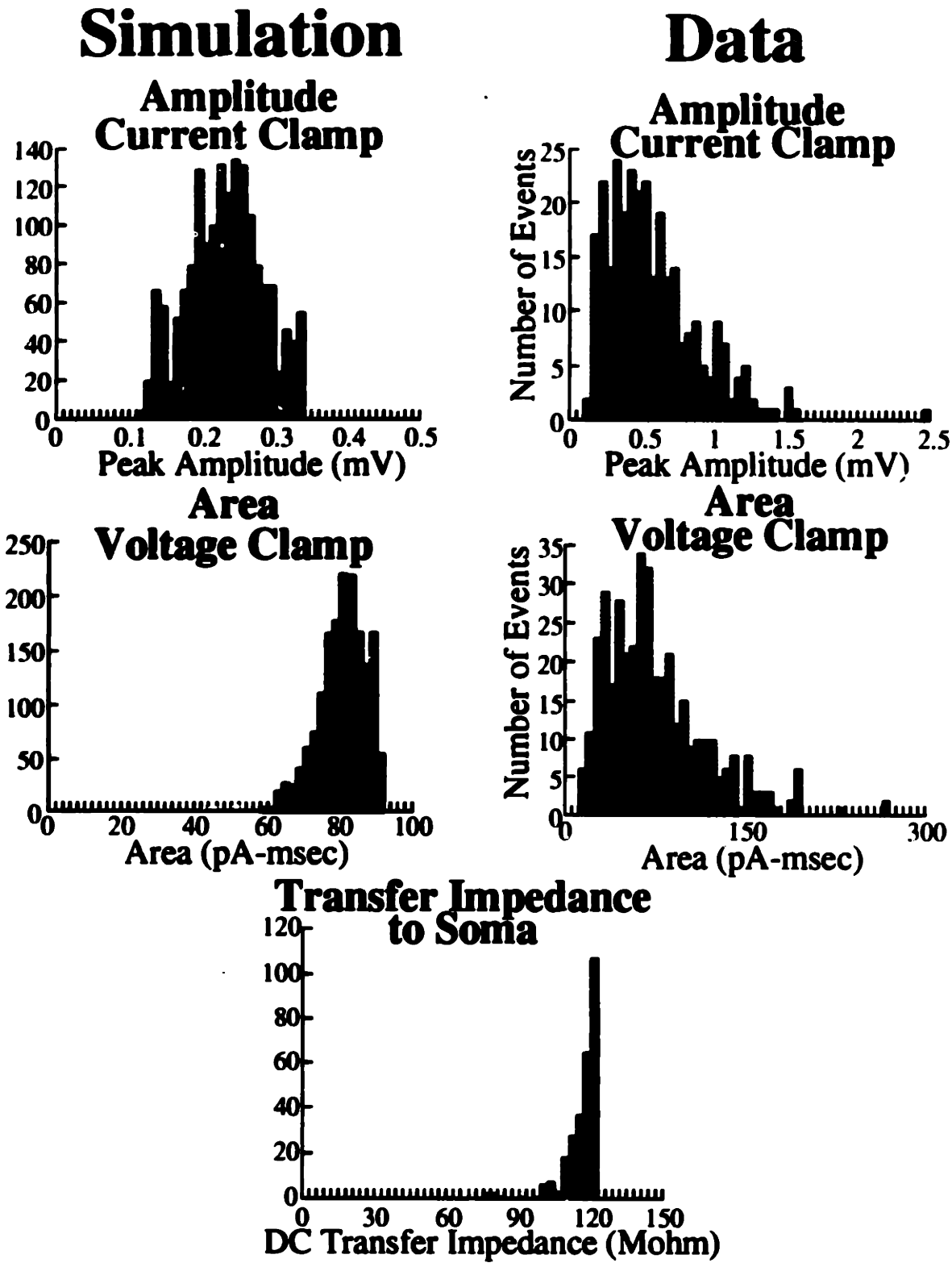
Simulation
Data
Amplitude
Current Clamp
Peak Amplitude (mV)
Number of Events
Area
Voltage Clamp
Area (pA-msec)
Transfer Impedance
to Soma
DC Transfer Impedance (Mohm)

Fig. 4 - 35

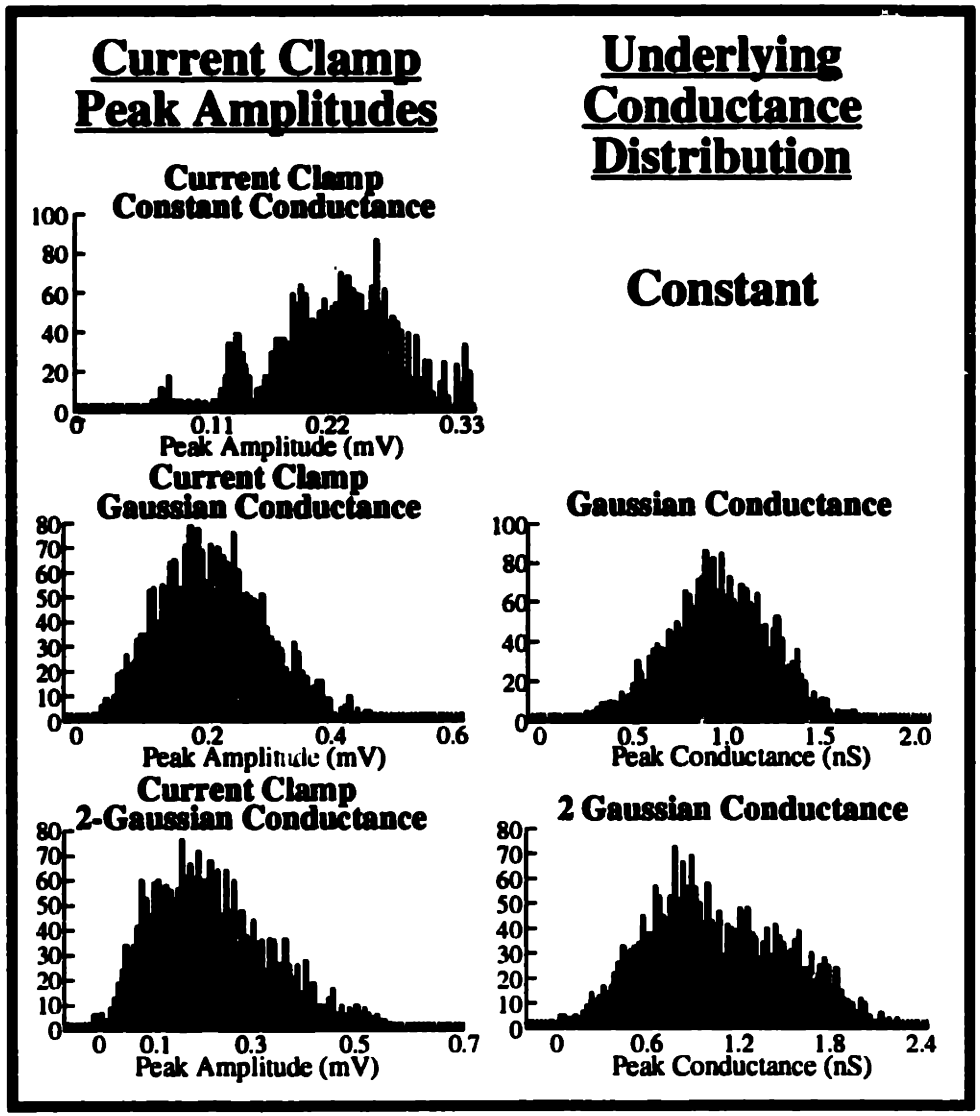

Effects on Other Parameters

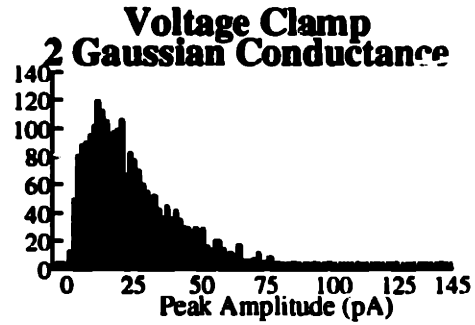

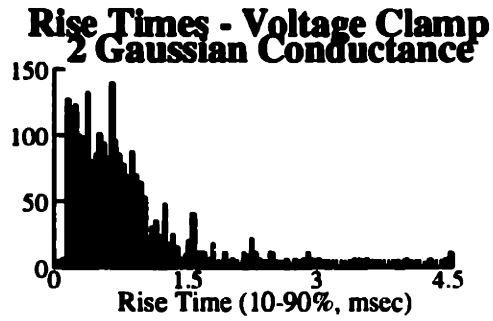

Fig. 4 - 36

Adding Conductance Variability:

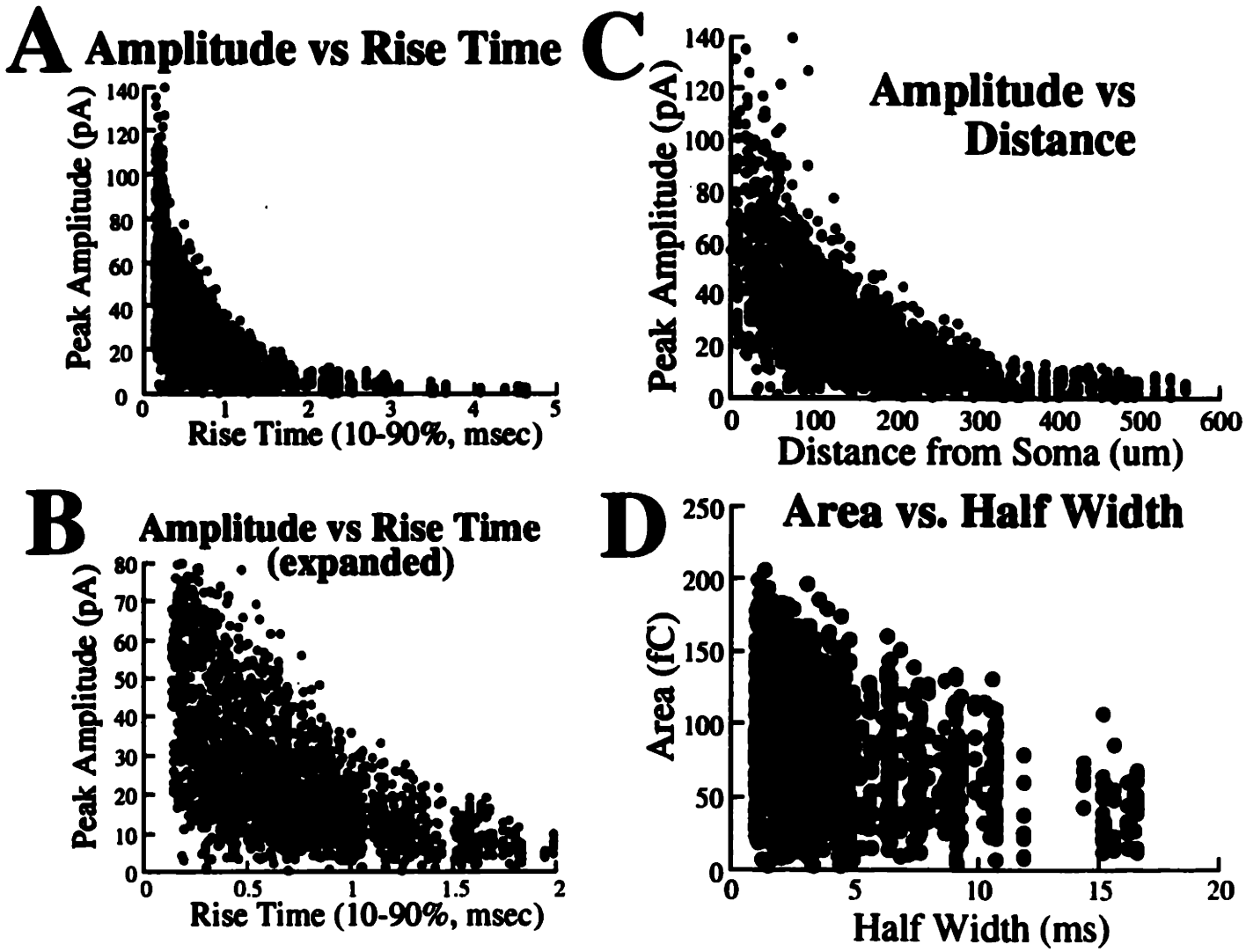

Fig. 4 - 37

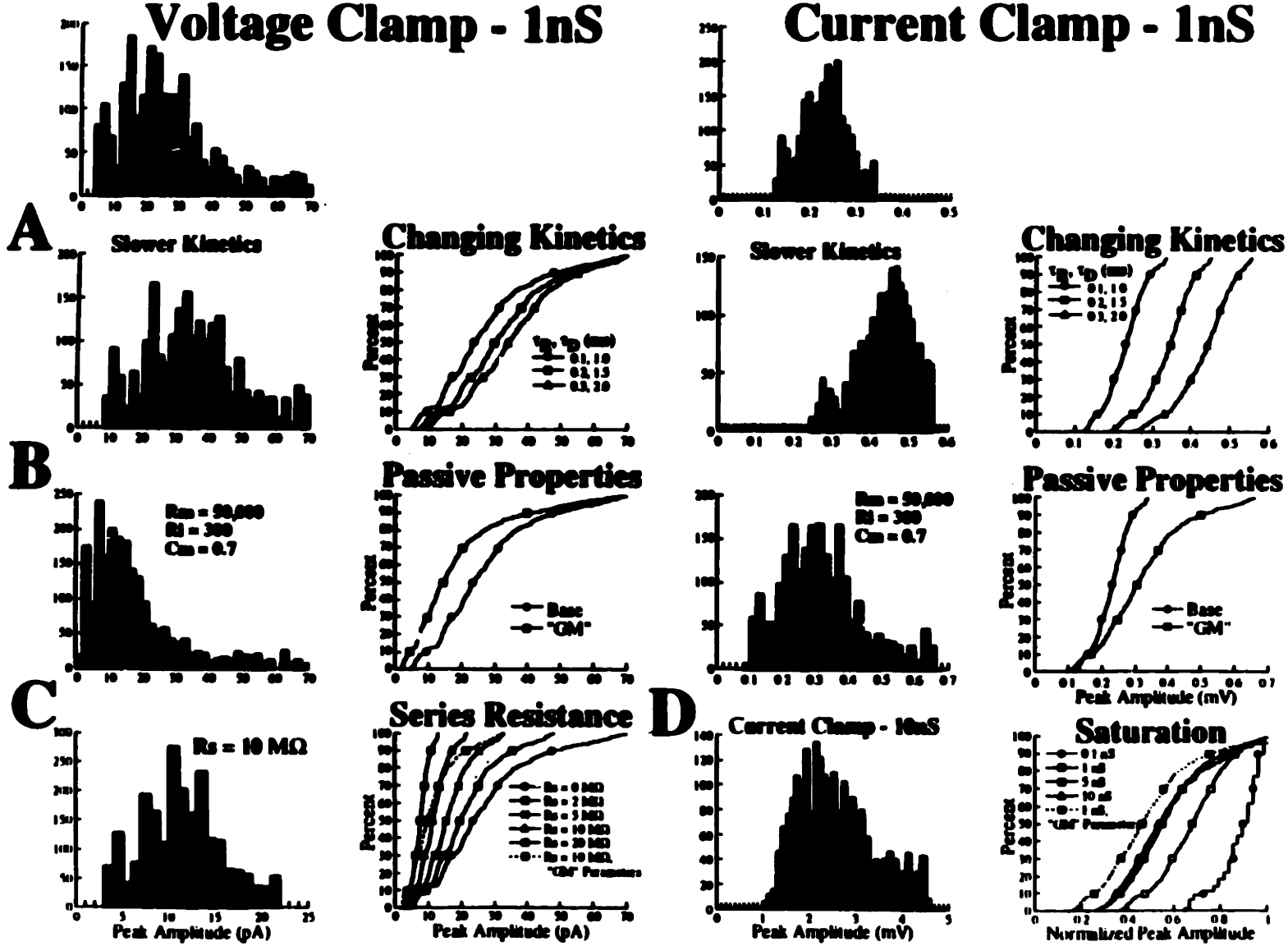
Voltage Clamp - 1nS
Current Clamp - 1nS
A
Slower Kinetics
Changing Kinetics
Slower Kinetics
Changing Kinetics
B
Rm = 50,000
Ri = 300
Cm = 0.7
Passive Properties
Rm = 50,000
Ri = 300
Cm = 0.7
Passive Properties
Base
"GM"
Base
"GM"
Peak Amplitude (mV)
C
Rs = 10 MΩ
Series Resistance
D
Current Clamp - 10nS
Saturation
Peak Amplitude (pA)
Peak Amplitude (pA)
Peak Amplitude (mV)
Normalized Peak Amplitude
Percent

Fig. 4 - 38

5

Experimental Evidence for Electrotonic Filtering in Visual Cortical Pyramidal Cells

Abstract

Cortical pyramidal cells receive thousands of synaptic inputs throughout their extensive dendritic tree. To understand the impact of synaptic location on synaptic function, it is important to assess the effects of electrotonic filtering on synaptic currents reaching the soma. In previous chapters, I have shown experimental and computational results suggesting that electrotonic filtering plays a role in the generation of mEPSC shape and amplitude. Here, I use local application of CNQX to block subpopulations of mEPSCs coming from particular regions of the cell, notably either from the soma and basal dendrites, or from the distal apical dendrite, allowing events arising from the remainder of the cell to be studied in isolation. Using this technique, it is possible to demonstrate three things suggested by the work in previous chapters. First, all of the very largest-amplitude mEPSCs are generated proximally. Second, most of the events are generated in the region of the basal dendrites and proximal apical obliques, consistent with the fact that the vast majority of synapses (>85%) are located here. And third, apically-generated events are small in amplitude and slow in kinetics compared to basal events. This suggests that electrotonic filtering does play a role in the control of mEPSC shape.

5.1 Introduction

In chapter 4, evidence and analysis was presented suggesting a role for electrotonic filtering in the generation of skewed mEPSC amplitude distributions. However, that evidence was in some sense circumstantial: while electrotonic filtering in combination with one other source of variability were shown to be sufficient to generate the recorded mEPSC parameter distributions, and the parameter correlations seen in experimental mEPSCs were consistent with that interpretation, it is possible that a clever combination of kinetic and conductance variability could mimic the effects of electrotonic filtering.

Can we provide experimental evidence for a role of electrotonic filtering in the generation of mEPSC amplitude distributions, beyond that given by simple parameter correlations? In this chapter, I have attempted to do just that, by correlating mEPSC amplitudes with their site of origin on the postsynaptic cell. By looking at mEPSCs generated on a limited region of the cell, I show the constraints on mEPSC amplitude imposed by electrotonic filtering (see section 4.3.5) do indeed apply to real mEPSCs.

In order to minimize the contribution of active dendritic currents and other sources of variability, I have examined the role of electrotonic filtering and synaptic location on the generation of mEPSC amplitude distributions recorded with whole-cell patch clamp techniques in the presence of TTX, APV, and bicuculline, to isolate as far as possible a pharmacologically uniform population of uniquantal synaptic events. Recording electrodes contained a CsF-based solution to minimize the contribution of other voltage-dependent conductances, and biocytin or Lucifer Yellow to allow reconstruction of cells.

To isolate populations of mEPSCs coming from either the region of the soma and basal dendrites, or from the apical dendrite, CNQX, marked with fast green was applied locally to the surface of the slice with a picospritzer. As this is a technically difficult experiment, we must be careful to restrict the conclusions drawn according to the risks - in some sense this evidence is just as circumstantial as that presented

above. However, the data presented here does provide strong support for the most important conclusions of Chapter 4.

Notably, the results of this chapter suggest that all of the largest, fastest mEPSCs are generated at proximal sites. Events generated distally on the apical dendrite are restricted to being small and slow. The bulk of mEPSCs appear to be generated in the basal and proximal apical dendrites of pyramidal cells, consistent with this being the location of the majority of synapses [134]. This data is consistent with the model of mEPSC generation consisting of a combination of electrotonic filtering and conductance variability[1], and strongly supports a role for electrotonic filtering in the generation of mEPSC amplitude distributions.

5.2 Methods

Preparation of slices Preparation of rat slices was performed as in the General Methods. For the experiments in this chapter, it was particularly important that recorded cells have their dendritic tree largely intact; that e.g. the apical dendrites were not severed during slicing. Several modifications were made to the techniques presented above to ensure that all cells recorded would be intact. First, instead of limiting attention to primary visual cortex, coronal slices were primarily made of more anterior regions of cortex containing higher visual areas. These regions of cortex were less sharply curved than primary visual cortex, and therefore a much larger percentage of the pyramidal cells maintained their apical dendrites intact after slicing. Second, recordings were limited to layer III or to the uppermost portion of layer V. This will, unfortunately, limit attention to smaller cells, many of whom do not have an apical dendrite which extends all the way to layer I [133]; but the proportion of large, deep layer V cells which were damaged during slicing makes them dangerous to study without simultaneous visualization. This may mean that the cells under study, being small, are less subject to filtering and have fewer distally-generated events (as they frequently lack the large apical tuft of "thick" layer V cells). Third, recordings were always made at least 50 μm below the surface of the slice to ensure that few dendrites were severed at the slice face, but above 250 μm to allow for easy penetration of surface-applied drugs (see below). Extracellular injections of biocytin (5%, slices

[1] However, it does not rule out a small contribution of kinetic variability.

allowed to survive for 3-6 hours in an incubation chamber, histology performed as for filled cells, see General Methods) provided a Golgi-like staining of large numbers of neurons, and showed that these constraints were guaranteed to yield recordings in intact neurons in the vast majority of cases. To confirm this, in all cases, either Lucifer Yellow or biocytin was included in the recording pipette, though it was not always possible to morphologically recover the recorded cell.

Electrodes and Recording Electrodes were filled with CsF-based solution (see General Methods), and either 0.3% Lucifer Yellow or 0.5% biocytin. In all experiments, the ACSF contained 1 μM TTX (Sigma), 50μM Bicuculline Methiodide (Sigma), and 30μM APV (RBI or Cambridge Research Biochemicals) to isolate purely AMPAergic mEPSCs. In most experiments, and all of those used for bath or local application of CNQX, the bath dextrose was increased to 50 mM. This drastically increased the baseline mEPSC frequency [224], and may also have increased mEPSC amplitude in some cases [92]. CNQX (100 μM (puffing), 10μM or 0.3μM(bath wash-in)) was dissolved in a very small quantity of DMSO, and then diluted with ACSF (containing the above drugs and dextrose concentration) to the concentration desired (final concentration of DMSO < 0.0006-0.006%; 6-10 μl in 1500ml for bath, or in 150ml for puff). Series resistance (R_s) was monitored by a pulse every 7 seconds (in early experiments, it was checked intermittently every few minutes). Data were not used if the series resistance changed by more than 20% from the control period. For cells that did change within this window of 20%, decreases in R_s occurred as often as increases, and so there is likely to be no systematic effect of R_s on responses across cells. Series resistance compensation was used whenever possible, and cells were discarded if R_s(before compensation) was >30$M\Omega$. In practice, almost all cells used here had R_s<15$M\Omega$.

5.2.1 Isolating subpopulations of mEPSCs.

A standard technique for evoking miniature synaptic events from particular regions of tissue is the local application of hyperosmolar solution [92, 17, 155, 157] or ruthenium red [92, 155, 157]. These approaches are typically used in cultured preparations, under visual control. I was unable to get them to work adequately under my recording conditions. Sucrose solution tended to move across the surface of the slice and spread a long distance, rather than entering the slice directly under the location where it was applied. Application of sucrose to the region near the recording electrode tended to cause the electrode to seal over due to increased osmotic pressure. Application of sucrose to the apical dendritic region caused little if any change in mEPSC frequency, presumably due to the difficulty in accurately localizing the puffer pipette under the blind conditions used here. Additionally, given the large asymmetry in the number

of basally- and apically-generated events suggested by the results presented in this chapter, even a several-fold increase in apical event frequency might not be easily seen against the background of larger numbers of basally-generated events.

Therefore, I turned to an alternate technique. Instead of evoking mEPSCs from a particular region of the cell, and attempting to pick them out from the ongoing background mEPSC activity in other parts of the dendritic tree, I used a subtraction technique of blocking mEPSCs coming from either the basal or apical dendritic regions. 50 mM dextrose was used in the ACSF to increase the baseline mEPSC frequency to a point where a reduction in frequency could easily be detected. Then CNQX was applied locally to either the basal or apical dendrites, to selectively block mEPSCs coming from that region of the cell.

Local application of drugs. To isolate populations of mEPSCs coming from either the region of the soma and basal dendrites, or from the apical dendrite, CNQX ($100\mu M$) was applied locally to the surface of the slice with a picospritzer. The CNQX solution was marked with 0.2-0.3% fast green to monitor the extent of its spread [212]. An interface chamber was used, and the puffed solution usually remained stationary on the slice after an initial period of spread, covering a final area proportional to the size of the puff. As recording was performed blind, CNQX was applied relative to the recording electrode and pial surface, assuming a pyramidal cell's orientation and shape (see schematic in Figure 5-39A). All recorded cells were filled with biocytin or Lucifer Yellow to allow later correlation between puff location and morphology. CNQX used for puffing was dissolved in ACSF of slightly different composition than that used in the bath[2]. Two vehicle solutions were used: one consisted of ACSF without dextrose or $CaCl_2$. The other contained $CaCl_2$, but only the standard (10 mM) concentration of dextrose. Neither contained TTX, APV, or Bicuculline. As the volumes applied were small, the concentrations of these compounds should rapidly equilibrate with the surrounding ACSF. Due to the lower dextrose (and hence osmolarity) of the vehicle solution, it alone may be expected to cause some reduction in mEPSC frequency. However, it too will be localized to the region under consideration, and so this will not significantly confound the results – it will act, if at all, as an additional mechanism to block events from that region. Both types of vehicle solutions were applied alone to the basal dendrites, in much larger quantities than ever used for CNQX application, and their (slight) effects are presented below. There were no differences between the two vehicle solutions, consistent with the Ca^{++}-independence of mEPSCs [11, 224].

Location and spread of applied CNQX were monitored with a dissecting microscope. Diagrams were kept of the slice, recording electrode, and puff location and extent. These were used later to correlate with the morphology of recovered cells. All

[2]Purely by oversight, not design.

mEPSCs were blocked by bath application of $10\mu M$ CNQX (n=4), or by repeated CNQX puffing sufficient to cover the whole extent of the cell (n=2).

Analysis MEPSCs were detected as described in the General Methods, using a detector that was sensitive to the presence of overlapping events. This was necessary due to the sometimes very high frequencies of events seen in the baseline periods. Shape parameters and amplitudes of these overlapping events were not measured unless they were unambiguous (i.e. the rise time and amplitude of the initial event), only their times of occurrence were recorded. A final version of the detector used for all the kinetic analysis shown here incorporated an improved rise-time measurement algorithm. The algorithm used in Chapter 4 was prone to overestimate the rise times of slow events. Differences in distributions of mEPSC parameters were tested using a Komolgorov-Smirnov test [200, 294], and differences between means were tested using a Mann-Whitney U test, and differences between paired means before and after drug application were tested initially with Signs or Maximum tests, then with a paired Wilcoxon Signed-Rank Test [221]. See General Methods for more details.

Analysis of the effects of CNQX puffing was performed both simply by visually examining the complete time course of changes in event amplitudes, frequency, and kinetics; and by extracting periods of events before and after the puff for quantitative analysis. The entire time course of the puff, plus a recovery period some time later if available, were recollected off-line and processed to detect mEPSCs. Then windows of mEPSCs were taken before and after CNQX application to allow quantitative comparison. Given the Poisson-like nature of mEPSCs, it was determined to be more accurate to compare identical windows of time before and after the puff, rather than identical numbers of events. In other words, consider the generation of mEPSC amplitudes as the sum of independent Poisson processes, and to ask how many events from each class of amplitudes are missing in the post-puff window. This approach also has the advantage of being more consistent from cell to cell, and easier to lock into the time course of CNQX application, regardless how dramatic the effect on event frequency. A nominal window of 60 seconds was used, for the baseline period ending just before the first puff, and for the post-puff period beginning a short while after the puff (10-20 sec) to allow the effect to equilibrate. In a number of cases, CNQX was applied slightly below the basal dendrites, and it took a few seconds to reach the cell. In these cases, the 60 second analysis window will contain a portion of time before the effect was maximal. In a few cells, a full 60 seconds of data were not available, and a shorter window was used (the window duration was always uniform for a single cell). In some cases, particularly in the earliest experiments where series resistance was not continually monitored and had to be checked intermittently, there were short blocks of time in which data were unavailable (indicated by hatched bars in the graphs). In this case the 60-second window was broken across these blocks. To

allow comparison of CNQX effects across cells, the values of mean mEPSC parameters for each block were expressed as a percentage of the value for the baseline block (0% change). Standard errors were computed for each parameter, and also normalized by the baseline mean to allow their expression as a percentage on the graphs at the same scale as their corresponding mean values.

5.3 Results

5.3.1 Most mEPSCs originate from the region of the basal dendrites.

Cortical pyramidal cells bear a stereotyped morphological relationship to the cortical layers and pial surface. While they are not as uniform as hippocampal pyramidal cells, it is true that if one records from a cortical pyramid, the location of the recording pipette almost always marks the location of the soma, and that the apical dendrite, however long, usually extends between that point and the pial surface.[3] This structure makes it possible to locally apply substances to particular regions of the cell even under conditions where the cell itself cannot be visualized until after the fact. In this study, blind whole-cell recordings were obtained in cells from a variety of layers. Recordings were assumed to be somatic, and cells were assumed to be pyramidal (both of these assumptions were true in >95% of recovered cells from the total population considered in this thesis, and for all of the cells used here which were recovered morphologically well enough to see their dendrites.[4] CNQX, marked with fast green, was applied locally to either the apical or basal dendrites. Basal dendrite puffs were applied near to the recording electrode, apical puffs were applied between the recording electrode and the pial surface.

Under conditions of high basal mEPSC frequency, local application of CNQX

[3]Rat cortex does contain a small number of inverted or atypically oriented pyramidal cells, whose apical dendrite extends obliquely, or even directly towards the white matter [177].

[4]A large fraction of the cells in this study were recovered morphologically, but for a number of those, only the soma was visible.

to a portion of the cell allows one to see events coming from the remainder of the cell in isolation; as well as to estimate the contribution of the blocked population to the whole. Such application appears specific and well-localized, having strikingly different effects on the cell depending on the location of the puff, even when two puffs are equidistant from the recording electrode. Figures 5-39B and C show the effect of CNQX application on two such sites on mEPSC inter-event intervals (IEIs), perhaps the most sensitive indicator of a decrease in mEPSC frequency. A decrease in event frequency can clearly be seen in such a plot as in increase in the number of long IEIs – points appearing in the upper part of the plot.

Blocking mEPSCs coming from the apical dendrite causes a small, slightly delayed, decrease in mEPSC frequency (Fig. 5-39B). In contrast, applying CNQX near the recording electrode to block mEPSCs coming from the region of the soma and basal dendrites causes a very large decrease in mEPSC frequency (Fig. 5-39C1). This change has a very rapid onset (Fig. 5-39C2), indicating that the CNQX is acting very locally to the puff site. The vast majority of events were blocked by basal CNQX application in every cell tested (n=19), and in 2 cases all events were blocked after a medium latency (at least partial recovery was obtained in 1 of these, see Discussion).

Vehicle Control It's possible that the sharp drop in mEPSC frequency seen with basal CNQX application is in fact due to the mechanical shock of puffing so near the recording electrode – perhaps the cell is damaged as a result. Given that partial or complete recovery from basal CNQX blockade was obtained in most cells showing a large effect of CNQX application (the others were lost before recovery occurred), this damage is obviously not so severe as to be permanent, but perhaps the cell goes through a temporary shock. To control for this, I placed a very large puff, much larger than that used for CNQX application, of vehicle solution onto the soma and basal dendrites near the recording electrode, to see if puffing alone would have an effect on mEPSC frequency or amplitude.

Puffing vehicle solution alone onto the basal dendrites has very little effect on

either mEPSC inter-event intervals (shown for two cells in Fig. 5-39D1 and E), or amplitudes (Fig. 5-39D2). There is a slight decrease in mEPSC amplitude at very long times post-puff, probably due to the slightly different composition of the puffing vehicle and the bath solutions (see Methods). However, the quantity of vehicle solution alone applied in these cases was much larger than that used for CNQX application, so this effect is overestimated here. It is clear, however, that the reduction in mEPSC frequency with CNQX puffing is not due to the mechanical stresses of puffing itself.

Therefore, the large, rapid, specific reduction in mEPSC frequency with basal but not apical CNQX application strongly suggests that the vast majority of events originate from synaptic sites on the basal dendrites, or proximal apical obliques. This is consistent with the fact that >85% of the spines, and hence the excitatory synapses, on these cells are located within this region (see Figure A-61A, [134]).

5.3.2 All of the largest events are generated proximally.

Applying CNQX to the basal dendrites preferentially blocks large-amplitude events. Figures 5-40A,C1, and C2 show the effect of basal CNQX application on mEPSC amplitudes in three cells, showing the consistency of the effect (population data presented in Figure 5-42). Across the 19 cells receiving basal CNQX application, there was a significant increase in mean IEI, a significant decrease in absolute frequency, and a significant decrease in mean event amplitude (Wilcoxon Signed-Rank Test, $p<0.05$).

In addition to blocking the majority of events in all three cells, basal CNQX application preferentially removes all or almost all of the largest mEPSCs. This is shown in Fig. 5-40D, by plotting cumulative mean event amplitude against amplitude for events in two identical periods before and after CNQX application. This simple, graphical technique is a sensitive indicator of a preferential loss or increase in large-amplitude events, without requiring artificial binning of the data [61, 277]. Events are

sorted into order of increasing amplitude, and then the cumulative mean is computed for points $i = [1..n]$ by averaging all of the amplitudes of events smaller than or equal to event i. The cumulative mean up to event i is then plotted against the amplitude of event i. It will increase as increasingly larger events are added, and then begin to plateau at the value of the mean for the whole population. If there is a selective loss of large-amplitude events, the curve for the distribution without such events will plateau at a lower cumulative mean value, diverging from the original distribution at the point at which events begin to be lost.[5]

In Figure 5-40D this technique shows a selective loss of large-amplitude events with basal CNQX application. Cumulative mean amplitude is plotted vs amplitude for the events in a 60-second period immediately before and shortly after CNQX application (see Methods). The two lines diverge for larger-amplitude events, suggesting a specific loss of those events post-puff [61]. This loss of large events can be seen again in Fig. 5-40E, where events from these two 60-second periods are averaged. There is a large decrease in amplitude, as well as an increase in rise time and half width post-CNQX, consistent with a loss of proximal events.

The effects of CNQX puffing were, again, specific, and not related to damage to the cell. The cell shown in Figure 5-40A is shown again in B, several minutes post-puff. Event amplitude and frequency has partially recovered, (CNQX is lipophilic and difficult to wash out), indicating that the cell is not damaged. At t=0, a second puff is applied in the same location as the first, showing that the effect is repeatable and is not likely to be due to partial blockade of mEPSCs.

[5]Unfortunately this technique does not reverse well, and so can't be used to show a selective loss of small-amplitude events; in theory if one sorted events in decreasing order and computed the cumulative mean from the top down, you should see a similar divergence at the point where small-amplitude events begin to be lost, but in practice as the large amplitude events continue to dominate the mean, hiding the effect.

5.3.3 Apical events are few in number and small in amplitude.

Applying CNQX to the apical dendrite to block distally-generated events had variable effects. As shown in Figure 5-39B for a cell selected from the middle of the range of CNQX effects, apical CNQX application caused a small decrease in mEPSC frequency (absolute frequency before: 23.15 Hz, after: 10.8 Hz; KS test on IEI distribution $p<=.0001$). Events, however still covered the entire range of amplitudes seen before CNQX puffing (Fig. 5-41A, cumulative amplitude distribution unchanged, shown in Fig 5-41D, KS test, $p>.05$), with no loss of large-amplitude events (Fig 5-41C). If anything, in this cell there was a slight increase in the number of large-amplitude events due to a burst shortly after the puff (Fig 5-41A,C), and a loss of small amplitude events, seen as a slight lightening of the points in (Fig 5-41A), resulting in a significant increase in mean amplitude ($p<.05$, Mann-Whitney U). The net effect was an increase in amplitude, and a decrease in rise time, of the average of events before and after CNQX application (Fig 5-41B1,2). The presence of this burst of large events (which did not seem to be related to CNQX application) makes interpretation somewhat difficult, but it is clear that after CNQX application to the apical dendrite, there is a loss in the absolute number of small-amplitude events. This can be seen by comparing the amplitude histograms for events in a 60-second window before and after CNQX application (Fig 5-41E1,2). The difference between these two histograms, binned at 1 pA intervals, can be seen in Fig 5-41E3. While the fractional loss of events is the same at all amplitudes (as can be seen by the lack of significant difference in the cumulative amplitude distributions); the largest absolute loss of events in a fixed time window occurs for events between 7 and 10 pA in amplitude,[6] with a more moderate loss between 10 and 15 pA.

The effects of apical puffing were also variable across cells, in contrast to the ef-

[6]There might be additional loss for events of 5-6 pA as well, but this will be masked due to the effects of approaching the detection threshold.

fects of basal CNQX application. Figure 5-42 shows both the population and single cell data over time for all of the cells in this study. The population as a whole did show a systematic increase in IEI (Fig. 5-42A), but this was not significant ($p>.05$, Wilcoxon Signed Rank Test). Similarly, the population average showed a slight but variable and nonsignificant increase in mEPSC amplitude after apical CNQX application ($2.67\pm6.35\%$). There was incredible heterogeneity across cells, making it difficult to see a systematic effect of apical CNQX application. All 7/7 cells showed a significant increase in mean IEI (decrease in frequency, Mann-Whitney U test, $p<0.05$; one cell did not show a significant change in the distribution of IEIs, Komolgorov-Smirnov test, $p>0.05$). The effects on amplitude, however, were variable, 4/7 cells showed a significant increase in mean amplitude (Mann-Whitney U, $P<0.05$), while 3/7 showed a decrease (only 2 cells showed a significant change in the distribution of event amplitudes (K-S test, $p<0.001$, all others $p>0.05$); but one of those showed an increase in event amplitudes, while the other showed a decrease.

There are several reasons why apical CNQX application is likely to produce varied results across cells. First, in spite of the precautions described above, a certain number of cells might not have apical dendrites; either because they were cut in the slicing or because they didn't have them to begin with. A large fraction of the cells in this study were recovered morphologically, all of which were found to be intact. Second, they might have an apical dendrite, it just might not be exactly in the place where CNQX was puffed. The upper layer V cells used frequently in this study because they were not usually injured by slicing (in contrast to the large lower layer V cells) were often of the "thin" variety [133, 108], and had an apical dendrite which did not extend all the way to layer I. CNQX was applied here either at layer I to hit the apical tuft, or somewhat closer to the soma to hit more of the bulk of the apical dendrite and upper obliques. A cell whose apical dendrite ended in layer II would not respond to a layer I puff.[7] Also, the apical dendrite might be obliquely oriented, inverted, or branch in

[7]This is in some sense also evidence for the localization of the CNQX, see below.

a way that placement of a small quantity of CNQX might partially or entirely miss it. Similarly, though the depth of the cell soma in the slice could be constrained by choosing where to patch onto cells, the apical dendrite might dive down from there into the slice, and therefore be too deep to allow easy access for the CNQX. If apical events are indeed smaller than basal events, then it might be that many of them are too small to detect - that in reality the study of mEPSCs is limited to the study of proximal mEPSCs, not because the number of apical mEPSCs is smaller, but because they go undetected. Finally, and most importantly especially in combination with these other factors, the signal-to-noise ratio might not be sufficient to clearly see the effect of apical CNQX application. As shown in Figure 5-40, the vast majority of events seem to be coming from the basal dendrites. If there is a loss of events with apical CNQX application, it may be too small of an effect to show up against this very high background.[8]

I therefore turned to an alternate approach; isolating apical events by applying CNQX to the basal dendrites, and then attempting to block the remaining small events with apical CNQX application (see Section 5.3.5).

5.3.4 Effects of CNQX application on the population of cells studied.

Across the population of cells, application of CNQX to the basal dendrites produced a dramatic reduction in mEPSC frequency and amplitude. On the whole, the effect was not stationary and increased in the period after the puff ("later"), presumably due to spread of CNQX (see below). However, for a number of cells, the effect was stationary over this period (see Figure 5-42C-E), and for one cell it even reversed, recovering almost completely before being repeated and even increased by a second puff. Applying CNQX again to the basal dendrites caused a further decrease in

[8]These might also be reasons why applying sucrose to the apical dendrite didn't produce significant increases in mEPSC frequency, see Methods.

both mEPSC amplitude and frequency. In contrast, applying CNQX to the apical dendrites after a basal puff decreased mEPSC frequency, but had no effect on mEPSC amplitudes (see below). Apical puffs, which will include a mix of cells with successful apical puffs and ones where the apical puff missed all or part of the target, showed a much smaller effect (see above). One cell showed an effect more typical of a basal puff in response to proximal apical application of CNQX, but after a complete recovery, a second, more restricted puff, showed a much less severe response more typical of that seen in other cells. On the population as a whole there is a nonsignificant decrease in mEPSC frequency and increase in mEPSC amplitude just after puffing the apical dendrite, which after time turns into a further decrease in mEPSC frequency and a decrease in mEPSC amplitude; probably due to spread towards the basal dendrites. Finally, as a control for any direct effect of puffing, puffing a large quantity of vehicle solution to cover the soma and basal dendrites (see Fig. 5-39D,E) causes no significant change in mean IEI, absolute frequency, or mean event amplitude ($p>.05$, $n=7$). It does cause a slight apparent decrease in event amplitudes at late times (probably due to solution composition, see above), but puffing itself overall is not sufficient to cause the changes in Figure 5-42A-E.

5.3.5 Dual-puffs reveal the nature of apically-generated events.

One important concern in interpreting the data in Figures 5-40 and 5-41 is to assess the real degree of spatial selectivity of CNQX application. Perhaps the CNQX rapidly spreads to cover the entire cell, and the remaining "events" are either not events at all, or are partially blocked by insufficient concentration of CNQX, resulting in their lower amplitudes.

All events are real All events were blocked by bath application of CNQX ($10\mu M$, $n=4$), or by deliberately puffing CNQX sufficient to cover the entire cell ($n=2$, one

held long enough for complete recovery, one partial), indicating that even the small, slow events remaining after basal CNQX application were indeed real mEPSCs.

Though CNQX application was initially well-localized, there did seem to be subsequent spread in a number of cases. However, this spread was slower than the onset of the original effect, and could be monitored both by observation of the fast green-marked CNQX through the microscope and by the progressive loss of events. The "stickiness" of the CNQX, which made washout difficult, seemed to also keep it from spreading too much beyond its initial location. This was in contrast to sucrose application, which seemed to spread rapidly across the surface of the slice. In two cases, basal application of CNQX caused an initial loss of most of the large events (as per the examples shown above), but over time the smaller events gradually disappeared as well (1 cell held long enough to show recovery). In these cases, the fast green-marked CNQX was clearly seen to spread beyond its initial location simultaneously with the loss of remaining events. Besides spread of CNQX, it is also possible that these cells themselves were simply limited in extent – e.g. had a short or amputated apical dendrite. Application of CNQX below, rather than directly on, the basal dendrites (i.e. in the space between the putative basal dendrite location and the white matter) had a very similar effect to direct basal application, however there was a much longer latency and the effect appeared to "sweep" across the population of putatively basal events in concert with the movement of the CNQX itself. In contrast, application of CNQX to the apical dendrites, not too much farther away from the recording electrode on the other side did not have such an effect. Finally, applying CNQX near to but not on the cell (e.g. the same distance away as an apical puff but at the level of the basals and laterally displaced) had at most a very small effect on event frequency (n=2).

Multiple puffs on the same cell

An even better estimate of the spatial selectivity of CNQX application is that after applying CNQX to the basal dendrites, and losing most of the events, then subsequently applying CNQX to the apical dendrite rapidly blocks most or all of the remaining events. This means that a) those events under study after basal CNQX application actually were coming from the apical dendrite, rather than being insufficiently blocked basal events.

Figure 5-42A and B show the population averages from 6 cells undergoing this protocol (a number of other cells received puffs first on the apical dendrite, then the basals, or on one half of the basals, then the other, but the number in any one group was too small to draw general conclusions from the results, though the case of one particular cell is presented on page 261, below). The data for each cell in the group is presented individually in Figure 5-43A,B. One cell showed effectively no change in IEI or amplitude with CNQX application. Of the others, after the first puff to the basal dendrites, all cells showed a significant increase in mean IEI, and a significant decrease in absolute frequency (data not shown) and mean amplitude ($p<.05$, Wilcoxon Signed Rank Test), as was typical for basal CNQX application.[9] This loss continued over time, presumably with slight spread of the CNQX; comparing events in the 60-second period immediately after the first puff, and the 60 second period immediately before the second ("later" on graphs, the absolute length of this interval varied from cell to cell, from 150 seconds to > 5 minutes) showed that the population mean IEI and the population mean amplitude continued to increase and decrease, respectively, over this period. This corresponded to an increase in IEI in 3 of the 6 cells, with 3 remaining approximately constant; and a decrease in amplitude in 3 cells with the other 3 remaining constant or increasing slightly. In the plots shown in Figure 5-42 and 5-43, the values are normalized as percentage of initial baseline means, so an

[9]The data from the first puff on these cells was included in the population of "basal" cells presented above, along with 13 cells receiving only basal CNQX application.

increase in amplitude after a first puff decrease is shown as a reduction in the % change back towards 0.

After this variable period of time, CNQX was then applied in the region between the initial puff and the pial surface, to see if the remaining events were in fact apically generated. 4 out of 6 cells showed a further increase in IEI, corresponding to a significant change in the paired population relative to the period immediately prior to the second puff ("later" period == "pre" for puff 2), this was matched by a significant decrease in absolute frequency ($p<.05$, Wilcoxon Signed Rank Test). 3 of these cells were held long enough to show complete, or almost complete recovery in event frequency to initial baseline values. This indicates that first these remaining events really are events (as would be expected by their blockade with bath CNQX), and more importantly, that these events really are coming from the apical dendrite. After apical CNQX application, there was a variable change in event amplitude. There was no significant change in the population as a whole ($p>.05$ Wilcoxon Signed Rank Test), 3 cells showed slight but frequently nonsignificant increases in mean amplitude (very few events remained at this point, making the standard errors quite large, see Figure 5-43B), while two showed a decrease and one showed no change. These results were similar to those obtained with apical puffs alone.

Figure 5-43C-E shows the time course of sequential CNQX application in one example cell. This cell was chosen because it was the cleanest example of the protocol, with the shortest interval between the two puffs (150 sec). It had an apical dendrite extending at least into layer II. As might be expected with this short inter-puff interval, there was no change in event amplitude or frequency in the period between puffs, except that which could be explained by a change in holding potential (see below).

At t=0, CNQX was applied to the soma and basal dendrites of this cell. There was a rapid increase in IEI (expansion of the band near 0 over the period 0-50 seconds in C), a loss of all large and medium-sized events (B), and a loss of events from throughout the range of rise times, but predominantly of faster events (E, difficult to see entirely because of too many points). At the time indicated by the black bar,

the holding potential was moved from -70 to -90 mV, to reveal more small-amplitude events. There was a loss of the very largest IEIs (C), corresponding to the detection of more events.[10] There is a concomitant increase in event amplitude (D), due to the increase in driving force, and an increase in the number of long rise time events (E); as such slow events are usually quite small (see Figure 4-19), it is not surprising that more of them are revealed by the increase in driving force.

After a baseline period at -90, during which period event characteristics are relatively stable, CNQX was applied to the apical dendrite at the time marked by the second dashed line (t= 150 sec). There is an immediate and drastic further decrease in event frequency (increase in IEI, C); and a loss of all remaining medium-amplitude events (which were revealed by the move to -90), and all but a few small-amplitude events. And, most notably, all long and medium rise-time events disappear (E), along with a fair number of fast events. At the time marked by the ending of the black bar, the holding potential was moved back to -70 mV to allow comparison with the state after the first puff. All but a very few events are gone, and towards the end of this period no further events appear. However, moving the cell back to -90 shows the beginnings of recovery, with a slight increase in event frequency and amplitude, and the reappearance of long rise time events.[11]

This example clearly shows that, at least in this cell, there are a number of clear apically-generated events (though a smaller number than those generated on the basal dendrites). These events are indeed truly events, being blocked by CNQX and showing standard voltage dependence. And they are indeed on the apical dendrite, showing very rapid blockade after local CNQX application in that region. And, most importantly, they are small in amplitude and comprise the majority of events with

[10]There is usually a very small increase in the absolute number of events detected when moving between -70 mV and more hyperpolarized voltages (see Section A.7), not usually sufficient to change event frequency or amplitude. However, after basal CNQX application this small increase in number of events comprises a relatively much larger fraction of the total.

[11]Recovery from apical CNQX application was always much more rapid than that from basal application, presumably because proximity to the edge of the slice allowed for better perfusion.

slow rise times.

Spatial selectivity of CNQX application. Comparing the responses of multiple very small CNQX placements onto a cell which was morphologically reconstructed provides evidence for at least a certain amount of spatial selectivity in CNQX application. In Figure 5-44, Inter-event interval and amplitude are plotted against time for a cell which received multiple CNQX applications at a holding potential of -60 mV (this cell was not included in the population data above, as its first puff was not categorically somatic). Puff times are indicated by the arrows. Puff location is indicated by the schematic for puffs 1-4, with the approximate location of the CNQX relative to the cell is indicated by the hatched blobs. Puff location was determined by comparing the reconstruction of the cell, which included outlines of the pial surface and gray-white border, with the drawings made of the slice and puff location during the experiment. The schematic is approximately representative of the size and branching structure of this cell, a very small layer V cell. The apical dendrite of this cell, which ended in lower layer III was not severed in the slicing, and simply happened to be that short.

Application of CNQX to the upper basals, and proximal apical dendrite (puff 1) caused a loss of all large-amplitude events, and a preferential loss of small and medium rise time events. Over the next 2 minutes, there is a slight further loss of events, at this point events of smaller amplitudes and both long and short rise times, presumably as the CNQX spreads both proximally and distally from the original puff location. There is a slight recovery of these small events just before puff 2. Application of CNQX to the small apical tuft of this cell caused no visible change in mEPSC amplitudes, but a loss of all the remaining medium and long rise time events, indicating that essentially all long rise time events, and a large number of medium rise time events (2-3 ms) are generated in this region.There is no visible loss of rapid events. Applying CNQX above the top of the apical dendrite (3) has no apparent further effect. After this point, applying CNQX to the middle of the apical dendrite

(4) shows no further obvious change in event amplitudes, but no long rise time events reappear, even though the medium rise time events (which are presumably generated more proximally) show a moderate recovery in this period. The fact that this recovery of medium rise time events occurs simultaneously to, or even before, the puff, indicates that it is due to recovery from the previous puff rather than a direct effect of this one. Eventually, deliberate, repeated puffing over all points of the cell (puff sites shown in B, plus several puffs in the lower basal dendrites) caused all events to vanish (data not shown), but over time the cell recovered almost completely, returning almost completely to its original rise time and amplitude distributions (right). These results support at least a limited degree of spatial selectivity in CNQX application.

5.3.6 Shape indices are reflective of mEPSC source location.

Do the methods presented in Chapter 4 for localizing mEPSCs actually work? I examined the effects of blocking selected subpopulations of events on their "shape indices" [203] - their location on the plot of rise time vs half width, which has been suggested to be the best metric for judging the location of a synaptic input from its shape (Chapter 4, [203, 206, 100, 98, 96, 211]). The shape indices of the events in 60-second windows before and after the basal and apical puffs on the cell shown in Figure 5-43 are plotted in Figure 5-45. Comparing shape indices for events before and after basal application of CNQX (Fig. 5-45A) shows that, though events are lost across the range of rise times, possibly indicating the presence of kinetic variability, there are events remaining at all shape index values after basal CNQX application. Particularly, there are still a large number of events with large rise times and half widths, indicative of a distal location. After moving to -90 ("pre" in Fig. 5-45B), many more events with long rise times and half widths appear, which were presumably too small to detect at -70. These events cover the whole range of shape indices shown for this cell at baseline, except a much larger proportion of them have indices indicative

of a distal location. After puffing CNQX onto the apical dendrite in this cell (Fig. 5-45B), all slow events with "distal" shape indices disappear. There are still a certain number of events with long rise times (e.g. there are 2 events with rise times > 3msec), but the remaining events seem all to come from much closer to the soma.

This indicates that, within the limits imposed by kinetic variability and experimental noise, location on the shape index plot is a good predictor of mEPSC source location.

5.3.7 Effect of event detection on parameter measurements.

One important consideration in estimating the fraction of mEPSCs which are generated at sites electrically remote from the soma, is that attenuation of their amplitudes may be so severe that we no longer detect them. If we don't detect the apical events in the first place, we will see no effect of blocking them; or we will see an effect which varies between cells, corresponding to the variable visibility of distal events with differences in cell size.[12] The analyses in Section 6.3.4 and section A.7 make it clear that there can be small, distal events which we will not detect. However, neither lowering the detection threshold (Fig. 5-46), and hyperpolarizing the cell to increase the size small events by increasing the driving force (Figs. 3-5, A-67) reveal any significant population of small, undetected mEPSCs; therefore we seem to be detecting the vast majority of events. This test does not protect us from letting apical events go undetected if those events are, as a population, qualitatively smaller in amplitude at source than the events we do detect (see Chapter 6 for discussion); but in that case, the major conclusion of this chapter – namely, that all the large, fast events we do detect are generated proximally, and that the apical events we detect are small and slow – will remain intact.

[12]Or even worse, if CNQX application blocks a resting conductance opened by ambient glutamate, CNQX application may suddenly make distal events more visible, by increasing the membrane resistivity. However, as mEPSC attenuation is much less severely affected by R_m than other parameters (Section A.5), this effect should be small at best.

Problems with other methods of testing detectability. In order to determine the effect of losing events below the baseline noise on mEPSC parameter distributions, and, more importantly, to control for the idea that the effects of CNQX application might be due to a partial blockade of spatially distributed receptors, rather than a total blockade of a localized subset of synapses, I have looked at the effects of partial CNQX blockade on mEPSC parameter distributions.

Unfortunately, I discovered that this seemingly simple approach carries its own set of technical complications. I studied partially blocked mEPSCs by examining events during the time course of washing in 10 μM CNQX.[13] Due to a slowly exchanging interface chamber with a long tubing lag, it was several minutes between the time the CNQX solution was started and the time when it had any effect. Once the drug made it through this lag, however, the time course from onset to total blockade was very rapid (Fig. 5-47A, amplitude series starts 50 seconds before any detectable reduction in mEPSC amplitudes). Intuitively, one would expect given the preceding results, that there will be a point where mEPSC amplitudes are reduced by 50%, but as this reduction is uniform over the cell, the distribution of mEPSC kinetic parameters should be unchanged. Unfortunately, the effects of the detection threshold get in the way. As mEPSC amplitude decreases (Fig. 5-47A), events that were smaller to begin with (and slower) fall out from under the threshold, so it ends up looking like we were looking at increasingly faster, proximal events (Fig. 5-47B). Plotting shape indices for events in non-overlapping intervals during the time course of CNQX wash (Fig. 5-47C,D) shows that the later the time, the more proximal the shape indices of the remaining events. This is consistent with the largest events being the most proximal and the last to become invisible with bath CNQX wash. It's also consistent with multiple populations of AMPA receptors with different kinetics and

[13] I attempted to partially block events with 0.3 μM CNQX, the published K_i value [104], but was unsuccessful - the only effect was a slight, temporary *increase* in mEPSC frequency in a subset of cells (n=2/4). As I didn't have time to do a full dose-response curve, I turned instead to analysis of the time course of the effect higher CNQX concentrations.

differential CNQX sensitivity, or by nonuniform wash-in of the CNQX from distal to proximal.[14] But the most parsimonious explanation is that the largest events are indeed proximally generated, and are the last to disappear under the detection threshold.

5.4 Discussion

Most events, and all of the largest events, arise from the basal dendrites.

Given the fact that > 85% of spines, and hence excitatory synapses, onto cortical pyramidal cells are located on their basal and proximal apical dendrites [134] it would seem very likely that the majority of mEPSCs would be generated from this region – most of the synapses generating most of the synaptic events. However, with the recent demonstration that, at least in culture, mEPSCs may be generated preferentially from particular synapses based on their history of activation [179], and the fact that different input pathways to the same postsynaptic cell can generate miniature synaptic events at different frequencies (see Chapter 6), this is not a foregone conclusion. It could be that for some reason, apical spines are massively overactive, and generate the bulk of mEPSCs. The fact that the vast majority of events are blocked by basal CNQX application shows that this is indeed the source of the bulk of mEPSCs. This supports the assumption made in Chapter 4 that, while mEPSC frequency might differ from synapse to synapse, such bias, if present, is relatively independent of synapse location on the postsynaptic cell.

Similarly, given the results presented in Figure 4-36, it is to be expected that the largest events, in spite of any intra- or inter-synapse variability in conductance, will be generated predominantly proximally. Again, this was shown to be the case, with the loss of all large-amplitude and most medium-amplitude events after basal CNQX

[14]This is actually slightly plausible. The top edge of the slice receives better perfusion as the CNQX washes out more quickly after apical puffs, and might reach equilibrium with the CNQX quicker than the middle of the slice.

application.

Spread of CNQX

For these conclusions to be valid, it is necessary that there is some degree of successful spatial control of CNQX application, that it doesn't immediately spread uniformly over the postsynaptic cell, and that the events lost with local application of CNQX to the basal dendrites were truly basal (or proximal apical) in origin. There are a number of facts that support there being sufficient spatial selectivity in CNQX application to warrant the limited conclusions drawn here.

First, after basal CNQX application, in the majority of cells, a fair number of unblocked events remained. Such events were truly mEPSCs subject to CNQX blockade, as bath application of 10 μMCNQX blocked all events (n=4), bath application of 10 μMCNQX after basal puff blocked the remaining events (n=1), and repeated puffing sufficient to deliberately cover the entire cell blocked all events (n=2). These events showed a degree of voltage dependence (complicated by the effects of detection threshold, see Figures 5-46 and 3-5) consistent with their synaptic origin.

These unblocked events came from regions of the cell spatially removed from those thought to be under CNQX blockade. Sequential application of CNQX to the same spot after recovery showed repeatability, and application of CNQX to first one half of the basal dendrites and then the whole basal region showed summation of effect. Most importantly, application of CNQX to the apical dendrite after basal CNQX application showed a rapid loss of a large number of presumed apical events. This shows that CNQX application to the basal dendrites spares at least a region of the apical dendrite, and thus there is a degree of spatial selectivity.

CNQX does spread after application in some cases. This can be seen most clearly in Figure 5-43A,B, comparing the change in IEI and amplitude immediately after basal CNQX application with that several minutes later. Similarly, in 2 cases, a single basal CNQX puff was sufficient to block all events, and in several cases basal CNQX

application was actually below the basal dendrites (closer to the white matter), and onset of CNQX was gradual. In these cases, the loss of events on the oscilloscope could be seen to "sweep" across the cell in time with movement of the dye. When all events disappeared, a check in the microscope confirmed that the dye had indeed moved beyond the desired restricted location. Thus, CNQX did spread after application. However, this spread was slow after the initial post-puff period (see time courses in all figures), and was able to be monitored by a combination of further change in the frequency of mEPSCs, and by spread of the fast green, which seemed to be a good predictor of CNQX location. The lipophilic, "sticky" nature of the CNQX, which made washout difficult, was beneficial in that it seemed to impede spread.

Spread of CNQX, and recovery from CNQX application does interfere with more detailed interpretation of these results – event distributions are not stationary. With multiple CNQX applications, it is possible that the response to the first puff changes over the period where we would like to study the effects of the second – not only might there be spread of CNQX, but recovery from the first puff can confound interpretation of the effects of the second. This is part of the reason that a less lipophilic AMPA blocker, such as kyurenic acid, was not used. Much more frequent, complete recovery would have been possible than shown here, but the response to an initial puff would not have been stable enough to allow interpretation of the response to the second. This is why more detailed conclusions have not been attempted from the dual puff study, and why in-depth analysis concentrated on the cell with the shortest inter-puff interval, which is most likely to be cleanly interpretable.

On the whole, while the spread of CNQX complicates detailed interpretation of these results, it does not interfere with the basic conclusions drawn from this study.

Properties of apically-generated events

The effects of apical CNQX application, either alone, or subsequent to basal CNQX application, were extremely variable. A number of reasons for this were discussed

above. The cell might not have an apical dendrite, either because it was severed in the slicing, it didn't have one to begin with, or it has one but it doesn't extend all the way to the place where the CNQX was applied. It might be obliquely oriented, or deep in the slice, so that the CNQX simply misses it. For instance, in one morphologically-recovered layer III cell, the apical dendrite bifurcated near the soma and the two branches diverged at a steep angle. A relatively small puff of CNQX was applied immediately between the branches, and not directly onto either of them. In any case, it is likely that the CNQX will have to travel farther to hit the apical dendrite than in the case of basal application; and that CNQX is not going to reach as significant a fraction of the apical membrane as it does of the basal membrane. And any effect of CNQX on apical events is more difficult to see because they are a much smaller population than the basal events, and also smaller and amplitude and thus more significantly affected by noise.

All of these things make it difficult to draw detailed conclusions about the nature of apical events. Three things can be said, however: first, they are lower in frequency, much lower, than basally-generated events, second, they are restricted predominantly to small amplitudes, and third, many of them have long rise times. The results from dual basal and apical puffs suggest that it is likely that all of the very longest rise time events are apically generated, but given the possibility of kinetic heterogeneity among the proximal events (see Chapter 4), this should be considered tentative without more data.

Loss of events due to detection.

One difficulty, considered in Sections 5.3.7, A.7, and 3.3.2 is that the fact that mEPSCs must be detected from the surrounding noise may bias their interpretation in some cases. This is particularly worrisome in the case of apically-generated events. Perhaps they are there, in large numbers, and we simply aren't detecting them.

This is not likely to be the case. Hyperpolarizing cells to -90 mV or -110 mV

(Figures 3-5 and A-67) does bring some events out of the noise via increased driving force, but the absolute number of such events is very small (30 events out of a population of 1500 at -110 mV). Certainly, no large peak of small events is lurking below the detection threshold just under the noise, this can be clearly seen from the analysis of voltage dependence cited above, and the effects of changing the detection threshold shown in Figure 5-46.

It is true that proximally-generated events are more sensitive to change of somatic voltage than are distal ones. However, given the fact that DC voltage control in these cells should be quite good, in spite of the problems with space clamp which give rise to filtering of mEPSCs [242, 150, 293], events of the same order of magnitude as those generated proximally, even if they are very far out on the apical dendrite, should be increased in amplitude to the same degree as a result of the change in holding potential; thus some fraction of them should be seen. It is possible that there are a large number of apical mEPSCs, which happen to be qualitatively smaller in amplitude (i.e. never detected under normal conditions) than the remainder of the mEPSC population. If so, we would be unable to detect them or determine their susceptibility to CNQX application. However, as the conclusions of this study are about the site of origin of those mEPSCs we *do* detect, this does not affect the results.

Other problems with detection of mEPSCs. Detection will induce some errors into the analysis of mEPSCs, unfortunately. While the number of small events lost due to threshold, and the number of noise events detected accidentally, should be equal or smaller in absolute number after CNQX application relative to the baseline period, these events will comprise a larger fraction of the total, given the smaller population size, and therefore exert a stronger influence skewing parameter measurements. When event frequency was very low, detected events were scanned more closely by hand to remove detected noise artifacts; this allowed very low thresholds to be used without significantly biasing the results due to unwanted garbage. Another error induced by the detector, is that measurement of event parameters is not independent of event

frequency. At high event frequencies (such as in some baseline periods), there will be larger numbers of overlapping events, which will not have their amplitudes or kinetic parameters measured (see Methods). At the same time, the detector will sometimes fail to detect an inflection, or an overlap, as multiple events, and will measure the properties of the composite event. This results in the generation of two classes of artifact: events with overly long rise times, and events with half widths too long for their rise. After CNQX application, event frequency is reduced to the point where these effects disappear. This means that there will be an apparent decrease in mEPSC rise time after CNQX application, due not to a real change in rise time, but instead simply to this detection artifact - this will mask a real increase in rise time which might be lurking underneath. A more advanced rise time measurement algorithm was developed, which was more robust against such errors; it was used for the measurement of all the kinetic data presented here. Population statistics were not presented for the effects of CNQX application on rise time because of the difficulty in adequately checking all detected events against this source of bias in more than a few cells. Another difficulty induced by detection is that of measuring the voltage dependence of low-frequency events. As shown in Figure 5-43C,D, moving the holding potential from -70 mV to -90 mV both increases the amplitudes of the largest events, and brings events out of the noise and into detection range (this can be seen by the reduction in long IEIs after the voltage change). Additionally, the largest (presumed more proximal) events will show a somewhat larger change in amplitude with hyperpolarization than the distal events. This, combined with any continuing spread of CNQX, makes it impossible to use the voltage dependence of events after CNQX application as a good metric of their conductance or reversal potential. When the cell is hyperpolarized, a small number of low-amplitude events appear out of the noise, but as frequency is low, these events comprise a large fraction of the total; there is a simultaneous increase in the amplitude of larger events, but when averaged the net result is no real change in amplitude with hyperpolarization for most cells. In cases where more hyperpolarized potentials were measured at later times during

periods where the CNQX was spreading, the average amplitude at -90 could be even lower than that at -70, as more of the proximal events were missing.

Insufficient CNQX – partial block of mEPSCs

The last potential problem with interpreting the effects of CNQX application is that of partial blockade. Perhaps the reason apical events appear smaller than basally-generated ones is that they are partially blocked by the initial application of CNQX. It is not the case that the small, apical events are actually partially blocked basal events; this can be seen from the arguments about the effects of dual CNQX puffing and spatial selectivity given above. Also, given the fact that all events are blocked by 10 μM CNQX applied in the bath, and the puffing solution contained 100 μM CNQX, the chance of only partially blocked events immediately under the puff is very low. The more conceivable risk is partially blocked synapses at a distance from the puff site, resulting in apparently small apically-generated mEPSCs. However, this is inconsistent with the fact that puffing CNQX directly onto the apical dendrite does not block the large-amplitude events; this indicates both that there aren't an undiscovered population of large apically-generated events partially blocked by basal CNQX application, and that it is almost definitely not the case that apical events are partially blocked by basal application – if that were so, apical application would (by simple reciprocity) be expected to partially block basal events, and so large-amplitude events would be reduced after apical CNQX application. Similarly, applying CNQX to one half of the basal dendrites (data not shown) reduced the frequency of large-amplitude events, without reducing the amplitude of all events, consistent with a model whereby a subset of proximal synapses are completely blocked but at least some of the others (which are physically nearby) are unaffected; all of these large events were blocked by a second, larger puff sufficient to cover all of the basal dendrites. Similarly, puffing different portions of the apical dendrite, or near the apical dendrite but not on it, caused only the expected reductions in mEPSC amplitude, not additional ones

likely to be due to partial block of more distant events (see Figure 5-44). Therefore it is extremely unlikely that partial receptor blockade is responsible for the results presented here (also see Section 5.3.7).

If there are multiple subtypes of AMPA receptors on these cells, it is conceivably possible that they have differential sensitivity to CNQX. The range cannot be particularly wide, as all events were blocked with 10 μMCNQX, and no consistent fraction of events were blocked with 0.3 μMCNQX applied in the bath. If this were true, it would somewhat obscure the results presented here, but would not change the basic conclusions.

Kinetic heterogeneity among events After CNQX application to the basal dendrites, some slow rise time events are lost (Fig. 5-43). This suggests that either there are some slow events arising from proximal input sites, presumably due to heterogeneity in AMPA receptor kinetics (see Chapter 6), that these events are the largest filtered events coming from sites close enough to be hit by a basal puff (e.g. the distal basal dendrites), or that these long rise times were artifacts due to inaccurate detection of overlapping events (see above); in that case the reduction of mEPSC frequency after CNQX application would as a consequence reduce the occurrence of such events. There are suggestions from the literature [82, 83, 143, 142, 70] and previous chapters of this thesis (see Figures 3-6, 3-7, and 3-8) that there is a certain degree of heterogeneity among mEPSC kinetics, at least between different cells, but possibly also in the form of identifiable subpopulations of mEPSCs within a single cell [70]. Data presented in Chapter 6 suggests that there might be such kinetic heterogeneity in GABAergic mIPSCs, with a population of very slowly-rising events coming from proximal sites; this is consistent with the known heterogeneity in the population of $GABA_A$ receptors on a single granule cell [225, 215, 91, 295, 272, 75, 186]. It is therefore quite possible that there are multiple kinetic subpopulations among the events studied here, corresponding to slightly different AMPA receptor subtypes, and

perhaps with tendencies towards different amplitudes.[15] This data cannot confirm or deny the presence of such events. However, it can say, that they too seem to be subject to the absolute constraints on amplitude and shape imposed by electrotonic filtering (see Section 4.3.5): proximal events can display the entire range of kinetic and amplitude variability afforded them by their underlying receptor makeup, but distally-generated events, as seen at the soma, will be small and slow.

[15]They might even have different sensitivities towards CNQX, though they are all clearly blocked by it.

5.5 Figure Legends

Figure 5-39: Local application of CNQX. A. Schematic of the experimental preparation. CNQX, marked with fast green, was applied locally to either the apical or basal dendrites of the recorded cell. B. Application of CNQX in the region of the apical dendrite causes a mild decrease in mEPSC frequency. Inter-event intervals (IEIs) are plotted against time relative to the application of CNQX (t=0). A decrease in event frequency is reflected by an increase in the number of long IEIs. Hatched bars indicate regions where data were unavailable for analysis (e.g. during seal test adjustment). At t=0, a drop of CNQX was applied to the apical dendrite. C1. Application of CNQX to the basal dendrites causes a dramatic reduction in mEPSC frequency. At t=0, a large drop of CNQX was applied in the region of the recording electrode. mEPSC frequency drops almost immediately. 2. Expansion of the region around t=0. D,E. Puffing by itself does not cause a change in mEPSC frequency or amplitude. At t=0 very large drop of vehicle solution was applied to the region containing the soma, basal dendrites, and proximal apical obliques. D. There is no large or rapid change in either (1) inter-event intervals or (2) amplitudes (larger events plotted downwards). E. Inter-event intervals for a vehicle solution puff in another cell.

Figure 5-40: Most mEPSCs originate from the basal dendrites. MEPSC amplitudes are plotted against time relative to a puff of CNQX onto the basal dendrites in three cells. CNQX is applied at t=0, larger mEPSC amplitudes are more negative (downwards). Hatched boxes represent stretches where data was unavailable. A. Application of a small puff of CNQX to the basal dendrites rapidly reduces event frequency and blocks all large-amplitude events. B. Same cell as A, several minutes later. Event amplitude and frequency has partially recovered. At t=0, a second puff is applied in the same location as the first. C. Basal CNQX puffs in two more cells. 1) CNQX is applied slightly below the basal dendrites and must diffuse a short distance before reaching full effect. 2) mEPSC amplitudes for cells whose IEIs are shown in Figure 5-39C. D. The effect of CNQX application is a selective loss of large-amplitude events. Cumulative mean amplitude is plotted vs. amplitude for events in a 60-second window before and shortly after CNQX application, for the cell shown in C1. E. Averages of all events in the two 60-second windows used in D. Pre: N: 1586, amplitude: -34.06 pA, rise time 0.6128 ms, half width 2.402 ms. Post: amplitude: N: 183, -23.09 pA, rise time 0.627 ms, half width 3.649 ms.

Figure 5-41: Apical mEPSCs tend to be smaller in amplitude. A. Amplitudes vs. time for apical application of CNQX, for the cell whose IEIS are shown in Figure 5-39B. B. Averages of all events in a 60-second window before (1) and shortly after (2) CNQX application for the cell shown in A. Pre: N: 845, amplitude: -13.35

pA, rise time 1.479 ms, half width 4.003 ms. Post: N: 505, amplitude: -14.48 pA, rise time 1.207 msec, half width 3.962 ms. C. Plotting cumulative mean amplitude vs. amplitude for the cell shown in A. B shows no loss of large-amplitude events. D. Cumulative amplitude distributions for these same pre- and post-puff periods. There is no significant difference between these distributions (K-S test, $p>.05$). E. Amplitude histograms of the events in these 60-second periods (1) before (n=845) and (2) after (n=505) CNQX application. (3) The difference between the histograms in (1) and (2), binned at 1 pA intervals.

Figure 5-42: Effects of CNQX application in the population of cells. Summary statistics on the change in mEPSC parameters with CNQX application to the basal or apical dendrites, or with vehicle puff. Values for IEI and amplitude are represented as % change, normalized to the value at the baseline period (0% change). A, B. Effects of puffing CNQX (or vehicle) on the population of cells. Mean change in IEI (A) and amplitude (B) across the population of cells is shown for the periods immediately post-puff, slightly later (or baseline for second puff), after a second puff if any, and a recovery period some minutes after the last puff. Each point is the mean for all the cells in a given category for whom data was collected (e.g. all cells have "pre" and "post", but not all cells were held for a second puff): basal puff (n=19), apical puff (n=7), dual puff (n=6), and vehicle puff onto the basal dendrites (n=7). "Dual" puff refers to first puffing CNQX onto the basal dendrites, collecting a post-puff period of data, and then applying CNQX to the apical dendrites (see Figure 5-43). The data for the first, basal, puff in these cells is included in the basal population. The second puff shown for the basal or apical cells refers to a second puff in the same location as the first. Error bars are standard error for each point, presented in the units of the graph (% of pre-puff mean). Where error bars are not visible, they are smaller than the symbols; except for the case of the post second puff value for apical application in A and B, where only one cell was in the group. 0% change is shown by dot-dashed line. A. CNQX application greatly increases inter-event interval. Effects of vehicle puff are almost indistinguishable from 0. B. CNQX application on the basal dendrites greatly decreases event amplitude, but apical application has a much more mixed effect (points from several cells overlaid, see above for details). Vehicle puffing causes a small average reduction in event amplitude at late times. C-E. Data for individual cells. For each cell in a category (basal, apical, or vehicle), the mean value of IEI (C) or amplitude (E), or the absolute frequency (D) (number of events divided by length of analysis window in seconds) is plotted against time period. Absolute frequencies are shown as raw values, not normalized to baseline. Error bars (almost always smaller than the symbol) are standard error across the population of events for that cell, normalized to the appropriate scale (no error bars shown for absolute frequency). Data for second puff of dual-puff cells shown in Figure 5-43.

Figure 5-43: Nature of apical events: dual-puff cells. A, B. Cell-by-cell data for the population data shown in Figure 5-42A, B. Error bars are smaller than the symbols. The difference between solid and dashed lines in B are there only to enable tracing of the data for a single cell from point to point. C-E. Single events are shown for a dual-puff cell. This cell was selected because it had the shortest interval between basal and apical puffs, thus leaving the least time for spread of the basally-applied CNQX. Consistent with this, its event parameters remained stationary over the period between puffs. Before the apical puff, the holding potential was moved from -70 mV to -90 mV to reveal more small-amplitude events, periods at -90mV are indicated by the thick black bars. Puff times are indicated by thick dashed lines. Basal puff occurred at t=0, apical puff indicated by the arrow. C. Inter-event intervals. D. Amplitudes. E. Rise times.

Figure 5-44: Correspondence between response and morphology. Responses to several small CNQX deposits onto a very small layer 5 cell. Inter-event interval and amplitude are plotted against time for a cell who received multiple CNQX applications (this cell was not included in the population data above, as its first puff was not categorically somatic). Puff times are indicated by the arrows and dashed lines. Recovery some minutes later shown at right in D,F. A. Puff location is indicated by the hatched patch on the cell for puffs 1-4. Scale bar to left is for 1-4. B. Reduced schematic, showing size of cell relative to the thickness of cortex, and a slightly expanded view (relative to A) of the reconstruction of this cell (scale bar is 100 μm). C. Amplitudes. D. Amplitude recovery several minutes after blocking all events via repeated puffing. E. Rise times. F. Rise time recovery. Holding potential in this cell was -60 mV.

Figure 5-45: Shape indices reflect event location. A. Rise time vs half width plot for all events in 60-second windows before and after application of CNQX to the basal dendrites for the cell shown in Figure 5-43C-F. "Post" points are plotted on top of, and hide, a mass of "pre" points, but these show no features different from the "post" points on top of them. B. Rise time vs half width plots for events immediately before and after the subsequent puff to the apical region. Holding potential -90mV. "Pre" points show the addition of a larger number of slow events not visible in A, presumably because the increased driving force allowed them to be detected. Puffing the apical dendrite removes all events with shape indices indicative of a distal location.

Figure 5-46: Effects of detection threshold. Figure 7: detectability effects

A: Effects of changing detection threshold on amplitude distribution of detected mEPSCs. The same stretch of data was detected with thresholds from 2-15 pA. Open

bars in 2-5 show the amplitude distribution of the baseline noise. A threshold of 2 pA detects the upper portion of the noise peak (large peak near 0), but does not add another peak of events below the mode predicted by detection with higher thresholds. B. Cumulative amplitude distributions resulting from the detection thresholds shown in A and D. C. Rise time distributions for the events detected in A, D. Detection of noise adds a significant number of very short rise-time events with a threshold of 2 pA, and a very high threshold (15 pA) misses some of the slower events.

Figure 5-47: Effects of bath CNQX. A. Time course of bath wash-in of 10 μM CNQX. CNQX wash was started several minutes before the data shown here (there is a long tubing lag in my setup). This period shows the stretch of time from initial change in mEPSC characteristics, until the point at which almost all events had disappeared. Event amplitudes are plotted vs. time, showing a progressive decrease in size. B. Event rise times plotted for data in A. As events disappear below the detection threshold due to loss of amplitude, those events that disappear first have the longest rise times (i.e. slow events are small, see Figure 4-19). C,D. Rise time vs half width plot for events in two arbitrarily chosen windows during the period of CNQX wash-in.[16] As CNQX washes in, events gradually move towards more proximal locations (according to their shape indices), presumably because the slowest events tend to go below detection threshold first. However, this effect is not completely monotonic, indicating that there are some larger slow events and suggesting the presence of conductance variability. Consistent with this, changing the holding potential to -90 (data not shown) restored some slower events. D. The final events left before total blockade all have very proximal shape indices. "Post" data in C replotted as "pre" data in D. Events from the final 15 seconds of the period shown here are plotted as filled triangles rather than empty ones, lie on top of the empty triangles, and can be seen on close examination and much squinting. They are all clustered near the origin, indicating that the largest events (those still above threshold) are the most proximal.

[16]They really were arbitrary. If I had chosen them deliberately, the effect would have been much more visible.

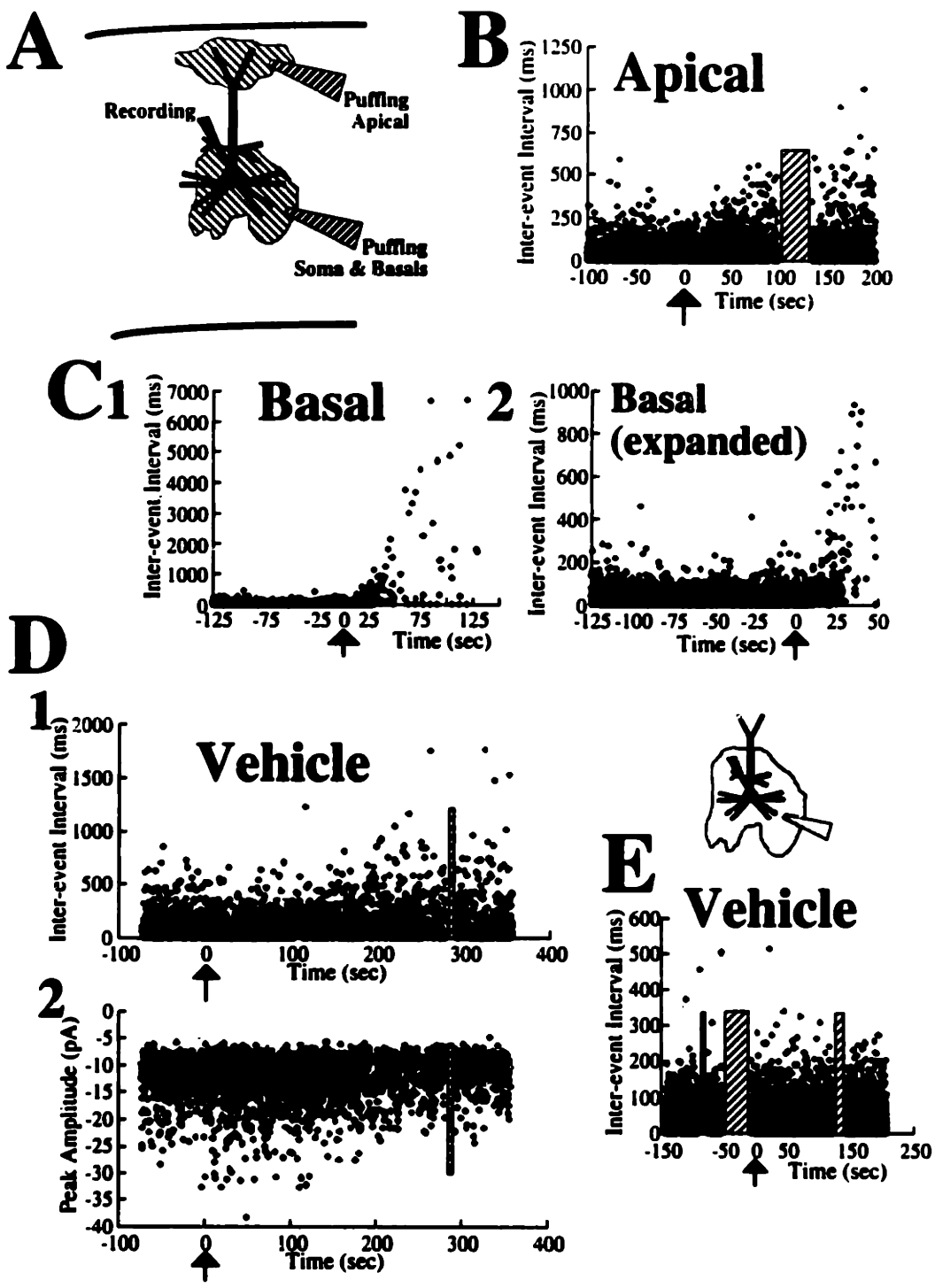
A
Recording
Puffing
Apical
Puffing
Soma & Basals
B
Apical
Inter-event Interval (ms)
Time (sec)
C1
Basal
Inter-event Interval (ms)
Time (sec)
2
Basal
(expanded)
Inter-event Interval (ms)
Time (sec)
D
1
Vehicle
Inter-event Interval (ms)
Time (sec)
2
Peak Amplitude (pA)
Time (sec)
E
Vehicle
Inter-event Interval (ms)
Time (sec)

Fig. 5 - 39

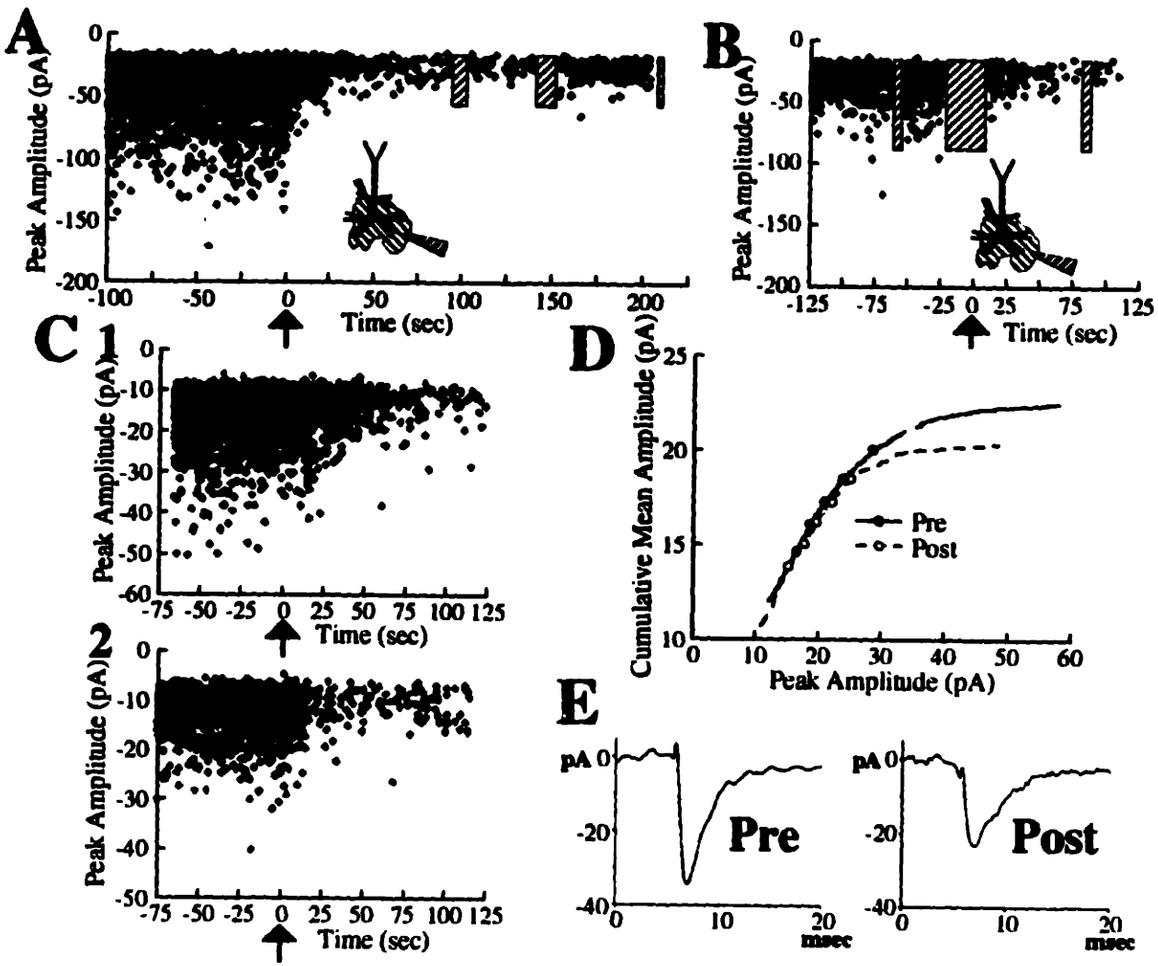
A
Peak Amplitude (pA)
0
-50
-100
-150
-200
-100 -50 0 50 100 150 200
Time (sec)
B
Peak Amplitude (pA)
0
-50
-100
-150
-200
-125 -75 -25 0 25 75 125
Time (sec)
C 1
Peak Amplitude (pA)
0
-10
-20
-30
-40
-50
-60
-75 -50 -25 0 25 50 75 100 125
Time (sec)
2
Peak Amplitude (pA)
0
-10
-20
-30
-40
-50
-75 -50 -25 0 25 50 75 100 125
Time (sec)
D
Cumulative Mean Amplitude (pA)
25
20
15
10
0 10 20 30 40 50 60
Peak Amplitude (pA)
Pre
Post
E
pA 0
-20
-40
Pre
0 10 20
msec
pA 0
-20
-40
Post
0 10 20
msec

Fig. 5 - 40

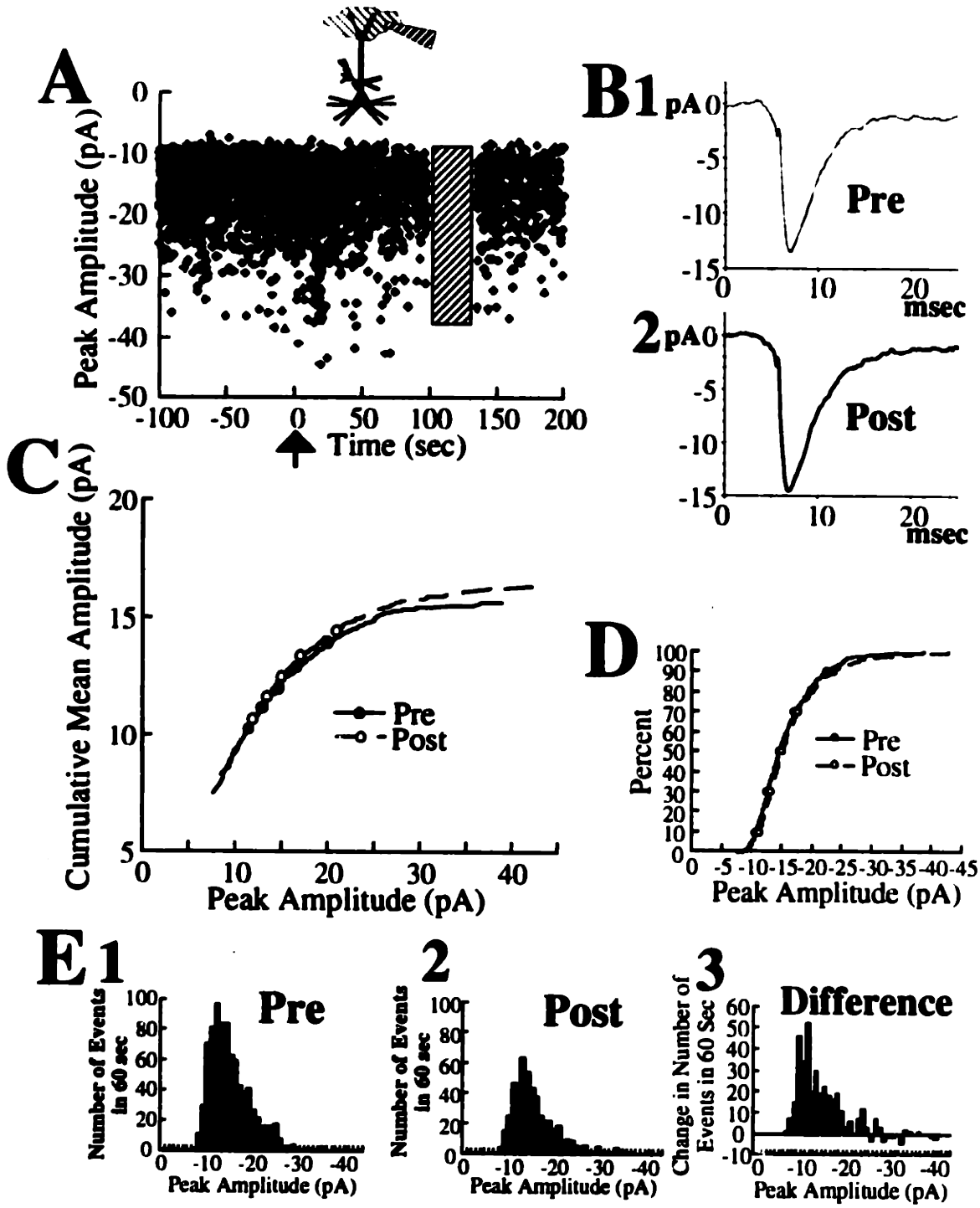
A
Peak Amplitude (pA)
0
-10
-20
-30
-40
-50
-100 -50 0 50 100 150 200
Time (sec)
B1
pA 0
-5
-10
-15
Pre
0 10 20
msec
2
pA 0
-5
-10
-15
Post
0 10 20
msec
C
Cumulative Mean Amplitude (pA)
20
15
10
5
0 10 20 30 40
Peak Amplitude (pA)
Pre
Post
D
Percent
100
90
80
70
60
50
40
30
20
10
0
0 -5 -10 -15 -20 -25 -30 -35 -40 -45
Peak Amplitude (pA)
Pre
Post
E1
Pre
Number of Events in 60 sec
100
80
60
40
20
0
0 -10 -20 -30 -40
Peak Amplitude (pA)
2
Post
Number of Events in 60 sec
100
80
60
40
20
0
0 -10 -20 -30 -40
Peak Amplitude (pA)
3
Difference
Change in Number of Events in 60 Sec
60
50
40
30
20
10
0
-10
0 -10 -20 -30 -40
Peak Amplitude (pA)

Fig. 5 - 41

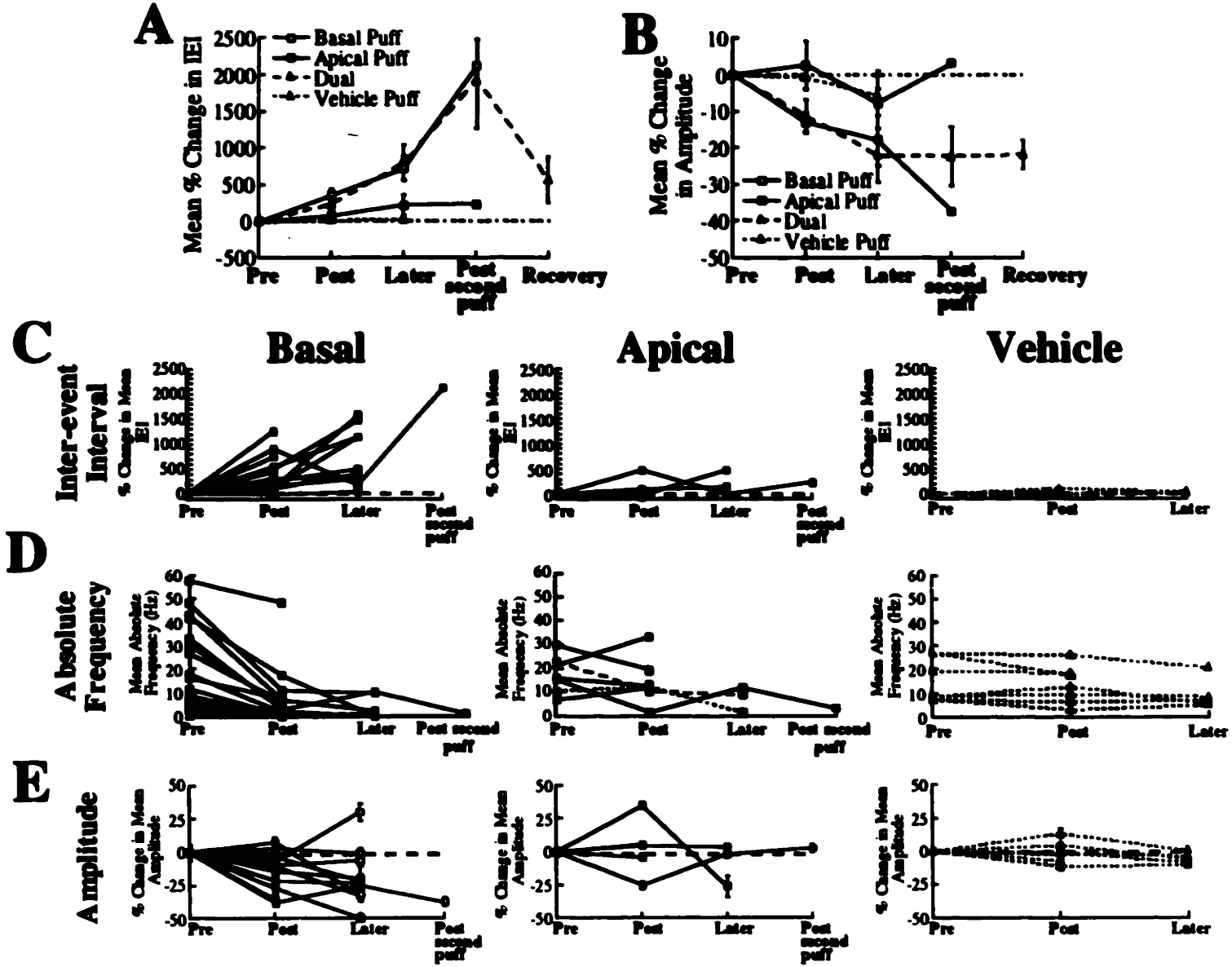
A
Mean % Change in IEI
Basal Puff
Apical Puff
Dual
Vehicle Puff
Pre
Post
Later
Post second puff
Recovery
B
Mean % Change in Amplitude
C
Basal
Apical
Vehicle
Inter-event Interval
D
Absolute Frequency
E
Amplitude

Fig. 5 - 42

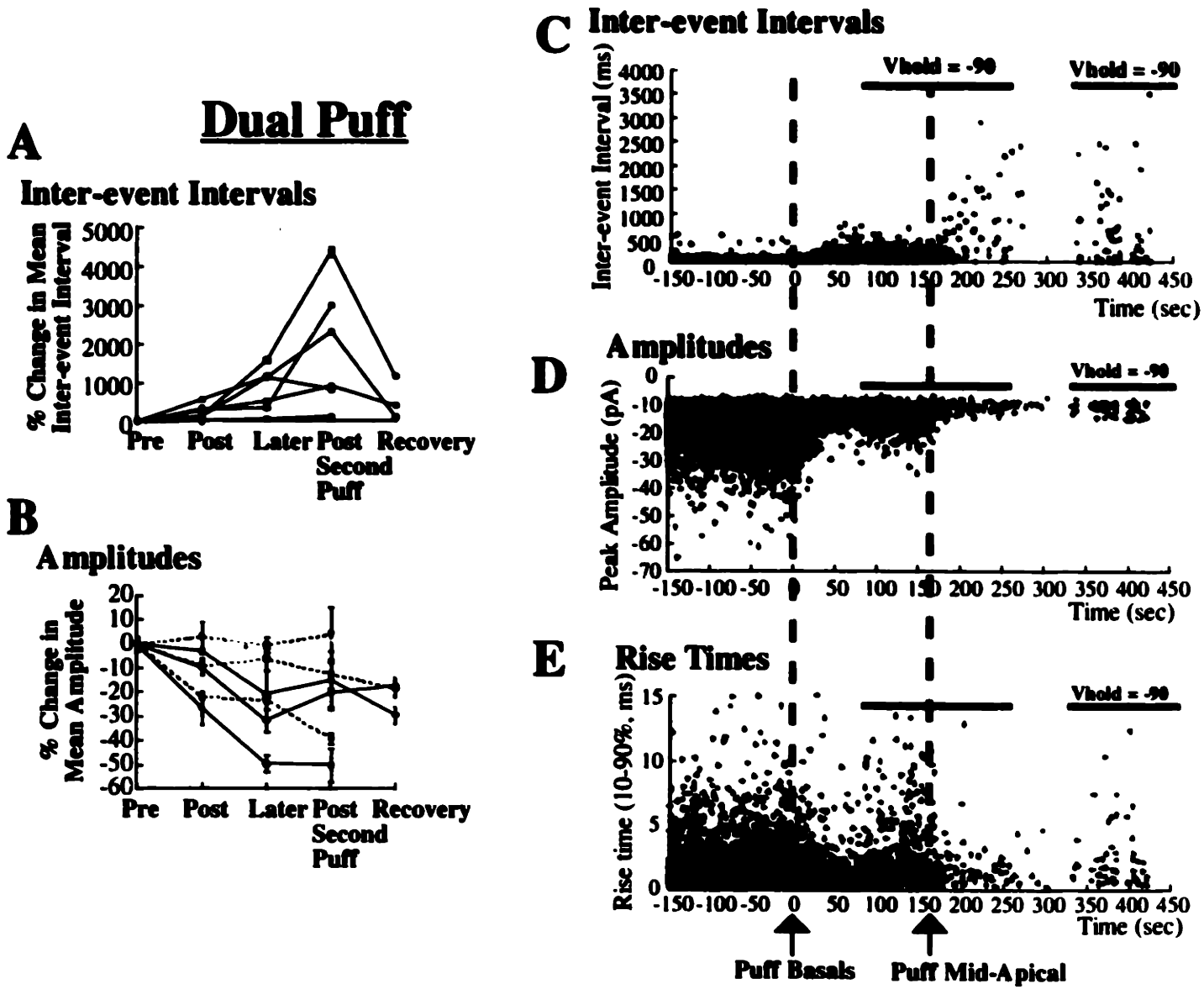
Dual Puff
A
Inter-event Intervals
% Change in Mean Inter-event Interval
5000
4000
3000
2000
1000
0
Pre
Post
Later Post
Recovery
Second Puff
B
Amplitudes
% Change in Mean Amplitude
20
10
0
-10
-20
-30
-40
-50
-60
Pre
Post
Later Post
Recovery
Second Puff
C
Inter-event Intervals
Inter-event Interval (ms)
Vhold = -90
Vhold = -90
4000
3500
3000
2500
2000
1500
1000
500
0
-150 -100 -50 0 50 100 150 200 250 300 350 400 450
Time (sec)
D
Amplitudes
Peak Amplitude (pA)
Vhold = -90
0
-10
-20
-30
-40
-50
-60
-70
-150 -100 -50 0 50 100 150 200 250 300 350 400 450
Time (sec)
E
Rise Times
Rise time (10-90%, ms)
Vhold = -90
15
10
5
0
-150 -100 -50 0 50 100 150 200 250 300 350 400 450
Time (sec)
Puff Basals
Puff Mid-Apical

Fig. 5 - 43

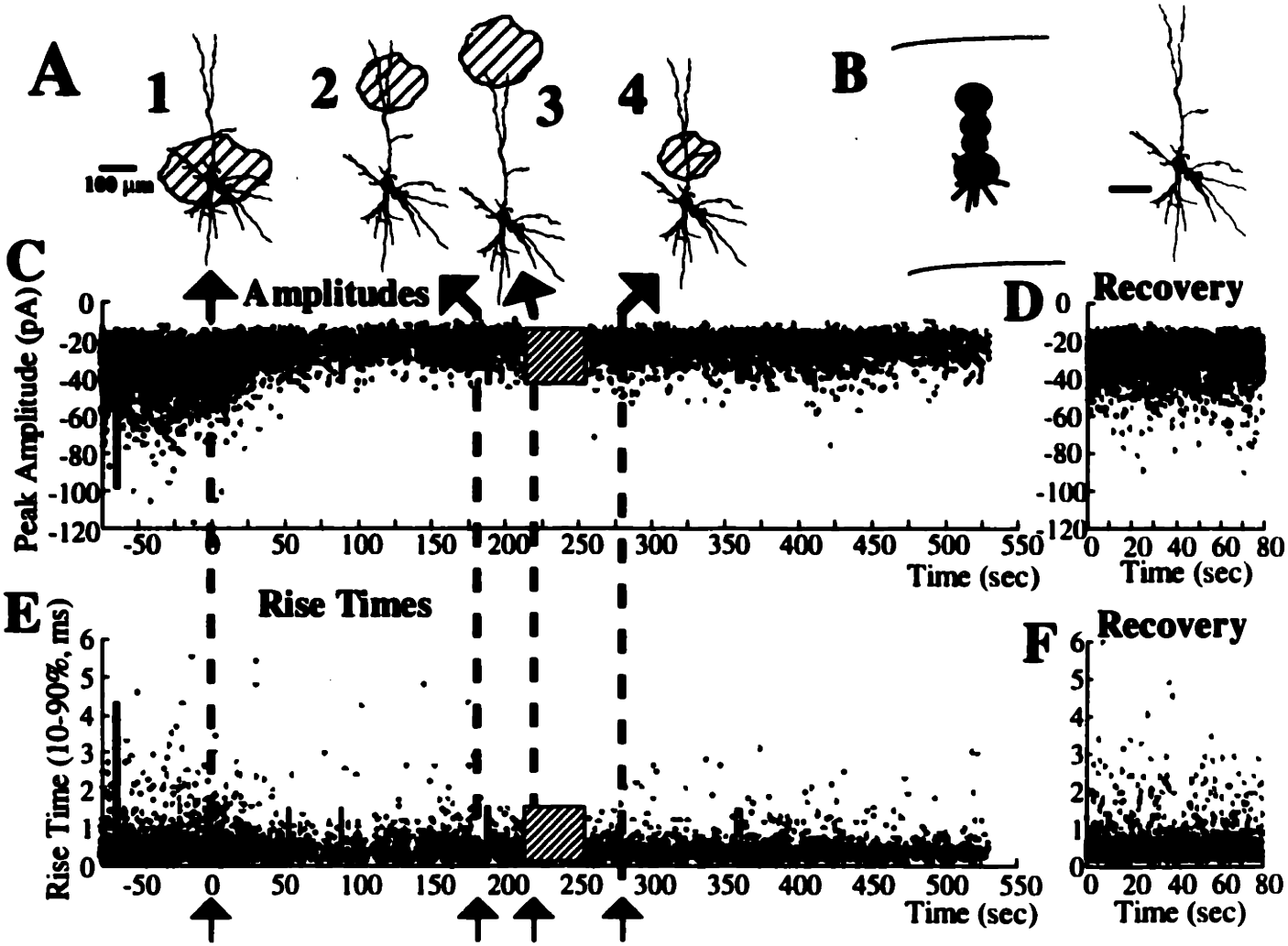
A
1
2
3
4
100 µm
B
C
Amplitudes
Peak Amplitude (pA)
0
-20
-40
-60
-80
-100
-120
-50
0
50
100
150
200
250
300
350
400
450
500
550
Time (sec)
D
Recovery
0
20
40
60
80
Time (sec)
E
Rise Times
Rise Time (10-90%, ms)
6
5
4
3
2
1
0
Time (sec)
F
Recovery
Time (sec)

Fig. 5 - 44

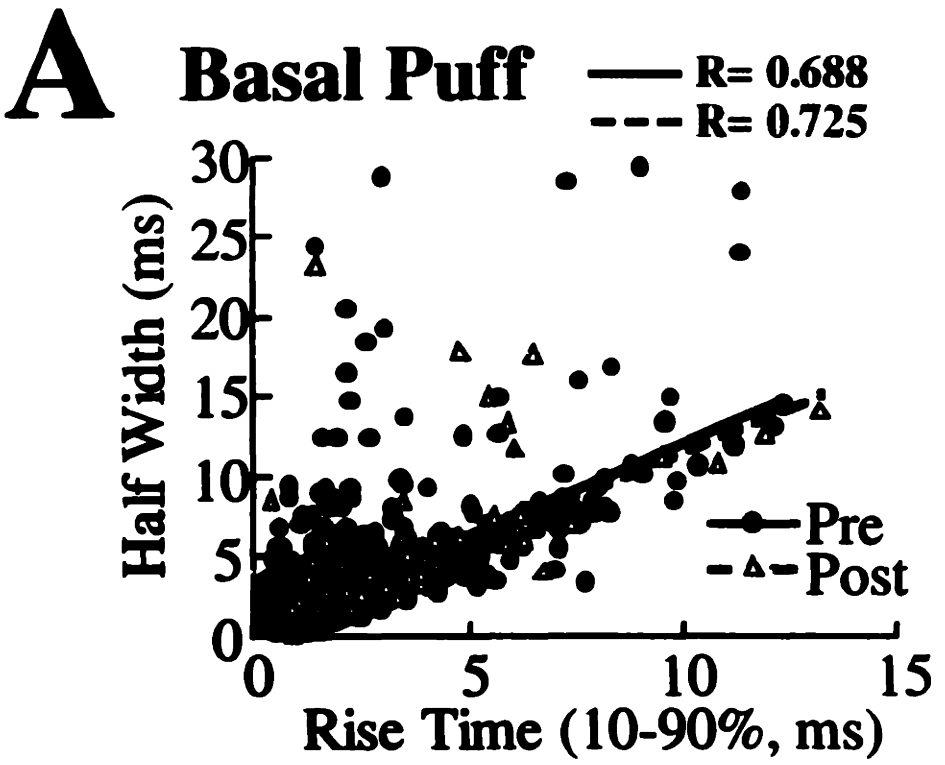
A
Basal Puff
R= 0.688
R= 0.725
Half Width (ms)
30
25
20
15
10
5
0
0
5
10
15
Rise Time (10-90%, ms)
Pre
Post

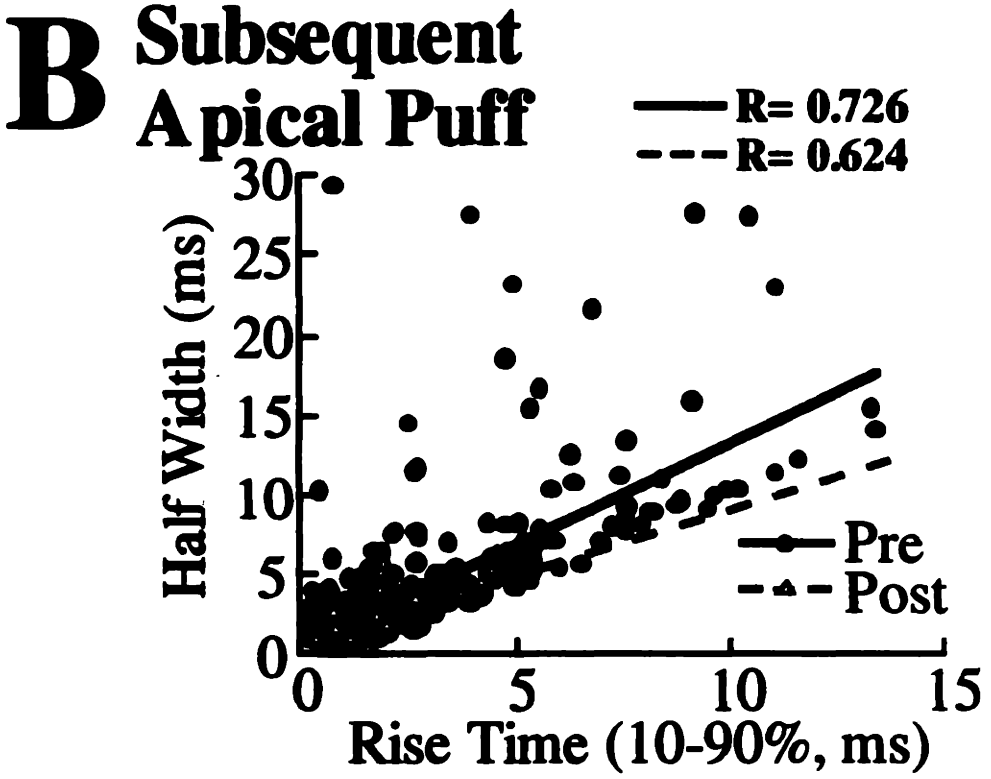
B
Subsequent
Apical Puff
R= 0.726
R= 0.624
Half Width (ms)
30
25
20
15
10
5
0
0
5
10
15
Rise Time (10-90%, ms)
Pre
Post

Fig. 5 - 45

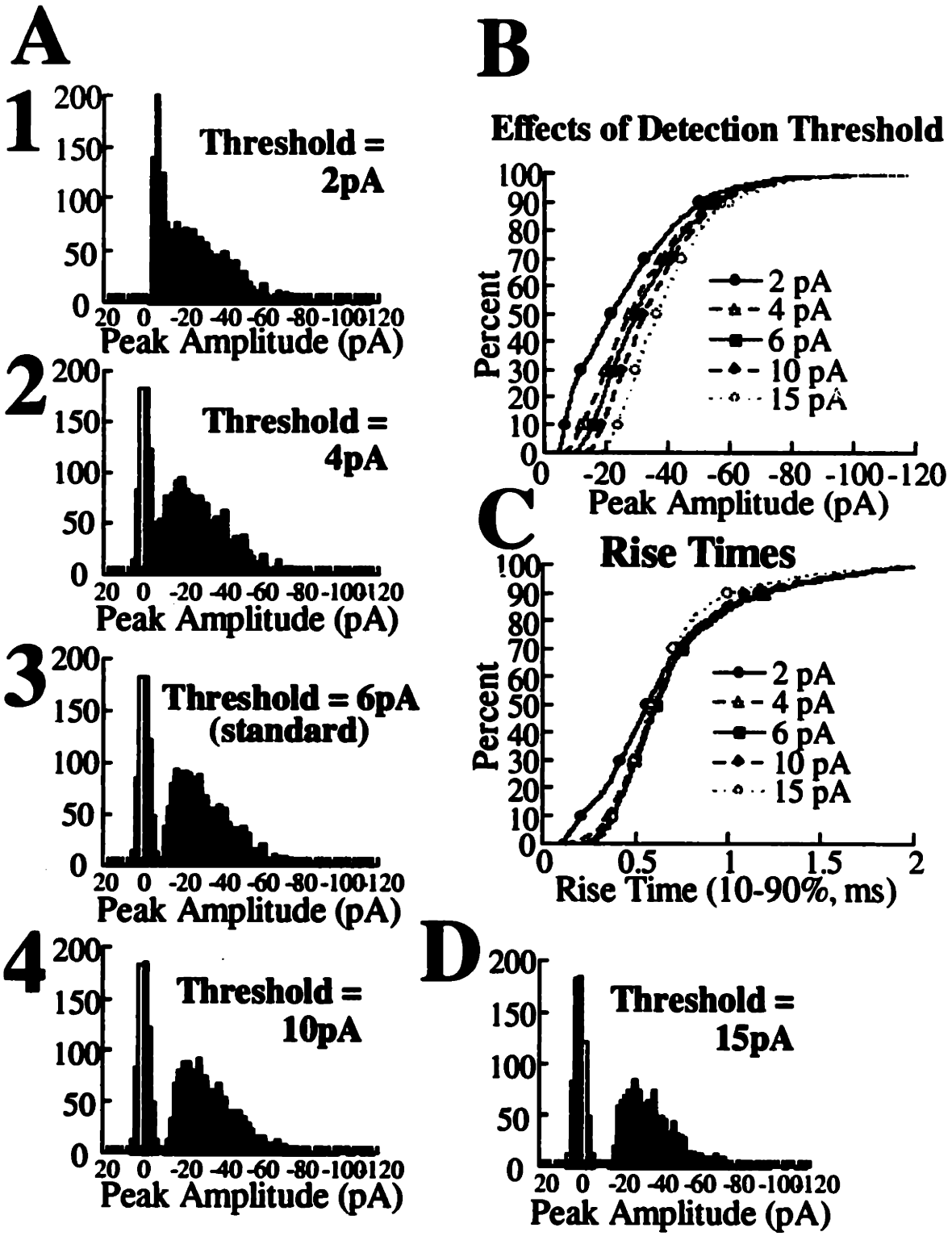
A
1
Threshold = 2pA
2
Threshold = 4pA
3
Threshold = 6pA (standard)
4
Threshold = 10pA
Peak Amplitude (pA)
B
Effects of Detection Threshold
Percent
2 pA
4 pA
6 pA
10 pA
15 pA
Peak Amplitude (pA)
C
Rise Times
Rise Time (10-90%, ms)
D
Threshold = 15pA

Fig. 5 - 46

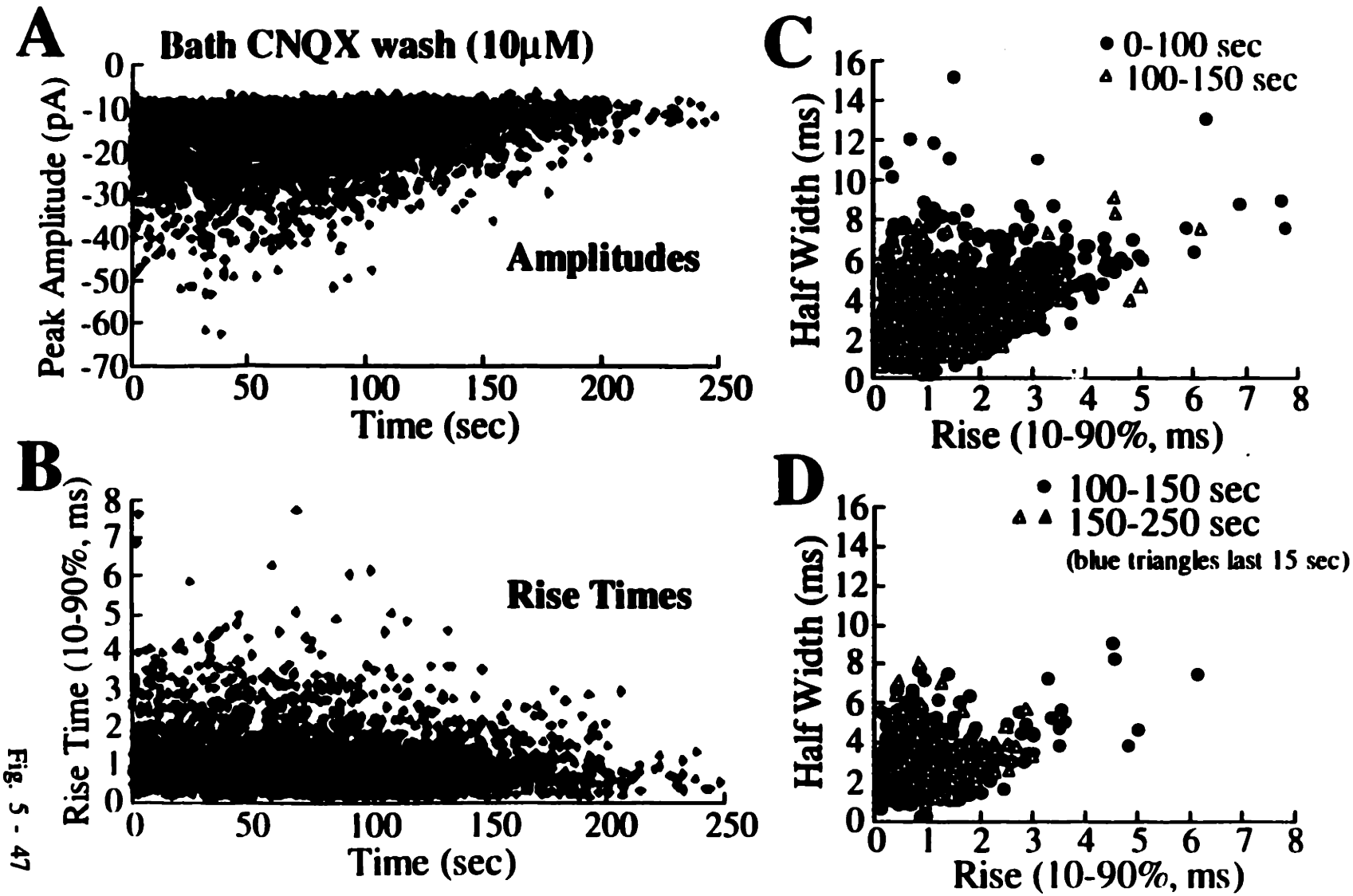
A
Bath CNQX wash (10μM)
Peak Amplitude (pA)
0
-10
-20
-30
-40
-50
-60
-70
Amplitudes
0
50
100
150
200
250
Time (sec)
B
Rise Time (10-90%, ms)
Rise Times
Time (sec)
C
0-100 sec
100-150 sec
Half Width (ms)
Rise (10-90%, ms)
D
100-150 sec
150-250 sec
(blue triangles last 15 sec)
Half Width (ms)
Rise (10-90%, ms)

Fig. 5 - 47

6

Electrotonic Structure in Dentate Gyrus Granule Cells: Filtering of IPSCs

Abstract

Many central neurons are subject to a tonic barrage of randomly occurring spontaneous inhibitory events (mIPSCs), resulting from the action potential-independent release of GABA. Do the terminals making synapses onto somatic vs dendritic sites, which arise from specific populations of interneurons, differ in their ability to generate mIPSCs? We have applied the techniques of Chapter 4 to whole cell recordings from dentate gyrus granule cells to demonstrate that most of the action potential independent inhibition, taking place as mIPSCs, originates from proximal sites. Indeed, removal of the bulk (>50%) of the dendritic tree does not change the characteristics of mIPSCs. Distal synapses, known to be present in equal or larger numbers than proximal ones [78, 79], are functional and generate responses to stimulation consistent with their being subject to considerable electrotonic filtering. These results document for the first time that a division of labor exists between GABAergic terminals synapsing at proximal vs distal portions of central neurons. Thus, proximal GABAergic terminals are responsible for sustained inhibition targeted at the soma.

6.1 Introduction

Electrotonic filtering is a fundamental property of the passive electrical structure of all neurons. Therefore, the analysis presented in Chapter 4, which depended only on the basic principles of cable theory applied to a specific cell morphology, should

be generally applicable across cell and synapse types. In this chapter we use these techniques to address a fundamental question about neuronal function.

In contrast to neocortical pyramidal cells from young rats (see Figure 3-4E,F), many neuronal types receive a high-frequency barrage of spontaneous and miniature GABAergic IPSCs. This tonic inhibition may act as a gain control, modulating the responsiveness of the cell. As the inhibitory innervation of many cell types comes from a number of interneuron types which are mapped onto particular parts of the granule cell somadendritic axis, information about the site of origin of these inhibitory inputs would tell us something about the functional properties of these interneuron subclasses. Computational studies have suggested functional differences between the roles of somatic and dendritic inhibition [284, 123, 120, 33]. Therefore which region of the cell generates these spontaneous inhibitory inputs are may have a powerful impact on their ability to shape the output of the cell. We have combined whole-cell patch clamp recording in granule cells with computational modeling to identify the site of origin of miniature IPSCs in dentate gyrus granule cells.[1]

6.1.1 Nature and location of inhibitory inputs to granule cells.

On most principal cells of the central nervous system, inhibitory terminals originating from distinct interneuron types specifically innervate spatially segregated parts of the neuron such as the axon initial segment, soma and various parts of the dendrites. In the case of granule cells of the hippocampal dentate gyrus, this inhibitory innervation arises from at least five types of GABAergic neuron [79, 80]. These interneurons terminate on essentially mutually exclusive domains along the longitudinal axis of the granule cell. The high specificity of their target selection makes it possible to predict the origin of GABAergic terminals from their location on the surface of the

[1]This work was performed in collaboration with Drs. I. Soltesz and I. Mody of the University of Texas Southwestern Medical Center at Dallas. See Section 1.2 for details.

postsynaptic cell [80, 186]. For example, axo-axonic or chandelier cells exclusively innervate the axon initial segment, while basket cells make contact with the somata and proximal dendrites of granule cells. These interneurons evoke short-latency, fast, $GABA_A$ receptor-mediated inhibitory synaptic events [26, 27]. The inhibitory innervation of the dendrites is supplied by other cells classified according to the location of their axonal and dendritic domains [80]. These include a type of hilar cell forming a dense axonal plexus in the inner third of the molecular layer, the termination zone of commissural and associational pathways; other hilar cells with axons in the outer two thirds of the molecular layer, the termination zone of the perforant pathway from the entorhinal cortex, as well as a molecular layer cell type which terminates exclusively in the distal dendritic region of granule cells. Such a strict spatial segregation of GABAergic afferents raises the possibility that these distinct inhibitory inputs may play different functional roles [185]. Granule cells of the hippocampal dentate gyrus have a morphology that is much simpler and more cable-like than cortical pyramidal cells (see Figure 6-52A), with 1-4 primary dendrites branching into a unipolar tree that extends, almost without tapering, for only 300 μm to the hippocampal fissure [57, 58, 44]. This means that the anatomical segregation of inhibitory inputs to these cells also results in an electrotonic segregation, with each presynaptic cell type corresponding to a unique electrical region of the postsynaptic cell.

The dendritic trees of these interneuron types can also occupy non- overlapping domains. For example, the hilar neuron with axon branches in the outer two- thirds of the molecular layer has its dendrites restricted to the hilus, indicating that it is devoid of direct cortical inputs, whereas basket and axo-axonic cells have dendrites in the termination zone of perforant path fibers. Accordingly, that these interneuron types may play distinct functional roles as a result of their differing excitatory and inhibitory inputs.

In contrast to the case of excitatory inputs, a major target of inhibitory axons is the postsynaptic neuron's soma and axon initial segment. This is often thought of as the predominant type of inhibitory input to most cells. However, most neurons also

receive a very large number of dendritic inhibitory synapses, predominantly onto dendritic shafts [192, 106]; but also onto spines and spine necks [106, 287]. Ultrastructural studies in the dentate gyrus have provided evidence for dendritic inhibition being as abundant, or even more abundant, than somatic inhibition. The numerical density of GABAergic synapses is similar in the somatic and dendritic regions of granule cells [78], which, combined with the greater volume of the dendritic layer, implies that granule cells probably receive a larger total number of their inhibitory synapses on their dendrites than on their soma. Immunocytochemical studies have demonstrated the presence of several of the α as well as $\beta 2/3$ $GABA_A$ receptor subunits in both dendritic and somatic layers [225, 215, 91, 295, 272, 75]. However, there has been no clear demonstration of the effect of the activation of distal dendritic GABAergic synapses on granule cells. These synapses may have different physiological properties from those present on the soma. Furthermore, synaptic events generated at different locations on granule cells may be distorted by cable filtering to different degrees, but as the detailed electrotonic structure of granule cells is not yet completely understood, it is difficult to ascertain what impact this will have on the functional importance of distal inhibitory synapses.

6.1.2 Properties of GABAergic synaptic currents

In addition to the normal, action potential-dependent release of GABA [2], inhibitory terminals are also capable of generating random inhibitory events in the absence of action potentials. The inter-event intervals of such events are exponentially distributed [188, 187, 238] and they occur in most cells at relatively high frequencies (1-50 Hz). Although the precise role and mechanism of transmitter release associated with this type of tonic inhibitory synaptic transmission is not yet known, it has received considerable attention, and such inhibitory events occurring at high frequencies are sufficient to exert a strong influence on the output of the cell. Removal of extracellular Ca^{++} or addition of Ca^{++} channel antagonists do not abolish mIPSCs [48, 188, 144], indicating

that these events are independent of Ca^{++} entry into terminals. It is possible that spontaneous Ca^{++} release from intracellular stores in inhibitory terminals is responsible for the generation of mIPSCs. Differences in the Ca^{++}-handling mechanisms between terminals belonging to distinct interneuron types may therefore result in important functional differences in GABA release. Different interneurons frequently express different calcium-binding proteins [38, 114]. Inhibitory cells which synapse on the proximal parts of granule cells, the axo-axonic and basket cells, are all immunoreactive for parvalbumin, whereas cells which terminate in the dendritic layers are immunopositive for other calcium-binding proteins such as calretinin and calbindin [38]. In addition, it has been reported that inhibitory terminals on dendrites are smaller and contain mitochondria much less frequently than somatic terminals [172], suggesting that inhibitory terminals on different parts of a given neuron may have different capacity of handling Ca^{++} and thus generating spontaneous GABA release.

6.1.3 Is there a functional role for GABAergic mIPSCs?

Many central neurons receive a tonic barrage of both spontaneous and miniature IPSCs [178, 238, 144, 188, 187]. While it has not been conclusively proven that such events occur at similar frequencies *in vivo*, the fact that they are dependent on the integrity of inhibitory input fibers [244], and can be modulated up or down in frequency by neuromodulators [155] strongly indicates that they may to play a functional role in the intact animal.

What functional role could they have? While the major role that has been suggested for random mEPSCs is to provide some sort of "noise" as is required by some computational network learning algorithms [141, 86, 28, 5, 76], the tonic inhibition provided by mIPSCs has an obvious potential role as a brake on the output of the cell. The frequency of mIPSCs is sensitive to a number of neuromodulatory factors

[47, 65, 128], which would act to control the level of tonic inhibition, and hence the excitability of the cell, in response to external stimuli.

$GABA_A$ receptors consist of a receptor-channel complex which is permeable to Cl^-. As the reversal potential of a Cl^- conductance is very close to the resting potential of the cell, this class of inhibitory input has been referred to as "shunting" or "silent" inhibition [122, 121, 245], and operates by acting as a current sink to draw excitatory current out of the cell, rather than by directly hyperpolarizing the membrane.[2] Computational studies have suggested that such inhibition may play very different roles depending on whether it is located on the soma or the dendrites of the postsynaptic cell [284].

If somatic and dendritic GABAergic terminals differ in their ability to generate random, action potential-independent mIPSCs, then this may have profound functional implications on the control of input-output relations of principal cells [284, 33]. In this study, we have combined whole-cell patch clamp recording and computational modeling to establish the site of origin of miniature IPSCs. This issue is fundamental to our understanding of how neuronal inhibition operates in cortical circuits. We find that action potential-independent random mIPSCs are restricted to GABAergic synapses situated on proximal parts of granule cells.

6.2 Methods

6.2.1 Preparation of slices

The preparation of slices was done as previously described [187, 246]. Briefly, adult (60-120 days old, 250-350 g) male Wistar rats were decapitated under pentobarbital

[2]In order to study these synapses experimentally, it is common to use recording solutions whose major anion is Cl^- itself. This will change the reversal potential of $GABA_A$-mediated IPSCs to approximately 0 mV, and make it possible to hold the cell near its normal resting potential and still see large IPSCs. In this configuration, used in this chapter, IPSCs are inward (negative) currents. This allows the "silent" signaling via a conductance change to be converted experimentally into a current signal, which can be easily measured.

sodium anesthesia (75 mg/kg *i.p.*) and the brains removed. The brain was cooled in 4°C artificial cerebrospinal fluid (ACSF), composed of (in mM) 126 NaCl, 2.5 KCl, 26 $NaHCO_3$, 2 $CaCl_2$, 2 $MgCl_2$, 1.25 NaH_2PO_4, and 10 glucose. Horizontal whole brain slices [244] (400 μm thick) were prepared using a vibratome tissue sectioner (Lancer Series 1000). The brain slices were sagittally bisected into two hemispheric components and submerged in a temporary storage chamber.

For the experiments involving the amputation of dendrites [239], the slices were pre-incubated at 32°C submerged in a temporary storage chamber in neuroprotective media containing 25 μM 2-amino-D-phosphonovaleric acid (APV; Cambridge Research Biochemicals) and 10 μM 6-cyano-7-nitroquinoxaline-2,3-dione (CNQX; Tocris Neuramin). Following preincubation, a cut was made parallel to the granule cell layer at the level of the outer edge of the inner third of the molecular layer on one of the two sides (blades) of the dentate gyrus. The cut part of the dendritic layer was removed. Both cut and uncut (control) slices were then transferred to a storage chamber where they were kept in ACSF at 32°C for at least 90 min before recording.

6.2.2 Electrophysiology

Electrodes and solutions. Patch electrodes were pulled from borosilicate (KG-33) glass capillary tubing (1.5 mm o.d.; Garner Glass) using a Narishige PP-83 two-stage electrode puller. The intracellular solution was made up in high- performance liquid chromatography (HPLC) grade water (Omnisolve, EM Science, Gibbstown, NJ) and was composed of (in mM): 135 CsCl, 2 $MgCl_2$, and 10 N-2- hydroxyethylpiperazine-N-2-ethanesulfonic acid (HEPES); the solution was buffered with CsOH to pH 7.2, and filtered through a 0.2 μm pore size filter (Nalgene). No exogenous Ca^{++} buffers were used. Final osmolarity for all solutions ranged between 260-280 mOsm. All salts were obtained from Fluka.

Recordings. Whole-cell recordings were obtained "blind" [24, 246] with an Axopatch-200A amplifier (Axon Instruments), digitized at 88 kHz (Neurocorder, NeuroData) before being stored on videotape. The ACSF contained (in μM) 25 APV, 10 CNQX (to record miniature IPSCs, 1 tetrodotoxin (TTX, Calbiochem) was also added). Access resistances were <15 $M\Omega$. Minimal stimulation was carried out as described previously [67, 128]. Briefly, patch pipettes filled with the extracellular medium were used to find and stimulate single fibers. The stimulating electrode was positioned at various distances from the granule cell layer (see Figure 6-49), and at least 300 μm away from the recorded cell. Low intensity stimuli elicited no response, but upon gradual increase in intensity IPSCs were evoked in an all-or-none fashion. When the stimulus intensity was raised above threshold, the percentage of failures decreased but in most cases did not alter the kinetics of the responses. Such narrow stimulus

thresholds indicated that the minimally evoked IPSCs probably resulted from the activation of single inhibitory fibers [67, 128]. Statistical analyses (t-test or F-test) were performed using SPSS for Windows^{TM} with a level of significance of $p < 0.05$. Data are presented as mean ± SEM (n = number of cells).

Analysis. Off-line, the recordings were filtered DC to 1-3 kHz (8-pole Bessel) before digitization at 20 kHz by computer (Data Translation DT 2821 A/D board in an Intel 486/66 MHz based computer). The digitization and analysis were done using the Strathclyde Electrophysiology software (courtesy of J. Dempster). Detection of individual miniature IPSCs was done using a software trigger previously described [187], 1992b) and supplied by Dr Dempster as part of the Strathclyde Electrophysiology software package. This detector is basically an amplitude-threshold based detector. A least squares Simplex based algorithm was used to fit the ensemble average with the sum of two (one rising and one decaying) exponentials:

$$I(t) = Ae^{-t/\tau_D} - Ae^{-t/\tau_R} \tag{6.1}$$

where I(t) is the mIPSC as a function of time (t), A is a constant, $\tau_R$and $\tau_D$are the rise and decay time constants respectively.

6.2.3 Simulations

Compartmental simulations were performed using a reconstructed dentate gyrus granule cell filled with biocytin in vivo during the course of another study [237], from an animal of similar age and size to those used here. The cell was reconstructed in 3D using a Eutectics NTS reconstruction system from 80 μm sections (100x objective, 1.3 n.a.), 10% shrinkage was assumed in the simulations presented here. Total dendritic extent in the Z dimension was under 400 μm, so it was assumed that the complete cell would have been present in a coronal slice and no additional cropping of the cell was performed. Simulations were performed using NEURON (courtesy M. Hines). The reconstructed cell was divided into compartments of less than 20 μm in length, and the presence of spines was corrected for by altering the values of R_m and C_m [89]. Spine densities and areas were taken from Desmond and Levy [59], and were consistent with spine counts taken directly from the cell used here. We used several sets of passive cellular parameters, chosen to be consistent with recent computational studies and the range of input resistances measured here. These included: R_m 40,000 Ωcm^2, R_i 100 Ωcm, C_m 1 $\mu F/cm^2$ [243]; R_m 50,000 Ωcm^2, R_i 200 Ωcm, C_m 1 $\mu F/cm^2$ [242]; R_m 50,000 Ωcm^2, R_i 300 Ωcm, C_m 0.7 $\mu F/cm^2$ [150]. Synaptic inputs were simulated as a difference of two exponentials, according to equation 6.1. Kinetics for all synapses were taken from the fit to the average of the largest, fastest

miniature IPSCs (those most likely to be purely somatic): τ_R= 0.146 ms, τ_D= 4.583 ms. The synaptic reversal potential was assumed to be 0 mV to compare with the Cl^--loaded cells studied here. The simulated cell was voltage clamped at -60 mV, in some simulations (including all those shown here) an explicit series resistance of 7 $M\Omega$ (the average of the experimental values) was included. Electrode capacitance was not explicitly modeled. There is additional potential source of error due to the fact that the Cl^--loaded granule cell dendrites may not rest at -60 mV, and therefore there may be a slight decrease in steady-state voltage and hence synaptic driving force with distance from the electrode. This was estimated to cause less than a 10% reduction in driving force, so was neglected. The X,Y,Z coordinates of each dendritic point were preserved in the simulation. These were used to calculate the distance of each simulated dendritic site from the midpoint of the cell body layer, taken as the centroid of the soma (the soma of this cell was in the middle of the cell body layer of the upper blade of the dentate gyrus).

6.3 Results

6.3.1 Miniature IPSCs are variable in amplitude and kinetics

One of the characteristic features of the amplitude and rise time distributions of spontaneously occurring IPSCs in all central neurons, recorded in the presence of glutamate receptor antagonists APV and CNQX, is that they are skewed towards larger amplitudes and rise-times (Figs 6-48A,6-50A) [238]. Such skewed amplitude and rise time distributions are found even when all action potential-dependent spontaneous IPSCs are blocked by the sodium channel blocker TTX [67, 188, 47, 187, 54]. In granule cells of the dentate gyrus, for example, the 10-90% rise-times of TTX-resistant miniature IPSCs range from 0.1 to 10 ms (Fig 6-48). Since all of these mIPSCs are blocked by the $GABA_A$ receptor antagonist bicuculline (25 μM, n=3), they all result from the activation of $GABA_A$ receptors. The skewed amplitude and rise-time distributions may be due to electrotonic filtering of the synaptic currents from different positions along the dendritic tree, or from the possible presence of un-

equal numbers of $GABA_A$ receptors with various subunit compositions and kinetic properties at different synapses on the same cell, or both [54] (also see Sections 4.3.5, 4.3.5, and 4.3.8).

As shown above, synaptic currents with identical kinetics at their site of origin would be attenuated in their amplitudes and slowed in their rise-times by varying degrees depending on how far the synapses are located from the site of recording, generally the soma [203, 242]. Most studies, however, have concluded that electrotonic filtering does not significantly affect the distribution of spontaneous PSCs because they do not show a negative correlation between rise time and amplitude [244, 144, 274]; this is also true for mIPSCs in granule cells (Fig. 6-48D). However, as shown in Section 4.3.2, these two parameters change with distance at drastically different rates [242, 232], so there should not be a simple linear relationship between them; therefore the lack of a negative correlation cannot be taken as evidence for the absence of cable filtering ([232, 233], also see Section 4.3.2). Additionally, any variability in underlying synaptic current amplitude or kinetics will mask the true relationship between these two parameters. If cable filtering does shape mIPSCs, then slower events should have a tendency to be smaller. This holds true for the mIPSCs recorded in dentate gyrus granule cells. While fast events cover the whole range of amplitudes, slow events are restricted to being very small; similarly the largest events tend to have very rapid rise times (Fig. 6-48D). We have examined this in more detail by dividing the population of mIPSCs into non-overlapping subpopulations with increasingly slower rise times (Fig. 6-48B,C). We divided mIPSCs into five subpopulations by fitting four Gaussians onto the distribution of 10-90% rise times, whereas the fifth population (which contained too few events to be reliably fitted) was lumped together from events with 3-10 ms rise times (see Figure Legend for details). Averages (Fig. 6-48B) and cumulative amplitude distributions (Fig 6-48C) for these subpopulations show that when populations of IPSCs were studied, slower events tended to be smaller and faster ones larger, consistent with a role for cable filtering in shaping these events.

If cable filtering is responsible at least in part for the varied kinetics of mIP-

SCs, some mIPSCs must be generated at a distance from the somatic recording site. However, because neither the underlying synaptic kinetics nor the degree by which individual miniature events are distorted by electrotonic filtering are not known, the exact site of generation of each event cannot be predicted. Consequently, from these data alone it is not possible to estimate the proportion of mIPSCs generated proximal vs distal sites. Thus we need to obtain direct evidence for the degree of electrotonic filtering occurring at various points along the dendritic tree.

6.3.2 Effects of cable filtering on proximal and distal inhibitory synaptic inputs

We obtained evidence of the amount of cable filtering occurring at different points along the granule cell dendritic tree by comparing the IPSCs generated by minimal stimulation of single GABAergic fibers in the outer vs inner molecular layers [128]. First, minimal stimulation was applied in the outer molecular layer (Fig. 6-49A). In order to minimize the possibility of fibers crossing laminar boundaries, a cut was made at mid-level parallel to the cell body layer, and the cut ended as close as possible to the recorded cell (Fig. 6-49A), stimulation was carried out in ACSF containing APV and CNQX (without TTX). As it is shown in Fig. 6-49B and C, IPSCs could be easily evoked from the level of the distal dendrites, demonstrating the presence of functionally intact distal inhibitory terminals and synapses. Next, we compared the IPSCs obtained by minimal stimulation of single GABAergic fibers in the outer molecular layer to those from the inner molecular layer as well as to the fastest of the spontaneously occurring events (10-90% rise times <0.34 ms) recorded from the same cells. Presumably, such fast events have been the least affected by cable filtering, so are the most likely to originate from somatic (i.e. the most proximal) sites. Furthermore, their kinetics are identical to those IPSCs which are evoked by minimal stimulation directly in the cell body layer [67, 128, 178]. As is shown in Fig. 6-49B, it was clear that the further away the IPSCs were generated, the

smaller and slower they became. Thus, the smallest (peak amplitude: -13.0±1.7 pA) and slowest (10-90% rise-time: 5.0±0.7 ms; range: 3.6-6.5 ms; n=6) events were observed when single fibers were stimulated in the outer molecular layer (Fig. 6-49C). These results show that functional GABAergic terminals and synapses are present on distal dendrites of granule cells. More importantly, they also demonstrate that the amplitude and kinetics of IPSCs originating distally but recorded at the soma are different from those of proximal IPSCs. These differences in IPSC amplitude and kinetics are consistent with the idea that cable filtering plays an important role in shaping the synaptic responses measured at the soma.

6.3.3 Removal of distal dendrites does not change the amplitude or kinetics of mIPSCs

Both the skewed distribution of mIPSC amplitudes and rise times, and the progressively smaller and slower responses seen at the soma to stimulation of increasingly distal inputs, suggest that cable filtering could play a large role in the determination of mIPSC shape. Logically, it would seem likely therefore that distal as well as proximal synapses contribute extensively to the generation of mIPSCs.

One direct way to test whether inhibitory terminals situated distally generate spontaneous mIPSCs is to study the effects of the removal of these inputs on the amplitude and rise-time distributions and mIPSC frequency. In order to achieve this, we surgically removed a large part of the dendritic tree. To avoid excitotoxic damage, dendrotomy was carried out in a neuroprotective medium [239], and mIPSCs were recorded from the dendrotomized granule cells (n=6).

Granule cells are ideally suited for such a manipulation, since they are tightly packed in a cell layer and in the rat they are devoid of basal dendrites. A cut is made at the outer edge of the inner molecular layer removes more than half of the total dendritic tree. Since the cut is made parallel to the granule cell layer and involves half of the dentate gyrus (the other half normally serves as control), there

is no possibility for any granule cell on the dendrotomized side to escape amputation of its dendrites. Removal of the bulk (>50%) of the dendritic tree with a cut was made at the outer edge of the inner molecular layer (see Fig. 6-50B, right panel) did not alter the amplitude and rise- time distributions of miniature IPSCs (Fig. 6-50) (Kolmogorov-Smirnov test based on cumulative distributions, $p>0.05$), nor did it change significantly the mean amplitude, rise-time (Fig. 6-50), or frequency (inter-event intervals: Control:273±64 ms, n=6; Dendrotomized: 325±49, n=6) of events.

Interestingly, the removal of the dendrites also did not change the percentage of slow (>3-3.5 to 6 ms) events (Control, 3.5%, n=3; Dendrotomized: 4%, n=3; Fig. 6-50, horizontal bar in the middle panels). Although we do not know for sure that these slow events in the cut cells are the same as the slow events in the control cells, it seems likely that even these slow events which could have conceivably originated from distal synapses may be generated at more proximal sites, albeit at very low frequency. This suggests the existence of proximal synapses with very different $GABA_A$ receptor subunit composition, and the low probability of occurrence of these slow events may be explained by either a relatively low frequency of GABA release from these terminals or by the small number of these synapses.

This result suggests strongly that the mIPSCs we record under control conditions originate preferentially from proximal sites. However, it does not necessarily imply that dendritic terminals do not generate miniature IPSCs. We know from the results obtained with minimal stimulation that, in our preparation, distal inhibitory terminals are functional and can release GABA. Distal mIPSCs may occur at relatively high frequencies, but attenuation by electrotonic filtering may render them undetectable at the soma. This result also does not necessarily imply that the variability seen in mIPSC peak amplitudes is not generated in part by cable filtering. It is possible that the filtering occurring even over the short (150 μm) length of remaining dendrite is sufficient to strongly attenuate mIPSCs.

6.3.4 Assessment of the ability of the event detector to detect distal IPSCs

An important consideration in estimating the number of very slow, small, presumably distal events is our ability to detect them (see Section 5.3.7). Perhaps there are a large population of these slow events, but our detection method only allows us to pick out the largest ones. This may explain why the slower events represent a progressively smaller percentage of the total population of mIPSCs (hence the skewed appearance of the rise-time distribution) (Fig. 6-48).

In order to determine the sensitivity of our method for detecting miniature IPSCs, we tested its ability to detect simulated events embedded in noise. We generated events of varying amplitude in different kinetic classes according to equation 6.1: proximal (τ_R=0.146 ms, τ_D=4.385 ms; obtained by fitting the average of the 25% fastest miniature IPSCs with the sum of a single exponential rise and single exponential decay) and "distal" (τ_R=6.242 ms, τ_D=6.422 ms; obtained by fitting the IPSCs evoked by minimal stimulation of the outer molecular layer, see Fig. 6-49C) (Fig. 6-51A). Simulated miniature IPSCs were embedded in Gaussian noise of σ = 1.6 pA, corresponding to the high end of the experimental range, and filtered at 3 kHz. These simulated data files were then run through the detector and the percentage of each event category that was successfully detected was measured. We successfully detected > 90% of the events of the proximal and distal classes with amplitudes of at least 6.5 pA (Fig. 6-51B). This indicates that we should detect almost all of those distal events with amplitudes over 6.5 pA and kinetics similar to or faster than our "slow" minimally evoked events. In fact, even in the extreme case of "ultra-slow" simulated events (τ_R=11.0 ms, τ_D= 14.0 ms, "ultra-slow"), we were still able to detect >90% of those events with amplitudes > 9.5pA. Such slow IPSCs were never observed experimentally (these kinetics were taken from the most distally-generated simulated IPSCs generated in a granule cell model (see Section 6.3.5).

6.3.5 Computational modeling of the influence of synaptic location on IPSC amplitude and kinetics in granule cells

Two important questions arise: First, what fraction of the distally-generated miniature IPSCs should we observe with our measured detection threshold of 6.5 pA? Based on the amplitudes of the minimally evoked IPSCs, we would expect that events originating 250 μm from the granule cell layer (i.e. the middle of the outer molecular layer, the region where we placed our stimulating electrodes to evoke distal minimal IPSCs) would be easily detectable. However, we do not know the number of terminals originating from an individual interneuron that synapse onto the dendrites of a single granule cell. Therefore, it is possible that the IPSCs evoked by minimal stimulation from distal sites are larger than distal mIPSCs because the evoked IPSCs may be elicited by several terminals belonging to the same axon. The second question is: are cable filtering and synaptic location sufficient to explain the amplitudes and kinetics of the distally-generated IPSCs? It could be that the underlying synaptic kinetics of distal synapses (which arise from a different population of inhibitory interneurons than the proximal ones do) are slower than those seen at the soma, or that the minimally evoked IPSCs are made up of multiple small quanta released asynchronously, thus extending the time course of the resulting synaptic current.

To answer these questions we have turned to compartmental modeling of a typical granule cell (Fig. 6-52A,B; see Experimental procedures for details). We estimated the underlying kinetics of the GABAergic synaptic current by selecting the 25% fastest of the miniature IPSCs (those most likely to be somatic) and fitting them with equation 6.1. We then placed a synapse with these kinetics onto each compartment of the granule cell model, and measured the amplitude and kinetics of the somatic response to that current. The distribution of response parameters with increasing distance from the granule cell layer is shown in Figure 6-52C and D. Peak amplitude decreases very rapidly as the synapse is moved away from the soma, and then plateaus after 50-

100 μm, showing only slight further decline. The 10-90% rise-time increases basically linearly with increasing distance from the soma.

Simulated 10-90% rise-times cover a very similar range to those seen in mIPSCs and minimally evoked IPSCs. This implies that cable filtering alone is sufficient to account for the slow kinetics and small amplitudes of the minimally evoked IPSCs from the outer molecular layer. Furthermore, the slow, small mIPSCs could be generated by synaptic events with the same kinetics of the putative somatic miniature IPSCs being placed onto a distal site (also see Fig. 6-53A). Figure 6-52C also shows that even in the most proximal region of the dendritic tree (the first 100 μm, which remains intact in the cut granule cells of Figure 6-50), there is still a significant effect of cable filtering on both mIPSC amplitude and rise time.

In order to test the integrity of our granule cell model, we placed a synaptic input with kinetics of the fastest, most probably somatic IPSCs, in the middle of the outer molecular layer (i.e. 250 μm away, indicated by the dashed line in Fig. 6-52A; the position of the synapse is indicated by an arrow), in the region where we evoked minimal IPSCs. As it is shown in Fig. 6-53A, the modeled response of this IPSC as seen at the somatic recording site perfectly matched the kinetics of the IPSC obtained by minimal stimulation. The conductance of the simulated distal input was 0.745 nS, which is not considerably different from the mean conductance of the putative somatic mIPSCs (0.83 nS, assuming a synaptic reversal potential of 0mV, Figure 6-52B), or the fastest, putatively somatic, spontaneous IPSCs recorded in the cell used for minimal stimulation in Fig. 6-49B (1.18 nS, events recorded in the absence of TTX). This result shows that our granule cell model describes well the cable properties of these neurons, and it also indicates that the at-source kinetics of distal IPSCs are similar to those of the presumed somatic mIPSCs.

6.3.6 Percent of miniature IPSCs from distal sites which should be detectable

For each synaptic site, we have estimated the miniature IPSC conductance at this site necessary to generate a 6.5 pA miniature IPSC at the soma (the "threshold miniature IPSC" for this site). We then calculated what the amplitude of this miniature IPSC would have been if it had been placed directly onto the soma (the "threshold somatic amplitude"). We assumed that the distal synapses show the same distribution of mIPSC peak conductances as the somatic miniature IPSCs. Next, we estimated how many of those events we should be able to see by looking at where the "threshold somatic amplitude" for each site fell on the distribution of somatic miniature IPSC peak amplitudes (generated by selecting the fastest-rising 25% of the miniature IPSCs; their cumulative amplitude distribution is shown in Fig. 6-53B). To take into account the variance between different dendrites, we averaged these threshold mIPSC amplitudes from sites in 20 μm bins from the soma (see Figure 6-54). Given the parameters used in Figs. 6-52 and 6-53A, the threshold somatic amplitude for those points from 240-260 μm from the soma (the region stimulated to obtain minimally evoked IPSCs) would be 38 pA (see also Fig. 6-53C). Sixty percent of the putative somatic miniature IPSCs are larger than 38 pA (Fig. 6B). If these distal synaptic sites draw their miniature IPSC amplitudes from a similar distribution as the somatic events do (which is suggested by the good match between simulated distal and slow IPSC in Fig. 6-53A), then we must be detecting 60% of the events generated 250 μm from the soma, as shown by the hatched region in Figure 6-53B. Naturally, we would detect a larger fraction of those events generated more proximally than 250 μm from the soma.

We have also explored the effects of changing the passive parameters of the model (see Methods for details). Figure 6-54A (expanded in B) shows the threshold event amplitude (amplitude of the somatic event which if placed into the dendrites at a particular location would generate a somatic event of 6.5pA) as a function of synaptic

distance from the granule cell layer for several sets of passive parameters. Increasing R_m several-fold slightly increases the percentage of distal events we should record, while at the same time slowing their kinetics even further [150, 242]; this would indicate that the bulk of events we see are generated even more proximally than postulated here. Increasing R_i to 200 or 300 Ωcm as has been suggested by recent studies [150, 154], does significantly increase the attenuation of distal events, and hence lower the fraction of those events we can detect. However, increasing R_i also slows event kinetics, meaning that events closer to the soma (whose amplitudes are less attenuated) will generate events with 3-6 msec rise times (data not shown). These two effects together indicate that we should still see a much larger number of events with long rise times than we do, if they were being generated at dendritic sites at the same rate as they are somatically. Using average input resistance (average input resistance for these cells is 256.36±18.42 $M\Omega$), as a guide to the most likely range of passive parameters for these cells, we can see from Figure 6-55 that it is likely that the range of parameters used here is plausible, and especially given that Cs^+ was used in the recordings here to increase R_m, to match the experimentally-recorded R_{in} in this relatively large cell, it is likely that R_i is not extremely high.

6.3.7 Source of amplitude variability in dendrotomized neurons.

We have shown that IPSCs in dentate gyrus granule cells are subject to cable filtering. As shown in Section 4.3.3, such filtering is sufficient to generate PSC variability and skewed amplitude histograms. However, we have also shown indirectly through computational modeling and directly by removal of the distal dendrites that mIPSCs in these cells are generated only by proximal synapses. What, therefore, explains the variability in mIPSC amplitude in granule cells, and in particular in the dendrotomized granule cells?

Cable cable filtering can cause large changes in PSCs generated very close to the

soma, within the region of dendrite that remains in the dendrotomized granule cells (see sections 6.3.5 and 4.3.3). However, this may not be enough. In particular, the presence of events with very long rise times (> 3ms) in dendrotomized granule cells (see Figure 6-50B) suggests that there must be some variability in the kinetics of mIPSCs (see section 4.3.5. It is therefore important to assess how much of the cable filtering in these cells takes place in this proximal dendritic range, and whether this is changed by the act of amputating the dendrites itself.

Dendrotomy is not an entirely benign procedure. It is a model for neuronal injury, and therefore there may be injury-mediated changes in cellular properties in addition to those simply due to the change in cell structure. If dendrotomy is not carried out under the neuroprotective conditions used here, cells either die, or undergo changes in the kinetics of their mIPSCs [239]. Even under conditions where cells appeared to survive dendrotomy relatively unscathed, it is possible that subtle changes in cellular or synaptic properties went unnoticed, or that the population of terminals giving rise to mIPSCs were affected by injury to the interneurons giving rise to them.

We have therefore used simulations to assess the effect of dendrotomy on granule cell properties, and to estimate how much of the remaining synaptic variability could be accounted for by cable filtering. The most obvious cellular property that would be expected to change with removal of more than half of the dendritic tree is the input resistance, R_{in} . The average input resistance of control granule cells is 256.36±18.42 $M\Omega$, while that of dendrotomized granule cells is 363.15±42.73 $M\Omega$, for a ratio of uncut to cut input resistances of 0.71. However, if one simply removes the dendrites of the modeled granule cell (Figure 6-52A) beyond 150 μm from the cell body layer, the input resistance of the modeled neuron goes up more than in the experimental case; the ratio of uncut to cut input resistances is close to 0.5, consistent with removal of half of the dendritic tree (in extensive cells such as these, the contribution of the soma to the total cell input conductance is minimal [205]). The exact ratio between simulated cut and uncut input resistances depends on the passive parameters of the model. If R_m is increased, (with R_i held constant), the effects of the presence (and

absence) of the dendrites is "seen" more clearly. and cutting the dendrites results in a larger increase in R_{in} than with lower R_m. If R_i is increased (with R_m held constant), it shields the soma from things happening in the dendrites. Therefore cutting the dendrites results in a smaller increase in R_{in} than with a smaller value of R_i. However, with any plausible combination of R_m and R_i (i.e. a combination giving an initial input resistance within the experimental range); cutting the dendrites *still* yielded a larger increase in R_{in} than was seen experimentally.

There are four obvious methods by which the input resistance of the dendrotomized cells could be lowered to be consistent with the experimental data. First, cutting the dendrites could induce an overall lowering of cellular membrane resistivity, R_m, due to calcium influx or other consequences of neuronal injury. Second, the cytoplasmic resistivity, R_i, could change, particularly in the region close to the cut. Third, recordings in the cut cells could be more likely to include a somatic shunt, possibly due to reduced membrane integrity in the injured neurons. And finally, the severed dendritic tips may not seal properly, inducing a leak conductance out the end of the dendrites [205]. The first and third possibilities have been discussed in detail in Sections A.5 and . A shunt conductance does not alter the kinetics or amplitude of PSCs recorded at the soma in voltage clamp, and so would be consistent with the data presented here (see sectionA.1.2); as is changing R_m all over the cell, which has little effect on PSC amplitude distributions (section A.5). Changing R_i does not have as significant an effect on R_{in} as does a change in R_m (see Figure 6-55), and is unlikely to account for the difference in input resistance measured here. Intuitively, the most biologically plausible account of the difference between predicted and measured input resistances is the last one; that the dendrites simply failed to seal after dendrotomy.

Figure 6-56A shows the effect of leaky dendritic tips on cell input resistance. The last segment of those dendritic tips which were severed at 150 μm from the soma to generate a "cut" cell model were given a local R_m which was some small fraction of the R_m for the rest of the cell. Cell input resistance is plotted here against the ratio of leaky to normal R_m, for a variety of passive parameters. As leakiness is increased

(indicated by a decreasing value of the leakiness ratio), R_{in} decreases.The horizontal lines indicate. for each set of parameters, the R_{in} of the uncut cell model (left line) and the expected cut cell R_{in} assuming a ratio between the two of 0.71 (right line). Each of the lines for the predicted cut cell R_{in} intersects with its respective plot of input resistance vs leakiness at a leakiness ratio of 0.075. This indicates that regardless of the passive parameters (across the range shown here), the cut dendritic tips must have a membrane that is 13 times more leaky than that of the rest of the cell to account for the measured difference in input resistances, if this is the source of the discrepancy with the experimentally measured R_{in} ratio.

How much variability can be caused by cable filtering in dendrotomized granule cells? In Figure 6-56B, mIPSC shape parameters are plotted as a function of dendritic distance from the soma (distance along the extended dendrites, *not* distance from the granule cell layer, allowing greater visibility of closely-spaced points) for the uncut cell, and the cut cell simulation with and without leaky dendrites. It can be seen that cutting off the dendrites, and inducing a termination close to the soma (see section A.1.1) reduces the attenuation of mIPSC amplitudes, areas and slopes, and prevents the usual increase in half width with distance. This would be expected in and of itself to increase mean mIPSC amplitude, even without the loss of any distally-generated, small events. Surprisingly, amputation of the dendrites increases mIPSC rise times over the remaining dendritic range, though rise times plateau after 100 μm and do not continue to increase with distance. None of the measured parameters except area are significantly affected by the presence of even the strong dendritic leak used here.

Depending on parameters, rise times in simulated cut cells can still be as long as 3 msec. This means that cable filtering should still contribute strongly to rise time and amplitude variability in dendrotomized neurons, but that we have been unable to use it to explain the continued presence of extremely slow events in cut cells. One possible explanation of this is simply that there is some other change in the passive properties

of the cut cells not taken into account in these simulations which would allow them to generate extremely slow events. Another possibility, however, and an attractive one given the striking similarity between the pooled amplitude and rise time distributions in cut and uncut cells, is that most of the mIPSCs are generated even more proximally than suggested above, in a region where they would be completely unaffected by the amputation of the dendrites.

6.4 Discussion

Taken together, these results indicate that distal miniature IPSCs should have rise-times comparable to those of the minimally evoked IPSCs from the outer molecular layer (3.5-6 ms) (because they would be subjected to the same amount of dendritic filtering). Since, as described above, our detector can detect 60% of the miniature IPSCs originating distally, there should be a large percentage of the total number of miniature IPSCs with 10-90% rise-times slower than 3 ms. However, there were very few (3%) miniature IPSCs with rise times in this range (Fig. 6-48A and 6-50A). This observation is consistent with the proximal origin of mIPSCs, as suggested by the experiments on removal of dendrites.

Seventy-five percent of all GABAergic synapses in the dentate gyrus are located in the dendritic layer of granule cells [78]. These terminals originate from distinct interneuron types each of which innervate particular parts of the dendritic tree [80, 26, 27]. The anatomical segregation of the inhibitory inputs to granule cells suggests heterogeneity in the functional roles of proximal vs distal inhibitory inputs, and possibly differences between the proximal and distal inhibitory terminals themselves. In addition to the anatomical differences between somatic and dendritic inhibitory terminals, notably in bouton size and content [172], there are also pharmacological differences between them. For example, in CA3, somatic and dendritic terminals show different degrees of presynaptic regulation of GABA release by $GABA_B$ receptors [128].

One powerful technique for exploring synaptic function across the population of inputs to a cell is the study of spontaneously-generated synaptic events. However, electrophysiological recordings of spontaneous IPSCs do not reveal the location of GABAergic synapses from which the individual events originate, making it difficult to study the functional impact of synapse location. Investigations aimed at revealing the site of origin of spontaneous IPSCs are also hampered by the lack of detailed knowledge of the extent to which synaptic currents are altered by electrotonic filtering in granule cells. In addition, the 11 different $GABA_A$ receptor subunits known to be expressed by granule cells [225, 215, 91, 295, 272, 75, 186] may be distributed differentially on the cell surface, forming receptor-channel pentamers with distinct kinetic properties, which would further complicate any study of the site of origin of miniature IPSCs. For example, in CA1 pyramids Pearce [190] showed the existence of distinct fast somatic and slower dendritic $GABA_A$ IPSCs and suggested that $GABA_A$ receptors with different kinetic properties may be activated by these two classes of inhibitory inputs, as cable filtering could not completely account for the slow decay kinetics of the dendritic IPSCs. On the other hand, as it has been shown to be the case for excitatory currents in pyramidal cells, electrotonic filtering can drastically influence synaptic signals [289, 104, 184].

We have demonstrated that cable filtering can play a role in shaping the kinetics and amplitudes of the different miniature IPSCs observable in a single neuron. Traditionally, the impact of cable filtering is assessed by measuring the degree of correlation between the rise-times and amplitudes of individual mIPSCs. Using this procedure no negative correlation can be found between mIPSC rise-times and amplitudes; this is also the case for excitatory spontaneous events in a variety of cell types (e.g. Figure 4-19, also see [244, 247, 163, 164, 274, 104]). However, populations of miniature events with distinct and progressively slower rise-times do show progressively smaller amplitudes (Fig. 6-48), and this is true irrespective of the precise algorithm used to sort miniature IPSCs into subpopulations. An alternative explanation of this result is that the GABAergic synapses on granule cells vary widely in their kinetics, and addi-

tionally those with slow kinetics are somehow restricted to having a smaller number of receptor-channels, and hence a lower total conductance. However, this is unlikely, as a similar relationship between amplitude and rise time (which can be simply derived from the appearance of the rise time *vs* amplitude plot (Fig. 6-48D), without the more complicated analysis shown here) can be seen across a wide variety of cell and synapse types ([244, 247, 163, 164, 274, 144, 104], also see Figures 4-19 and 4-31. This result, then, suggests that miniature IPSC kinetics and amplitudes are altered by cable filtering. Thus, in all likelihood some mIPSCs are generated at a distance from the soma.

On the other hand, these results do not provide information as to exactly how far from the soma the most distal mIPSCs are generated. We tested this by removing the bulk of the dendritic tree. When the amputation of dendrites is carried out in neuroprotective media [239], the neurons survive and the kinetics of the miniature IPSCs are not affected. There is no change in the distribution of mIPSC amplitudes or rise times, and the mean frequency of mIPSCs is identical to control. Thus, mIPSCs recordable at the soma must all be generated more proximally than the outer edge of the inner molecular layer. Simulations of these cut cells (Figure 6-56) suggest that many of these events are generated even more proximally than that, however this conclusion is speculative as it relies on many assumptions about the changes granule cells undergo as a result of dendrotomy.

Experiments with minimal stimulation in the proximal and distal dendritic layers provided direct evidence for a strong degree of cable filtering of GABAergic IPSCs. In addition, these experiments dismissed the possibility that the lack of distally-generated mIPSCs was a result of the inability of inhibitory synapses situated on distal dendrites to release GABA onto functional receptors. As has been described before, the narrow stimulus intensity threshold, the fixed latency and the kinetics of the minimally evoked IPSCs are all consistent with the activation of single fibers [67, 128]. As the site of minimal stimulation was moved farther out along the dendritic axis of the cell, the amplitude and rise-time of the resulting evoked IPSCs changed in

a manner consistent with the effect of electrotonic filtering. Importantly, simulations showed that the kinetics of the distally-evoked IPSCs at source were likely to be very similar to the kinetics of the somatic spontaneous IPSCs (Fig. 6-52C,D, 6-53A). According to this finding there are no major systematic differences between the kinetic properties of $GABA_A$ receptors in the outer molecular layer vs those located on the soma, although subtle differences may occur. In addition, the near-perfect match shown in Fig. 6-53A between the distally-evoked IPSC and the somatic "recording" of the distally positioned fastest spontaneously occurring IPSCs in the model also provided an independent check on the validity of the parameters used in the compartmental model, since it is extremely unlikely to have come about only by chance.

Since the model proved to be a realistic representation of granule cells, we could use it to estimate the percentage of the distal miniature IPSCs that we should detect if they occured with the same amplitude distribution as the putative somatic miniature IPSCs (see below) (Fig. 6-53B). We could conclude that more than 60% of these spontaneous dendritic events should be detectable in our system. However, the population of events with >3 ms rise-times (i.e. those potentially originating in the outer molecular layer) comprised only a very small fraction of the total population of miniature IPSCs, approximately 3%. In fact, as shown by the experiments involving the amputation of dendrites, even this small population of slow miniature IPSCs were generated at sites closer than the middle molecular layer.

The simulations also showed that even those miniature IPSCs generated close to the soma would have their amplitudes drastically attenuated by cable filtering (Fig. 6-52C), and the rise-times of events generated within the inner molecular layer could be slowed to as long as 3 ms (Fig. 6-52D). Although this paper does not address the question of whether the effects of cable filtering or those of different $GABA_A$ receptors with distinct kinetics are the more important factors underlying the generation of non-uniform mIPSCs in a single cell, it is interesting to note that the considerable effects of cable filtering acting on IPSCs generated within the first 100 μm from the cell body can, in principle, explain a large part of the mIPSC variability in both

control and dendrotomized cells. The presence in both control and dendrotomized neurons of a small percentage of very slow (>3-3.5 to 6 ms) events may suggest the existence of a small number of proximal synapses with distinct $GABA_A$ receptor subunit composition and kinetics, although it should be stressed that we do not know for sure that these slow events in the cut cells are the same as the slow events in the control cells, and we cannot say with certainty that those events could not have been generated through cable filtering in the remaining dendrites via some mechanism which we did not consider in our simulations.

Additionally, the lack of detailed knowledge of the distribution of GABAergic synapses on the dendrites of a single granule cell left us unable to generate simulated amplitude and rise time distributions as was done in previous chapters. In the case of excitatory synapses onto cortical cells, the location and number of dendritic spines serves as a marker of the anatomical synapse distribution. Inhibitory synapses have no such marker discernible with the light microscope, and while ultrastructural studies have examined the relative densities of GABAergic synapses in the somatic and dendritic layers [78], no study has yet undertaken the mammoth task of measuring the density of GABAergic synapses onto particular granule cells at different levels of their dendritic trees. Therefore, we have not tried to explain the source of the shape of the mIPSC distribution, and have limited ourselves to assessing what the relationship is between values of the measured shape parameters and their source locations on the dendritic tree. An interesting finding of this type is the clear mapping between rise time values and locations on the dendritic tree (also see Section 4.3.4). In spite of the small number of very slow events, which would have been expected to be generated in the far distal dendrites, there are a large number of events with rise times between 0.5 and 1.5 ms (Figure 6-48A). Simulations suggest that events with these characteristics would be recorded from synapses in the inner molecular layer (Fig. 6-52D), and these kinetics are consistent with those of responses evoked with minimal stimulation in the IML (Fig. 6-49).

The apparent lack of major differences between the somatic vs distal dendritic

$GABA_A$ receptors allowed us to make assumptions about the possible distributions of distal IPSC amplitudes from the distribution of somatic event amplitudes, as we did when we estimated the percentage of distal miniature IPSCs (Fig. 6-53B). We cannot rule out the possibility that at distal inhibitory terminals the number of $GABA_A$ receptors per synapse may be lower and thus the distal events may be of significantly smaller amplitude at source. However, the immunostaining for $GABA_A$ receptor subunits studied so far appears to be homogeneous in the dendritic layer [225, 215, 91, 295, 272, 75, 186]. In addition, even if the percentage of distal mIPSCs that we could see would be lower than the 60% estimated here because of amplitude differences at source we should still observe many more than the observed 3% of the total number of events with >3 ms rise-times. Therefore, distal terminals cannot substantially contribute to the generation of mIPSCs. We conclude that the frequent and random mIPSCs are predominantly generated at proximal synapses and therefore are likely to have a functional impact on the site of action potential initiation. Even if there was an undetectable population of very small distal mIPSCs, given their "electrotonic invisibility" at the soma these would be expected to have a limited impact on the output of the cell.

At present we can only speculate why only proximal inhibitory terminals are capable of releasing GABA independently of action potentials. It should be emphasized that the dendritic synapses appeared fully functional in our preparation, since minimal stimulation could evoke IPSCs from the outer molecular layer. It seems likely that the anatomical differences between somatic vs dendritic terminals [172] may underlie some functional difference between them. It is interesting to note that local application of sucrose in the granule cell layer results in a many-fold increase in the frequency of miniature IPSCs with a very short latency (1-3 sec), whereas the application of sucrose in the outer molecular layer in the same cell causes only a small and rather delayed (>10 sec) increase (see e.g. Fig 5 in Mody et al., 1994 [178]). Although the precise mechanism of action of high osmolarity sucrose solutions on transmitter release is not well understood, the failure of sucrose to increase GABA

release from distal terminals may also be associated with the smaller size or other anatomical differences between dendritic and somatic GABAergic terminals.

Functional implications for cortical inhibition Our findings reveal that the sustained, action potential-independent GABA release takes place preferentially or perhaps exclusively at sites close to the action potential initiation site in granule cells. A functional division of labor may thus exist between subclasses of inhibitory cells which innervate proximal vs distal regions of principal neurons. Based on our data, the random tonic inhibition is primarily a result of miniature events generated by the neurons with proximal termination zones, probably basket and axo-axonic cells. A perpetual release of GABA onto the somata of granule cells will allow only precisely timed EPSPs to fire the cell. Unimpeded by distal spontaneous inhibitory events, the action potentials may actively back-propagate [252] down the dendrites. A possible functional difference between these two classes of synaptic inputs has been described. Proximal inhibition can block excitatory inputs so that no amount of excitation may bring the cell to firing threshold, whereas distal dendritic inhibition can operate only relatively, in the sense that any amount of it can be overcome by sufficient excitation [284]. This would mean that tonic inhibition located proximally on the cell could maintain a basal restraint on cell firing regardless of whether excitatory synaptic inputs were active at any one time. Tonic inhibition at the dendrite, if it were present, would not have any functional impact in the absence of nearby excitatory activity [123, 120], and would have to be set relative to the amount of excitatory activity present at the moment. The restricted nature of tonic, action potential-independent GABAergic inhibition is likely to play an important role in regulating the input-output relations of central neurons.

6.5 Figure Legends

Figure 6-48: Role of cable filtering in the generation of mIPSC amplitude variability. A. Distribution of the 10-90% rise times of granule cell mIPSCs. Three granule cells were selected on the basis of similar access resistances (8-10 $M\Omega$), and 1100 events from each were pooled to generate this population distribution (total N = 3300). Rise times range from 0.1-10 msec, and the rise time distribution is skewed. The distribution of mIPSCs with rise times <3 msec were fitted with 4 Gaussians as shown (mean and S.D. of each distribution indicated in figure). Those IPSCs with rise times from 3-10 msec could not reliably be fitted with a single or multiple Gaussians, so they were pooled and are represented by a separate bar on the right (population 5). B. Averages of the mIPSC subpopulations defined in A. Events were selected with 10-90% rise times within 1 S.D. around each of the five means shown in A, resulting in 5 non-overlapping subpopulations. This figure shows averages of mIPSCs belonging to each of the five populations. Note that populations of mIPSCs with distinct and progressively slower rise times show progressively smaller amplitudes (see Figure 4-31). C. Cumulative amplitude distributions for the five subpopulations shown in A and B. Note that while fast events (population '1') cover the whole range of amplitudes[3], slow events (population '5') are restricted to being small. D. There is no negative correlation between rise time and amplitude. The plot of rise time vs amplitude shown here is very similar in shape to that seen in cortical neurons (Figure 4-19, note that abscissa and ordinate are exchanged, and that larger amplitudes are represented to the left in the figure shown here).

Figure 6-49: Effects of cable filtering on minimally evoked IPSCs. A. Schematic drawing of the experimental paradigm. A granule cell was recorded at the level of its soma, and a stimulating electrode was positioned in either the inner or the outer third of the molecular (dendritic) layer. A cut made parallel to the granule cell layer halfway up the molecular layer ensured that fibers stimulated distally did not branch into the proximal dendritic tree. Abbreviations: HIL: hilus; GCL: granule cell layer; IML, MML, OML: inner, middle and outer molecular layer, respectively. B. Minimally evoked IPSCs (meIPSCs) from the OML showed slow rise times and small amplitudes (trace 1) when compared to those evoked from the IML (trace 2) or to the fastest spontaneous IPSCs (sIPSCs) (trace 3). These fast sIPSCs (the fastest 25% of sIPSCs, with 10-90% rise times < $0.34msec$) are the least affected by cable filtering, and are likely to originate from somatic (proximal) sites.

[3]Larger events, with progressively more negative peak currents, are shown to the left in this and subsequent figures in contrast to the practice in other chapters.

Figure 6-50: Are there significant numbers of distally-generated events? There is no significant effect of removal of the bulk of the dendritic tree on the properties of mIPSC's. The distal half of the granule cell dendritic tree was amputated in neuroprotective medium (see methods), in order to identify which, if any, mIPSC's arise from this part of the tree (the level at which dendrotomy was carried out is indicated in the schematic drawings at far right). Amplitude (left) and rise time (right) distributions of mIPSCs from 3 control (A) and 3 dendrotomized (B) granule cells (each distribution is from 3300 mIPSCs, 1100 from each cell; the cells were recorded with similar access resistances (8-10 $M\Omega$)). Note that there is no significant change in the distributions, the mean amplitude, or the mean rise time of events as a result of dendrotomy. Note also that slow events with rise times >3 msec (marked by a horizontal bar in the middle panel) could readily be seen in neurons with amputated dendrites with a low frequency similar to that seen in control cells.

Figure 6-51: Are slow distal events escaping detection? A. Examples of simulated mIPSCs of varying amplitudes (-0.5 to -19.5 pA) and kinetics (fast ("proximal"), slow ("distal"), and very slow ("ultra-slow"), see text and methods for details) used to test the sensitivity of the detector. Simulated mIPSCs are embedded in Gaussian noise of σ = 1.6 pA, and filtered at 3 kHz. B. Percentage of events successfully detected in each kinetic class as a function of peak event amplitude. More than 90% of the fast and slow events over 6.5 pA are detected. Even with the very slow events, we can detect more than 90% of those events with amplitudes over 9.5 pA.

Figure 6-52: Effects of cable filtering on mIPSC shape. A. Camera lucida image of the reconstructed granule cell used in the simulations, and B its corresponding dendrogram. C,D. Plot of simulated IPSC amplitudes (C) and 10-90% rise times (D) as a function of synaptic distance from the granule cell layer (R_m=40,000 $\Omega cm2$, R_i=100 Ωcm, R_s=7 $M\Omega$, g_{syn}=0.75 nS, synaptic parameters from fit to 25% fastest, "proximal" mIPSCs: τ_R=0.146 msec, τ_D=4.583 msec). The measured amplitude decays rapidly over the first 50-100 μm, and then plateaus at approximately 10 pA. Rise times show a linear relationship with distance, and cover the same range as both the recorded minimally evoked IPSCs and the slowest mIPSCs.

Figure 6-53: What proportion of distal mIPSCs should we be able to detect? A. Simulated mIPSCs show similar kinetics to the evoked meIPSCs, using synaptic input kinetics measured at the soma. Traced labeled "Simulated IPSC at source in OML" is a simulated somatic mIPSC measured at the soma for an input synaptic current with the same kinetics as the average of the fastest, most probably somatic mIPSCs (parameters same as in Figure 6-52). In trace B, the same input is

placed onto a dendrite 250 μm from the granule cell layer (indicated by the dashed line in figure 6-52A; the position of the synapse is indicated by an arrow), in the middle of the outer molecular layer, in the region from which we evoked minimal IPSCs), and the response measured at the soma. The overlying trace is the fit to an actual minimally evoked IPSC stimulated at a site 250 μm from the granule cell layer, indicating both the plausibility of the model and, more importantly, that cable filtering alone is sufficient to generate a very good match to the slow kinetics of both the distal minimally evoked IPSCs and the slowest mIPSCs (also see Figure 6-52), without requiring different distal synaptic kinetics or temporal dispersion of bouton release. B. Assuming that distal mIPSCs have the same underlying distribution of amplitudes at source as the "somatic" mIPSCs (the fastest events, population '1' in Figure 6-48A), we estimated from the model that we should be able to detect 60% of distally-generated mIPSCs (see text for details). The plot shows the cumulative probability distribution of amplitudes of putative "somatic" mIPSCs. The shaded region on the cumulative probability plot shows the proportion of events which would remain undetectable if generated in the distal dendrites.

Figure 6-54: Could cable filtering contribute to amplitude variability? A. Amplitude of threshold event if it were placed onto the soma, for several sets of passive parameters (expanded in B). Figure 6-54A (expanded in B) shows the threshold event amplitude (amplitude of the somatic event which if placed into the dendrites at a particular location would generate a somatic event of 6.5pA) as a function of synaptic distance from the granule cell layer for several sets of passive parameters. The key indicates the passive parameters used for each set of simulations. The first number is R_m in $k\Omega cm^2$(i.e. 40k = 40,000 Ωcm^2), the second is R_i (Ωcm), and the third, where present, is C_m ($\mu F/cm^2$, where not indicated C_m= 1.0 $\mu F/cm^2$), in all cases R_s=7 $M\Omega$ and synaptic kinetics as in Figure 6-53. Increasing R_m several-fold slightly increases the percentage of distal events we should record, while at the same time slowing their kinetics even further [150, 242]; this would indicate that the bulk of events we see are generated even more proximally than postulated here. Increasing R_i to 200 or 300 Ωcm as has been suggested by recent studies [150, 154], however, does significantly increase the attenuation of distal events, and hence lower the fraction of those events we can detect.

Figure 6-55: Effects of passive parameters on simulated input resistance. A. R_{in} as a function of R_m for several values of R_i. Over the physiologically plausible ranges shown here, R_{in} is much more dependent on R_m than R_i. B. R_{in} as a function of R_i for several values of R_m. In each case, points with increasing R_{in} for the same R_i value represent increasing values of R_m. Data same as A. C. R_{in} as a function of R_m for different methods of correcting for cell shrinkage during fixation

and histochemical processing. Unscaled refers to the original direct reconstruction. Z-dimension corrected refers to the scaling in the Z dimension applied to correct for the additional shrinkage seen in that dimension coupled with optical foreshortening effects (see General Methods), it is only noticeably different from no correction for very high values of R_m. The third method, used for all the other simulations in this chapter, takes the Z-corrected morphology and corrects for presumed 10% shrinkage due to histochemical processing (see General Methods and Section A.1.3). Not all R_m values were tested on all morphologies. For some values of R_m, two values of R_i were tested, in each case the higher value of R_{in} corresponds to the higher value of R_i. The smaller the cell (the less correction applied), the higher the values of R_{in} for any set of passive parameters. In any case, only a narrow range of passive parameters are within the range of R_{in} values seen in this study. These are also consistent with previous computational studies of granule cells using whole-cell recording [243].

Figure 6-56: How much cable filtering is going on in cut cells? A. The effect of leaky dendritic tips on cell input resistance. The last segment of those dendritic tips which were severed at 150 μm from the soma to generate a "cut" cell model were given a local R_m which was some small fraction of the R_m for the rest of the cell. Cell input resistance is plotted against the ratio of leaky to normal R_m, for a variety of passive parameters. The key indicates the passive parameters used for each set of simulations. The first number is R_m in $k\Omega cm^2$ (i.e. 40k = 40,000 Ωcm^2), the second is R_i (Ωcm) (R_{in} is independent of C_m). As leakiness is increased (indicated by a decreasing ratio), R_{in} decreases.The horizontal lines indicate, for each set of parameters (identified by the symbols at the ends of the lines), the R_{in} of the uncut cell model (left line) and the expected cut cell R_{in} assuming a ratio between the two of 0.71 (right line, see text). Each of the lines for the predicted cut cell R_{in} intersects with its respective plot of input resistance vs leakiness at a leakiness ratio of approximately 0.075. This indicates that regardless of the passive parameters (across the range shown here), the cut dendritic tips must have a membrane that is 13 times more leaky than that of the rest of the cell to account for the measured difference in input resistances. B. mIPSC shape parameters are plotted as a function of dendritic distance from the soma (distance along the extended dendrites, as in the dendrogram shown in Figure 6-52B, *not* distance from the granule cell layer, allowing greater visibility of closely-spaced points) for the uncut cell, and the cut cell simulation with and without leaky dendrites (leak ratio used = 0.075). It can be seen that cutting off the dendrites, and inducing a termination close to the soma (see section A.1.1) reduces the attenuation of mIPSC amplitudes, areas and slopes, and prevents the usual increase in half width with distance. This would be expected in and of itself to increase the mean mIPSC amplitude, even without the loss of any distally-generated, small events. Surprisingly, amputation of the dendrites increases mIPSC rise times over the

remaining dendritic range, though rise times plateau after 100 μm and do not continue to increase with distance. None of the parameters except area are significantly affected by the presence of even the strong dendritic leak used here. Parameters used (standard for all simulations in this chapter): R_m=40,000 $\Omega cm2$, R_i=100 Ωcm, R_s=7 $M\Omega$, g_{syn}=1.0 nS, synaptic kinetics τ_R=0.146 msec, τ_D=4.583 msec.

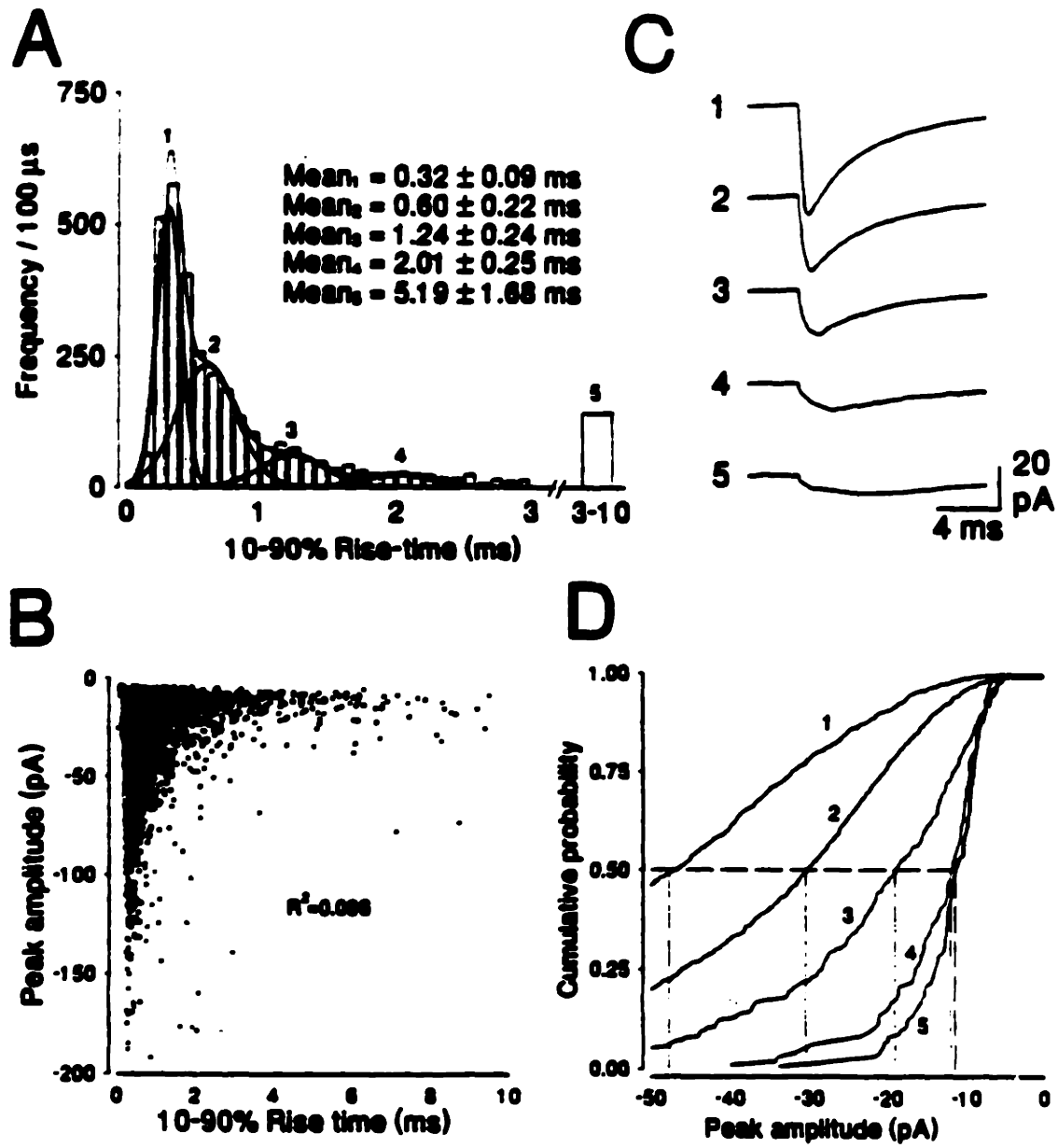
A
750
500
250
0
Frequency / 100 µs
Mean1 = 0.32 ± 0.09 ms
Mean2 = 0.60 ± 0.22 ms
Mean3 = 1.24 ± 0.24 ms
Mean4 = 2.01 ± 0.25 ms
Mean5 = 5.19 ± 1.68 ms
1
2
3
4
5
0
1
2
3
3-10
10-90% Rise-time (ms)
C
1
2
3
4
5
20
pA
4 ms
B
0
-50
-100
-150
-200
Peak amplitude (pA)
R²=0.096
0
2
4
6
8
10
10-90% Rise time (ms)
D
1.00
0.75
0.50
0.25
0.00
Cumulative probability
1
2
3
4
5
-50
-40
-30
-20
-10
0
Peak amplitude (pA)

Fig. 6 - 48

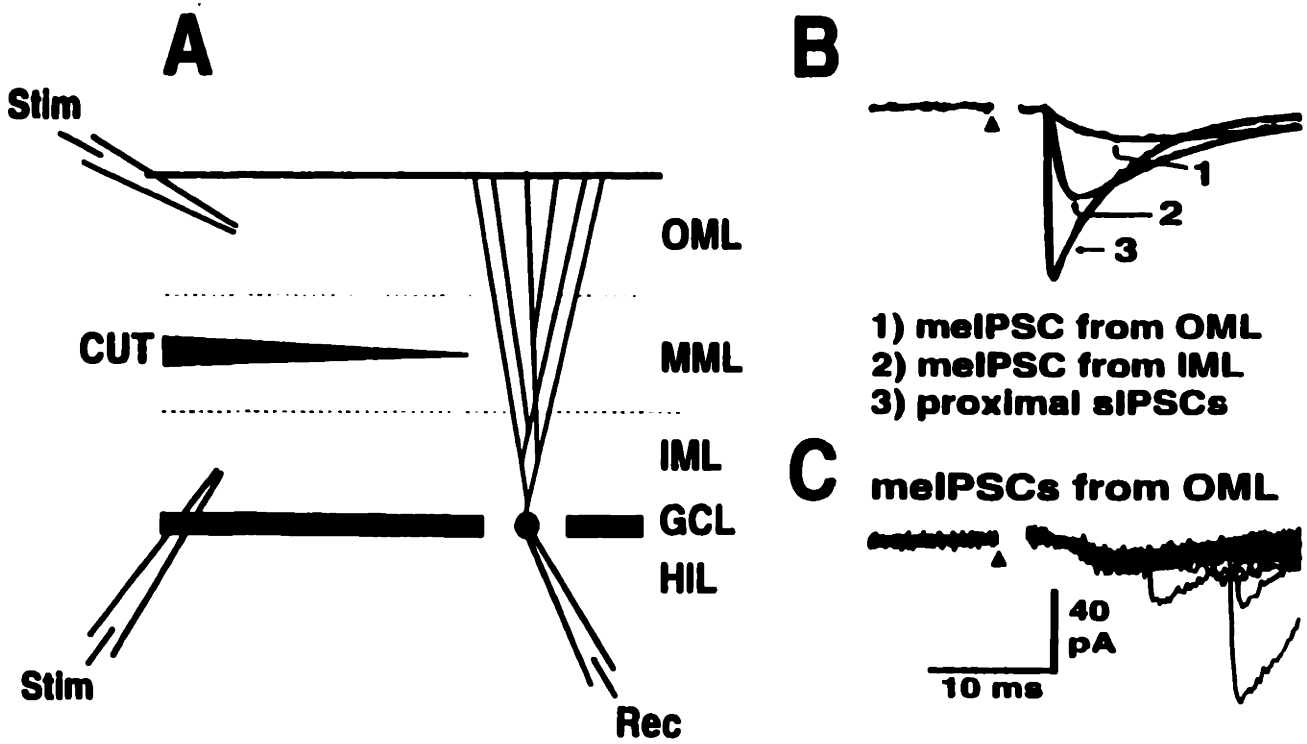
A
Stim
OML
CUT
MML
IML
GCL
HIL
Stim
Rec
B
1
2
3
1) melPSC from OML
2) melPSC from IML
3) proximal sIPSCs
C
melPSCs from OML
40
pA
10 ms

Fig. 6 - 49

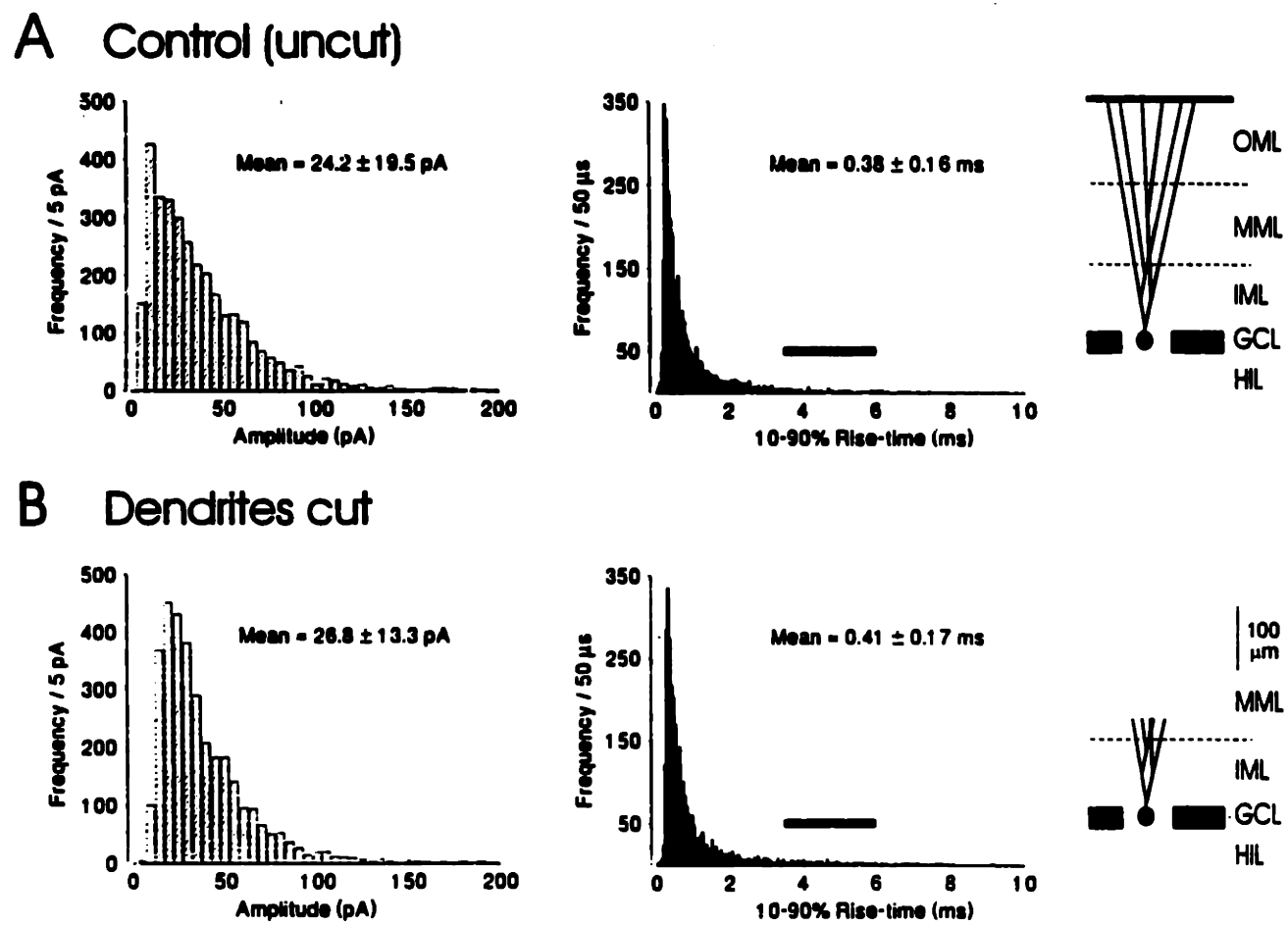
A Control (uncut)
Mean = 24.2 ± 19.5 pA
Frequency / 5 pA
Amplitude (pA)
Mean = 0.38 ± 0.16 ms
Frequency / 50 µs
10-90% Rise-time (ms)
OML
MML
IML
GCL
HIL
B Dendrites cut
Mean = 26.8 ± 13.3 pA
Mean = 0.41 ± 0.17 ms
100 µm

Fig. 6 - 50

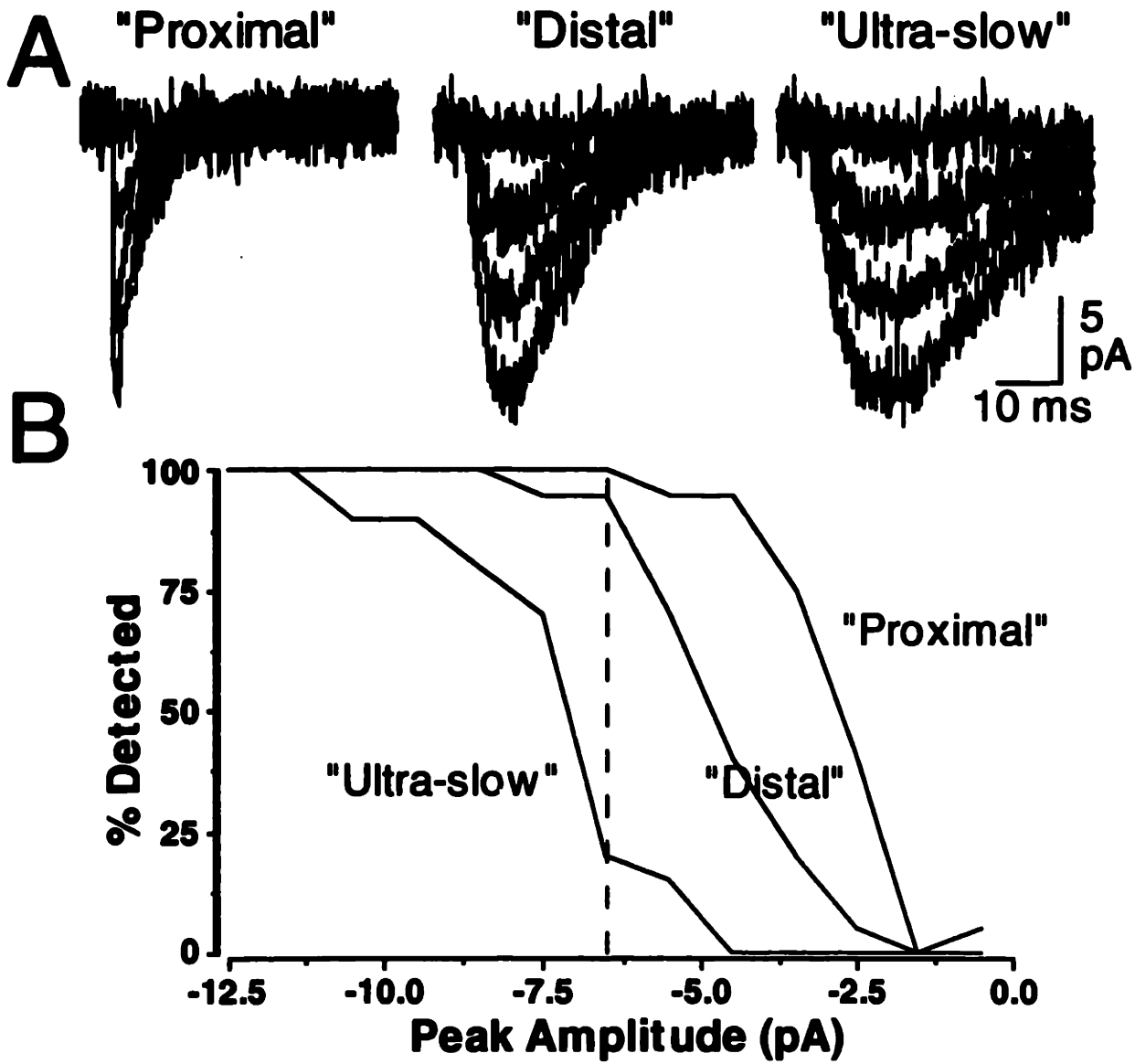
A
"Proximal"
"Distal"
"Ultra-slow"
5
pA
10 ms
B
100
75
50
25
0
% Detected
"Proximal"
"Distal"
"Ultra-slow"
-12.5
-10.0
-7.5
-5.0
-2.5
0.0
Peak Amplitude (pA)

Fig. 6 - 51

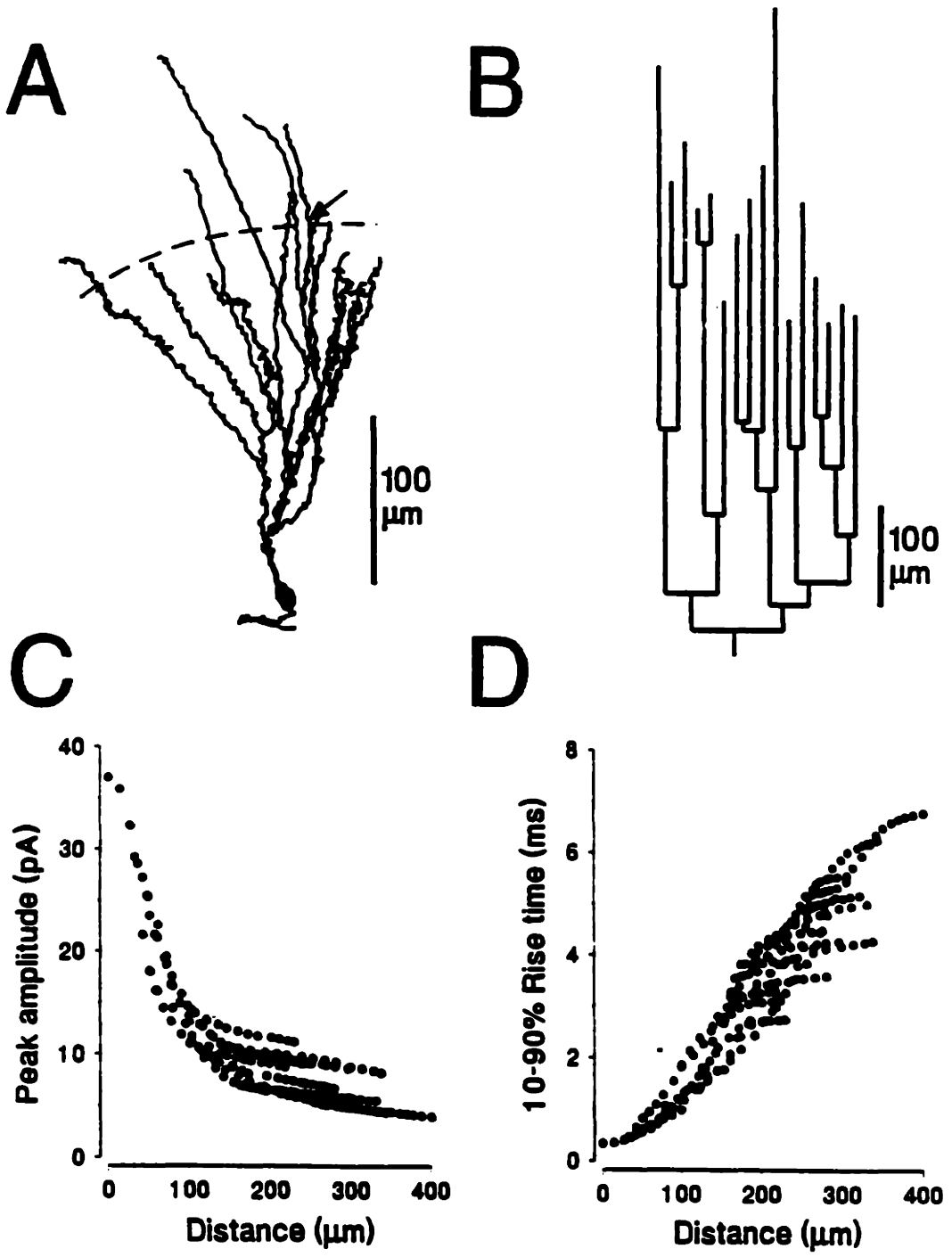
A
100
µm
B
100
µm
C
Peak amplitude (pA)
40
30
20
10
0
0
100
200
300
400
Distance (µm)
D
10-90% Rise time (ms)
8
6
4
2
0
0
100
200
300
400
Distance (µm)

Fig. 6 - 52

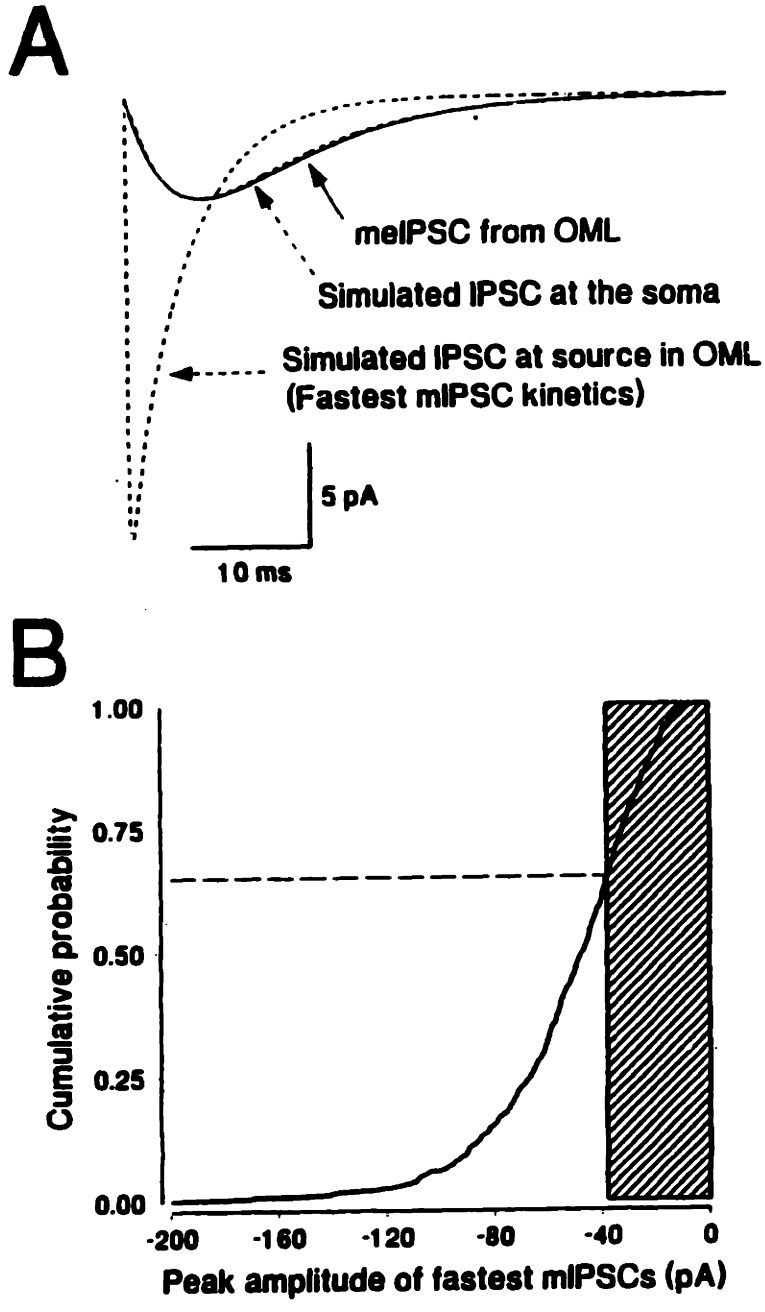
A
melPSC from OML
Simulated IPSC at the soma
Simulated IPSC at source in OML
(Fastest mIPSC kinetics)
5 pA
10 ms
B
1.00
0.75
0.50
0.25
0.00
Cumulative probability
-200
-160
-120
-80
-40
0
Peak amplitude of fastest mIPSCs (pA)

Fig. 6 - 53

A

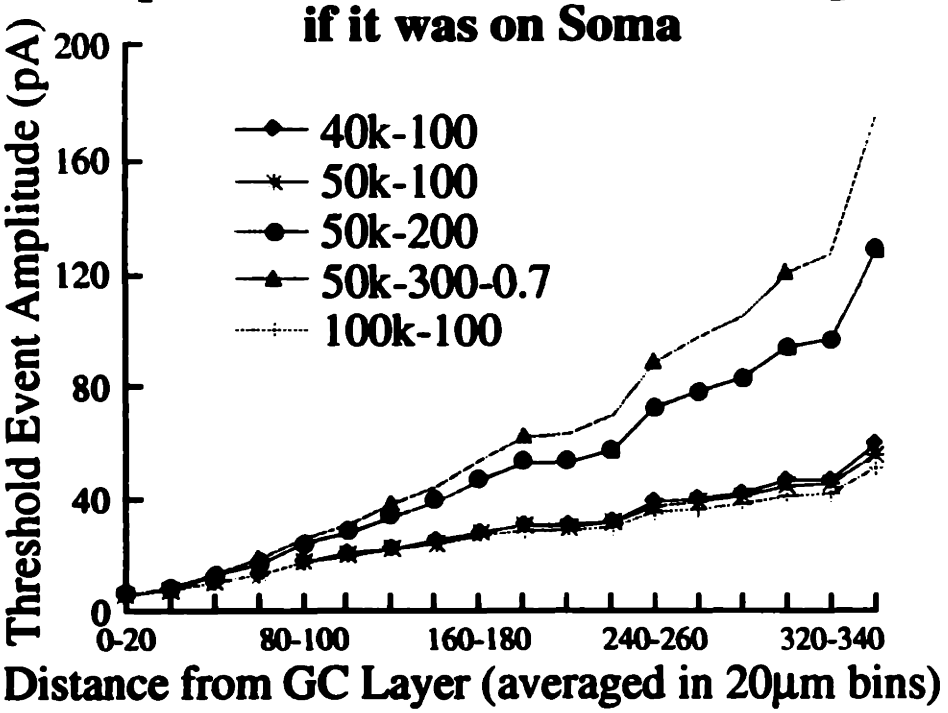
Amplitude of Threshold Event (6.5pA)
if it was on Soma
Threshold Event Amplitude (pA)
200
160
120
80
40
0
40k-100
50k-100
50k-200
50k-300-0.7
100k-100
0-20
80-100
160-180
240-260
320-340
Distance from GC Layer (averaged in 20µm bins)

B

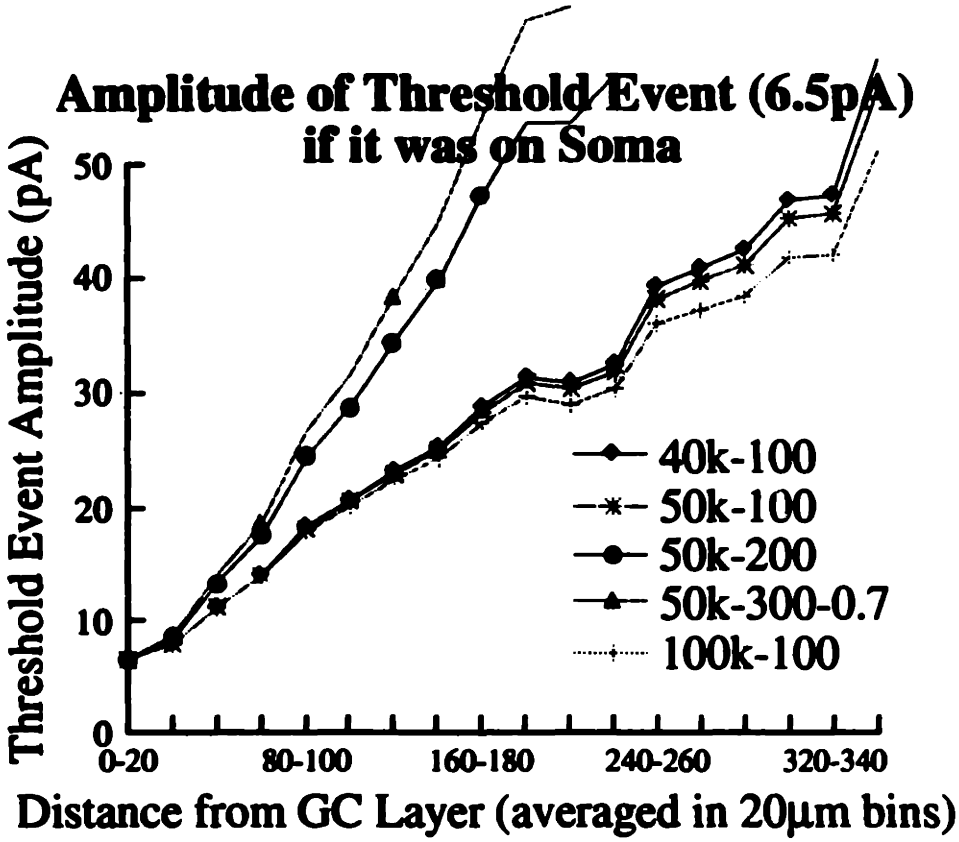
Amplitude of Threshold Event (6.5pA)
if it was on Soma
Threshold Event Amplitude (pA)
50
40
30
20
10
0
40k-100
50k-100
50k-200
50k-300-0.7
100k-100
0-20
80-100
160-180
240-260
320-340
Distance from GC Layer (averaged in 20µm bins)

Fig. 6 - 54

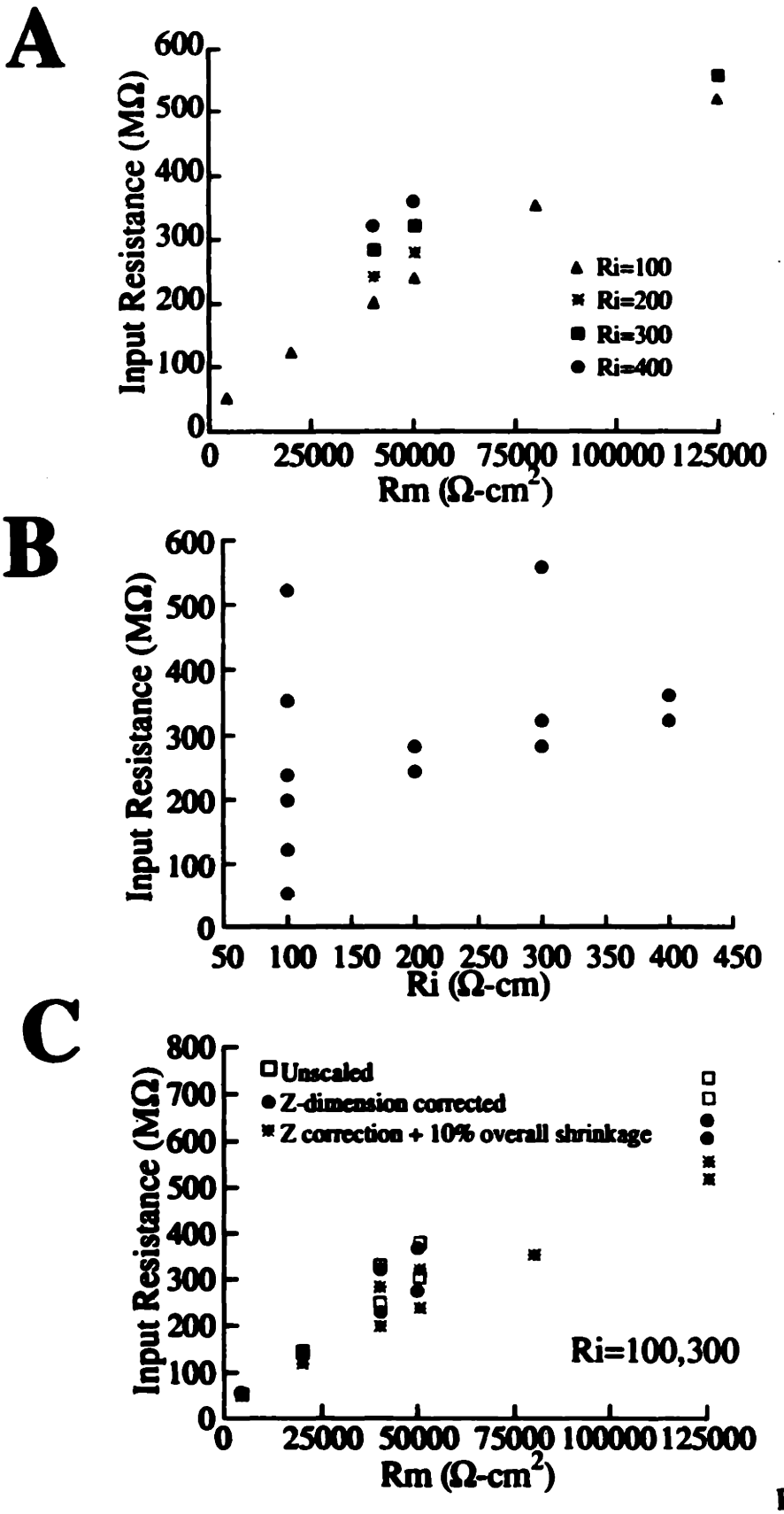
A
Input Resistance (MΩ)
600
500
400
300
200
100
0
0
25000
50000
75000
100000
125000
Rm (Ω-cm²)
Ri=100
Ri=200
Ri=300
Ri=400
B
Input Resistance (MΩ)
600
500
400
300
200
100
0
50
100
150
200
250
300
350
400
450
Ri (Ω-cm)
C
Input Resistance (MΩ)
800
700
600
500
400
300
200
100
0
Unscaled
Z-dimension corrected
Z correction + 10% overall shrinkage
Ri=100,300
0
25000
50000
75000
100000
125000
Rm (Ω-cm²)

Fig. 6 - 55

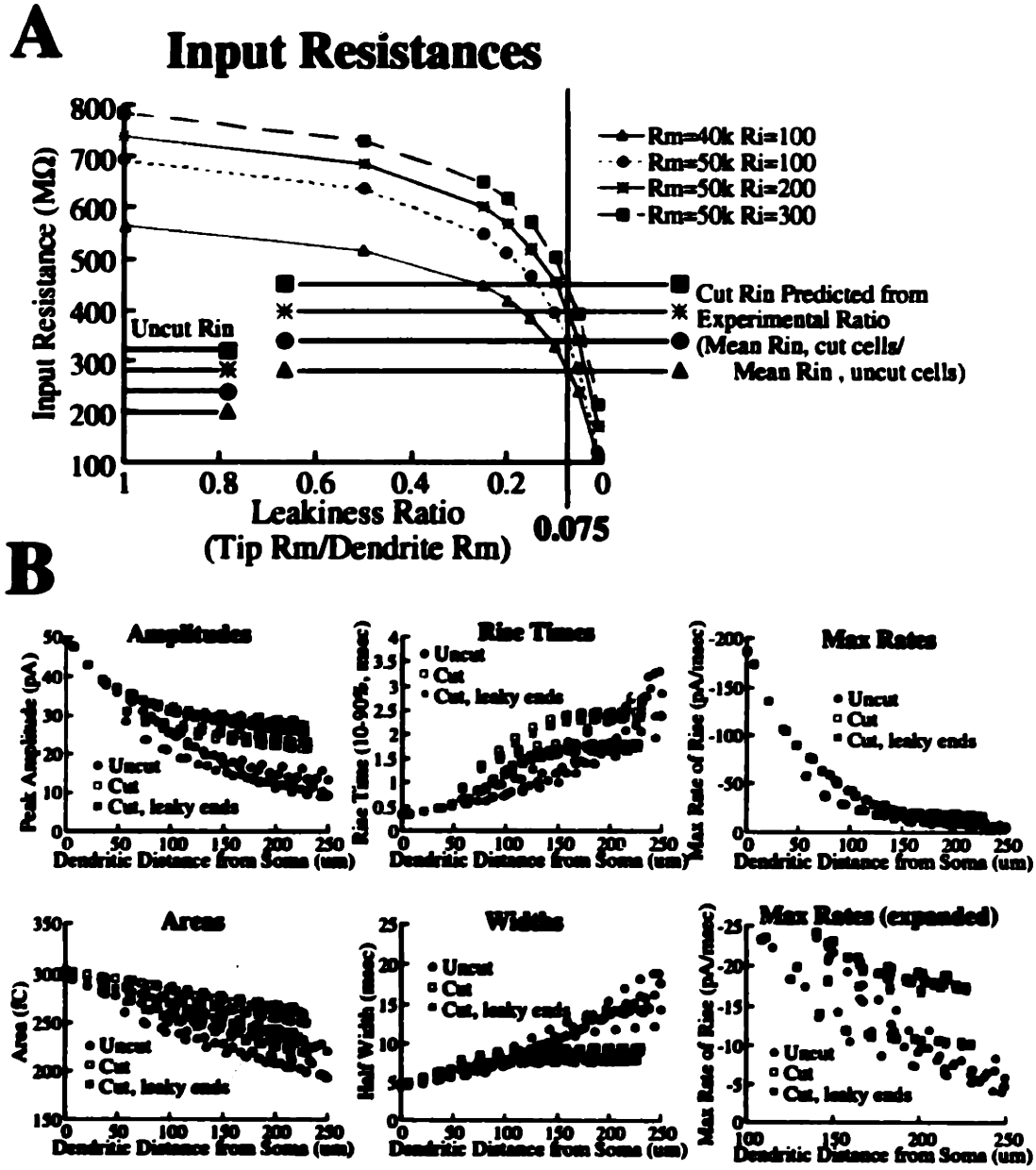
A
Input Resistances
Input Resistance (MΩ)
800
700
600
500
400
300
200
100
Uncut Rin
Rm=40k Ri=100
Rm=50k Ri=100
Rm=50k Ri=200
Rm=50k Ri=300
Cut Rin Predicted from
Experimental Ratio
(Mean Rin, cut cells/
Mean Rin , uncut cells)
1
0.8
0.6
0.4
0.2
0
Leakiness Ratio
(Tip Rm/Dendrite Rm)
0.075
B
Amplitudes
Peak Amplitude (pA)
Rise Times
Rise Time (10-90%, msec)
Max Rates
Max Rate of Rise (pA/msec)
Areas
Area (fC)
Widths
Half Width (msec)
Max Rates (expanded)
Uncut
Cut
Cut, leaky ends
Dendritic Distance from Soma (um)

Fig. 6 - 56

7

Summary and Conclusions

Wow. You've actually made it to the end of the thesis. Quite a long trip, eh? I wish I could give you a prize, or at least a cookie or something. But wait - you're not one of those who skips to the end to see how the whole thing comes out, are you? Make sure that the good guys ride off into the sunset happily before you dive into that stressful scene where the membrane capacitance is threatening to drastically cut the EPSC's amplitude before it can reach the soma and generate an action potential.... Nah, not you. But just to remind you, here are the high points:

Functional convergence onto visual cortical neurons

In Chapter 3, I showed that single-fiber inputs to cortical neurons are large, fast, and extremely variable in amplitude, both between the inputs to different cells and across the population of inputs to a single cell. Single inputs fluctuate in amplitude over time, frequently fail to release transmitter at all, and are made up of no more than a few quanta in amplitude at most, even given their large size. Assuming linear summation, only 5-50 simultaneous input are necessary to generate an output spike. This very low functional convergence means that the variability intrinsic to the synaptic inputs of a cortical cell will, in many cases, be reflected in its output.

Generation of synaptic variability in cortical neurons

What generates the incredible amount of synaptic variability described in Chapter 3. In that chapter, several candidate mechanisms were identified, including the measured variability in single inputs over time, and factors such as animal age, and access resistance, which will generate variation in EPSC distributions between cells. In Chapters 4 and 5, I addressed the question of what generates the variability seen in the population of inputs to a single cell. Most importantly, I asked the question of what role synapse location on the postsynaptic cell, in the form of electrotonic filtering, plays in the generation of amplitude variability. In chapter 4, I showed that electrotonic filtering alone is in fact sufficient to generate the characteristic skewed amplitude and rise time distributions seen for mEPSCs of cortical pyramidal cells. I then explored methods for detecting the effects of electrotonic filtering, as well as several other potential sources of mEPSC variability, in populations of real mEPSCs. As usual, the best method for assessing the contribution of electrotonic filtering to mEPSC shape was originally suggested by Rall - simple plots of rise time vs half width [203, 206]. Using this technique, as well as some others, I showed that mEPSCs are almost definitely shaped by electrotonic filtering, and that it is likely to generate a large fraction of their amplitude variability. However, I also showed that it is not completely sufficient to explain all of the characteristics of experimentally measured mEPSCs. A simple model combining electrotonic filtering and the variation in conductance between synapses (or at the same synapse over time) suggested by this and other studies [19, 17], is sufficient to replicate all of the data on mEPSC variability in cortical neurons.

Given that it would be nice to have an independent, experimental, confirmation of these conclusions, in Chapter 5 I attempted to provide experimental evidence for a role for electrotonic filtering in the generation of mEPSC amplitude variability in cortical cells. Using local application of CNQX, I showed that the largest, fastest mEPSCs all come from the region of the basal and proximal apical dendrites, consistent with

the predictions above. Additionally, the vast majority of the events arose from this region, consistent with >85% of the spines being located there. Events localized from the apical dendrites tended to be smaller and slower than the average basal event. Finally, applying the kinetic analysis of the last section to localized subpopulations of events provides experimental support for the use of rise time vs half width shape indices as an experimental metric for synaptic source location [97, 269, 100, 94].

Extension to other systems

In Chapter 6, the results of Chapter 4 were used to answer a functional question: what is the site of origin of synaptically-generated mIPSCs? With excitatory inputs to cortical pyramidal cells, the location of the spines (the most common input site), and the fact that the majority of inputs come from other pyramids, lead us to the answer that mEPSCs are very likely to come in from all over the cell.[1] In the case of inhibitory inputs to dentate gyrus granule cells, in contrast, those inputs arise from different source interneurons which target particular postsynaptic regions. Analysis of mIPSCs using techniques developed in previous chapters suggests strongly that those events are generated predominantly from proximal sites, in spite of the fact that an equal or larger number of GABAergic synapses are onto the dendrites [78, 79]. It was shown that distal mIPSCs, if present, would for the most part be detectable at the soma. Distal synapses were shown to be functional, and give responses at the soma identical to the predictions of a computational model on the effects of filtering on the shapes of such events. In spite of these facts, spontaneous events arose only from the soma and most proximal dendrites, and this analysis was confirmed by cutting off the distal half of the dendritic tree and showing no change in mIPSC amplitude, rise time, or frequency distribution.

[1]The results of Chapter 5 are consistent with a model where mEPSCs are equally likely to come from anywhere on the cell; that if particular inputs are unusually likely to generate a mEPSC [179], this bias is not preferentially distributed to particular parts of the postsynaptic cell.

7.1 Paradoxes of Cortical Function

There is a striking paradox which is brought into graphic relief by the data presented here. On one hand, there is the old picture of neurons as stochastic, noisy creatures, responding to repeated presentation of the same stimuli with random patterns of spikes [232, 35, 14, 289], and capable of signaling information only by their average firing rate. This contrasts sharply with the new, improved neuron – one which in fact responds to the same input with exactly the same output [12], which represents the detailed fluctuations of its synaptic inputs exactly in the detailed patterns of its spikes [150], and one which is optimal, or nearly optimal, in its transmission of information about the sensory world [24].

If this is indeed our "new" neuron, one which is capable of representing information in the detailed patterns of its spikes, how do we reconcile this with the facts shown here, that the response to one of those spikes in the next cell down the line is in fact variable, both fluctuating widely in amplitude and even failing to release transmitter at all on many occasions, and that these inputs are so large that their fluctuations are not averaged away in the eyes of the postsynaptic cell by the law of large numbers.

We have three choices: first, we assume that there is some biological reason for this "noise" in synaptic transmission (i.e. it can't get any better), and we go back to our picture of the average-rate neuron trying to overcome the insufficiencies in its inputs. Second, we accept that there is some functional requirement for noise in the nervous system, perhaps to take it out of local minima [87]. Third, and perhaps, most intriguing, is the idea that these inputs aren't noisy at all. This variability can be modulated, by the history of firing of the presynaptic neuron [182, 251], and might be affected by neuromodulators. The nervous system obviously has control over the degree of reliability of any particular connection, as some are designed to be extremely large and extremely reliable; either by having the presynaptic axon make several hundred contacts onto a single postsynaptic cell as in the case of retinogeniculate synapses, or by making one enormous bouton containing hundreds of release sites,

as in the case of the endbulbs of Held in the cochlear nucleus. It might be that neurons simply can't afford to make these strong connections except where absolutely necessary, and so do without in the rest of the brain. It also might be that these more variable connections allow for greater synaptic plasticity and a more flexible response to the ongoing patterns of sensory input. The answer to this paradox will determine both the nature of the neural code, how neurons represent information, and what synaptic plasticity of the bewildering number of forms described in recent years will actually mean to the cells involved.

7.2 Cortical microcircuitry and function

The fundamental point of this thesis is that single-fiber connections between cortical cells are large, fast, and extremely variable. This variability is expressed between the inputs to different cells or perhaps different cell types, between the inputs to a single cell, and even in the response to a single input over time. This variability between inputs is determined by a number of factors, not the least of which is the combination of the morphology of the postsynaptic cell, and the location of the synapse in its dendritic tree. All of these facts must be taken into account when we ask how cells generate the emergent properties so important in visual information processing. These properties provide a rich substrate for both cortical information processing, and cortical plasticity; and may allow a single cell to participate in a wide array of ongoing computations.

Appendix A

Additional Analysis of Filtering Effects

This appendix demonstrates some basic features of cable filtering and experimental analysis which are important for understanding, interpreting, and extrapolating from the results presented elsewhere in the thesis. Many of these results are well-known consequences of basic cable theory, I have simply provided systematic examples of them here (sometimes for the first time) in case they are not familiar to the reader. Other of the results presented here are important to the detailed interpretation of the experimental data presented above, but would perhaps distract from the flow of presentation and be too esoteric for some readers. They are presented here for reference.

A.1 Effects of morphology.

The underlying premise of cable theory is that the shape of a cell, via its electrotonic architecture, will transform signals as they pass along it. It is clear that integration of electrical signals in a very large cell with long, branching dendrites, will be very different from that occurring in a small cell with little or no dendritic tree. What fundamental building-blocks of cell morphology affect electrical signals, and what effects do they have?

A.1.1 Effects of cable shape.

The most basic morphological features of the cell are the length and diameters of its dendrites, and how they branch. These features shape electrical signals in complex ways, and the simple notion that inputs coming from farther away are always smaller at the soma is too naive. In fact, dendrites can be tuned to pass some electrical signals more effectively than others [89].

Dendritic diameters. Holmes [89] has shown that dendritic diameters can be selected to maximize the amplitude of the somatic response to an input at a given distance away. While inputs onto a thinner dendrite will be more severely attenuated as they propagate from the input site to the soma, the higher input impedance at that dendritic site means the subsynaptic response there will be larger than in a larger-diameter dendrite. The net effect can be a larger response at the soma.[1]

This can be seen in Figure A-57A, where response amplitudes are larger for inputs into an intermediate-diameter cable than for inputs into either a thinner or thicker dendrite. The response to a somatic synapse in a 2.5 μm diameter cable is much smaller than that seen in a thinner cable, in spite of the much more severe attenuation in the thinner cable. However, the response to a very distal synapse in the 2.5 μm diameter cable is much larger than that seen in a 0.2 μm diameter cable. But both of these are smaller than the response in a cable of intermediate size. The higher input resistance of the thinner cable means that the amplitude at the input site is larger to begin with, and more remains after propagation to the soma - the net transfer attenuation is less severe in the thinner cable. This indicates an amplitude tuning effect with cable diameter.

For somatic inputs, amplitude (and input resistance) varies significantly with cable

[1] It is important to keep in mind that on a single dendrite, as you move a synapse progressively farther away from the soma, the somatic response will decrease monotonically. However, as you move an input out different dendrites of differing structure, the somatic response may be larger from a more distal site on one dendrite than from a more proximal site on another, and this is not easily predictable a priori from examination of their diameters.

diameter, while for the most distal dendritic inputs, somatic response amplitude is independent of diameter. The rate of attenuation of the response with distance from the soma is very dependent on cable diameter - if the attenuation profiles in Figure A-57A were normalized relative to the peak amplitude on the soma, their shapes would differ greatly, and would not be monotonically related to diameter. This can be seen more clearly in Figure A-57B, where the data in A-57A is replotted as a function of cable diameter. As diameter is increased, the response amplitude at the soma at first increases and then decreases, giving rise to an optimal diameter to produce the peak somatic response [89]. These curves also show that the optimal diameter is slightly different for each synaptic location - as the synapse is moved distally, a larger optimal diameter is required to overcome the resulting increase in attenuation. The shape of the attenuation curves in A and the tuning curves in B are both dependent on the frequency response of the cable (see Fig. A-64) and the frequency components of the synaptic current (see Fig. A-63).

Branching. Synaptic response shape is also affected by dendritic branching, indicating that synapse position alone does not control somatic response shape. Comparing the response to a synapse placed either immediately before or immediately after a branch point with that to an equidistant t synapse on an unbranched cable shows that placing a synapse near a branch point attenuates the response amplitude and changes its time course (Fig. A-57C). The presence of a branch decreases the somatic response amplitude, presumably due to the decrease in input resistance. If the branch is more distal than the input its effect is limited to the later portions of the synaptic current - rise time is unchanged, the peak amplitude is only slightly reduced, but the decay is much faster as the branch acts as a current sink. Proximal branches affect the entire time course of the synaptic response: the rise time is slowed, the peak amplitude is attenuated more severely, and the decay is actually slowed relative to control.

Effects of other dendrites. It has been shown ([242, 150, 153, 151], see Chapter 4) that in cells with extended dendrites only rarely is there sufficient space clamp to adequately bring distal synapses under true voltage control. What, then, is the real difference between current and voltage clamp? There are two primary differences. First, the frequency range each lets pass to the soma (see Figure A-63 and Figure A-60), and second, the interaction between the primary dendrites. In perfect voltage clamp (R_s=0), there is no interaction between synapses on different dendrites, as they are separated from each other by the clamped soma, short-circuiting transmission from one dendrite to another. In current clamp, the other dendrites act as a frequency-dependent conductance load upon the soma, filtering the response to a synaptic input onto one dendrite. This effect is simulated in Figure A-57C, where responses in a simple soma-cable model are compared with those in which the rest of the dendritic tree, represented as a lumped load, is present. In current clamp, addition of a load drastically reduces the amplitude of the response seen at the soma, and smoothes its time course. The load exerts its effects as current reaches the soma, so it will not affect interactions between inputs occurring within a single dendrite at the input site itself (left graph in Figure A-57E). For every synaptic site, the somatic response is reduced significantly by the dendritic load, while in contrast, the subsynaptic voltage response is independent of the load, except at the most proximal synaptic locations. In perfect voltage clamp, the load has no effect on the response as the somatic clamp isolates the dendrites from one another.

Effects of dendritic terminations. In addition to dendritic diameter, length, and branching, there is one other basic morphological feature that has an impact on the nature of electrotonic filtering: dendritic terminations. The effect of terminations was studied in detail in some of the earliest papers on cable theory [201, 202, 211, 99], as it was not obvious *a priori* what the appropriate mathematical model was for the end of a dendrite. The standard approach today is to simply treat dendritic terminal

segments as cylinders whose ends are sealed with membrane,[2] rather than as a short-circuit to ground. This means that current propagating towards the termination will be reflected back into the cell [201]. If the termination is far enough from the soma this reflected current will not impact the somatic response, but as discussed above (Section 4.3.3), many cortical pyramidal cell dendrites terminate (electrically) relatively close to the soma.

The effects of terminations can be seen by comparing the somatic response to a synaptic input at a particular dendritic location onto a very long dendrite and a dendrite which ends just beyond the synapse (Fig. A-57E,F). There is a strong effect of dendritic termination in both voltage (E) and current clamp (F). While the subsynaptic response amplitude follows approximately the same pattern over the course of the dendrite regardless of length (left, squares at top), the amplitude of the somatic response is the same over the initial part of the cable, and then diverges about 150 μm from the soma. In the short cable, instead of continuing to decrement with distance, the response plateaus – the current cannot escape down into a long dendrite, is reflected back towards the soma, and shows up as increased amplitude of the somatic response in the short cable to an equidistant input. This indicates that in relatively short dendrites, even ones as long as the basal dendrites of pyramidal cells, close terminations will be reflected in decreased attenuation of the synaptic current as it propagates to the soma.

Characteristic features of attenuation profile. These two effects combine to generate a stereotyped three-part pattern of subsynaptic voltage response[3] as the synapse is moved farther out the dendrite (Figure A-57E,F). The first part is controlled by the relative input impedance of the soma and proximal dendritic cable. If the soma has a lower input impedance than the dendrite (e.g. due to a load on the

[2]See Section 6.3.7 for a more detailed examination of a particular case.

[3]This should be the same as the pattern of subsynaptic voltage escape in voltage clamp, at least for distal synapses [242].

soma from the other dendrites), the subsynaptic amplitude will increase steeply as the synapse is moved away from the soma. If the input impedance of the soma is higher than that of the proximal dendritic cable (due to a small soma diameter and large cable, and no load), the subsynaptic voltage response will remain relatively constant over some region of the proximal dendrite, or will even decrease. The second part is a plateau region, which can be quite long in the case of the long cable, or almost nonexistent in the short one. The plateau region is generated when both ends of the dendrite are electrically far away, and the input impedance approaches that at the midpoint of an infinite cable. Finally, as the input impedance increases near the dendritic termination, the subsynaptic voltage also increases dramatically. If the termination is close enough to the soma, this massive increase in subsynaptic voltage with distance is enough to partially (but never completely) overcome the attenuation between the synaptic site and the soma, causing the plateau in the somatic response. The first (soma) and last (termination) parts are always present, however the length of the plateau region depends on the length of the dendrite; in short dendrites it may disappear entirely. This type of impedance matching is also responsible for the diameter tuning effect seen in Figure A-57A and B.

A.1.2 Effects of somatic shunt: comparison to sharp electrode studies.

To estimate the functional convergence onto a cortical cell, it is critically important to accurately measure the amplitudes of single-fiber inputs. However, one striking difference in the measurements of single-fiber response amplitude and mEPSPs given in Table 1.3.3 and Chapter 3 is that the amplitudes seen with sharp electrode recordings are much smaller than those with whole cell patch. The most likely underlying causes for this all relate to that cells recorded using whole cell patch techniques typically have much higher input resistances (150-500 $M\Omega$) and longer time constants (20-100 msec) than those seen with sharp electrodes (5-80 $M\Omega$, 5-30 msec). While somatic

input resistance is not the major determinant of response amplitude in current clamp (see Figure A-60), it is clear from Figure A-57F that cells with higher input resistances will show generally larger current clamp peak amplitudes for the same synaptic input current. To understand whether this change alone can account for the change in synaptic amplitudes, it is important to identify the mechanism underlying the change in input resistance. Several candidate factors have been suggested to contribute to all or part of this difference in input resistance. First, whole cell recordings are typically performed in much younger animals than those used for sharp electrode studies (see Section 1.3.1). Therefore the cells used in whole cell studies may be smaller to start with, and thus have intrinsically higher input resistances. Second, many whole cell studies are performed at room temperature (22°C), while sharp electrode studies are typically performed at > 32°C. This could also contribute to some of the more extreme differences in input resistance which have been reported [111]. However, when these two factors are controlled for, there still remains a significant difference in input resistance between cells recorded with sharp electrodes and with whole cell patch techniques [246, 243].[4]

Two further mechanisms have been put forth to explain this remaining difference in input resistance. In the first, dialysis of the cell during whole-cell recording washes out some factor necessary for maintaining a normal source of membrane conductance, thereby effectively increasing the membrane resistivity of the cell [36]. This would not explain the maintained difference in input resistance seen with perforated patch recording,[5] or the fact that the difference in input resistance is apparent immediately

[4]There is also a significant difference in input resistance seen between *in vivo* and *in vitro* recordings. This has been partially attributed to the increased background synaptic activity *in vivo* [22, 208]. Several of the early sharp electrode studies in Table 4.3.1 were actually performed *in vivo*. However, cells recorded *in vivo* with whole-cell electrodes show much higher input resistances than those recorded either *in vitro* or *in vivo* with sharp electrodes (S. Nelson, C. Moore, pers. comm.), indicating that in this case as well, the difference in recording technique accounts for at least part of the difference in R_{in}.

[5]In this technique, the patch of membrane underneath the electrode is not sucked away to create a true whole-cell recording. Instead, a substance in the pipette, usually a detergent such as nystatin or an antibiotic such as amphoceterin is used to make small non-ion-specific pores in the

on breaking into the cell, suggesting that prolonged dialysis is not necessary to increase the membrane resistivity. The other candidate mechanism for the lower input resistance in sharp electrode recordings is the presence of a shunt, or leak conductance, around the barrel of the sharp electrode where it has punctured the cell membrane [36, 66, 69, 101, 152, 198, 199, 218, 265, 288]. A whole-cell patch pipette, with its tight seal to the membrane of the cell, is expected to allow no such leak.[6] The leak conductance around a sharp electrode is postulated to be somewhat ion-selective, or to induce the opening of an ion-selective conductance due to influx of Ca^{++} or other ions through the leak. Such a complication is necessary to explain the preserved resting membrane potential in intracellular recordings. If a large shunt conductance with a reversal potential of 0 mV were opened in the cell membrane, it would be expected that the neuron would rapidly depolarize [36, 66, 69, 101, 152, 198, 199, 218, 265, 288]. Such a change in membrane potential may also be partially prevented by leakage of K^+ from the electrode tip, as most sharp electrodes are filled with very high-concentration solutions with K^+ as the dominant cation.

To answer the question of functional effectiveness and size of single-fiber synaptic inputs, it is therefore important to distinguish between these two mechanisms of input resistance change. Figure A-58A illustrates the difference between spontaneous EPSPs recorded with sharp electrodes and whole-cell patch pipettes. The four cells recorded with whole-cell patch electrodes under standard conditions show remarkably similar amplitude distributions. An interneuron, also recorded under the same conditions, has an amplitude distribution of similar shape, but shifted in favor of larger amplitudes.[7] In contrast, recording mEPSPs in the presence of bicuculline, which will

patch membrane. Membrane voltage and current can be monitored through these channels without washout of any major cytoplasmic constituents larger than the pore size [243, 222, 220].

[6] Although it is clear that not all whole-cell recordings are created equal, and in the case of a bad seal or break-through, or an unhealthy cell, the whole-cell recording could actually have somewhat of a shunt conductance around the electrode, or even be a quasi-intracellular recording.

[7] Interneurons have larger input resistances than pyramidal cells, due to their smaller size. However, they also have shorter dendrites and excitatory inputs directly onto their somata, both of which will contribute to the larger synaptic inputs seen in these cells.

increase the level of spontaneous firing in the slice and hence the relative fraction of action potential-dependent events (see Chapter 3), simply added a greater percentage of large events, while leaving the small events unchanged as a fraction of the total. These three known conditions are compared to distributions recorded in two pyramidal cells with sharp electrodes.[8]. In contrast to both the effects of bicuculline and the differences between cell types seen with whole cell recording, the distributions seen in sharp electrode recordings are changed in slope as well as in absolute amplitude from the "standard" whole-cell recordings, suggesting more than a simple effect of cell size. One confounding factor, however, is the increased baseline noise in the sharp electrode recordings, which makes detection of small events difficult. In fact, in most sharp electrode recordings, spontaneous synaptic events cannot be seen. However, the difference between amplitude distributions with sharp electrodes and whole cell is not consistent with a simple effect of event detectability, as sharp electrode recordings show very few or none of the easily detectable, large amplitude events ($> 0.5mV$) seen commonly with whole-cell recordings (see Section 5.3.7).

The difference in slope seen between the cumulative amplitude distributions of cells recorded with sharp electrodes and whole-cell patch clamp is not consistent with the predictions of a simple shunt conductance (Fig. A-58B,C). Adding a somatic shunt conductance simply shifts the simulated cumulative amplitude distribution to the left by 0.05 mV,[9] with no change in slope. Increasing the synaptic conductance into the partial saturation range, and generating event amplitudes even larger than those seen commonly in experiments, does not change the effect of the added shunt (though the amplitude of the shift is increased). The shift in the amplitude distributions seen between whole-cell and sharp electrode recordings is consistent with what one would

[8]These events were recorded under otherwise identical conditions as the "standard" whole-cell events, however the animals used were several weeks older. The cells themselves, which were filled with biocytin and recovered, were not substantially larger in size than those used for whole-cell recording.

[9]Notice that the simulated amplitudes here are smaller than those seen experimentally, and increasing the synaptic conductance (Fig. A-58C) does increase the size of the shift.

see with an overall reduction in membrane resistivity (see section A.5) in the sharp electrode case. However, it might be that in sharp electrode recordings the amplitude distributions are shifted dramatically to the left by a shunt, (more dramatically than would be expected for the previously suggested range of shunt conductances), and the lower end of the distribution is lost in the noise, generating the measured change in distribution slope (see Section 5.3.7).

Although the effect of a shunt conductance on amplitude is independent of synaptic input location, its effect on the other synaptic parameters is not. Figure A-58D plots the value of each parameter in the presence of a 10 nS somatic shunt against its value in the unshunted case for all locations on a layer V cell. Parameters that are dependent on the integration of current over time are the ones most affected. All areas and half widths are reduced by the presence of the shunt, but proximal events are more affected than distal ones. The shunt conductance only affects the rise times of slow, distally generated events: these are uniformly smaller than is seen in the unshunted case. Maximum slope is only slightly affected, and only for the very fastest (most proximal) events. In general, the presence of a somatic shunt speeds the time course of all parts of the synaptic response (though the change in time course and amplitude come together to cause little or no change in maximum slope), by providing an additional direct current sink to ground and partially short-circuiting the somatic capacitance. This is consistent with the difference in shape parameter values seen between sharp electrode and whole cell recordings.

Without further experimental analysis, it is not possible to decide categorically between a change in passive properties and the presence of a somatic shunt together with noise to explain the differences in mEPSP distributions. There are other theoretical analyses which provide good evidence for the presence of a somatic shunt in sharp electrode recordings [243, 246]. And even if at least part of the measured change is due to a change in membrane resistivity, it is not easy to say what the "true" value is - perhaps R_m increases with whole cell recording, due to dialysis of cellular constituents, but perhaps it decreases with sharp electrode recording as a consequence

of the injury induced by cell puncture. It simply indicates that measurements of synaptic "efficacy" must be taken with a grain of salt.

A.1.3 Effects of errors in morphological reconstruction.

Synaptic responses are sensitive to detailed aspects of cell morphology (Fig. A-57). Errors in the morphological reconstruction of the cells used for these simulations might therefore affect the simulated response distributions, and it is important to assess the implications of such possible errors for the conclusions above [36]. The most likely source of error in the reconstructions is in the diameter of the dendrites [36, 150]. Fine dendrites can approach the limits of resolution of the light microscope, and areas where the dendritic cross-section is not circular are subject to errors in diameter estimation. Finite accuracy in the diameter digitization system and difficulty in resolving spines from their parent dendrite both lead to diameter overestimation. It is also much harder to asses the effect, if any, of shrinkage on dendritic diameters. The other likely source of error is incorrect compensation for shrinkage. In chapter 5, a certain amount of correction in the z-dimension was made (see General Methods), but no systematic correction for shrinkage was applied due to the difficulty of assessing how reflective overall slice shrinkage is of cellular shrinkage; the HRP reaction product may form a kind of skeleton inside cells causing them to wrinkle instead of shrink [150].

Figure A-59A-D shows the effect of errors in dendritic diameters on simulated amplitude distributions. Diameters were scaled to 80% or 120% of their measured values (compare to Figure 4-22C). EPSC amplitude increased or decreased with the change in diameter, however the change was much larger when the dendrites were made thinner (Fig. A-59D). The change is slightly more pronounced for those inputs at the distal sections of the basal dendrites (the center of the range of distances from the soma, Fig. A-59C); events located more distally than that are close to the floor (plateau) region for filtering effects. This shifts the peak of the distribution without

much affecting the tail, stretching or compressing it from its control shape.

Surprisingly, when both the dendritic diameters and dendritic lengths are scaled by 110%, which is the most common approach for shrinkage correction in histological material processed as this was [36, 25], the increase in length compensates for the increase in diameter and the net effect is a reduction in EPSC amplitudes and an increase in their variability (Figure A-59D). For the pure changes in diameter, increasing diameters resulted in increasing amplitudes (means 24.86 pA for 80%, 30.71 pA for standard, 32.30 pA for 120%). Surprisingly, scaling both lengths and diameters by 110% had the net effect of reducing mEPSC amplitude (mean=28.38 pA) and increasing the skew of the distribution. This suggests that errors in the material used here due to inaccuracies in diameter measurements or (more importantly) the lack of correction for shrinkage, will result in an underestimation of the variability caused by electrotonic filtering. This result led me to incorporate such a 10% correction for shrinkage in simulations attempting to match simulations and physiology [36].

Errors in diameter measurements also affect the other EPSC shape parameters. In Figure A-59E,F, the parameters of inputs to a simple soma-cable model are measured in current clamp for several values of the cable diameter (amplitudes for this model are shown in Figure A-57A,B). All parameters are altered by changing dendrite diameter, but the effects are most pronounced for more distal inputs.[10]

A.2 Current vs. voltage clamp.

A naive response to the strong similarity between amplitude distributions of spontaneous events in current and voltage clamp in the same cell (e.g. Fig. 4-17A) is to assume there is a simple ohmic relationship between them, depending on the input resistance of the cell. However, due to the fact that events undergo different amounts of

[10]Except in the case of area, where effects are more pronounced for proximal inputs. However, as these simulations were performed in current clamp, this may have more to do with the increase in input resistance (and hence response amplitude) seen in the smaller diameter dendrite.

filtering in current and voltage clamp, this simple translation is not accurate, and can be very misleading. Current clamp measurements are in some sense highly low-passed filtered by the time constant of the cell membrane. The direct ohmic translation will be most accurate for those events most filtered in voltage clamp – the distally generated events (Figure A-60A, Left), and those recorded with high series resistance (Figure A-60B, Left). Events which are less subject to filtering in voltage clamp will not bear a simple ohmic relationship to their current-clamp counterparts at the soma. Similarly, if one reduces the high-frequency components present in the synaptic input, by either slowing the input current kinetics (Figure A-60A, Left), or by increasing the series resistance (Figure A-60B, Left), the resulting synaptic I-V relationship begins to more closely approach that predicted for the steady-state case (given by the solid line in both graphs). In contrast, area, which already is an extremely low-frequency measure (approaching DC as the integration period increases), is basically identical in current and voltage clamp, and is not affected by additional filtering due to slower current kinetics (Figure A-60A, Right) or additional series resistance (Figure A-60B, Right).

A.3 Effects of spines.

A.3.1 Effects of spine incorporation on simulated parameter distributions.

A surprising finding about cortical pyramidal cells is that, in spite of the visual prominence of their apical dendrite, more than 85% of their spines and hence their excitatory inputs are actually onto the basal dendrites [134] (Figure A-61A,B). This implies both that the basal tree may be the most significant integration region in the cell, and that most of the synapses onto the cell are within 200 μm of the soma. In generating the simulated parameter distributions used in this study, we have had to make assumptions about the distribution of spines onto each modeled cell at two points:

when spine membrane is incorporated into that of the cell (see General Methods), and when using spine location as a metric of synapse location to generate expected event distributions. It is important to assess how sensitive the results presented here are to either of these two factors. To some extent, the effect of spine incorporation (which is performed by changing R_m and C_m[89]) is equivalent to changing the passive properties of the cell, so this question was addressed somewhat by the exploration of passive parameter effects presented in Chapters 4 and Section A.5. However, errors in the spine incorporation function are equivalent to changing the cell's passive properties differentially across the cell's dendritic tree, whose effect on simulated parameter distributions has not been addressed.

A variety of spine distribution functions were tested both for spine incorporation and the generation of parameter distributions. Using three different spine density functions (one constant, two diameter-dependent) suggested by the literature (Fig. A-61C) had only a very small effect on the distribution of event amplitudes in voltage clamp. Most notably there is a smaller number of large-amplitude events with the constant spine density. In current clamp (Fig. A-61D), the differences between these distributions were larger. The most important factor appeared to be the spine density assumed for spine incorporation into the cell membrane; when a diameter-dependent spine density function was used for incorporation and then a constant density function was used to generate the histogram, the final result was more similar to the diameter-dependent density used alone (Fig. A-61D, similar data for voltage clamp not shown).[11] The changes in the amplitude distribution with changes in the spine density were somewhat similar to those seen with changes in R_m and C_m(see Section A.5). In a large layer V cell (shown in Fig. 4-22A), a diameter-dependent spine density function generates a larger number of smaller events from the distal dendrites (Fig. A-61E). However, even these relatively large changes do not significantly change the resulting amplitude histograms (Fig. A-61F)[12], and would not affect any of the

[11]Such mixed distributions were occasionally used in the simulations presented here.

[12]These additional small points appear as a bump at the left end of the histogram. In practice,

conclusions above. In fact, a typographical error led me to run simulations on a cell with a completely inappropriate spine distribution function (the number of spines became negative for some compartments). Even in this case, the basic shape of the parameter distributions were preserved, and their quantitative changes were slight. This suggests that the results presented above are robust to errors in the assumed spine density function. However, it also points out that the spine density function (just as the passive parameters of the cell) can affect the fine details of event amplitude and distribution shape, or weighting. Therefore it may affect the outcome of quantitative comparisons between experimental and simulated distributions.

While simulations of inputs across the surface of the cell tells us unequivocally what range of parameter values cable filtering alone can generate for that particular cell-parameter combination, the actual weighting, in terms of numbers of points we are likely to see taking on any particular value, is a sensitive function of the details of the spine distribution. While it is easy to simulate a distribution with the same general shape as the experimental data, and the shapes of these simulated parameter distributions are robust to small errors, I have been wary of taking on any more quantitative analyses of these distributions which can be influenced by subtle errors in spine distribution. Notably, besides any errors in the anatomically assumed spine distribution, the fact that in a finite amount of time one will not see inputs from every spine, that some spines may overproduce events [179], and that inputs from some spines may be too small or distorted to be detected at the soma (see Chapter 6), all indicate that these distributions are likely to be inaccurate in terms of their weighting – what fraction of the points take on a given range of parameter values. This is why, for instance, correlation coefficients are not usually presented for simulated parameter relationships.

such events would probably be below the experimental detection threshold.

A.3.2 Effects of spine head input location on parameters of synaptic response.

While spine incorporation takes into account the effects of the thousands of other spines on the response properties of the cell, it does not replace the spine which is underneath an active input synapse. In these simulations, synaptic inputs were placed directly onto dendritic shafts, rather than onto an explicitly-simulated spine (mostly to save computation time). I have compared these simulations with those incorporating an explicit spine model in order to ensure that this simplification does not introduce significant errors into the results; and to see what if any effect there is of the spine on the synaptic response. Although a number of early studies [119] suggested that spines may play a computational role via their passive electrical properties, current dogma suggests that spines serve as biochemical, rather than electrical, compartments [125]. Therefore this simplification should not significantly affect the results.

A two-compartment spine model was placed onto the midpoint of a basal dendrite and fairly distally onto an apical dendrite of the cell shown in Figure 4-21B. The properties of a synaptic input of varying kinetics onto the spine head were then compared with the responses to that synapse when placed directly onto the dendritic shaft below the spine location (comparable to the rest of the simulations performed above). The increased input impedance of the spine head relative to the dendritic shaft did attenuate somatic response amplitudes (Figure A-62A) due to reduced driving force, but this effect was limited predominantly to larger inputs (> 5 nS), and was much more pronounced in voltage than current clamp.[13] The presence of the spine also had a small effect on synaptic kinetics (as can be seen for rise times in Figure A-62B), but again this effect was limited to large amplitude, slow inputs and primarily to voltage clamp.

In contrast, omission of the interposed spine will result in errors in the simulated

[13]Note that the simulations here do not incorporate NMDA receptors.

subsynaptic voltage. Due to the higher input impedance at the spine head, a spine synapse will generate a much larger subsynaptic (spine head) voltage than will a synapse placed onto the shaft below (Figure A-62C). This effect is identical in current and voltage clamp, as the voltage escape for distal synapses in current clamp is the same as the subsynaptic voltage response there in current clamp [242]. There is also a much larger degree of voltage attenuation from the spine head to the shaft than vice versa. If a synapse is put onto a spine head (Figure A-62D,E), the resulting spine head voltage will be strongly attenuated by the spine neck, yielding a much lower voltage in the shaft below. In contrast, there is no voltage attenuation in the other direction; the voltage response to a shaft synapse will be identical in the subsynaptic shaft and in a spine head above [293]. The shaft voltage with a shaft synapse will be intermediate between the spine head and shaft voltages with a spine synapse (Figure A-62D,E).

Together these results indicate that while placing synapses directly onto the dendritic shaft instead of onto an interposed spine will not incur significant errors in the synaptic amplitudes or kinetics measured at the soma, at least over the range of synaptic conductances used here. There will be errors in the simulated subsynaptic voltage, which must be kept in mind when considering the implications of the results presented here for the activation of dendritic nonlinearities.

A.4 Effects of synaptic kinetics.

Electrotonic filtering occurs essentially because the membrane circuit of the cell forms a low-pass filter. How significant an effect this filter will have on synaptic signals depends, of course, on the frequency characteristics of the signals themselves. Figure A-63A demonstrates the fact that fast synaptic inputs will be more significantly attenuated by the cable than will slow ones [242, 150]. Two equal-conductance inputs with different kinetics were placed onto the soma and two dendritic locations of a simple soma-cable model. At the soma, their amplitudes were identical. However, as the synapse moved farther out the dendrite, the faster input was much more

severely attenuated than the slow one. The quantitative effect of filtering by cables of different electrotonic structure; as well as different values of the series resistance (in combination with the whole-cell capacitance, see below), will depend on the absolute frequency-dependence of the synaptic current. I have therefore plotted in Figure A-63B the power spectra generated by several sets of synaptic kinetics (parameters given in figure legend), from the Fourier transform of Equation 2.1 (f in Hz, τ_R,τ_D in ms):

$$G(f) = \frac{1}{Norm}\left(\frac{1}{2\pi f j + \frac{1000}{\tau_D}}\right) - \left(\frac{1}{2\pi f j + \frac{1000}{\tau_R}}\right) \quad (A.1)$$

The same data are shown normalized for clarity in Figure A-63C. Only the slowest set of kinetics has essentially no power above 500Hz, and the fastest two sets (those most resembling real mEPSCs) have significant power up too 2000Hz. In the best case, the filter formed by the series resistance (see below) will have a cutoff of 2000Hz, in the worst (but still commonly considered experimentally usable, e.g. a large cell with a middling R_s) case it might be as low as 100Hz. The cell membrane itself, in current clamp, will act as a filter with a frequency cutoff on the order of 100Hz, and it falls off very rapidly in voltage clamp as well; thus even these slower synaptic inputs are not immune to cable effects (as shown in A).

A.5 Effects of passive parameters.

A linear membrane model is controlled by three passive parameters: R_m, the intrinsic resistivity of the cell membrane, C_m, the capacitance per unit area of membrane, and R_i, the intracellular axial resistivity; any or all of these might vary within a cell. A vast body of literature is devoted to estimating these parameters [15, 14, 25, 103, 36, 46, 51, 101, 90, 99, 98, 104, 135, 139, 150, 154, 203, 206, 204, 211, 226, 271, 270, 274, 293], however in spite of 40 years of effort, the accepted values of these parameters are still in flux. This figure compares the shape of somatic responses recorded at the soma of a simple cable model for several synaptic input sites and two sets of passive pa-

rameters: the "standard" parameters used for a baseline in the simulations presented here (R_m 40,000 Ωcm^2, R_i 100 Ωcm, C_m 1.0 $\mu F/cm^2$ [243]), and those estimated recently for cortical pyramidal cells by G. Major (R_m 50,000 Ωcm^2, R_i 300 Ωcm, C_m 0.7 $\mu F/cm^2$ [150, 152, 153, 151, 154, 104]). Most of the contention over the "true" value of passive parameters has centered on the value of R_m (see discussion of somatic shunt, Section A.1.2, above). Only this recent work has brought into question the assumed values for the other two parameters.

The effects of these parameters on synaptic response waveform for different input locations can be seen clearly using a simple cable model, and comparing "standard" and "GM" parameters, which differ in R_m, R_i, and C_m. In voltage clamp, (R_s=0), the somatic response is independent of these parameters, and is identical to the underlying synaptic current. However, as the synaptic input is moved out the cable, it is more severely slowed and attenuated with the "GM" parameters than the standard values. This is due to the increased value of R_i, which is sufficient to strongly attenuate the propagating currents in spite of the increase in R_m which should protect them from loss of amplitude (but not slowing of kinetics [242]). In striking contrast, in current clamp the increased input resistance due to the change in both R_m and R_i results in a much larger response with the "GM" parameters to both the somatic and proximal dendritic input. The response also rises faster due to the decrease in C_m. Only at the more distal input location does the increase in R_i succeed in attenuating the "GM" response more than the standard one. This result is extremely interesting in light of the fact that a) the "GM" parameters are the average best fit for the responses in cortical pyramidal cells in an extensive study [150, 154], and b) the simulations in chapter 4, which were performed using "standard" parameters, consistently gave current clamp responses that were too small, while voltage clamp responses were within observed ranges or if anything slightly too large. As discussed in the description of Figure 4-38, the "GM" parameters may allow a much better fit of the experimental distribution of mEPSCs and mEPSPs.

Comparing cumulative amplitude distributions generated for various sets of pas-

sive parameters in a full cell model in current (Fig. A-64C) and voltage clamp (Fig. A-64D) shows clearly that for these rapid synaptic inputs, the overwhelming determinant of response amplitudes is the axial resistivity, R_i, and to a lesser extent, C_m. They are almost entirely independent of membrane resistivity. Attenuation of the peaks of these rapid currents occurs almost entirely through capacitive filtering, especially in current clamp where capacitive filtering is so important, and via low-pass filtering by the axial resistance of the cell. Almost none takes place as a result of passive loss across the membrane conductance of the cell. In contrast, attenuation of lower-frequency parameters like area are much more likely to depend on the value of R_m. The effects of these parameter changes on simulated response distributions can be seen in Figure 4-38.

A.6 Effects of series resistance.

A.6.1 Series resistance and filtering.

Access, or series resistance, refers to a resistance in series with the cell membrane in the form of the resistance of the recording pipette, possibly increased by partial clogging with cell membrane or other cellular detritus [229, 220, 222]. Series resistance has two effects on the responses recorded through the pipette. The first, and most commonly known, is a voltage error [229, 220]. The recording amplifier is clamping the potential at the end of the pipette. However, the access resistance between the pipette end and the cell interior allows a voltage drop to exist between these two points; thus the cell's interior will not be clamped to $V_{command}$, but instead offset from that by the voltage drop across the access resistance. This voltage drop, in turn, is a function of the command current flowing across R_s: $V_{drop} = R_s I_{command}$ by Ohm's law. In the case of the command currents, synaptic currents, and series resistances used here, however, this voltage drop is not terribly large - only 1-2mV at resting potential. The DC voltage drop can become significant when an attempt

is made to depolarize the cell significantly, for instance to reverse mEPSCs. This effect of series resistance is much more important when very large command currents are necessary: when synaptic currents are very large (e.g. 1 nA synaptic currents in cochlear nucleus cells [268]), or when an attempt is made to voltage-clamp large active currents (e.g. Na^+ currents [212]); or when series resistance is very high, as in the case of sharp electrode recording. In the latter case, the amplifiers typically used for such applications contain bridge circuitry for compensating the DC voltage effects of series resistance in current clamp, and voltage clamp is performed using switch-clamp circuitry, where current is never being passed while voltage is recorded, thus eliminating this source of error.

A second effect of series resistance, and one much more relevant to this study, is that the resistance in series with the membrane capacitance acts as a low-pass, RC filter. The cutoff for this filter is approximately $1/R_sCm_{cell}$, where R_s is the access resistance, and Cm_{cell} is the total cell capacitance. Given the large size of cortical pyramidal cells, this term can be quite large; the effect of this type of filtering can be quite significant even with very low values of R_s (Fig. A-65) [231]. As series resistance increases, the increasingly filtered responses measured at the soma are attenuated in their amplitudes and slowed in their kinetics similarly to the effects of cable filtering. Careful comparison shows that this effect is most severe for the largest, fastest events – those arising from locations closest to the soma. The effect of series resistance is different for two groups of parameters: amplitude and slope; and rise time, half width, and area. While increasing R_s affects the values of all parameters [242], the relative effect on amplitude and slope (the "high-frequency parameters", see Section 4.3.4) is much more pronounced, and much different for the proximal vs distal synaptic inputs. In the case of the other parameters, the effect is more of a uniform increase in values (for rise and width, decrease for area) across all locations.

Additionally, in the presence of a non-zero series resistance, the dendrites are no longer entirely isolated from one another in voltage clamp. In Section A.2 it was noted that perhaps the most pronounced practical difference between current and

voltage clamp is the interaction between dendrites in the former and their individual isolation in the latter. However, because the filtering effects of R_s depend on the total cell capacitance. the presence of the other dendrites in and of itself increases the degree of filtering, and hence the attenuation of synaptic currents. In this figure, the same somatic and proximal dendritic inputs are simulated with R_s=5 in the presence (black) and absence (gray) of a somatic load representing the other dendrites. in the former case the synaptic responses at the soma are attenuated and slowed relative to the unloaded case for the same value of series resistance. With R_s=0, the traces would be identical with and without load. This interaction between dendrites is a passive one. An active interaction between dendrites can exist in the presence of non-zero series resistance if a synaptic current into one dendrite is large enough to cause a significant voltage error at the soma, this can effect the measured response to a synaptic input in another dendrite. In either case, however, the interaction between dendrites is still much more limited and artificial than in current clamp.

A.6.2 Parameters controlling the effects of series resistance.

The quantitative effectiveness of series resistance in filtering synaptic inputs depends on a number of parameters. It is not possible to compare recordings simply on the numeric value of their series resistance, without also making sure they are matched on these other parameters as well.

Morphology: cell size effects the filtering properties of series resistance. As noted in the caption to Figure A-65C, simply an increase in cell size (as with adding dendrites) increases the total cell capacitance, and hence decreases the cutoff frequency of the filter formed by the series resistance and the cell membrane [231]. This is independent of synaptic location, and is not due to additional cable filtering of synaptic inputs in a larger cell; it is due purely to the simple addition to total membrane.

In fact, addition of membrane close to the soma is likely to have more of an effect than, say, elongation of dendrites: addition of membrane distally is shielded from the somatic recording by the axial resistivity of the dendrites. This effect is demonstrated for a somatic synapse onto a simple cable model. The response to a somatically-placed synapse is shown for three values of the series resistance in the case of a normal cell and a cell with a soma twice as large (implemented by increasing the specific capacitance of the somatic membrane 4-fold). With R_s=0, the responses are identical for both cells (fastest, largest response). However, with R_s=5 (gray traces) and R_s=20 (dark gray/black traces), there is a marked difference between the somatic responses measured in the small and large cells; in the large cell the response is slowed and attenuated as by a much larger value of R_s. The difference would also exist in a model composed only of an isopotential soma. This means that it is very difficult to use the numeric value of R_s as a measure of comparability of recordings between cell types of different sizes; the "identical" R_s values may actually be responsible for very different degrees of filtering.

Location: Series resistance filtering effects are more severe for proximal synaptic locations. The response to a proximal and a distal synaptic input is shown for three values of R_s. For the proximal input, its amplitude is sharply attenuated by increasing R_s. For the distal input, however, while its time course is somewhat slowed, its amplitude is much less affected, and both effects are much less severe than that seen for the proximal input. This is because most of the high-frequency components of this synaptic input have already been filtered away by the dendritic cable, so there is not much left for the series resistance to affect. This also means that series resistance will severely mask the effect of cable filtering - with high enough R_s, the difference between the proximal and distal input due to their electrotonic location would disappear as the proximal input was filtered down to match the distal one; the absence of indicators of cable filtering in high series resistance recordings is therefore not evidence that filtering does not occur.

Kinetics: Series resistance will attenuate fast events much more severely than slow ones (the same is true for cable filtering of events with different kinetics (see Fig. A-63, [242]). Figure A-66C shows the effects of increasing R_s on faster and slower somatic inputs. The faster input (right), which has much more high-frequency energy in its waveform, will be significantly attenuated, while a slower event will be relatively unaffected by increasing R_s (the same is true for cable filtering of events with different kinetics, see Figure A-63, [242]).

Passive properties: As noted above, the degree of filtering due to R_s depends on the total cell capacitance, which depends both on C_m, and on the values of R_m and R_i, which determine how much of the cell's capacitance is "seen" by the somatic electrode. Here, again a somatic input is simulated for three values of R_s and two sets of passive cellular parameters: standard (left), and "GM" (right) (see caption to Figure A-64). The latter, with its lower value of C_m and higher value of R_i, undergoes slightly less attenuation with increasing series resistance relative to the standard parameters.

A.7 Effects of detection threshold.

If we are to use spontaneous events as a metric for the range of input variability seen by a cortical neuron, and more importantly, as a marker of the "standard" size of an input, it is important that we are detecting all, or almost all, of the spontaneous events. If there is in reality a large population of very small events we do not detect, this will cause us to strongly overestimate the functional convergence to a cortical cell.

Section 3.3.2 demonstrated this problem, by showing the effect of changing holding potential (and hence synaptic driving force and sEPSC size) on the number and characteristics of detected sEPSCs. The loss of events behind the "detection window" as the cell was depolarized made detailed analysis of the voltage dependence of these events difficult. Figure 5-46 showed that the detection method used in this study does

approach the limits of the experimental noise – by lowering our detection thresholds we pick up few or no additional true events, and instead only begin to detect noise fluctuations.

The real question, however, is not whether we could do any better with a better detector, or whether we will run into problems at depolarized potentials. The question is, at our standard holding potential at -70 mV, which is close to the resting potential of the average cortical cell so the relevant voltage for the larger question at hand; are we seeing all of the spontaneous events present?

Figure A-67 suggests that while doing so is difficult if events are not large, that events are in fact large enough so that we are capable of detecting them. First, we can estimate over what region of the cell we can in fact see events of a certain size by assuming a nominal detection threshold of 5 pA, and asking, for various values of the synaptic conductance, at what point on the dendritic tree we would no longer be able to detect a synaptic input at the soma (Fig. A-67A). For an input with a peak conductance of 100 pS, the answer is pretty dismal – we wouldn't be able to detect it unless it was less than 50 μm from the soma, in the region where there are very few excitatory synaptic inputs.[14] For a larger input (1 nS), more of the size suggested both by the events measured here and in other recent studies [17], the answer is somewhat reassuring – we should be able to "see" it up to about 500 μmaway in dendritic path distance, a value which encompasses most of the dendritic tree of even the largest cells (also see Figure 6-53).

The question remains, then, how large are the synaptic inputs? Figure A-67B shows clearly that we are in fact probably not losing a large population of events below the level of the noise. If instead of depolarizing the cell from -70, we hyperpolarize it and increase the synaptic driving force, we should expect to see both an increase in EPSC size, and, if we are losing events, an increase in EPSC number as events come out from under the detection threshold. When we move the cell from -70 to -90 mV,

[14]The nominal conductance of a single AMPA channel is 10 pS.

no such occult population appears. There is an increase of only about 2% in the total number of events in a fixed time window, indicating that, in fact, at -70 the bulk of the EPSC amplitude distribution is visible. There is a slightly larger increase in number of EPSCs detected as the cell is further hyperpolarized to -110 mV, indicating that there may in fact be a small population of extremely small synaptic inputs; but again, these events are not numerous enough to change the shape of the amplitude distribution or the conclusions of this study.

A.8 Figure Legends

Figure A-57: Effects of morphology. A. Effects of cable diameter on current clamp peak amplitudes and attenuation. In a soma and cable model, a single synapse is moved sequentially out the dendrite, and the peak amplitude of the response at the soma is plotted as a function of synapse position for several values of dendritic cable diameter. B. Diameter tuning curves. The EPSP amplitudes shown in A are replotted as a function of dendritic diameter for 4 synaptic locations (indicated schematically on the inset). Cable structure (A,B): soma diameter 20 μm, cable length 1000 μm, R_m 50,000 Ωcm^2, R_i 200 Ωcm, C_m 1.0 $\mu F/cm^2$. C. The shape of the current response at the soma is affected by the detailed branching structure of the cell. Responses to the same synaptic input at the same location on the dendritic cable are compared for three cases (indicated schematically): branch before the synapse, branch after the synapse, and no branching. Cable structure: soma diameter 20 μm, cable length 1000 μm, cable diameter 1.0 μm, branch length 200 μm, branch diameter 0.5μm, R_m 40,000 Ωcm^2, R_i 100 Ωcm, C_m 1.0 $\mu F/cm^2$. D. Effects of other dendrites. The response to a synapse on the dendrite and the soma are shown in the case of a pure soma and cable model (black lines), and when the rest of the dendritic tree, in the form of a lumped load is added (gray lines). Cable structure: soma diameter 20 μm, cable length 1000 μm, cable diameter 1.0 μm, load length 500 μm, load diameter 4 μm, R_m 40,000 Ωcm^2, R_i 100 Ωcm, C_m 1.0 $\mu F/cm^2$. E. End-effects in voltage clamp. The response at the synapse (squares) and at the soma (triangles, shown alone to right) to a synaptic input moved sequentially out the dendrite in the standard soma and 1000 μm cable model, that model with an added load (load length 1800 μm, load diameter 8 μm), and the model plus load with the dendritic cable shortened to 250 μm, similar to the maximal extent of a pyramidal cell's basal dendrites. As in D, with perfect voltage clamp, there is no difference between the loaded and unloaded case. F. Current clamp responses for the models described in E. The response for all three models at soma and at synapse is shown at left, the somatic response of the models with incorporated load can be seen expanded at right.

Figure A-58: Effects of somatic shunt: comparison to sharp electrode studies. A. Cumulative probability distributions of spontaneous events recorded from pyramidal cells with sharp electrodes (dotted lines at left, n=2, 4M KAc), whole-cell recording under standard conditions (solid lines in center, n=4, KGlu-based recording solution), whole-cell recording in the presence of 50 μm bicuculline, which increases spontaneous activity and the selectively increases the number of large events (dashed line with asterisks, KGlu-based solution), and whole-cell recording from an interneuron, a much smaller cell with a higher input resistance than the pyramidal cells (dashed line with triangles, KGlu-based recording solution, upper layer V. B. Simu-

lated current clamp amplitude distributions generated according to the methods of Chapter 4 (synaptic conductance: 1 nS). An additional shunt conductance was placed in the soma, with a reversal potential the same as the resting membrane potential [36, 66, 69, 101, 152, 198, 199, 218, 265, 288]. Cumulative amplitude distributions are shown for several values of the shunt conductance (0-20 nS) , they are simply shifted to the left rather than scaled as in the experimental case. C. Effects of shunt on larger inputs. Synaptic inputs were 5 nS. All other conditions were the same as in B. D. Effect of shunt on other parameters. For each parameter, the value in the unshunted condition is plotted against the value of that parameter for that synapse with a 10 nS somatic shunt. The solid lines indicate the identity relationship.

Figure A-59: Effects of errors in morphological reconstruction. A. The dendritic diameters of the cat layer V cell shown in Figure 4-22C were scaled to 80% of their reconstructed values, and the resulting voltage-clamp amplitude distribution for the cell is shown in A (compare to Figure 4-22C). B. As in A, except diameters scaled to 120% of their measured values. C. Peak amplitudes vs distance are plotted for the two amplitude distributions shown in A and B. D. Cumulative amplitude distributions are directly compared for control, the two diameter scalings shown in A and B, and for an overall shrinkage compensation, in the form of a 10% increase in dendritic diameters and lengths. This was implemented as a linear shrinkage correction, scaling all X,Y, and Z values by 110% (0,0,0, is centered on the soma). In practice, this is the appropriate correction for a linear shrinkage of the slice/sections, and it will result in dendritic lengths being scaled by more or less than 10% depending on their orientation in the tissue. E, F. Effect of diameter change on the values of all of the shape parameters, shown for a simple soma-cable model in current clamp. Cable diameters were 0.5, 1.0, and 1.5 μm , all other parameters were as in Figure A-57A,B.

Figure A-60: Relationship between current and voltage clamp. A. Synaptic inputs along the length of a simple dendritic cable were simulated in both current and voltage clamp for three sets of synaptic kinetics: fast (τ_R= 0.1 ms, τ_D= 1.0 ms), medium (τ_R= 0.2 ms,τ_D= 1.5 ms), and slow (τ_R= 0.5 ms,τ_D= 3.0 ms). Left: The peak amplitude measured at the soma in current clamp is plotted against that in voltage clamp for each event type at each location. The solid line shows the predicted steady-state relationship between voltage and (DC) current injected into the soma based on the cell's input resistance ($V = IR_{in}$). Right: The area measured at the soma in current clamp is plotted against the area measured in voltage clamp (the black line shows the identity relationship). The unusually low values of voltage clamp area for a few events with slow kinetics are due to premature termination of the simulation before the event had really finished. Note that in this graph only, current clamp values are on the abscissa. B. A similar relationship is shown for

increasing values of the series resistance in the voltage-clamp measurements. Left: Voltage clamp peak amplitude is plotted against current clamp amplitude for the same input, for increasing values of the series resistance used in voltage clamp. The solid line shows the relationship predicted from R_{in} assuming a steady-state input current. Right: The same relationship is plotted for area in voltage clamp and current clamp; the black line shows the identity relationship. The relationship between these two variables is independent of the value of R_s. In fact, the relationship between these two variables is the identity relationship, but the values of voltage clamp area measured here are underestimated due to using too short of an integration period (this is the same error as in A, Right; note exchanged axes in A). The error has been left here in order to demonstrate its affect on area measurements. The largest area values, those for the most proximal and hence shortest-duration events, are correct.

Figure A-61: Effects of spine incorporation function of parameter distributions. A. Distribution of spines with distance, assuming a constant spine density (1.4 spines/μm) for all dendrites in a medium-sized rat layer V cell (Figure 4-21C). B. Cumulative probability distribution for the location of spines from the histogram in A. More than 85% of spines, and hence probably a similar fraction of excitatory synapses, are within 200 μm of the soma. C. Effect of different assumptions about the distribution of spines in both the incorporation of spine membrane (see General Methods) and the generation of amplitude distributions. Cumulative amplitude distributions were generated in voltage clamp for the cell used for A,B. Three underlying spine densities are used: one constant, 1.4 spines/μm, and two diameter-dependent, $(1.1 + 1.3\ diameter)$ *spines*/μm [150], and $(-0.39 + 2.6\ diameter)$ *spines*/μm [134]; all of these generate somewhat higher spine densities than the actual spine counts for this particular cell.[15] D. Effects of spine density assumptions on current clamp amplitude distributions. Cumulative amplitude distributions generated in current clamp using the same conditions as in B. One additional condition was used: a diameter-dependent spine incorporation function was used, but the histogram was generated assuming a constant spine density. E. Effects of spine density in a different cell. Using a diameter-dependent spine density function in a large rat layer V cell (shown in Fig. 4-22A) generates a larger number of smaller events from the distal dendrites. F. Amplitude histograms for the cases shown in E. Constant spine density histogram is on top. The additional small points appear as a bump at the left end of the histogram. In practice, such events would probably be below the experimental detection threshold.

[15]Spine counts were not routinely made do to the difficulty in adequately resolving spines and accurately correcting for occlusion, etc. I have therefore taken the approach of relying on the work of others who have devoted significant time and effort into getting it right.

Figure A-62: Effects of spine input on parameters of synaptic response. Effects of interposed spine on synaptic response measured at soma. A. The peak somatic amplitude in current and voltage clamp is measured in response to a synaptic input of varying kinetics placed onto a basal dendritic spine (open squares) and onto the dendritic shaft immediately underneath it (filled circles), as a function of synaptic conductance. B. Rise times at the soma are plotted for the same simulations shown in A. Simulations in A and B incorporated a spine with head diameter 0.65 μm, head length 0.65 μm, neck diameter 0.15μm, neck length 1.2 μm, placed onto the middle section of a basal dendrite of a rat layer V pyramidal cell (Figure 4-21B). Synaptic kinetics used were (τ_R, τ_D(ms)): 0.1,1.0; 0.2,1.5; 0.3,2.0; 0.5,3.0. C. Subsynaptic voltage for the simulations shown in A and B. D,E. Voltage transfer between spine and shaft. An input with the fastest kinetics used in A-C was placed onto the basal spine from A-C (D) and a distal apical spine of the same size (E), and onto the dendritic shaft beneath each spine. The peak amplitude of the current clamp voltage response was measured at the soma, shaft, and spine head in both cases. As shown in A, the somatic voltage is similar in both cases. If the synaptic input is onto the spine head, the voltage in the head (black squares) is much higher than that in the underlying shaft (gray diamonds) . If the synapse is on the dendritic shaft, the subsynaptic voltage and the overlying spine head voltage (overlying traces, dashed line) are identical.

Figure A-63: Effects of synaptic kinetics. A. Faster inputs are subject to more severe attenuation. Traces show the responses to fast (τ_R=0.1, τ_D=1.0 ms) and slow (τ_R=0.5, τ_D=3.0 ms) 1nS synaptic inputs onto the soma; and 0.1 and 0.6 λ out the dendrite of a soma-cable model (locations indicated by schematic). B. Power spectra of several candidate synaptic current waveforms, showing their frequency-dependence. τ_R, τ_D(ms) = 0.1,1.0; 0.2,1.5; 0.3,2.0; 0.5,3.0. C. Data in B, with each trace normalized to its value at 0 Hz.

Figure A-64: Effects of passive parameters. A. Effect of passive parameters on response shape in current (left) and voltage clamp (right). A synaptic input was placed onto three locations of a 1 λ-long cable model: the soma, and 0.1 and 0.5 λ along the dendrite. Responses with "standard" (R_m= 40,000 Ωcm^2, R_i= 100 Ωcm, C_m= 1 $\mu F/cm^2$) parameters are shown in black, those with "GM" parameters (R_m= 50,000 Ωcm^2, R_i= 300 Ωcm, C_m= 1 $\mu F/cm^2$) are in gray; input location is given by the symbols above (below) each set of traces and the model schematic (left). B. Cumulative amplitude distributions generated for the cell shown in Figure 4-21B for a variety of passive parameters, in both current and voltage clamp. C_m was 1.0 $\mu F/cm^2$ unless otherwise noted. Synaptic parameters for A and B: τ_R=0.1 ms, τ_D=1.0 ms.

Figure A-65: Effects of series resistance. A. An identical synaptic input was simulated on the soma and sequential locations on the dendrite of a simple cable model. These responses are plotted on top of each other, as the synapse is moved more distally, the responses at the soma are smaller and slower. This same set of simulations is repeated for 7 values of R_s, each set is displaced to the right from the previous one and plotted in a different shade of gray. The R_s value used is shown below. B. The simulations in A are quantified in terms of their synaptic shape parameters. For each location, the value of each parameter is plotted for each value of R_s. In some cases, the algorithm used to measure synaptic events was unable to determine that an event was present, it was so small and slow, in these cases the value is recorded as 0. C. In the presence of a non-zero series resistance, the dendrites are no longer entirely isolated from one another in voltage clamp. In this figure, the same somatic and proximal dendritic inputs are simulated with R_s=5 in the presence (black) and absence (gray) of a somatic load representing the other dendrites. With R_s=0, the traces would be identical with and without load. D. Cumulative probability distributions are shown for rise time, half width, area, and maximum slope for the cell shown in Figure 4-21B, for two values of R_s (0 and 10 $M\Omega$, all other parameters standard), demonstrating that the effects described in B also occur in a full cell model.

Figure A-66: Parameters controlling effect of series resistance. The parameters controlling the quantitative value of R_s. A. Morphology: cell size effects the filtering properties of series resistance. The response to a somatically-placed synapse onto a simple soma-cable model is shown for three values of the series resistance in the case of a normal cell and a cell with a soma twice as large (implemented by increasing the specific capacitance of the somatic membrane 4-fold). With R_s=0, the responses are identical for both cells (fastest, largest response). However, with R_s=5 (gray traces) and R_s=20 (dark gray/black traces), there is a marked difference between the somatic responses measured in the small and large cells. B. Location: series resistance filtering effects are more severe for proximal synaptic locations. The response to a proximal and a distal synaptic input is shown for three values of R_s. C. Kinetics: series resistance will attenuate fast events much more severely than slow ones. A somatic event is simulated with two different sets of kinetics (τ_R= 0.1,τ_D= 1.0 ms, left, and τ_R= 0.5,τ_D= 5.0 ms, right) for three values of R_s. For the faster kinetics (right), increasing R_s has a much more significant affect on the amplitude of the response. D. Passive properties: the passive properties of the cell help to determine the effectiveness of R_s. A somatic input is simulated for three values of R_s and two sets of passive cellular parameters: standard (left), and "GM" (right) (see caption to Figure A-64). The latter, with its lower value of C_m and higher value of R_i, undergoes slightly less attenuation with increasing series resistance relative to the standard parameters.

Figure A-67: Effects of detection threshold. A. Approximate distances (measured as dendritic path length from soma) from which most or all events can be detected, for 7 simulated cells, one of which was simulated with 3 spine distribution functions. The open bars show the distance at which all 0.1 nS inputs can be detected. The black bars show the distance at which almost all 1 nS inputs can be detected. The hatched bars shows the distance at which almost all 1 nS inputs can be detected with a series resistance of 10 $M\Omega$. Parameters as in Figure 4-21. B. Amplitude histograms for one cell recorded at several holding potentials. Same data as shown in Figure 3-5B.

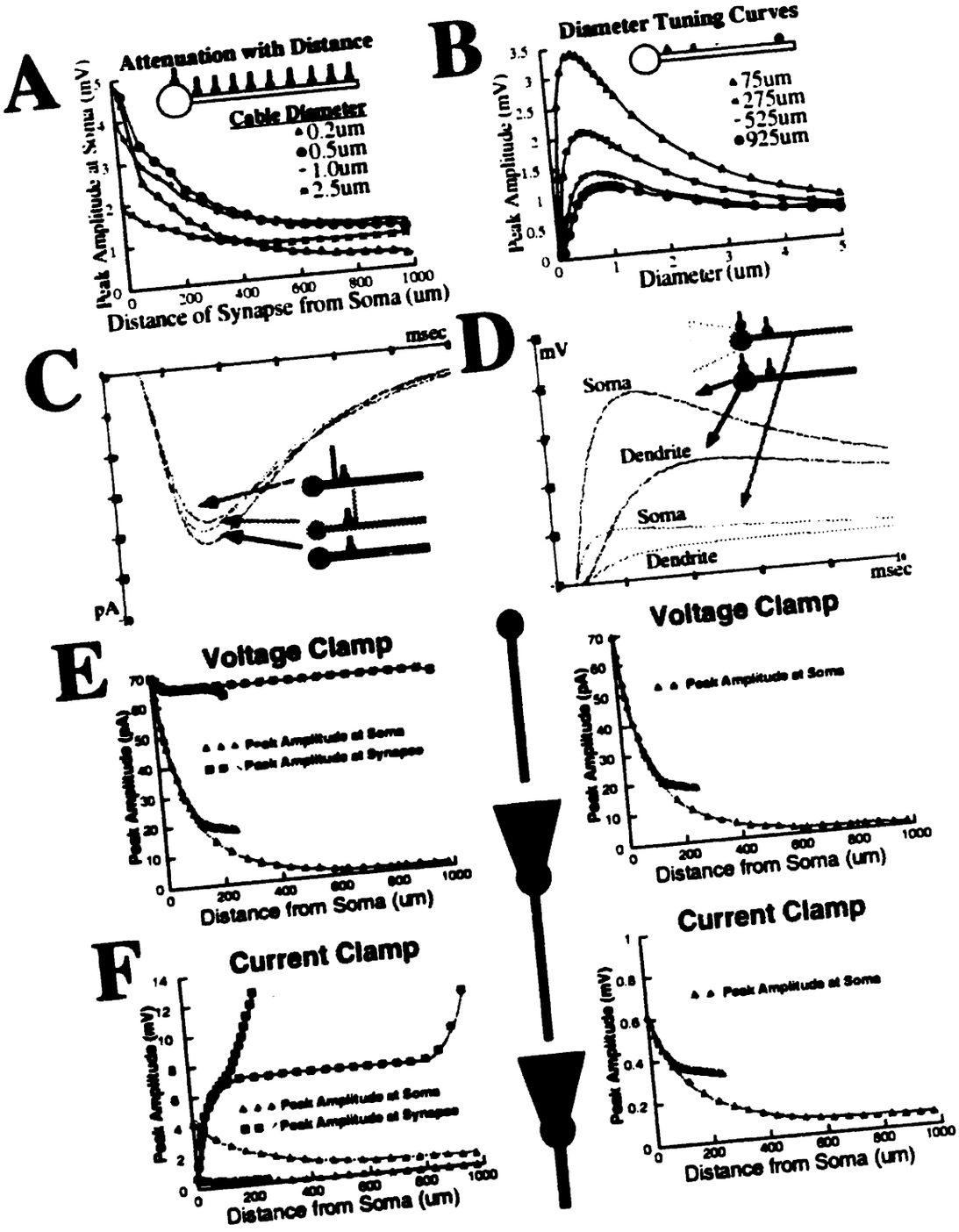
A
Attenuation with Distance
Cable Diameter
0.2um
0.5um
1.0um
2.5um
Peak Amplitude at Soma (mV)
Distance of Synapse from Soma (um)
B
Diameter Tuning Curves
75um
275um
525um
925um
Peak Amplitude (mV)
Diameter (um)
C
msec
pA
D
mV
Soma
Dendrite
Soma
Dendrite
msec
E
Voltage Clamp
Peak Amplitude at Soma
Peak Amplitude at Synapse
Peak Amplitude (pA)
Distance from Soma (um)
Voltage Clamp
Peak Amplitude at Soma
Peak Amplitude (pA)
Distance from Soma (um)
F
Current Clamp
Peak Amplitude at Soma
Peak Amplitude at Synapse
Peak Amplitude (mV)
Distance from Soma (um)
Current Clamp
Peak Amplitude at Soma
Peak Amplitude (mV)
Distance from Soma (um)

Fig. A - 57

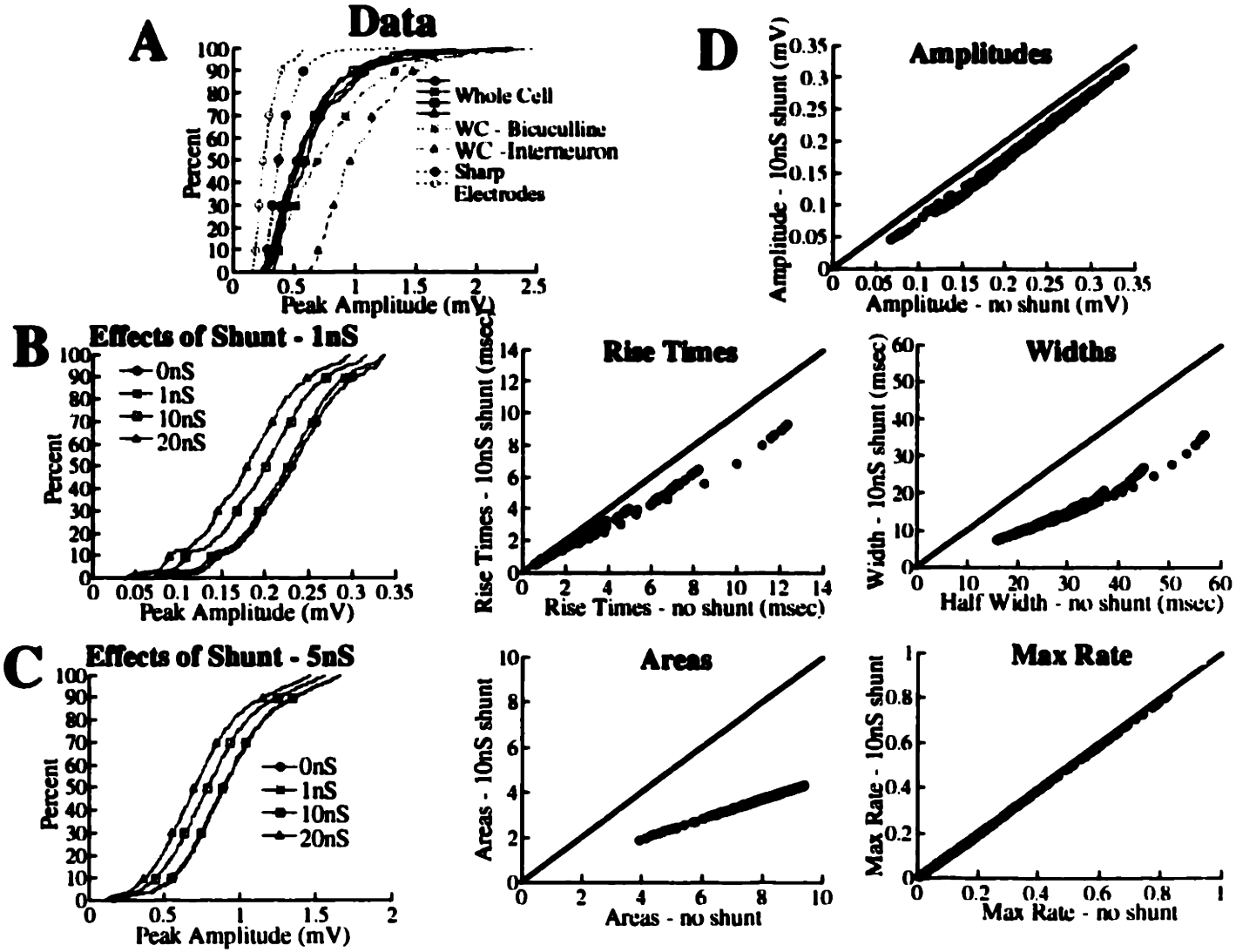
A
Data
Percent
Peak Amplitude (mV)
Whole Cell
WC - Bicuculline
WC -Interneuron
Sharp Electrodes
B
Effects of Shunt - 1nS
0nS
1nS
10nS
20nS
Percent
Peak Amplitude (mV)
C
Effects of Shunt - 5nS
0nS
1nS
10nS
20nS
Percent
Peak Amplitude (mV)
D
Amplitudes
Amplitude - 10nS shunt (mV)
Amplitude - no shunt (mV)
Rise Times
Rise Times - 10nS shunt (msec)
Rise Times - no shunt (msec)
Widths
Width - 10nS shunt (msec)
Half Width - no shunt (msec)
Areas
Areas - 10nS shunt
Areas - no shunt
Max Rate
Max Rate - 10nS shunt
Max Rate - no shunt

Fig. A - 58

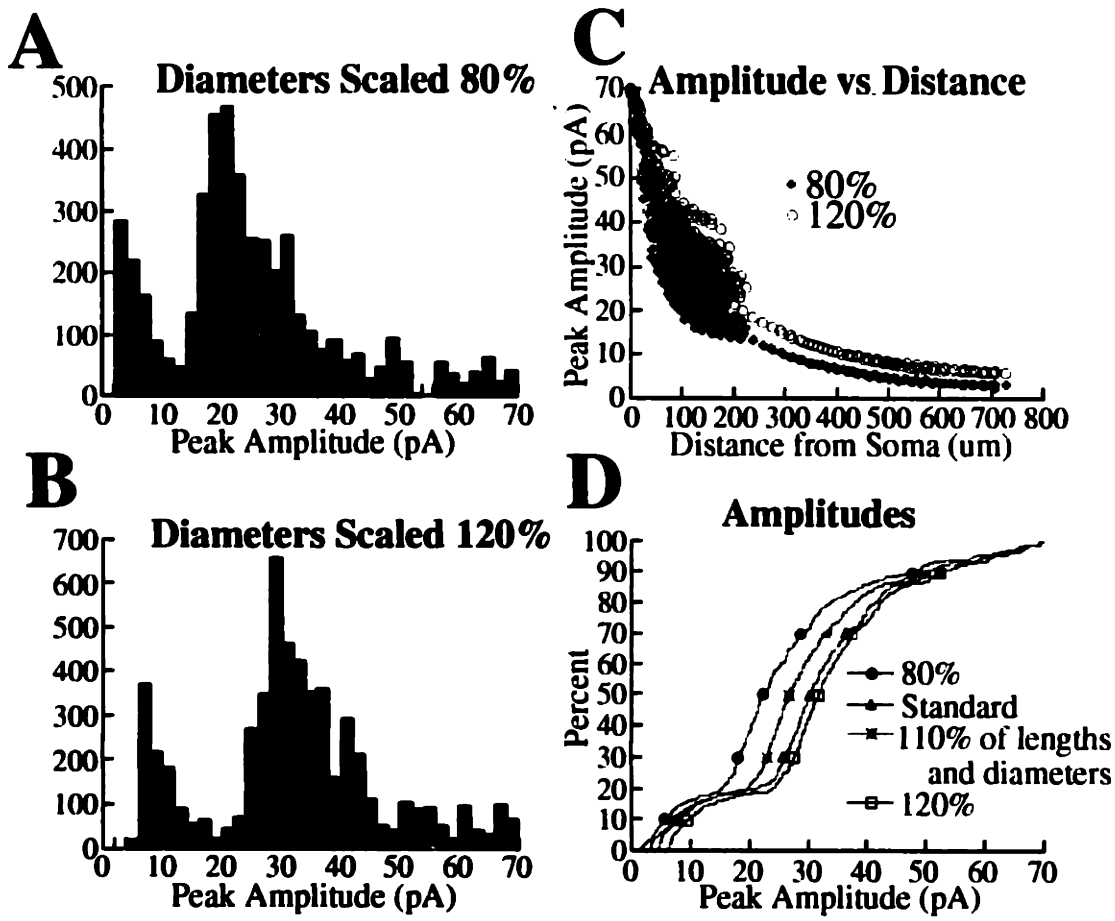

Effects of Diameter Change on Other Parameters

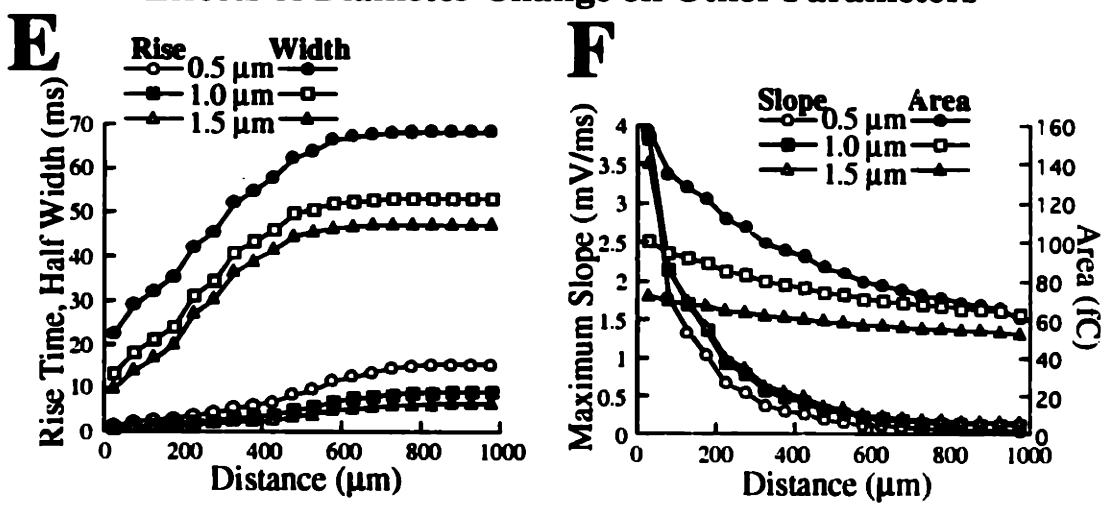

Fig. A - 59

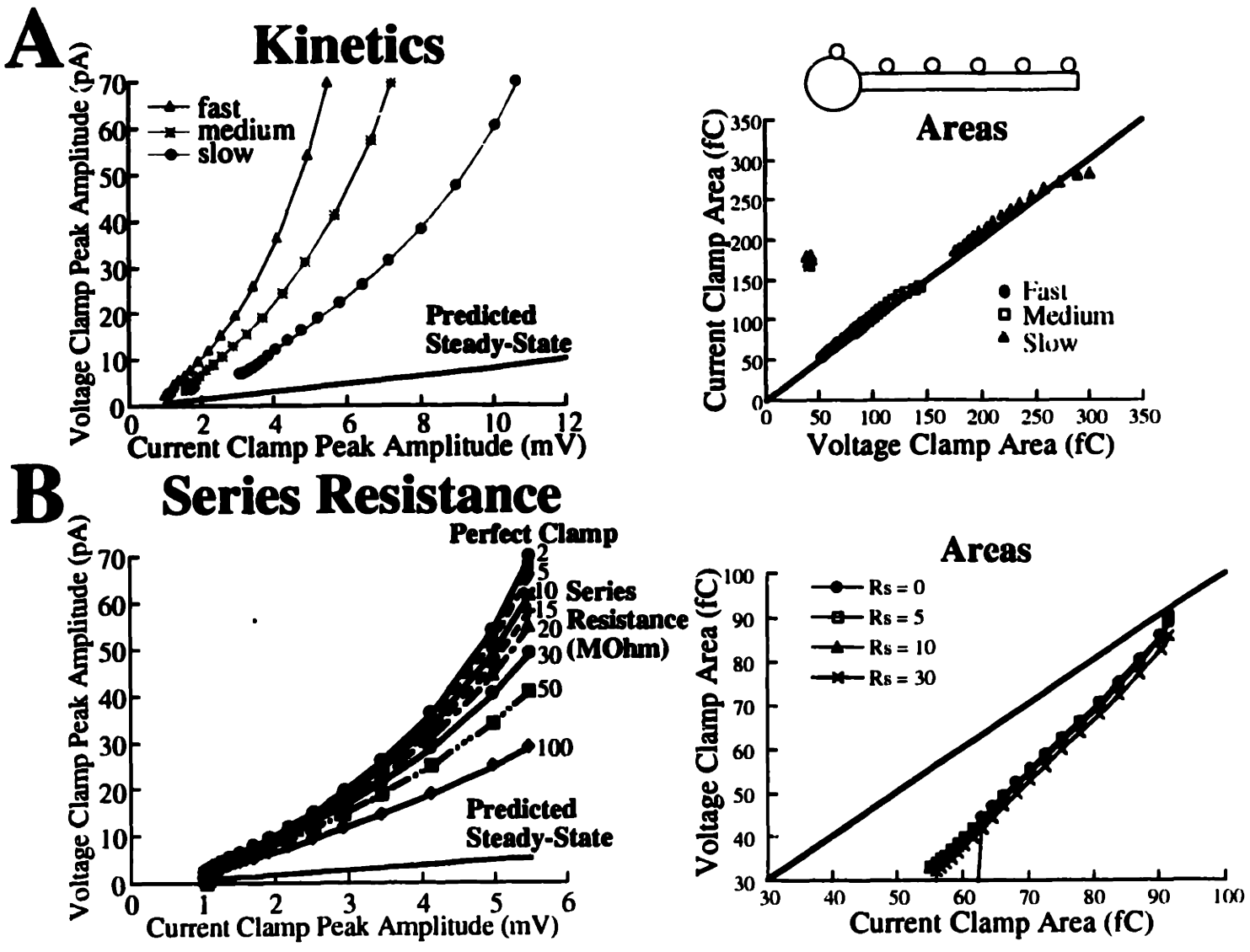
A
Kinetics
fast
medium
slow
Predicted
Steady-State
Voltage Clamp Peak Amplitude (pA)
Current Clamp Peak Amplitude (mV)
Areas
Fast
Medium
Slow
Current Clamp Area (fC)
Voltage Clamp Area (fC)
B
Series Resistance
Perfect Clamp
2
5
10
15
20
30
50
100
Series
Resistance
(MOhm)
Predicted
Steady-State
Areas
Rs = 0
Rs = 5
Rs = 10
Rs = 30
Voltage Clamp Area (fC)
Current Clamp Area (fC)

Fig. A - 60

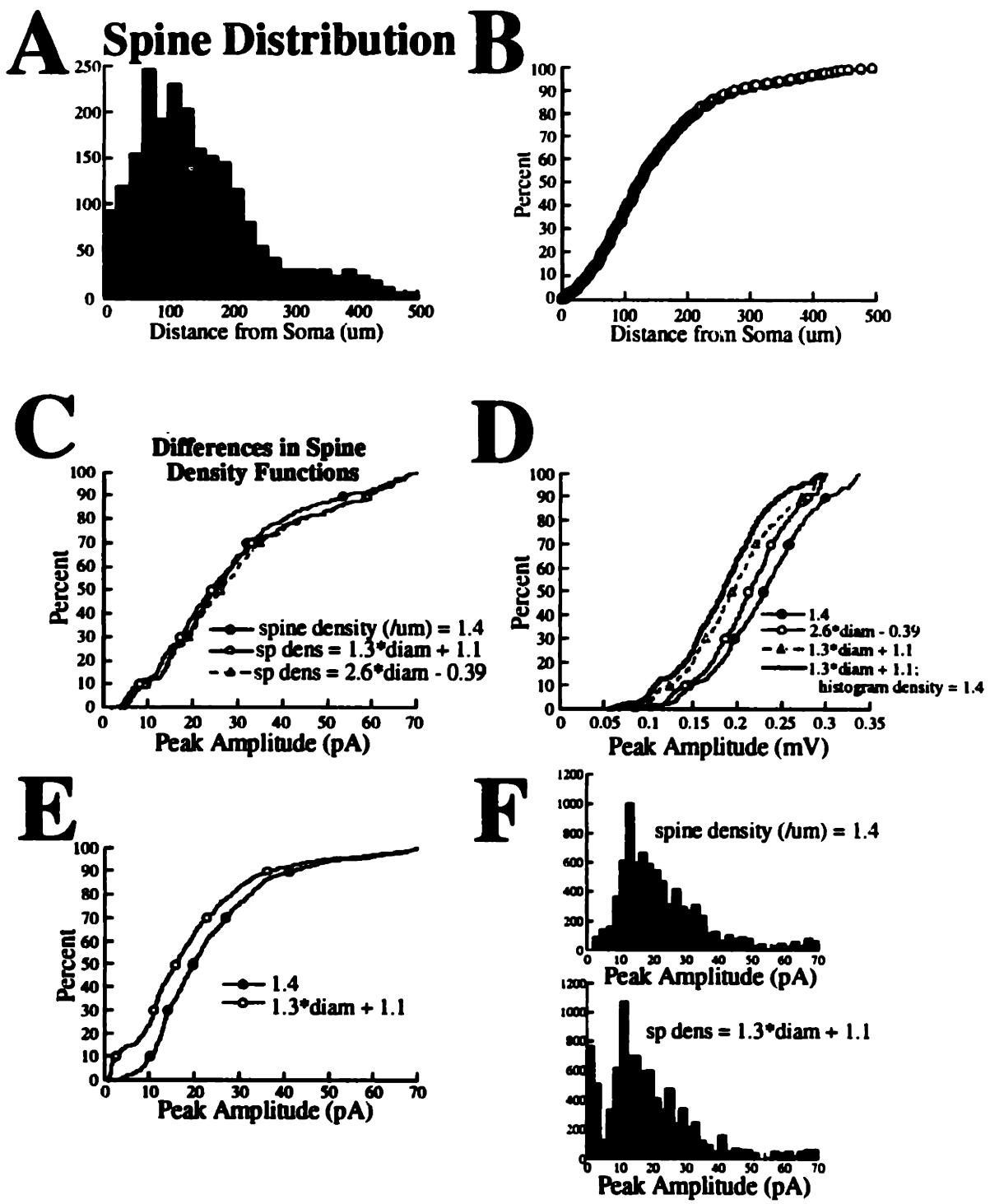
A
Spine Distribution
Distance from Soma (um)
B
Percent
Distance from Soma (um)
C
Differences in Spine Density Functions
Percent
spine density (/um) = 1.4
sp dens = 1.3*diam + 1.1
sp dens = 2.6*diam - 0.39
Peak Amplitude (pA)
D
Percent
1.4
2.6*diam - 0.39
1.3*diam + 1.1
1.3*diam + 1.1: histogram density = 1.4
Peak Amplitude (mV)
E
Percent
1.4
1.3*diam + 1.1
Peak Amplitude (pA)
F
spine density (/um) = 1.4
Peak Amplitude (pA)
sp dens = 1.3*diam + 1.1
Peak Amplitude (pA)

Fig. A - 61

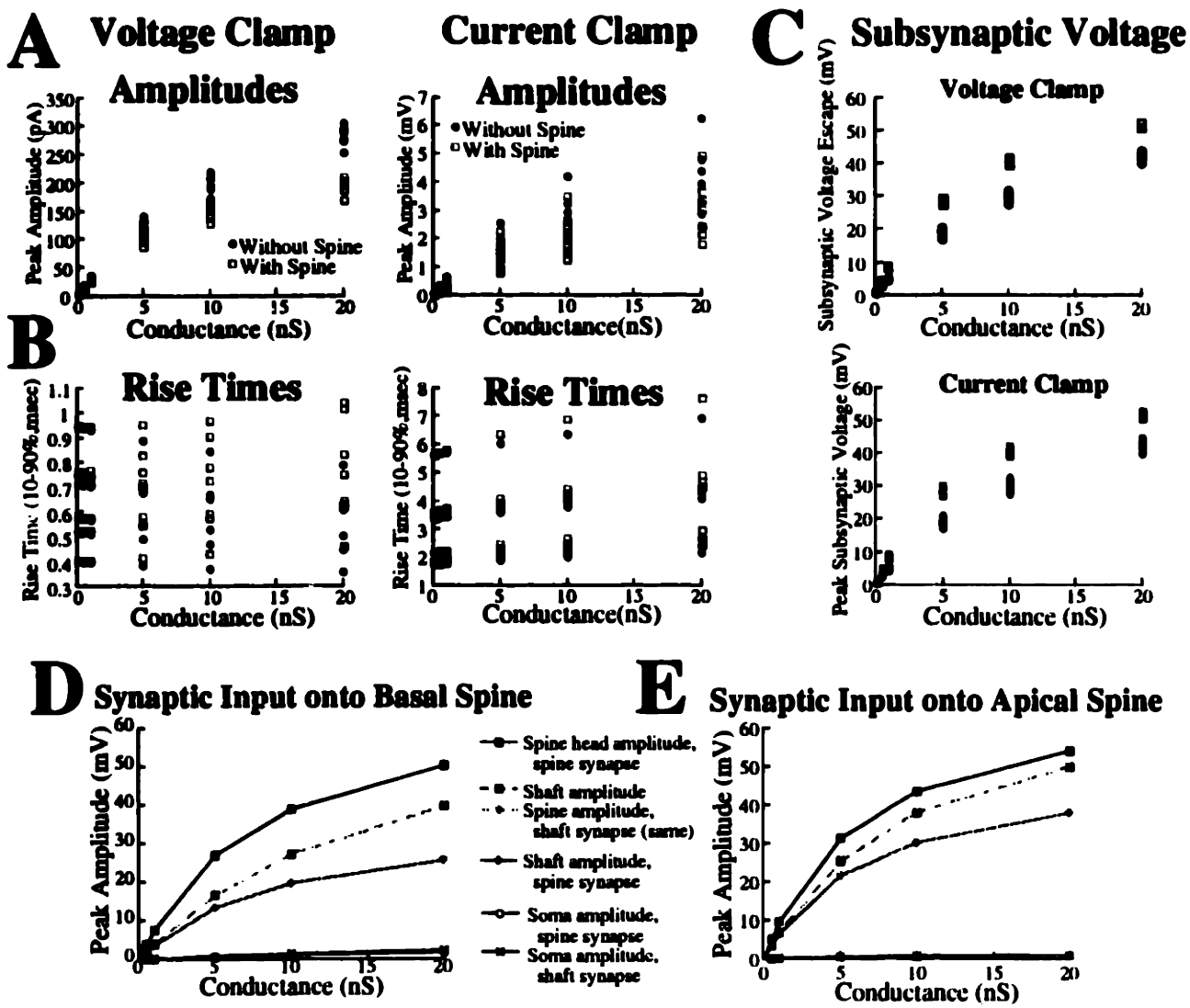
A
Voltage Clamp
Amplitudes
Peak Amplitude (pA)
Without Spine
With Spine
Conductance (nS)
Current Clamp
Amplitudes
Peak Amplitude (mV)
Without Spine
With Spine
Conductance(nS)
B
Rise Times
Rise Time (10-90%,msec)
Conductance (nS)
Rise Times
Rise Time (10-90%,msec)
Conductance(nS)
C
Subsynaptic Voltage
Voltage Clamp
Subsynaptic Voltage Escape (mV)
Conductance (nS)
Current Clamp
Peak Subsynaptic Voltage (mV)
Conductance (nS)
D
Synaptic Input onto Basal Spine
Peak Amplitude (mV)
Conductance (nS)
Spine head amplitude, spine synapse
Shaft amplitude
Spine amplitude, shaft synapse (same)
Shaft amplitude, spine synapse
Soma amplitude, spine synapse
Soma amplitude, shaft synapse
E
Synaptic Input onto Apical Spine
Peak Amplitude (mV)
Conductance (nS)

Fig. A - 62

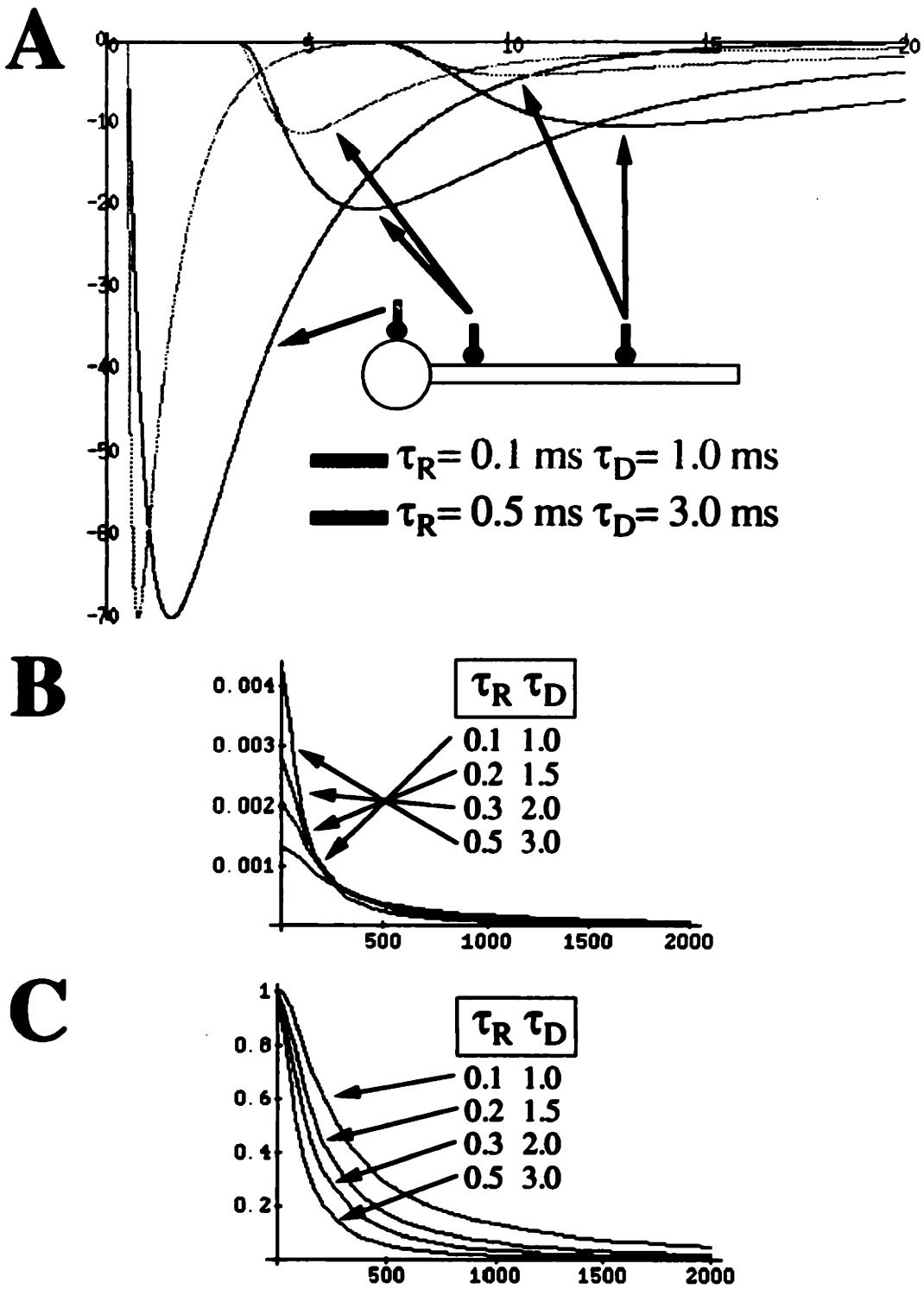
A
0
5
10
15
20
-10
-20
-30
-40
-50
-60
-70
τR= 0.1 ms τD= 1.0 ms
τR= 0.5 ms τD= 3.0 ms
B
0.004
0.003
0.002
0.001
τR τD
0.1 1.0
0.2 1.5
0.3 2.0
0.5 3.0
500
1000
1500
2000
C
1
0.8
0.6
0.4
0.2
τR τD
0.1 1.0
0.2 1.5
0.3 2.0
0.5 3.0
500
1000
1500
2000

Fig. A - 63

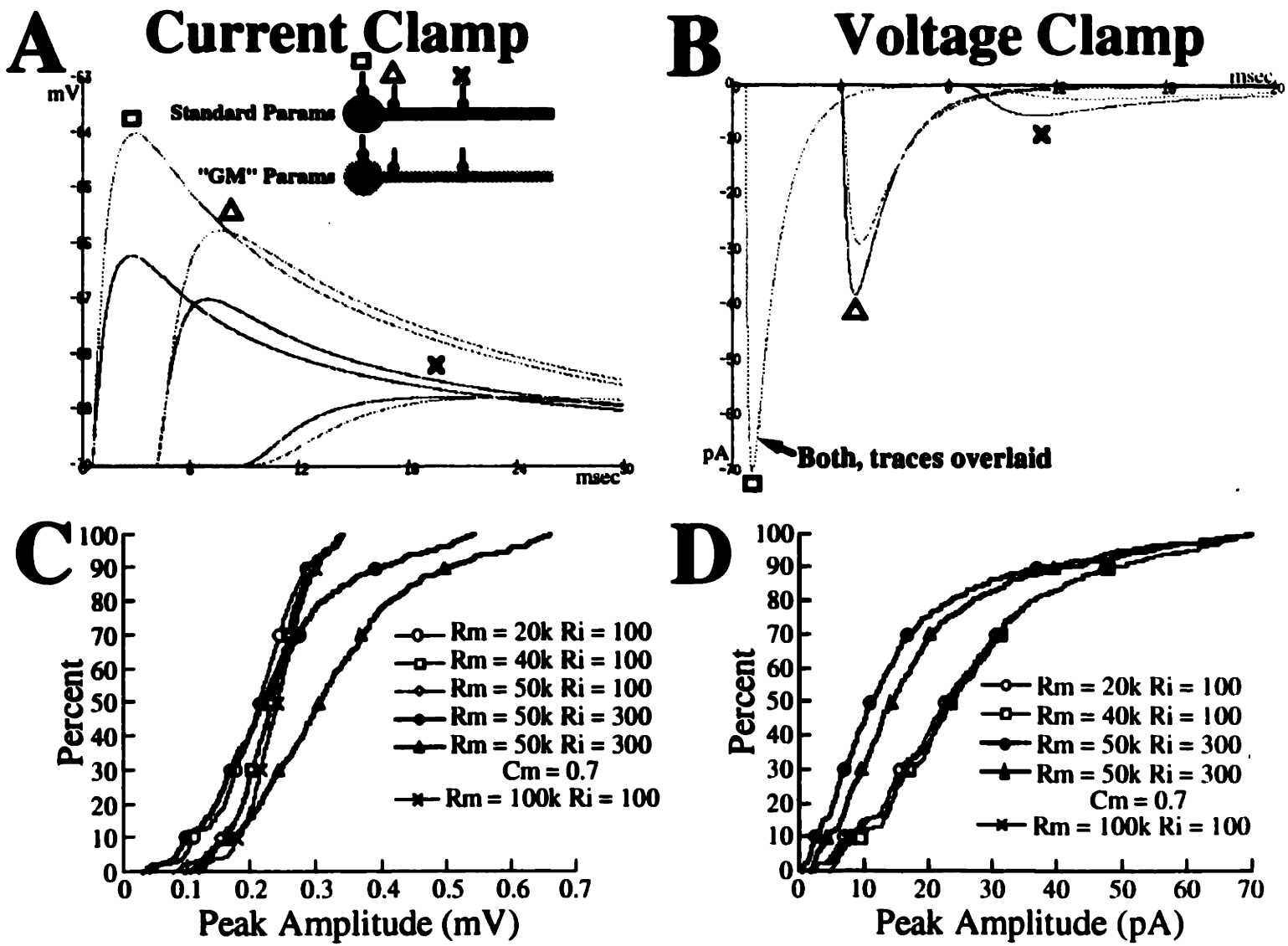
A
Current Clamp
mV
Standard Params
"GM" Params
msec
B
Voltage Clamp
msec
pA
Both, traces overlaid
C
Percent
Peak Amplitude (mV)
Rm = 20k Ri = 100
Rm = 40k Ri = 100
Rm = 50k Ri = 100
Rm = 50k Ri = 300
Rm = 50k Ri = 300
Cm = 0.7
Rm = 100k Ri = 100
D
Percent
Peak Amplitude (pA)
Rm = 20k Ri = 100
Rm = 40k Ri = 100
Rm = 50k Ri = 300
Rm = 50k Ri = 300
Cm = 0.7
Rm = 100k Ri = 100

Fig. A - 64

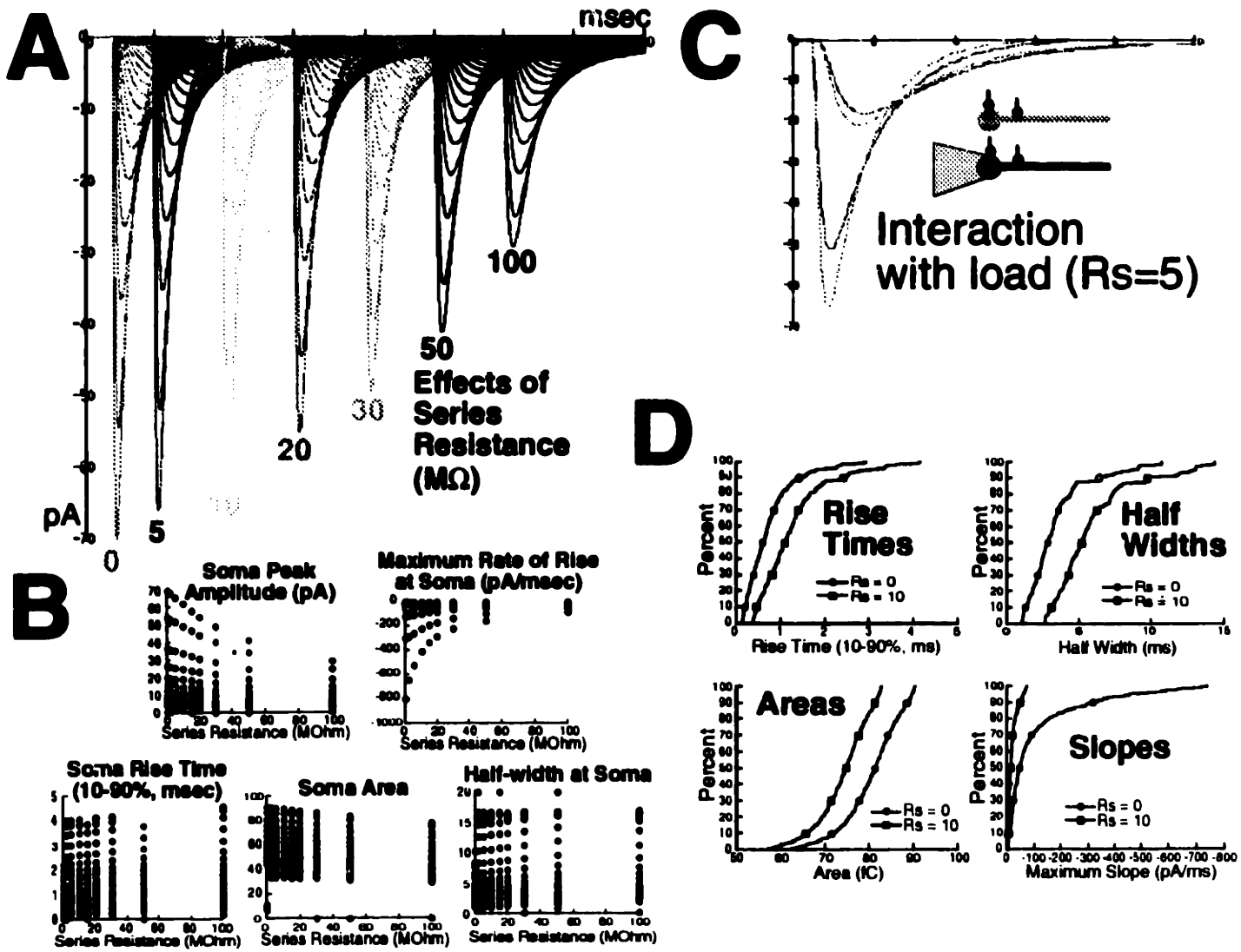
A
msec
pA
0
5
10
20
30
50
100
Effects of Series Resistance (MΩ)
B
Soma Peak Amplitude (pA)
Maximum Rate of Rise at Soma (pA/msec)
Soma Rise Time (10-90%, msec)
Soma Area
Half-width at Soma
Series Resistance (MOhm)
C
Interaction with load (Rs=5)
D
Rise Times
Rise Time (10-90%, ms)
Half Widths
Half Width (ms)
Areas
Area (fC)
Slopes
Maximum Slope (pA/ms)
Percent
Rs = 0
Rs = 10

Fig. A - 65

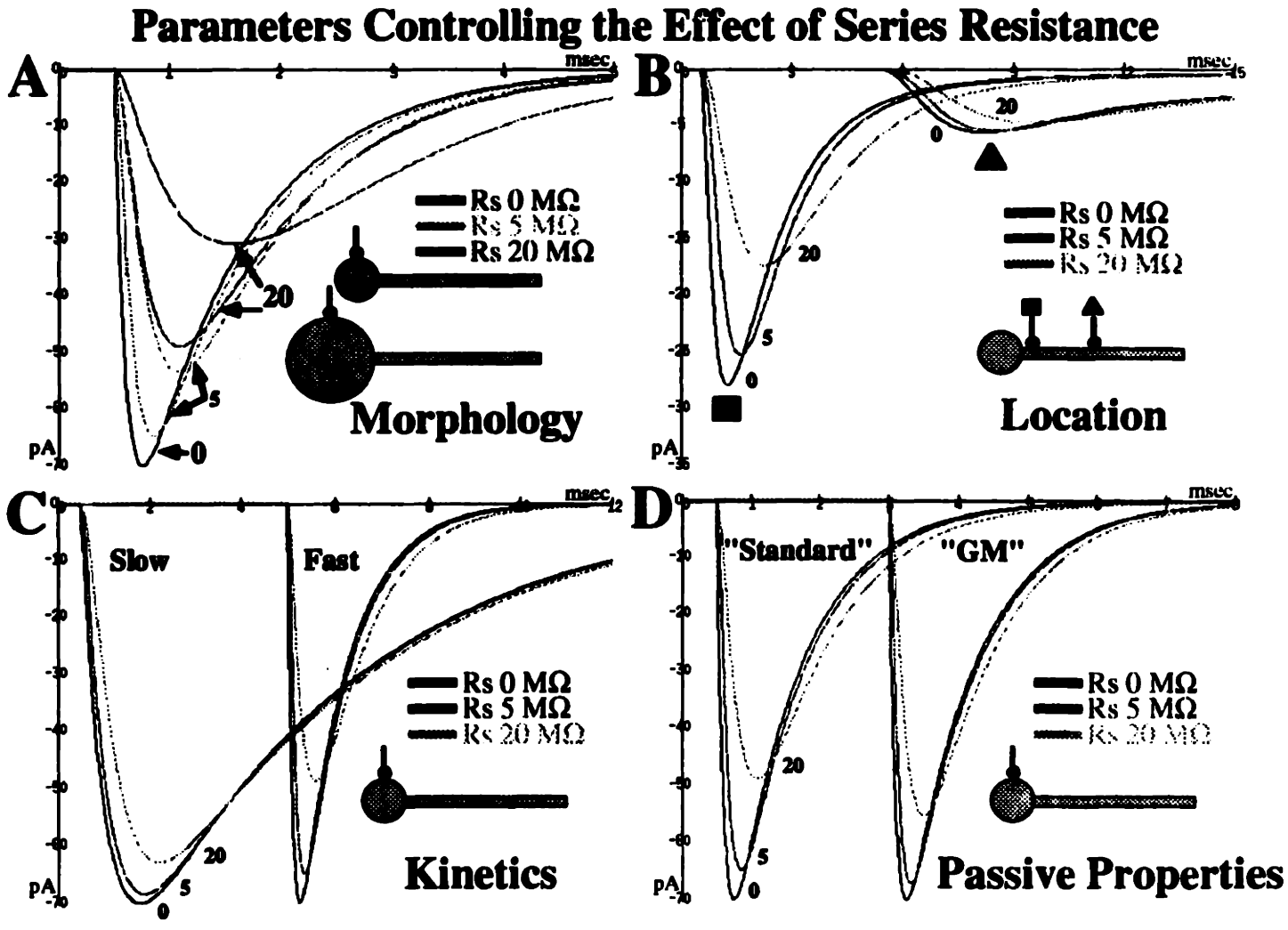
Parameters Controlling the Effect of Series Resistance
A
msec
pA
Rs 0 MΩ
Rs 5 MΩ
Rs 20 MΩ
20
5
0
Morphology
B
msec
20
0
20
5
0
Rs 0 MΩ
Rs 5 MΩ
Rs 20 MΩ
Location
C
msec
Slow
Fast
pA
Rs 0 MΩ
Rs 5 MΩ
Rs 20 MΩ
20
5
0
Kinetics
D
msec
"Standard"
"GM"
20
5
0
pA
Rs 0 MΩ
Rs 5 MΩ
Rs 20 MΩ
Passive Properties

Fig. A - 66

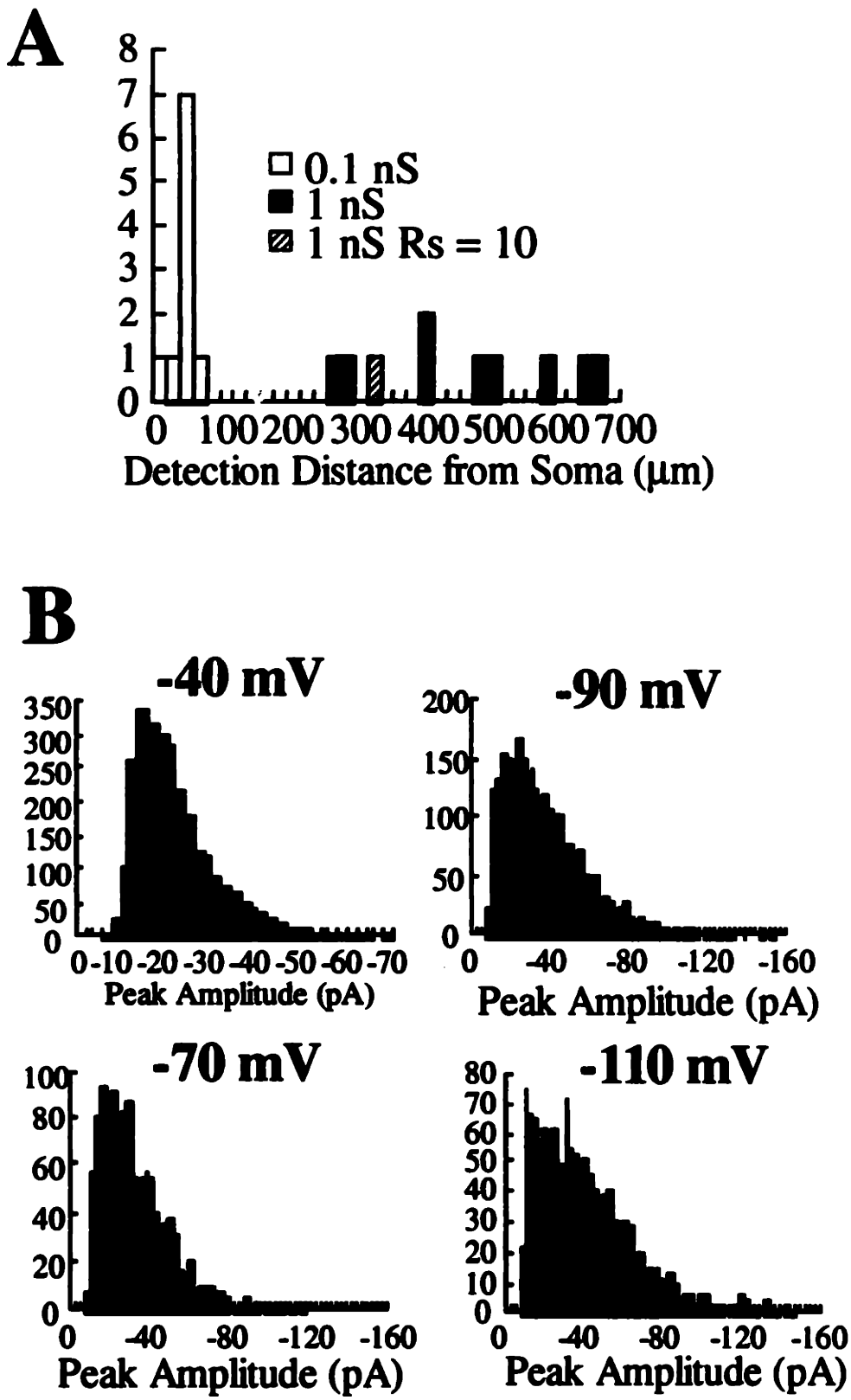
A
8
7
6
5
4
3
2
1
0
0.1 nS
1 nS
1 nS Rs = 10
0 100 200 300 400 500 600 700
Detection Distance from Soma (µm)
B
-40 mV
350
300
250
200
150
100
50
0
0 -10 -20 -30 -40 -50 -60 -70
Peak Amplitude (pA)
-90 mV
200
150
100
50
0
0 -40 -80 -120 -160
Peak Amplitude (pA)
-70 mV
100
80
60
40
20
0
0 -40 -80 -120 -160
Peak Amplitude (pA)
-110 mV
80
70
60
50
40
30
20
10
0
0 -40 -80 -120 -160
Peak Amplitude (pA)

Fig. A - 67

Bibliography

[1] Agmon, A. and O'Dowd, D. K. (1992). NMDA receptor-mediated currents are prominent in the thalamocortical synaptic response before maturation of inhibition. *Journal of Neurophysiology*, 68:345–349.

[2] Alger, B. E. and Nicoll, R. A. (1980). Spontaneous inhibitory post-synaptic potentials in hippocampus: Mechanism for tonic inhibition. *Brain Research*, 200:195–200.

[3] Allen, C. and Stevens, C. F. (1994). An evaluation of causes for unreliability of synaptic transmission. *Proc. Natl. Acad. Sci.*, 91:10380–10383.

[4] Alzheimer, C., Schwindt, P. C., and Crill, W. E. (1993). Postnatal development of a persistent Na^+ current in pyramidal neurons from rat sensorimotor cortex. *Journal of Neurophysiology*, 69:290–292.

[5] Amit, D. J. and Treves, A. (1989). Associative memory neural network with low temporal spiking rates. *Proc. Natl. Acad. Sci.*, 86:7871–7875.

[6] Andersen, P., Raastad, M., and Storm, J. F. (1992). Excitatory synaptic integration in hippocampal pyramids and dentate gyrus cells. In *Cold Spring Harbor Symposia on Quantitative Biology Volume LV*. Cold Spring Harbor Laboratory Press.

[7] Andersen, P., Storm, J., and Wheal, H. V. (1987). Thresholds of action potentials evoked by synapses on the dendrites of pyramidal cells in the rat hippocampus in vitro. *Journal of Physiology*, 383:509–526.

[8] Anderson, J. C., Douglas, R. J., Martin, K. A., and Nelson, J. C. (1994a). Map of the synapses formed with the dendrites of spiny stellate neurons of cat visual cortex. *Journal of Comparative Neurology*, 341:25–38.

[9] Anderson, J. C., Douglas, R. J., Martin, K. A., and Nelson, J. C. (1994b). Synaptic output of physiologically identified spiny stellate neurons in cat visual cortex. *Journal of Comparative Neurology*, 341:16–24.

[10] Ankri, N., Legendre, P., Faber, D. S., and Korn, H. (1994). Automatic detection of spontaneous synaptic responses in central neurons. *Journal of Neuroscience Methods*, 52:87–100.

[11] Arancio, O., Korn, H., Gulyas, A., Freund, T., and Miles, R. (1994). Excitatory synaptic connections onto rat hippocampal inhibitory cells may involve a single release site. *Journal of Physiology*, 481:395–405.

[12] Bair, W., Koch, C., Newsome, W., and Britten, K. (1994). Power spectrum analysis of bursting cells in area MT in the behaving monkey. *Journal of Neuroscience*, 14:2870–2892.

[13] Barbour, B. (1993). Synaptic currents evoked in Purkinjie cells by stimulating individual granule cells. *Neuron*, 11:759–769.

[14] Barrett, J. N. and Crill, W. E. (1974a). Influence of dendritic location and membrane properties on the effectiveness of synapses on cat motoneurones. *Journal of Physiology*, 239:301–324.

[15] Barrett, J. N. and Crill, W. E. (1974b). Specific membrane properties of cat motoneurones. *Journal of Physiology*, 239:301–324.

[16] Bayer, S. A. and Altman, J. (1991). *Neocortical Development.* Raven Press.

[17] Bekkers, J. M., Richerson, G. B., and Stevens, C. F. (1990). Origin of variability in quantal size in cultured hippocampal neurons and hippocampal slices. *Proc. Natl. Acad. Sci.*, 87:5359–5362.

[18] Bekkers, J. M. and Stevens, C. F. (1989). NMDA and non-NMDA receptors are co-localized at individual excitatory synapses in cultured rat hippocampus. *Nature*, 341:230–233.

[19] Bekkers, J. M. and Stevens, C. F. (1990). Two different ways evolution makes neurons larger. *Progress in Brain Research*, 83:37–45.

[20] Bekkers, J. M. and Stevens, C. F. (1991). Application of quantal analysis to the study of long-term potentiation: Errors, assumptions, and predictions. In Baudry, M. and Davis, J. L., editors, *Long Term Potentiation: A Debate of Current Issues.* MIT Press.

[21] Bell, A. J. (1992). Self-organisation in real neurons: Anti-Hebb in 'channel space'? In *Neural Information Processing Systems 4.*

[22] Bernander, O., Douglas, R. J., Martin, K. A. C., and Koch, C. (1991). Synaptic background activity determines spatio-temporal integration in single pyramidal cells. *Proc. Natl. Acad. Sci.*, 88:11569–11573.

[23] Bialek, W., Rieke, F., de Ruyter van Steveninck, R. R., and Warland, D. (1991). Reading a neural code. *Science*, 252:1854–1856.

[24] Blanton, M. G., LoTurco, J. J., and Kriegstein, A. R. (1989). Whole cell recording from neurons in slices of reptilian and mammalian cerebral cortex. *Journal of Neuroscience Methods*, 30:203–210.

[25] Bloomfield, S. A., Hamos, J. E., and Sherman, S. M. (1987). Passive cable properties and morphological correlates of neurones in the lateral geniculate nucleus of the cat. *Journal of Physiology*, 383:653–692.

[26] Buhl, E. H., Halasy, K., and Somogyi, P. (1994a). Diverse sources of hippocampal unitary inhibitory postsynaptic potentials and the number of synaptic release sites. *Nature*, 368:823–828.

[27] Buhl, E. H., Han, Z. S., Lõrinczi, Z., Stezhka, V. V., Karnup, S. V., and Somogyi, P. (1994b). Physiological properties of anatomically identified axo-axonic cells in the rat hippocampus. *Journal of Neurophysiology*, 71:1289–1307.

[28] Buhmann, J. and Schulten, K. (1987). Influence of noise on the function of a "physiological" neural network. *Biological Cybernetics*, 56:313–327.

[29] Burgard, E. C. and Hablitz, J. J. (1993a). Developmental changes in NMDA and non-NMDA receptor-mediated synaptic potentials in rat neocortex. *Journal of Neurophysiology*, 61:230–240.

[30] Burgard, E. C. and Hablitz, J. J. (1993b). NMDA receptor-mediated components of miniature excitatory synaptic currents in developing rat neocortex. *Journal of Neurophysiology*, 61:230–240.

[31] Burke, R. E. (1967). Composite nature of the monosynaptic excitatory postsynaptic potential. *Journal of Neurophysiology*, 30:1114–1137.

[32] Busch, C. and Sakmann, B. (1992). Synaptic transmission in hippocampal neurons: Numerical reconstruction of quantal IPSCs. In *Cold Spring Harbor Symposia on Quantitative Biology Volume LV*. Cold Spring Harbor Laboratory Press.

[33] Bush, P. C. and Sejnowski, T. J. (1994). Effects of inhibition and dendritic saturation in simulated neocortical pyramidal cells. *Journal of Neurophysiology*, 71:2183–2193.

[34] Calvin, W. H. and Stevens, C. F. (1967). Synaptic noise and other sources of randomnesss in motoneuron interspike intervals. *Journal of Neurophysiology*, pages 574–587.

[35] Cattaneo, A., Maffei, L., and Morrone, C. (1981). Patterns in the discharge of simple and complex visual cortical cells. *Proc. R. Soc. Lond. B*, 212:279–297.

[36] Cauller, L. J. and Connors, B. W. (1992). Functions of very distal dendrites: Experimental and computational studies of layer I synapses on neocortical pyramidal cells. In McKenna, T., Davis, J., and Zornetzer, S. F., editors, *Single Neuron Computation*. Academic Press.

[37] Cauller, L. J. and Connors, B. W. (1994). Synaptic physiology of horizontal afferents to layer I in slices of rat SI neocortex. *Journal of Neuroscience*, 14:751–762.

[38] Celio, M. R. (1990). Calbindin D-28k and parvalbumin in the rat nervous system. *Neuroscience*, 35:375–475.

[39] Chagnac-Amitai, Y., Friedman, A., Connors, B. W., and Gutnick, M. J. (1993). Regenerative activity in apical dendrites of pyramidal cells in neocortex. *Cerebral Cortex*, 3:26–38.

[40] Chagnac-Amitai, Y., Luhmann, J. J., and Prince, D. A. (1990). Burst generating and regular spiking layer 5 pyramidal neurons of rat neocortex have different morphological features. *Journal of Comparative Neurology*, 296:598–613.

[41] Chattarji, B. F. S. and Brown, T. (1994). Spontaneous synaptic currents in visualized neurons ofthe rat amygdala and perirhinal cortex. In *Society for Neuroscience Abstracts.*

[42] Chung, S., Raymond, S. A., and Lettvin, J. Y. (1970). Multiple meanings in single visual units. *Brain, Behavior and Evolution*, 3:72–101.

[43] Claiborne, B. J. (1992). *Use of Computers for Quantitative, Three-Dimensional Analysis of Dendritic Trees*, pages 315–330. Academic Press.

[44] Claiborne, B. J., Amaral, D. G., and Cowan, W. M. (1990). Quantitative, three-dimensional analysis of granule cell dendrites in the rat dentate gyrus. *Journal of Comparative Neurology*, 302:206–219.

[45] Clamann, H. P., Riolt-Pedotti, M., and Lüscher, H. (1991). The influence of noise on quantal EPSP size obtained by deconvolution in spinal motoneurons in the cat. *Journal of Neurophysiology*, 65:67–75.

[46] Clements, J. D. and Redman, S. J. (1989). Cable properties of cat spinal motoneurones measured by combining voltage clamp, current clamp, and intracellular staining. *Journal of Physiology*, 409:63–87.

[47] Cohen, G. A., Doze, V. A., and Madison, D. V. (1992). Opiod inhibition of GABA release from presynaptic terminals of rat hippocampal neurons. *Neuron*, 9:325–335.

[48] Collingridge, G. L., Gage, P. W., and Robertson, B. (1984). Inhibitory post-synaptic currents in rat hippocampal CA1 neurones. *Journal of Physiology*, 356:551–564.

[49] Connors, B. W., Gutnick, M. J., and Prince, D. A. (1982). Electrophysiological properties of neocortical neurons in vitro. *Journal of Neurophysiology*, 48:1302–1320.

[50] Croner, L. J., Purpura, K., and Kaplan, E. (1993). Response variability in retinal ganglion cells of primates. *Proc. Natl. Acad. Sci.*, 90:8128–8130.

[51] De Schutter, E. and Bower, J. M. (1993a). An active membrane model of the cerebellar purkinjie cell: I. simulation of current clamps in slice. Submitted to J. Neurophysiol.

[52] De Schutter, E. and Bower, J. M. (1993b). An active membrane model of the cerebellar purkinjie cell: II. simulation of synaptic responses. Submitted to J. Neurophysiol.

[53] De Schutter, E. and Bower, J. M. (1993c). Are cerebellar purkinjie cell responses independent of the dendritic location of granule cell synaptic inputs? Submitted to Nature.

[54] DeKoninck, Y. and Mody, I. (1994). Noise analysis of miniature IPSCs in adult rat brain slices; properties and modulation of synaptic $GABA_A$ receptor channels. *Journal of Neurophysiology*, 71:1318–1335.

[55] del Castillo, J. and Katz, B. (1954a). Quantal components of the end-plate potential. *Journal of Physiology*, 124:560–573.

[56] del Castillo, J. and Katz, B. (1954b). Statistical factors involved in neuromuscular facilitation and depression. *Journal of Physiology*, 124:574–585.

[57] Desmond, N. L. and Levy, W. B. (1982). A quantitative anatomical study of the granule cell dendritic fields of the rat dentate gyrus using a novel probabilistic method. *Journal of Comparative Neurology*, 212:131–145.

[58] Desmond, N. L. and Levy, W. B. (1984). Dendritic caliber and the 3/2 power relationship of dentate granule cells. *Journal of Comparative Neurology*, 227:589–596.

[59] Desmond, N. L. and Levy, W. B. (1985). Granule cell spine density in the rat hippocampus varies with spine shape and length. *Neuroscience Letters*. 54:219–224.

[60] Deuchars, J., Thomson, A. M., and West, D. C. (1994). Single axon excitatory postsynaptic potentials in neocortical interneurons exhibit pronounced paired pulse facilitation. *Journal of Physiology*, 478:423–435.

[61] Doherty, P., Hagwood, B. J., and Smith, I. C. H. (1984). Changes in miniature end-plate potentials after brief nervous stimulation at the frog neuromuscular junction. *Journal of Physiology*. 356:349–358.

[62] Douglas, R. J. and Martin, K. A. C. (1990). Neocortex. In Shepherd, G. M., editor, *The Synaptic Organization of the Brain*, pages 389–438. Oxford University Press.

[63] Douglas, R. J. and Martin, K. A. C. (1991). Opening the grey box. *Trends in Neurosciences*, 14:286–293.

[64] Douglas, R. J., Martin, K. A. C., and Whitteridge, D. (1989). A canonical microcircuit for neocortex. *Neural Computation*, 1:480–488.

[65] Doze, V. A., Cohen, G. A., and Madison, D. V. (1991). Synaptic localization of adrenergic disinhibition in the rat hippocampus. *Neuron*, 6:889–900.

[66] Durand, D. (1984). The somatic shunt cable model for neurons. *Biophysical Journal*, 46:645–653.

[67] Edwards, F. A., Konnerth, A., and Sakmann, B. (1990). Quantal analysis of inhibitory synaptic transmission in the dentate gyrus of rat hippocampal slices: a patch-clamp study. *Journal of Physiology*, 430:213–249.

[68] Edwards, F. A., Konnerth, A., Sakmann, B., and Takahashi, T. (1989). A thin slice preparation for patch clamp recordings from neurones of the mammalian central nervous system. *Pflugers Archives*, 414:600–612.

[69] Evans, J. D., Kember, G. C., and Major, G. (1992). Techniques for obtaining analytical solutions to the multi-cylinder somatic shunt cable model for passive neurones. *Biophysical Journal*, 63:350–365.

[70] Finch, D. M., Fisher, R. S., and Jackson, M. B. (1990). Miniature excitatory synaptic currents in cultured hippocampal neurons. *Brain Research*, 518:257–268.

[71] Fitzhugh, R. (1960). Thresholds and plateaus in the hodgkin-Huxley nerve equations. *Journal of General Physiology*, 43:867–895.

[72] Foehring, R. C., Lorenzon, N. M., Herron, P., and Wilson, C. J. (1991). Correlation of physiologically and morphologically identified neuronal types in human association cortex in vitro. *Journal of Neurophysiology*, 66:1825–1837.

[73] French, R. J. and Shoumikas, J. J. (1985). An ion's view of the potassium channel. *Journal of General Physiology*, 85:669–698.

[74] Gabbott, P. L. A., Martin, K. A. C., and Whitteridge, D. (1987). Connections between pyramidal neurons in layer 5 of cat visual cortex (area 17). *Journal of Comparative Neurology*, 259:364–381.

[75] Gao, B. and Fritschy, J. M. (1994). Selective allocation of $GABA_A$ receptors containing the a1 subunit to neurochemically distinct subpopulations of rat hippocampal interneurons. *European Journal of Neuroscience*, 6:837–853.

[76] Gibson, W. G., Robinson, J., and Bennett, M. R. (1991). Probabilistic secretion of quanta in the central nervous system: Granule cell synaptic control of pattern separation and activity regulation. *Phil. Trans. Roy. Soc. (Lond.) B*, 332:199–220.

[77] Gulyás, A. I., Miles, R., Sik, A., Tóth, K., Tamamaki, N., and Freund, T. F. (1993). Hippocampal pyramidal cells excite inhibitory neurons through a single release site. *Nature*, 366:683–687.

[78] Halasy, K. and Somogyi, P. (1993a). Distribution of GABAergic synapses and their targets in the dentate gyrus of rat: a quantitative immunoelectron microscopic analysis. *J. Hirnforschung*, 34:299–308.

[79] Halasy, K. and Somogyi, P. (1993b). Subdivisions in the multiple GABAergic innervation of granule cells in the dentate gyrus of the rat hippocampus. *European Journal of Neuroscience*, 5:411–429.

[80] Han, Z.-S., Buhl, E. H., Lörinczi, Z., and Somogyi, P. (1993). A high degree of spatial selectivity in the axonal and dendritic domains of physiologically identified local-circuit neurons in the dentate gyrus of the rat hippocampus. *European Journal of Neuroscience*, 5:395–410.

[81] Hessler, N. A., Shirke, A. M., and Malinow, R. (1993). The probability of transmitter release at a mammalian central synapse. *Nature*, 366:569–572.

[82] Hestrin, S. (1992). Activation and desensitization of glutatmate-activated channels mediating fast excitatory synaptic currents in the visual cortex. *Neuron*, 9:991–999.

[83] Hestrin, S. (1993). Diferent glutamate receptor channels mediate fast excitatory synaptic currents in inhibitory and excitatory cortical neurons. *Neuron*, 11:1083–1091.

[84] Hestrin, S., Nicoll, R. A., Perkel, D. J., and Sah, P. (1990). Analysis of excitatory synaptic action in pyramidal cells using whole-cell recording from rat hippocampal slices. *Journal of Physiology*, 422:203–225.

[85] Hines, M. (1989). A program for simulation of nerve equations with branching geometries. *Int. J. Biomed. Comput.*, 24:55–68.

[86] Hinton, G., Sejnowski, T. J., and Ackley, D. H. (1984). *Boltzmann Machines: Constraint Satisfaction Networks that Learn.* Carnegie-Mellon University Press, Pittsburgh.

[87] Hirsch, J. A. and Gilbert, C. D. (1991). Synaptic physiology of horizontal connections in the cat's visual cortex. *Journal of Neuroscience*, 11:1800–1809.

[88] Holmes, W. (1994). Does glutamate saturate NMDA receptors at at synapse? In *Society for Neuroscience Abstracts.*

[89] Holmes, W. R. (1989). The role of dendritic diameter in maximizing the effectiveness of synaptic inputs. *Brain Research*, 478:127–137.

[90] Holmes, W. R. and Rall, W. (1992). Estimating the electrotonic structure of neurons with compartmental models. *Journal of Neurophysiology*, 68:1438–1452.

[91] Houser, C. R., Olsen, R. W., Richards, J. G., and Möhler, H. (1988). Immunohistochemical localization of benzodiazepine/$GABA_A$ receptors in the human hippocampal formation. *Journal of Neuroscience*, 8:1370–1383.

[92] Hubbard, J. I., Llinas, R., and Quastel, D. M. J. (1969). *Electrophysiological Analysis of Synaptic Transmission.* E. Arnold Publishers, London.

[93] Huguenard, J. R., Hamill, O. P., and Prince, D. A. (1988). Developmental changes in Na^+ conductances in rat neocortical neurons: Appearance of a slowly inactivating component. *Journal of Neurophysiology*, 59:778–795.

[94] Iansek, R. and Redman, S. J. (1973). The amplitude, time course and charge of unitary excitatory post-synaptic potentials evoked in spinal motoneurone dendrites. *Journal of Physiology*, 234:665–688.

[95] Jack, J. J. B., Kullman, D. M., Larkman, A. U., Major, G., and Stratford, K. J. (1992). Quantal analysis of excitatory synaptic mechanisms in the mammalian nervous system. In *Cold Spring Harbor Symposia on Quantitative Biology Volume LV*. Cold Spring Harbor Laboratory Press.

[96] Jack, J. J. B., Miller, S., Porter, R., and Redman, S. J. (1971). The time course of minimal excitatory post-synaptic potentials evoked in spinal motoneurons by group Ia afferent fibers. *Journal of Physiology*, 215:353–380.

[97] Jack, J. J. B., Noble, D., and Tsien, R. W. (1975). *Electric Current Flow in Excitable Cells*. Oxford University Press.

[98] Jack, J. J. B. and Redman, S. J. (1971a). An electrical description of the motoneurone, and its application nfo the analysis of synaptic potentials. *Journal of Physiology*, 215:321–352.

[99] Jack, J. J. B. and Redman, S. J. (1971b). The propagation of transient potentials in some linear cable structures. *Journal of Physiology*, 215:283–320.

[100] Jack, J. J. B., Redman, S. J., and Wong, K. (1981). The components of synaptic potentials evoked in cat spinal motoneurons by impulses in single group 1a afferents. *Journal of Physiology*, 321:65–96.

[101] James W. Fleshman, J., Segev, I., and Burke, R. E. (1988). Electrotonic architecture of type-identified α-motoneurons in the cat spinal cord. *Journal of Neurophysiology*, 60:60–85.

[102] Jaslove, S. W. (1992). The integrative properties of spiny distal dendrites. *Neuroscience*, 47:495–519.

[103] Johnston, D. and Brown, T. H. (1983). Interpretation of voltage-ciamp measurements in hippocampal neurons. *Journal of Neurophysiology*, 50:464–486.

[104] Jonas, P., Major, G., and Sakmann, B. (1993). Quantal components of unitary EPSCs at the mossy fibre synapse on CA3 pyramidal cells of the rat hippocampus. *Journal of Physiology*, 472:615–663.

[105] Jones, E. G. (1988). What are the local circuits? In Rakic, P. and Singer, W., editors, *Neurobiology of Neocortex*, pages 137–152. Dahlem Konferenzen, John Wiley and Sons Limited.

[106] Jones, E. G. and Hendry, S. H. C. (1984). Basket cells. In Peters, A. and Jones, E. G., editors, *Cerebral Cortex*, volume 1, pages 309–336. Plenum Press.

[107] Jones, K. A. and Baughman, R. W. (1991). Both NMDA and non-NMDA subtypes of glutamate receptors are concentrated at synapses on cerebral cortical neurons in culture. *Neuron*, 7:593–603.

[108] Kasper, E. M., Larkman, A. U., Lübke, J., and Blakemore, C. (1994a). Pyramidal neurons in layer 5 of the rat visual cortex: I. correlation among morphology, intrinsic electrophysiological properties, and axon targets. *Journal of Comparative Neurology*, 339:459–474.

[109] Kasper, E. M., Larkman, A. U., Lübke, J., and Blakemore, C. (1994b). Pyramidal neurons in layer 5 of the rat visual cortex: II. development of electrophysiological properties. *Journal of Comparative Neurology*, 339:475–494.

[110] Kasper, E. M., Lübke, J., Larkman, A. U., and Blakemore, C. (1994c). Pyramidal neurons in layer 5 of the rat visual cortex: III. differential maturation of axon targeting, dendritic morphology, and electrophysiological properties. *Journal of Comparative Neurology*, 339:495–518.

[111] Kawaguchi, Y. (1993). Groupings of nonpyramidal and pyramidal cells with specific physiological and morphological characteristics in rat frontal cortex. *Jounal of Neurophysiology*, 69:416–430.

[112] Kawaguchi, Y. (1994). Physiological subgroups of nonpyramidal cells in layer II/III of rat frontal cortex. In *Society for Neuroscience Abstracts*.

[113] Kawaguchi, Y. (1995). Physiological subgroups of nonpyramidal cells with specific morphological characteristics in layer II/III of rat frontal cortex. *Jounal of Neuroscience*, 15.

[114] Kawaguchi, Y. and Kubota, Y. (1993). Correlation of physiological subgroupings of nonpyramidal cells with parvalbumin- and calbindin$_{D28K}$-immunoreactive neurons in layer V of rat frontal cortex. *Jounal of Neurophysiology*, 70:387–396.

[115] Kim, H. G. and Connors, B. W. (1993). Apical dendrites of the neocortex: Corrlation between sodium- and calcium-dependent spiking and pyramidal cell morphology. *Journal of Neuroscience*, 13:5301–5311.

[116] Kisvarday, Z. F., Cowey, A., and Somogyi, P. (1986). Synaptic relationships of a type of GABA-immunoreactive neuron (clutch cell), spiny stellate cells and lateral geniculate nucleus afferents in layer IVC of the monkey striate cortex. *Neuroscience*, 19:741–761.

[117] Koch, C. (1985). Understanding the intrinsic circuitry of the cat's dLGN: Electrical properties of the spine-triad arrangement. *Philosophical Transactions of the Royal Society London, Series B*. 225:365–390.

[118] Koch, C., Bernander, Ö., and Douglas, R. J. (1995). Do neurons have a voltage or a current threshold for action potential initiation? *Journal of Computational Neuroscience*, in press.

[119] Koch, C. and Poggio, T. (1983). A theoretical analysis of the electrical properties of spines. *Philosophical Transactions of the Royal Society London, Series B*, 218:455–477.

[120] Koch, C. and Poggio, T. (1984). Nonlinear interactions in a dendritic tree: Localization, timing, and role in information processing. *Proceedings of the National Academy of Sciences, U.S.A.*, 80:2799–2802.

[121] Koch, C. and Poggio, T. (1987). Biophysics of computation. In Edelman, G. M., Gall, W. E., and Cowan, W. M., editors, *Synaptic Function*. Wiley.

[122] Koch, C. and Poggio, T. (1992). Multiplying with synapses and neurons. In McKenna, T., Davis, J., and Zornetzer, S. F., editors, *Single Neuron Computation*. Academic Press.

[123] Koch, C., Poggio, T., and Torre, V. (1982). Retinal ganglion cells: a functional interpretation of dendritic morphology. *Philosophical Transactions of the Royal Society London, Series B*, 298:227–264.

[124] Koch, C. and Segev, I. (1989). *Methods in Neuronal Modeling*. MIT Press.

[125] Koch, C. and Zador, A. (1993). The function of dendritic spines: Devices subserving biochemical rather than electrical compartmentalization. *Journal of Neuroscience*, 13:413–422.

[126] Korn, H. and Faber, D. S. (1987). Regulation and significance of probabilistic release mechanisms at central synapses. In Edelman, G. M., Gall, W. E., and Cowan, W. M., editors, *Synaptic Function*. Wiley.

[127] Kullmann, D. M. and Nicoll, R. A. (1992). Long-term potentiation is associated with increases in quantal content and quantal amplitude. *Nature*, 357:240–244.

[128] Lambert, N. A. and Wilson, W. A. (1993). Heterogeneity in presynaptic regulation of GABA release from hippocampal inhibitory neurons. *Neuron*, 11:1057–1067.

[129] Langdon, R. B. and Sur, M. (1990). Components of field potentials evoked by white matter stimulation in isolated slices of primary visual cortex: Spatial distributions and synaptic order. *Journal of Neurophysiology*, 64:1484–1501.

[130] Langmoen, I. A. and Andersen, P. (1983). Summation of excitatory postsynaptic potentials in hippocampal pyramidal cells. *Journal of Neurophysiology*, 50:1320–1329.

[131] Larkman, A., Hannay, T., Stratford, K., and Jack, J. (1992). Presynaptic release probability influences the locus of long-term potentiation. *Nature*, 360:70–73.

[132] Larkman, A., Stratford, K., and Jack, J. (1991). Quantal analysis of excitatory synaptic action and depression in hippocampal slices. *Nature*, 350:344–347.

[133] Larkman, A. U. (1991a). Dendritic morphology of pyramidal neurones of the visual cortex of the rat: I. branching patterns. *Journal of Comparative Neurology*, 306:307–319.

[134] Larkman, A. U. (1991b). Dendritic morphology of pyramidal neurones of the visual cortex of the rat: III. spine distributions. *Journal of Comparative Neurology*, 306:332–343.

[135] Larkman, A. U. (1991c). Dendritic morphology of pyramidal neurones of the visual cortex of the rat: IV. electrical geometry. *Journal of Comparative Neurology*, 323:137–152.

[136] Larkman, A. U. and Mason, A. (1990a). Correlations between morphology and electrophysiology of pyramidal neurons in slices of rat visual cortex. II. electrophysiology. *Journal of Neuroscience*, 10:1415–1428.

[137] Larkman, A. U. and Mason, A. (1990b). Correlations between morphology and electrophysiology of pyramidal neurons in slices of rat visual cortex. I. establishment of cell classes. *Journal of Neuroscience*, 10:1407–1414.

[138] LeMasson, G., Marder, E., and Abbott, L. F. (1993). Activity-dependent regulation of conductances in model neurons. *Science*, 259:1915–1917.

[139] Lev-Tov, A., Miller, J. P., Burke, R. E., and Rall, W. (1983). Factors that control amplitude of EPSPs in dendritic neurons. *Journal of Neurophysiology*, 50:399–412.

[140] Liao, D., Jones, A., and Malinow, R. (1992). Direct measurement of quantal changes underlying long-term potentiation in CA1 hippocampus. *Neuron*, 9:1089–1097.

[141] Little, W. A. and Shaw, G. L. (1975). A statistical theory of short and long term memory. *Behavioral Biology*, 14:115–133.

[142] Livsey, C. T., Costa, E., and Vicini, S. (1993). Glutamate-activated currents in outside-out patches from spiny versus aspiny hilar neurons of rat hippocampal slices. *Journal of Neuroscience*, 13:5324–5333.

[143] Livsey, C. T. and Vicini, S. (1992). Slower spontaneous excitatory postsynaptic currents in spiny versus aspiny hilar neurons. *Neuron*, 8:745–755.

[144] Llano, I. and Gerschenfeld, H. M. (1993). Inhibitory synaptic currents in stellate cells of rat cerebellar slices. *Journal of Physiology*, 468:177–200.

[145] Llano, I., Marty, A., Armstrong, C. M., and Konnerth, A. (1991). Synaptic- and agonist-induced excitatory currents of Purkinjie cells in rat cerebellar slices. *Journal of Physiology*, 434:183–213.

[146] LoTurco, J. J., Mody, I., and Kriegstein, A. R. (1990). Differential activation of glutamate receptors by spontaneously released transmitter in slics of neocortex. *Neuroscience Letters*, 114:265–271.

[147] Luhmann, H. J. and Prince, D. A. (1991). Postnatal maturation of the GABAergic system in rat neocortex. *Journal of Neurophysiology*, 65:247–263.

[148] Maffei, L. and Galli-Resta, L. (1990). Correlation in the discharges of neighboring rat retinal ganglion cells during prenatal life. *Proc. Natl. Acad. Sci.*, 83:2861–2864.

[149] Mainen, Z. and Sejnowski, T. J. (1995). Reliability of spike timing in neocortical neurons. *Science*, In Press.

[150] Major, G. (1992). *The Physiology, Morphology and Modelling of Cortical Pyramidal Neurones.* PhD thesis, Oxford University.

[151] Major, G. (1993). Solutions for transients in arbitrarily branching cables: III. voltage clamp problems. *Biophysical Journal*, 65:469–491.

[152] Major, G., Evans, J. D., and Jack, J. J. B. (1993a). Solutions for transients in arbitrarily branching cables: I. voltage recordings with a somatic shunt. *Biophysical Journal*, 65:423–449.

[153] Major, G., Evans, J. D., and Jack, J. J. B. (1993b). Solutions for transients in arbitrarily branching cables: II. voltage clamp theory. *Biophysical Journal*, 65:450–468.

[154] Major, G., Larkman, A. U., Jonas, P., Sakmann, B., and Jack, J. J. B. (1994). Detailed passive cable models of whole-cell recorded CA3 pyramidal neurons in rat hippocampal slices. *Journal of Neuroscience*, 68:16–27.

[155] Malgaroli, A. and Tsien, R. W. (1992). Glutamate-induced long-term potentiation of the frequency of miniature synaptic currents in cultured hippocampal neurons. *Nature*, 357:134–139.

[156] Malinow, R. (1991). Transmission between pairs of hippocampal slice neurons: Quantal levels, oscillations, and LTP. *Nature*, 252:722–724.

[157] Manabe, T., Renner, P., and Nicoll, R. A. (1992). Postsynaptic contribution to long-term potentiation revealed by the analysis of miniature synaptic currents. *Nature*, 355:50–55.

[158] Markram, H. and Sakmann, B. (1994). Calcum transients in dendrites of neocortical neurons evoked by single subthreshold excitatory postsynaptic potentials via low-voltage-activated channels. *Proc. Natl. Acad. Sci.*, 91:5207–5211.

[159] Marr, D. (1970). A theory for cerebral neocortex. *Proceedings of the Royal Society of London, Series B*, 176:161–234.

[160] Martin, A. R. (1966). Quantal nature of synaptic transmission. *Physiological Reviews*, 46:51–66.

[161] Martin, A. R. (1977). Junctional transmission II. presynaptic mechanisms. In *Handbook of Physiology*, chapter 10, pages 329–355. Physiological Society.

[162] Mason, A., Nicoll, A., and Stratford, K. (1991). Synaptic transmission between individual pyramidal neurons of the rat visual cortex *in vitro*. *Journal of Neuroscience*, 11:72–84.

[163] McBain, C. J. and Dingledine, R. (1992). Dual-component miniature excitatory synaptic currents in rat hippocampal CA3 pyramidal neurons. *Journal of Neurophysiology*, 68:16–27.

[164] McBain, C. J. and Dingledine, R. (1993). Heterogeneity of synaptic glutamate receptors on CA3 stratum radiatum inteneurones of rat hippocampus. *Journal of Physiology*, 462:373–392.

[165] McCormick, D. A. (1990). Membrane properties and neurotransmitter actions. In Shepherd, G. M., editor, *Synaptic Organization of the Brain*, pages 32–66. Oxford University Press.

[166] McCormick, D. A., Connors, B. W., Lighthall, J. W., and Prince, D. A. (1985). Comparative electrophysiology of pyramidal and sparsely spiny stellate neurons of the neocortex. *Journal of Neurophysiology*, 54:782–806.

[167] McCormick, D. A. and Prince, D. A. (1987). Post-natal development of electrophysiological properties of rat cerebral cortical pyramidal neurones. *Journal of Physiology*, 393:743–762.

[168] McNaughton, B. L., Barnes, C. A., and Andersen, P. (1981). Synaptic efficacy and EPSP summation in granule cells of rat fascia dentata studied in vitro. *Journal of Neurophysiology*, 46:952–966.

[169] Mel, B. W. (1992). NMDA-based pattern discrimination in a modeled cortical neuron. *Neural Computation*, 5:???

[170] Mel, B. W. (1994). Information processing in dendritic trees. *Neural Computation*, 6:1031–1085.

[171] Miles, R. (1990). Synaptic excitation of inhibitory cells by single CA3 hippocampal pyramidal cells of the guinea-pig in vitro. *Journal of Physiology*, 428:61–77.

[172] Miles, R., Tóth, K., Gulyás, A. I., Hajós, N., and Freund, T. F. (1995). Different functions for dendritic and somatic inhibitory cells of the hippocampus. *Journal of Physiology*, 480:32P.

[173] Miles, R. and Wong, R. K. S. (1986). Excitatory synaptic interactions between CA3 neurons in the guinea-pig hippocampus. *Journal of Physiology*, 373:397–418.

[174] Miller, M. W. (1981). Maturation of rat visual cortex: I. a quantitative study of golgi-impregnated pyramidal neurons. *Journal of Neurocytology*, 10:859–878.

[175] Miller, M. W. (1986). Maturation of rat visual cortex: III.postnatal morphogenesis and synaptogenesis of local circuit neurons. *Developmental Brain Research*, 25:271–285.

[176] Miller, M. W. (1988a). Development of projection and local circuit neurons in neocortex. In Peters, A. and Jones, E. G., editors, *Cerebral Cortex*, volume 7, pages 133–175. Plenum Press.

[177] Miller, M. W. (1988b). Maturation of rat visual cortex: IV. the generation, migration, morphogenesis, and connectivity of atypically oriented pyramidal neurons. *Journal of Comparative Neurology*, 274:387–405.

[178] Mody, I., DeKoninck, Y., Otis, T. S., and Soltesz, I. (1994). Bridging the cleft at GABA synapses in the brain. *Trends in Neuroscience*, 17:517–525.

[179] Murphy, T. H., Baraban, J. M., Wier, W. G., and Blatter, L. A. (1994). Visualization of quantal synaptic transmission by dendritic calcium imaging. *Science*, 263:529–532.

[180] Nakanishi, S. (1994). Metabotropic glutamate receptors: Synaptic transmission, modulation, and plasticity. *Neuron*, 13:1031–1037.

[181] Nicoll, A. and Blakemore, C. (1993a). Patterns of local connectivity in the neocortex. *Neural Computation*, 5:665–680.

[182] Nicoll, A. and Blakemore, C. (1993b). Single-fibre EPSPs layer 5 of rat visual cortex *in vitro*. *NeuroReport*, 4:167–170.

[183] Nicoll, A., Larkman, A., and Blakemore, C. (1992). EPSPs in rat neocortical pyramidal neurones *in vitro* are prolonged by NMDA receptor-mediated currents. *Neuroscience Letters*, 143:5–9.

[184] Nicoll, A., Larkman, A., and Blakemore, C. (1993). Modulation of EPSPs shape and efficacy by intrinsic membrane conductances in rat neocortical pyramidal neurons in vitro. *Journal of Physiology*, 468:693–710.

[185] Nicoll, R. A. (1994). Neuroscience. Cajal's rational psychology. *Nature*, 368:808–809.

[186] Nusser, Z., Roberts, J. D. B., Baude, A., Richards, J. G., Sieghart, W., and Somogyi, P. (1995). Immunocytochemical localization of the $\alpha 1$ and $\beta 2/3$ subunits of the $GABA_A$ receptor in relation to specific GABAergic synapses in the dentate gyrus. *European Journal of Neuroscience*, in press.

[187] Otis, T. S. and Mody, I. (1992). Modulation of decay kinetics and frequency of $GABA_A$ receptor-mediated spontaneous inhibitory postsynaptic currents in hippocampal neurons. *Neuroscience*, 49:13–32.

[188] Otis, T. S., Staley, K. J., and Mody, I. (1991). Perpetual inhibitory activity in mammalian brain slices generated by spontaneous GABA release. *Brain Research*, 545:142–150.

[189] Otmakhov, N., Shirke, A. M., and Malinow, R. (1993). Measuring the impact of probabilistic transmission on neuronal output. *Neuron*, 10:1101–1111.

[190] Pearce, R. A. (1993). Physiological evidence for two distinct $GABA_A$ responses in rat hippocampus. *Neuron*, 10:189–200.

[191] Perkel, D. and Nicoll, R. A. (1993). Evidence for all-or-none regulation of neurotransmitter release: Implications for long-term potentiation. *Journal of Physiology*, 471:481–500.

[192] Peters, A. (1987). Numbers of neurons and synapses in primary visual cortex. In Peters, A. and Jones, E. G., editors, *Cerebral Cortex*, volume 6, pages 267–294. Plenum Press.

[193] Peters, A. and Jones, E. G. (1984). Classification of cortical neurons. In Peters, A. and Jones, E. G., editors, *Cerebral Cortex*, volume 1, pages 107–121. Plenum Press.

[194] Peters, A. and Kara, D. A. (1985a). The neuronal composition of area 17 of rat visual cortex I. the pyramidal cells. *Journal of Comparative Neurology*, 234:218–241.

[195] Peters, A. and Kara, D. A. (1985b). The neuronal composition of area 17 of rat visual cortex III. numerical considerations. *Journal of Comparative Neurology*, 238:263–274.

[196] Peters, A. and Kara, D. A. (1987). The neuronal composition of area 17 of rat visual cortex IV. the organization of pyramidal cells. *Journal of Comparative Neurology*, 260:573–590.

[197] Peters, A. and Marie, R. L. S. (1984). Smooth and sparsley spinous nonpyramidal cells forming local axonal plexuses. In Peters, A. and Jones, E. G., editors, *Cerebral Cortex*, volume 1, pages 419–445. Plenum Press.

[198] Pongracz, P. (1991). Electrotonic structure of olfactory sensory neurons analyzed by intracellular and whole cell patch techniques. *Journal of Neurophysiology*, 65:747–758.

[199] Poznanski, R. R. (1987). Techniques for obtaining analytical solutions for the somatic shunt cable model. *Mathematical Biosciences*, 83:1–23.

[200] Press, W. H., Teulosky, S. A., Vetterling, W. T., and Flannery, B. P. (1992). *Numerical Recipies in C*. Cambridge University Press.

[201] Rall, W. (1959). Branching dendritic trees and motoneuron membrane resistivity. *Experimental Neurology*, 1:491–527.

[202] Rall, W. (1960). Membrane potential transients and membrane time constant of motoneurons. *Experimental Neurology*, 2:503–532.

[203] Rall, W. (1967). Distinguishing theoretical synaptic potentials computed for different soma-dendritic distributions of synaptic input. *Journal of Neurophysiology*, 30:1138–1168.

[204] Rall, W. (1969). Time constants and electrotonic length of membrane cylinders and neurons. *Biophysical Journal*, 9:1483–1508.

[205] Rall, W. (1977). Core conductor theory and cable properties of neurons. In Kandel, E. R., editor, *Handbook of Physiology (Sect. I): The Nervous System*, pages 39–97. American Physiological Society.

[206] Rall, W., Burke, R. E., Smith, T. G., Nelson, P. G., and Frank, K. (1967). Dendritic location of synapses and possible mechanisms for the monosynaptic EPSP in motoneurons. *Journal of Neurophysiology*, 30:1169–1193.

[207] Ramon y Cajal, S. (1988). *Cajal on the Cerebral Cortex*. Oxford University Press.

[208] Rapp, M., Yarom, Y., and Segev, I. (1992). The impact of parallel fiber background activity on the cable properties of cerebellar purkinjie cells. *Neural Computation*, 4:518–533.

[209] Rastaad, M., Storm, J. F., and Andersen, P. (1992). Putative single quantum and single fibre excitatory postsynaptic currents show similar amplitude range and variability in rat hippocampal slices. *European Journal of Neuroscience*, 4:113–117.

[210] Redman, S. (1990). Quantal analysis of synaptic potentials in neurons of the central nervous system. *Physiological Reviews*, 70:165–198.

[211] Redman, S. J. (1971). The attenuation of passively propagating dendritic potentials in a motoneurone cable model. *Journal of Physiology*, 234:637–664.

[212] Regehr, W., Kehoe, J., Ascher, P., and Armstrong, C. (1993). Synaptically triggered action potentials in dendrites. *Neuron*, 11:145–151.

[213] Regehr, W. and Tank, D. (1992). Calcium concentration dynamics produced by synaptic activation of CA1 hippocampal pyramidal cells. *Journal of Neuroscience*, 12:4202–4223.

[214] Reuveni, I., Friedman, A., Amitai, Y., and Gutnick, M. J. (1993). Stepwise repolarization from Ca^{2+} plateaus in neocortical pyramidal cells: Evidence for non-homogenous distribution of HVA Ca^{2+} channels in dendrites. *Journal of Neuroscience*, 13:4609–4621.

[215] Richards, J. G., Schoch, P., Haring, P., Takacs, B., and Möhler, H. (1987). Resolving $GABA_A$/benzodiazepine receptors: Cellular and subcellular localization in the CNS with monoclonal antibodies. *Journal of Neuroscience*, 7:1866–1886.

[216] Roe, A. W. (1991). PhD thesis, Massachusetts Institute of Technology.

[217] Ropert, N., Miles, R., and Korn, H. (1990). Characteristics of miniature inhibitory postsynaptic currents in CA1 pyramidal neurones of rat hippocampus. *Journal of Physiology*, 428:707–722.

[218] Rose, P. K. and Dagum, A. (1988). Nonequivalent cylinder models of neurons: Interpretation of voltage transients generated by somatic current injection. *Journal of Neurophysiology*, 60:125–148.

[219] Rosenmund, C., Clements, J. D., and Westbrook, G. L. (1993). Nonuniform probability of glutamate release at a hippocampal synapse. *Nature*, 262:754–757.

[220] Rudy, B. and Iverson, L. E. (1991). *Ion Channels.* Academic Press, San Diego.

[221] Sachs, L. (1982). *Applied Statistics: A Handbook of Techniques.* Springer-Verlag.

[222] Sakmann, B. and Neher, E. (1983). *Single-Channel Recording.* Plenum.

[223] Sayer, R. J., Redman, S. J., and Andersen, P. (1989). Amplitude fluctuations in small EPSPs recorded from CA1 pyramidal cells in the guinea pig hippocampal slice. *Journal of Neuroscience*, 9:840–850.

[224] Scanziani, M., Capogna, M., Gahwiler, B. H., and Thompson, S. M. (1992). Presynaptic inhibition of miniature excitatory synaptic currents by bacolofen and adenosine in the hippocampus. *Neuron*, 9:919–927.

[225] Schoch, P., Richards, J. G., Haring, P., Takacs, B., Stahli, C., Staehlin, T., Haefly, W., and Möhler, H. (1985). Co-localization of GABA receptors and benzodiazepine receptors in the brain shown by monoclonal antibodies. *Nature*, 314:168–171.

[226] Segev, I., James W. Fleshman, J., and Burke, R. E. (199?). Computer simulation of group Ia EPSPs using morphologically realistic models of cat α-motoneurons. *Journal of Neurophysiology*, 6?:648–660.

[227] Segev, I., Rapp, M., Manor, Y., and Yarom, Y. (1992). Analog and digital processing in single nerve cells: Dendritic integration and axonal propagation. In McKenna, T., Davis, J., and Zornetzer, S. F., editors, *Single Neuron Computation*. Academic Press.

[228] Shadlen, M. and Newsome, W. (1994). Noise, neural codes, and cortical organization. *Current Opinion in Neurobiology*, 4:569–576.

[229] Sherman-Gold, R., editor (1993). *The Axon Guide for Electrophysiological and Biophysical Laboratory Techniques*. Axon Instruments, Inc., Foster City, CA.

[230] Siebert, W. M. (1965). Some implications of the stochastic behavior of primary auditory neurons. *Kybernetik*, 2:206–215.

[231] Silver, R. A., Traynelis, S. F., and Cull-Candy, S. G. (1992). Rapid-time-course miniature and evoked excitatory currents at cerebellar synapses *in situ*. *Nature*, 355:163–166.

[232] Smetters, D. K. and Nelson, S. B. (1993). Estimates of functional synaptic convergence in rat and cat visual cortical neurons. In *Society for Neuroscience Abstracts*.

[233] Smetters, D. K. and Nelson, S. B. (1995). Electrotonic structure and synaptic variability in cortical neurons. In Bower, J., editor, *Proceedings of Computation and Neural Systems 1994*. Kluwer.

[234] Snyder, D. L. and Miller, M. I. (1991). *Random Point Processes in Time and Space*. Springer-Verlag.

[235] Softky, W. R. (1994). Sub-millisecond coincidence detection in active dendritic trees. *Neuroscience*, 58:13–41.

[236] Softky, W. R. and Koch, C. (1993). The highly irregular firing of cortical cells is inconsistent with temporal integration of random EPSPs. *Journal of Neuroscience*, 13:334–350.

[237] Soltesz, I. and Deschênes, M. (1993). Low- and high-frequency membrane potential pscillations during theta activity in CA1 and CA3 pyramidal neurons of the rat hippocampus under ketamine-xylazine anesthesia. *Journal of Neurophysiology*, 70:97–116.

[238] Soltesz, I. and Mody, I. (1994). Patch-clamp recordings reveal powerful GABAergic inhibition in dentate hilar neurons. *Journal of Neuroscience*, 14:2365–2376.

[239] Soltesz, I. and Mody, I. (1995). Ca^{++}-dependent plasticity of miniature inhibitory postsynaptic currents following amputation of dendrites in central neurons. *Journal of Neurophysiology*, In Press.

[240] Soltesz, I., Smetters, D. K., and Mody, I. (1995). Tonic inhibition originates from synapses close to the soma. *Neuron*, In Press.

[241] Somogyi, P. and Cowey, A. (1984). Double bouquet cells. In Peters, A. and Jones, E. G., editors, *Cerebral Cortex*, volume 1, pages 337–360. Plenum Press.

[242] Spruston, N., Jaffe, D. B., Williams, S. H., and Johnston, D. (1993). Voltage- and space-clamp errors associated with the measurement of electrotonically remote synaptic events. *Journal of Neurophysiology*, 70:781–802.

[243] Spruston, N. and Johnston, D. (1992). Perforated patch-clamp analysis of the passive membrane properties of three classes of hippocampal neurons. *Journal of Neurophysiology*, 67:508–529.

[244] Staley, K. J. and Mody, I. (1991). Integrity of perforant path fibers and the frequency of action potential independent excitatory and inhibitory synaptic events in dentate gyrus granule cells. *Synapse*, 9:219–224.

[245] Staley, K. J. and Mody, I. (1992). Shunting of excitatory input to dentate gyrus granule cells by a depolarizing $GABA_A$ receptor-mediated postsynaptic conductance. *Journal of Neurophysiology*, 68:197–212.

[246] Staley, K. J., Otis, T. S., and Mody, I. (1992). Membrane properties of dentate gyrus granule cells: Comparison of sharp microelectrode and whole-cell recordings. *Journal of Neurophysiology*, 67:1346–1358.

[247] Stern, P., Edwards, F. A., and Sakmann, B. (1992). Fast and slow components of unitary EPSCs on stellate cells elicited by focal stimulation in slices of rat visual cortex. *Journal of Physiology*, 449:247–278.

[248] Stevens, C. F. (1993). Quantal release of neurotransmitter and long-term potentiation. *Neuron*, 10:55–63.

[249] Stevens, C. F. and Wang, Y. (1994). Changes in reliability of synaptic function as a mechanism for plasticity. *Nature*, 371:704–707.

[250] Storm, J. F. and Lipowsky, R. (1994). Evidence that changes in presynaptic fibers may affect paired-pulse facilitation in hippocampal slices. In *Society for Neuroscience Abstracts*.

[251] Stratford, K. J., Mason, A. J. R., Larkman, A. U., Maajor, G., and Jack, J. J. B. (1989). The modeling of pyramidal neurones in the visual cortex. In Durbin, R., Miall, C., and Mitchison, G., editors, *The Computing Neurone*, pages 296–321. Addison-Wesley.

[252] Stuart, G. and Sakmann, B. (1994). Active propagation of somatic action potentials into neocortical pyramidal cell dendrites. *Nature*, 367:69–72.

[253] Sutor, B. and Hablitz, J. J. (1989a). EPSPs in rat neocortical neurons in vitro i. electrophysiological evidence for two distinct EPSPs. *Journal of Neurophysiology*, 61:607–620.

[254] Sutor, B. and Hablitz, J. J. (1989b). EPSPs in rat neocortical neurons in vitro II. involvement of N-methyl-D-aspartate receptors in the generation of EPSPs. *Journal of Neurophysiology*, 61:621–634.

[255] Szentágothai, J. (1975). The "module-concept" in cerebral cortex architecture. *Brain Research*, 95:475–496.

[256] Szentágothai, J. (1979). Local neuron circuits of the neocortex. In Schmitt, F. O. and Worden, F. G., editors, *The Neurosciences Fourth Study Program*. MIT Press.

[257] Thompson, S. M., Masukawa, L. M., and Prince, D. A. (1985). Temperature dependence of intrinsic membrane properties and synaptic potentials in hippocampal CA1 neurons in vitro. *Journal of Neuroscience*, 5:817–824.

[258] Thomson, A. M. (1986). A magnesium-sensitive post-synaptic potential in rat cerebral cortex resembles neuronal responses to N-methylaspartate. *Journal of Physiology*, 370:531–549.

[259] Thomson, A. M. and Deuchars, J. (1994). Temporal and spatial properties of local circuits in neocortex. *Trends in Neuroscience*, 17:119–126.

[260] Thomson, A. M., Deuchars, J., and West, D. C. (1993a). Large, deep layer pyramid-pyramid single axon EPSPs in slices of rat motor cortex display pared pulse and frequency-dependent depression, mediated presynaptically and self-facilitation, mediated postsynaptically. *Journal of Neurophysiology*, 70:2354–2369.

[261] Thomson, A. M., Deuchars, J., and West, D. C. (1993b). Single axon excitatory postsynaptic potentials in neocortical interneurons exhibit pronounced paired pulse facilitation. *Neuroscience*, 54:347–360.

[262] Thomson, A. M., Girdlestone, D., and West, D. C. (1988). Voltage-dependent currents prolong single-axon postsynaptic potentials in layer III pyramidal neurons in rat neocortical slices. *Journal of Neurophysiology*, 60:1896–1907.

[263] Thomson, A. M. and Rhadpour, S. (1991). Excitatory connections between CA1 pyramidal cells revealed by spike triggered averaging in slices of rat hippocampus are partially NMDA receptor mediated. *European Journal of Neuroscience*, 3:587–601.

[264] Thomson, A. M. and West, D. C. (1993). Fluctuations in pyramid-pyramid excitatory postsynaptic potentials modified by presynaptic firing pattern and postsynaptic membrane potential using paired intracellular recordings in rat neocortex. *Neuroscience*, 54:329–346.

[265] Thurbon, D., Field, A., and Redman, S. (1993). Electrotonic profiles of interneurons in stratum pyramidale of the CA1 region of rat hippocampus. *Journal of Neurophysiology*, 70:2354–2369.

[266] Traynelis, S. F., Silver, R. A., and Cull-Candy, S. G. (1993). Estimated conductance of glutatmate receptor channels activated during EPSCs at the cerebellar mossy fiber-granule cell synapse. *Neuron*, 11:279–289.

[267] Trussell, L. O., Raman, I. M., and Zhang, S. (1994). AMPA receptors and rapid synaptic transmission. *Seminars in the Neurosciences*, 6:71–79.

[268] Trussell, L. O., Zhang, S., and Raman, I. M. (1993). Desensitization of AMPA receptors upon multiquantal neurotransmitter release. *Neuron*, 10:1185–1196.

[269] Tuckwell, H. (1988). *Introductaion to Biological Cable Theory*. Cambridge University Press.

[270] Turner, D. A. (1984). Conductance transients onto dendritic spines in a segmental cable model of hippocampal neurons. *Biophysical Journal*, 46:85–96.

[271] Turner, D. A. (1988). Waveform and amplitude characteristics of evoked responses to dendritic stimulation of CA1 guinea-pig pyramidal cells. *Journal of Physiology*, 395:419–439.

[272] Turner, G. D., Bodewitz, G., Thompson, C. L., and Stephenson, F. A. (1993). Immunohistochemical mapping of gamma-aminobutyric acid type-A receptor alpha subunits in rat central nervous system. *Psychopharmacol. Ser.*, 11:29–49.

[273] Turrigiano, G., Abbott, L. F., and Marder, E. (1994). Activity-dependent changes in the intrinsic properties of cultured neurons. *Science*, 264:974–977.

[274] Ulrich, D. and Lüscher, H.-R. (1993). Miniature excitatory synaptic currents corrected for dendritic cable properties reveal quantal size and variance. *Journal of Neurophysiology*, 69:1769–1773.

[275] Van der Kloot, W. (1987). Pretreatment with hypertonic solutions increases quantal size at the frog neuromuscular junction. *Journal of Neurophysiology*, 57:1536–1554.

[276] Van der Kloot, W. (1988). Acetylcholine quanta are released from vesicles by exocytosis (and why some think not). *Neuroscience*, 24:1–7.

[277] Van der Kloot, W. (1989). Statistical and graphical methods for testing the hypothesis that quanta are made up of subunits. *Journal of Neuroscience Methods*, 27:81–89.

[278] Van der Kloot, W. (1991). The regulation of quantal size. *Progress in Neurobiology*, 36:93–130.

[279] Van der Kloot, W., Balezina, O. P., Molgo, J., and Naves, L. A. (1994). The timing of channel opening during miniature endplate currents at the frog and mouse neuromuscular junctions: Effects of fasiculin-2, other anticholinesterases, and vesamicol. *Pflugers Archives*, 428:114–126.

[280] Van der Kloot, W. and Molgo, J. (1994). Quantal acetylcholine release at the vertebrate neuromuscular junction. *Physiological Reviews*, 74:899–991.

[281] Van der Kloot, W. and Spielholz, N. (1987). Effects of changes in tonicity of the extracellular solution on the size of vesicles in the frog motor nerve terminals. *Journal of Neurocytology*, 16:77–84.

[282] Van Essen, D. C. (1985). Functional organization of primate visual cortex. In Peters, A. and Jones, E. G., editors, *Cerebral Cortex*, volume 3, pages 259–329. Plenum Press.

[283] Voronin, L. L., Kuhnt, U., Gusev, A. G., and Hess, G. (1992). Quantal analysis of long-term potentiation of "minimal" excitatory postsynaptic potentials in guinea pig hippocampal slices: Binomial approach. *Experimental Brain Research*, 89:275–287.

[284] Vu, E. T. and Krasne, F. B. (1992). Evidence for a computational distinction between proximal and distal inhibition. *Science*, 255:1710–1712.

[285] Walmsley, B., Edwards, F. R., and Tracey, D. J. (1987). The probabilistic nature of synaptic transmission at a mammalian excitatory central synapse. *Journal of Neuroscience*, 7:1037–1046.

[286] Walmsley, B. and Stuklis, R. (1989). Effects of spatial and temporal dispersion of synaptic input on the time course of synaptic potentials. *Journal of Neurophysiology*, 61:681–687.

[287] White, E. L. (1989). *Cortical Circuits.* Birkhauser.

[288] White, J. A., Manis, P. B., and Young, E. D. (1992). The parameter identification problem for the somatic shunt model. *Biological Cybernetics*, 66:307–318.

[289] Williams, S. H. and Johnston, D. (1991). Kinetic properties of two anatomically distinct excitatory synapses in hippocampal CA3 pyramidal neurons. *Journal of Neurophysiology*, 66:1010–1020.

[290] Wuarin, J.-P. and Dudek, F. E. (1993). Patch-clamp analysis of spontaneous synaptic currents in supraoptic neuroendocrine cells of the rat hypothalamus. *Journal of Neuroscience*, 13:2323–2331.

[291] Xiang, Z., Greenwood, A. C., Kairiss, E. W., and Brown, T. H. (19943). Quantal mechanism of long-term potentiation in hippocampal mossy-fiber synapses. *Journal of Neurophysiology*, 71:2552–2556.

[292] Yuste, R., Gutnick, M. J., Saar, D., Delaney, K. R., and Tank, D. W. (1994). Ca^{2+} accumulations in dendrites of neocortical pyramidal neurons: An apical band and evidence for two functional compartments. *Neuron*, 13:23–43.

[293] Zador, A. M. (1993). *Biophysics of Computation in Single Hippocampal Neurons.* PhD thesis, Yale University.

[294] Zar, J. (1974). *Biostatistical Analysis.* Prentice Hall.

[295] Zimprich, F., Zezula, J., Sieghart, W., and Lassmann, H. (1991). Immunohistochemical localization of the alpha 1, alpha 2, and alpha 3 subunit of the $GABA_A$ receptor in the rat brain. *Neuroscience Letters*, 127:125–128.